THERMAL CHARACTERIZATION AND KINETIC ANALYIS OF SARA FRACTIONS OF CRUDE OILS BY TGA AND DSC METHODS

A THESIS SUBMITTED TO
THE GRADUATE SCHOOL OF NATURAL AND APPLIED SCIENCES
OF
MIDDLE EAST TECHNICAL UNIVERSITY

BY

KIYMET GİZEM GÜL

IN PARTIAL FULFILLMENT OF THE REQUIREMENTS
FOR
THE DEGREE MASTER OF SCIENCE
IN
PETROLEUM AND NATURAL GAS ENGINEERING

SEPTEMBER 2011

Approval of the thesis:

THERMAL CHARACTERIZATION AND KINETIC ANALYSIS OF SARA FRACTIONS OF CRUDE OILS BY TGA AND DSC METHODS

submitted by **KIYMET GİZEM GÜL** in partial fulfillment of the requirements for the degree of **Master of Science in Petroleum and Natural Gas Engineering Department, Middle East Technical University** by,

Prof. Dr. Canan Özgen _____
Dean, Graduate School of **Natural and Applied Sciences**

Prof. Dr. Mahmut Parlaktuna _____
Head of Department, **Petroleum and Natural Gas Engineering**

Prof. Dr. Mustafa Verşan Kök _____
Supervisor, **Petroleum and Natural Gas Engineering Dept., METU**

Examining Committee Members

Prof. Dr. Mahmut Parlaktuna _____
Petroleum and Natural Gas Engineering Dept., METU

Prof. Dr. Mustafa Verşan Kök _____
Petroleum and Natural Gas Engineering Dept., METU

Prof. Dr. Nurkan Karahanoğlu _____
Geological Engineering Dept., METU

Assist. Prof. Dr. Çağlar Sınayuç _____
Petroleum and Natural Gas Engineering Dept., METU

Dr. A.Gürkan İşcan _____
Çalık Energy, ANKARA

Date: 14/09/2011

I hereby declare that all information in this document has been obtained and presented in accordance with academic rules and ethical conduct. I also declare that, as required by these rules and conduct, I have fully cited and referenced all material and results that are not original to this work.

Name, Last name : Kıymet Gizem Gül

Signature :

ABSTRACT

THERMAL CHARACTERIZATION AND KINETIC ANALIYSIS OF *SARA* FRACTIONS OF CRUDE OILS BY TGA AND DSC METHODS

Gül, Kıymet Gizem
M.Sc., Department of Petroleum and Natural Gas Engineering
Supervisor: Prof. Dr. Mustafa Verşan Kök

September 2011, 183 pages

In this thesis, four different crude oil samples and their saturate, aromatic and resin fractions were analyzed by two different thermoanalytical methods, thermogravimetric analysis (TGA) and differential scanning calorimetry (DSC). The experiments were performed at three different heating rates (5, 10 and 15 °C/min) under air atmosphere. Same gas flow rate and same pressure were applied to all samples.

The aim is to determine the kinetic analysis and combustion behavior of crude oils and their fractions and also determining the effect of heating rate on all samples.

For all samples two main reaction regions were observed in thermogravimetry (TG), differential thermogravimetry (DTG) and DSC curves due to the oxidative degradation of crude oil components. It was deduced that the free moisture, volatile hydrocarbons were evaporated from the crude oils, light hydrocarbons were burned and fuel was formed in the first reaction region. The second reaction region was the

main combustion region where the fuel was burned. From the TGA curves, it was detected that the heavier fraction, resins, lost considerable amounts of their initial mass, approximately 35%, while saturates lost only approximately 3% of their initial mass in the second reaction region. DSC curves of the samples were also examined and observed that as the sample got heavier, the heat of the reaction increased. Saturates, lightest part of the crude oil fractions, gave minimum heat of reaction. As the heating rate increased, shift of peak temperatures to high values and higher reaction regions were observed.

The kinetic analysis of crude oils and their fractions were also performed using different kinetic methods. Activation energies (E), mean activation energies (E_{mean}) and Arrhenius constants were found for crude oils and fractions. It was deduced that the resins gave the highest activation energy and Arrhenius constant for both reaction regions. Moreover, it was encountered that heating rate has no effect on activation energies.

Keywords: thermogravimetry, differential scanning calorimetry, combustion, SARA fractions, kinetic analysis

ÖZ

TGA VE DSC METHOTLARI YOLUYLA HAM PETROLLERİN *SARA* FRAKSİYONLARININ TERMAL KARAKTERİZASYONU VE KİNETİK ANALİZİ

Gül, Kıymet Gizem
Yüksek Lisans, Petrol ve Doğal Gaz Mühendisliği Bölümü
Tez Yöneticisi: Prof. Dr. Mustafa Verşan Kök

Eylül 2011, 183 sayfa

Bu tez çalışmasında, dört farklı petrolün ve bu petrollerin doymuş hidrokarbon, aromatik ve polar fraksiyonları iki farklı termoanalitik yöntem ile incelenmiştir. Bu metotlar termogravimetrik analiz (TGA) ve türevsel taramalı kalorimetridir (DSC). Tüm deneyler üç farklı ısıtma hızında (5, 10 and 15 °C/dk) hava kullanılarak gerçekleştirilmiştir. Bütün deneyler aynı gaz akış hızında ve basıncında yapılmıştır.

Çalışmanın amacı, petrol örnekleri ve fraksiyonlarının yanma özelliklerinin incelenmesi, kinetik hesaplamalar ve ısıtma hızının etkisinin belirlenmesidir.

Termogravimetri (TG), türevsel termogravimetri (DTG) ve DSC yanma eğrilerinde iki farklı reaksiyon aralığı gözlemlenmiştir. Birinci reaksiyon bölgesinde numunelerin içerdiği yüksek nem ve uçucu hidrokarbonların uçtuğu, hafif hidrokarbonların yandığı, ikinci reaksiyon aralığının ise asıl yanma bölgesi olduğu anlaşılmıştır. TGA eğrilerinden, ikinci reaksiyon aralığında, polar fraksiyonların

başlangıç ağırlıklarının ortalama %35'ini kaybederken doymuş hidrokarbonların ortalama %3 ünü kaybettiği gözlemlenmiştir. DSC eğrileri incelendiğinde numune ağırlaştıkça reaksiyon ısı miktarının arttığı gösterilmiştir. Petrollerin en hafif fraksiyonları olan doymuş hidrokarbonların en az reaksiyon ısısına sahip olduğu gözlemlenmiştir. Artan ısıtma hızının petroller ve fraksiyonlarında tepe sıcaklıklarında artmaya neden olduğu anlaşılmıştır.

Farklı kinetik modeller kullanılarak petrollerin ve fraksiyonlarının kinetik parametereleri hesaplanmıştır. Bütün numuneler için aktivasyon enerjisi, ortalama aktivasyon enerjisi ve Arrhenius katsayısı belirlenmiştir. Bunun sonucunda da polar fraksiyonların en fazla aktivasyon enerjisine ve Arrhenius katsayısı sahip olduğu gözlemlenmiştir. Isıtma hızının aktivasyon enerjisinde herhangi bir değişikliğe neden olmadığı görülmüştür.

Anahtar sözcükler: termogravimetri, türevsel taramalı kalorimetri, yanma, SARA fraksiyonları, kinetik analiz

to my family

ACKNOWLEDGMENTS

I would like to express my deepest gratitude to my supervisor Prof. Dr. Mustafa Verşan Kök for his guidance, advice, criticism, encouragements and support from initial to the final level enabled me to develop an understanding of the subject.

Besides my advisor, I would like to thank the rest of my thesis committee: Prof. Dr. Mahmut Parlaktuna, Prof. Dr. Nurkan Karahanoğlu, Assist. Dr. Çağlar Sınayuç, Dr. Gürkan İşcan for their comments.

I would like to thank to my workmates especially to Göker Ertunç, Aslı Satı Gündoğar, Sevtaç Bülbül for their suggestions, technical and moral support.

Lastly but most importantly, my heartfelt gratitude goes to my family, Ayhan and Zümrüt, for their unflagging love and support throughout my life; this study is simply impossible without them. I am indebted to my grandfather, Mehmet, for his care and love. Although he is no longer with us, he will be remembered and loved forever.

TABLE OF CONTENTS

LIST OF FIGURES

FIGURES

LIST OF TABLES

TABLES

NOMENCLATURE

ASTM	American Society of Testing Materials
EOR	Enhanced Oil Recovery
TGA	Thermogravimetric Analyzer/Analysis
TA	Thermal Analysis
TG	Thermogravimetry
DSC	Differential Scanning Calorimetry
DTA	Differential Thermal Analysis
DTG	Differential Thermogravimetry
TA	Thermal Analysis
T	Temperature
T_p	Peak Maximum Temperature
HTO	High-Temperature Oxidation
LTO	Low-Temperature Oxidation
SARA	Saturate, Aromatic, Resin, Asphaltene
API	American Petroleum Institute
α	Conversion degree
β	Heating rate
C_p	Heat capacity
A	Arrhenius constant (Pre-exponential factor)
E	Activation energy
n	Reaction order
t	Time
R	Universal gas constant

CHAPTER 1

INTRODUCTION

Fossil fuels have been widely used as an energy source since the Industrial revolution. World primary energy consumption grew by 5.6% in 2010, the largest increase (in terms of percentage) since 1973 [1]. However, the old oil reserves are declining and finding the location of new reserves is getting harder. Therefore, there occurs an emphasis on recovering the remaining oil in old reserves. The enhanced oil recovery (EOR) methods were developed to recover that untapped oil from partially depleted reservoirs. The in situ combustion, burning the fuel in its place, i.e. reservoir, is one of the thermal enhanced oil recovery techniques that have been more widely and successfully applied [2]. In in situ combustion, the energy is generated through a combustion front that is propagated in the reservoir. This process involves important physical and chemical reactions that take place in the reservoir. During the oil recovery process, any gas that is containing oxygen is injected into the reservoir. This injected gas reacts with the fuel in the reservoir, produce heat and ignites oil in surrounding area. This creates a combustion front and this front propagates through the reservoir. Therefore, the unburned oil is recovered from the reservoir. The coke that is formed in the reservoir is an important parameter for the continuity of the combustion front [3].

Although extensive research has been done on the thermal and fluid dynamics aspect of the in situ combustion process, it is equally important to learn the chemical reaction kinetics of the phenomenon of in situ combustion. However, limited data are

available on the rates and the nature of the partial oxidation reactions and the high temperature combustion reactions of crude oils.

The combustion kinetics necessary for the petroleum industry can be achieved by thermal analysis techniques. Thermal analysis is the measurement of the any physical or chemical change of a property of a sample as a function of temperature or time. The most widely used thermal analysis methods applied in petroleum industry are thermogravimetry (TG) and differential scanning calorimetry (DSC).

Thermogravimetry is a technique in which the mass of sample is measured as a function of temperature or time while the substance is subjected to a controlled temperature program. The controlled temperature program means heating/cooling at a constant linear rate, isothermal measurements or the combination of heating, cooling and isothermal stages. The commonly investigated processes are the mass loss or mass gain in oxidation, dehydration, determination of volatile content, decomposition and other compositional analysis. The most common application in petroleum industry is heating at constant linear heating rate. TG gives general information about the reaction kinetics.

Differential scanning calorimetry is a technique in which the amount of heat required to change the temperature of a sample and a reference sample is measured as a function of temperature. During the experiment, both the sample and the reference sample are tried to keep at same temperature. These measurements provide quantitative and qualitative information about the physical and chemical changes that involve exothermic and endothermic processes.

In this thesis, four different crude oil samples from southeastern region of Turkey and their saturate, aromatic and resin fractions were used. The crude oil samples separated to their fractions by using column chromatography technique. The asphaltene fractions of these could not be obtained at the end of column chromatography process. The crude oil samples and their fractions were subjected to

same pressure, same gas flow rate despite different heating rates (5, 10 and 15 °C/min). The different combustion behavior of crude oils and SARA fractions by means of TG/DTG and DSC methods were studied and also the heating rate effect on the combustion behavior was analyzed. Moreover, different model fitting (Arrhenius and Coats & Redfern methods) and isoconversional (Ozawa – Flynn – Wall and Kisssinger – Akkahira – Sunose methods) methods were applied to the samples to evaluate the kinetic parameters. The kinetic parameters of the samples were discussed and also the effect of heating rate on the kinetic parameters was examined.

CHAPTER 2

LITERATURE REVIEW

There have been many studies on the application of the thermal analysis techniques to the combustion behavior of the crude oils. These studies back to 1959, when Tadema [4] first applied the thermal analysis to the effects of combustion on mixture of crude oils and clays. Two different reaction regions were identified in all the studied crude oil samples. One of them occurred at low temperatures and the other one at high temperatures.

Bae [5] investigated the thermo-oxidative behavior of the crude oils using TGA and differential thermal analyzer (DTA) instruments. The results revealed that the crude oils could be grouped according to their thermo-oxidative behavior and also the viscosity and density of crude oils did not correlate well with this behavior. The available oxygen at low temperatures changed the quantity and quality of the available fuel. Moreover, this available fuel did not consume at lower temperatures. In fireflooding, the heat generated at low temperature was significant.

Vossoughi and Willhite [6] developed a kinetic model of the in situ combustion process from the data that is obtained from TGA and DSC. The acquired data were used to figure out the fuel deposition and fuel combustion rate in a combustion tube. The gases that were released from the TGA were examined by gas chromatography to determine the reactions taking place during TGA combustion experiments.

Kok and Karacan [7] studied the pyrolysis behavior of crude oils and their saturate, aromatic, resin, asphaltene (SARA) fractions using thermogravimetry and differential scanning calorimetry. The aim of this study was to describe the complex behavior of whole oil by less complex constituents. The experiments were performed with 10 °C/min heating rate under nitrogen environment. This study showed that the chemical nature of the fractions determines the pyrolysis mechanisms and also the fractions in whole crude oil follow their own pathway (distillation and cracking) independent of the existence of other fractions.

Kok and Karacan [8] studied the pyrolysis behavior and kinetic analysis of six different crude oils by DSC and TG/DTG. Two main mass loss regions were observed during the pyrolysis of crude oils. One of these regions was the distillation region where light to medium gravity crude oils were evaporated. The second region was the visbreaking and cracking region during which the heavy parts of the crude oils were evaporated and this region was characterized by the relatively steep peak in the TG/DTG curve. For the kinetic analysis, they used the Arrhenius kinetic model. They observed that as the asphaltene content was increasing or the °API gravity of crude oils was decreasing (oil gets heavier), the cracking activation energy was increasing. The DSC curves were showed endothermic effect both in distillation and visbreaking and cracking region. The calorific value due to the cracking reaction was increasing with increase in asphaltene content or decrease in °API gravity.

Kok and Pamir [9] studied the pyrolysis behavior and kinetics of oil shale by TG/DTG and DSC in non-isothermal environment. All the DSC experiments were endothermic and no exothermic effect was observed. Moreover, two reaction regions were observed in TG/DTG. The first region was distillation and the second one was the visbreaking and cracking. The start of pyrolysis reaction for rich grade shale was lower than the poor grade shale. The kinetic parameters were determined by Coats and Redfern method. The advantage of using this method is determining the reaction order rather than assuming it and consider the heating rate effect.

Kok and Karacan [10] studied behavior of whole oil and fractions during combustion by TGA and DSC by using air and a heating rate 10 °C/min for two Turkish crude oils. The TGA and DSC experiments are used to determine the weight loss and reaction enthalpies of individuals due to the reactions. The experiments showed that saturates lost most of their mass in low-temperature oxidation (LTO), aromatics and resins lost in middle-temperature oxidation (MTO) and the asphaltenes lost in high-temperature oxidation (HTO) regions for the two crude oils. Moreover, saturates gave the highest amount of heat release in LTO, resins and aromatics in MTO and asphaltenes in HTO.

Al-Saffar et al. [11] used DISC reactor to investigate the oxidation behavior of North Sea light crude oil and its SARA fractions in consolidated cores. The results demonstrated that the light crude oils were adequately reactive for the air combustion at reservoir conditions. The burned fuel concentration was determined from the SARA fractions of the crude oil. The light crude oils were highly reactive at low temperatures since they were highly composed of saturates fraction and saturates were mainly contribute to the fuel deposition and oxygen consumption at low temperatures.

Kok and Iscan [12] applied DSC to the combustion of crude oils in the presence and absence of metal chlorides. The experimental data showed that the grain size distribution is important in the low percentage of metallic additive. However, as the percentage of the additive increased, the effect of additives become more important. Three different reaction regions were observed, LTO, (fuel deposition) FD and HTO. Two different kinetic methods (Roger-Morris and Arrhenius) were used to analyze the data obtained from DSC. The data indicated that the crude oils with catalyst had lower activation energy. This is attributed to the fact that catalysts lowered the energy need for commencing the reactions and catalysts provided additional pathways for the reactions.

Li and Yue [13] studied the pyrolysis of oil shale samples from Fushun and Maoming using TGA at four different heating rates. The kinetic parameters were determined using integral method, differential method, Friedman procedure, maximum rate method and parallel first order reaction model. The results obtained from differential and integral methods are almost same. Moreover, the activation energies obtained from maximum rate method and Friedman method were also close. They also observed that for oil shale the parallel reaction model was more reasonable than the other reaction models based on the assumption that oil shale follows six parallel first order reactions with different activation energies.

Kok and Pamir [14] studied the pyrolysis behavior and the kinetics of oil shales using DSC and TGA. Two reaction regions were observed, distillation region between ambient temperature and 500 K and cracking region between the 500-800 K. Kinetic parameters of the samples were also calculated using different kinetic methods. Activation energies differed from each other and these were attributed to different type of kerogen in oil shale samples.

Li et al. [15] examined the behavior of pure paraffinic components and mixtures of pure paraffinic components with crude oils by using TG/DTG thermal analysis techniques. For the pure components, the fractions between C16 and C26 were distilled significantly in low temperature region. The heavier fractions distilled in low and high temperature regions but distilled significantly in high temperature oxidation region. As the molecular weight increased, the peak temperatures for low and high temperature oxidation regions increased. Mixing heavier paraffins with crude oils increased the heat evaluation in low temperature oxidation; therefore, some paraffin samples could be used as igniter in reservoir.

Kok et al. [16] investigated the combustion behavior of the crude oils (Beykan and Karakus) limestone matrix mixtures by TG/DTG methods. The experiments were performed at a heating rate of 10 °C/min under air atmosphere. In combustion experiments, three different reaction regions were observed such as LTO, FD, HTO.

The kinetic parameters were determined by Arrhenius kinetic model. The activation energies for these reaction regions were distinct from each other. These individual activation energies were attributed to the different reaction mechanisms and these differences did not give any indication to the overall combustion reactivity of crude oil.

Bagci and Kok [17] studied the combustion reaction kinetics of Turkish crude oils (Bati Raman, Camurlu, Raman, Adiyaman, Garzan, Karakus and Beykan) in limestone medium. The limestone and the crude oil were mixed and heated at constant air flow rate. The molar CO_2/CO ratios determined by analyzing the produced gas vary during LTO, FD, HTO but these values were determined at different heating rates. The H/C ratio was decreasing with an increase in the temperature for all runs. The activation energies of Bati Raman and Camurlu crude oils were similar for HTO and FD reactions. The activation energies of Adiyaman and Garzan medium gravity oils for the HTO reaction were higher than the FD reaction. The activation energy of the LTO reaction was the twice of HTO and FD reaction. The activation energies and Arrhenius constants were almost independent of the gravity of the crude oils.

Ambalae et al. [18] studied the pyrolysis and combustion behavior of both crude oil and its asphaltenes each mixed with the reservoir sand using TGA. Temperature-rated and isothermal pyrolysis experiments were performed to determine the activation energy and the temperature at which the coke formation was maximized. Arrhenius method was applied for the determination of kinetic parameters. The activation energy calculated for the whole oil and the asphaltene were in close agreement.

Mendez Kuppe et al. [19] studied the heat of combustion of three different crude oils and their respective SARA fractions. They concluded that the heating values of saturates and aromatics were higher than the heating values of the resins and

asphaltenes. The heating values of the resins and asphaltenes were almost similar and lower than saturates and aromatics.

Murugan et al. [20] examined the thermal behavior of Fostern whole oil mixed with reservoir sand and the coke derived from the whole oil by TGA under nitrogen and air atmospheres at 10 °C/min heating rate up to 800 °C. Three reaction regions (LTO, FD, HTO) were observed similar to previous studies in non-isothermal combustion experiments. Higher activation energy values were obtained at higher temperatures. The coke derived from the whole oil was subjected to isothermal combustion at different temperatures from 375 to 500 °C. The kinetic parameters were calculated using Arrhenius model. The experimental data and the kinetic model showed a close relationship for different combustion temperatures. It was also observed that the apparent order of reaction approaches unity.

Castro and Vazquez [21] analyzed the four different Mexican crude oils and their SARA fractions with different densities ranging from 9 to 39 °API using TGA and DSC techniques. TGA technique was used to characterize the volatilization and decomposition temperature of crude oils and observed that the decomposition temperature was increased with the increasing average molecular mass of crude oil. DSC experiments showed the transition regions of SARA fractions. DSC has shown to be a good indicator for the fingerprinting of crude oils and SARA fractions.

Kok [22] examined the characteristics of heavy and medium gravity crude oils in limestone matrix by DSC and TGA. The crude oil limestone mixtures were subjected to oxidizing atmosphere under constant heating rate environment. Two different zones were observed known as LTO and HTO in TGA and DSC curves. Two different kinetic methods were applied both to the LTO and HTO regions. It was observed that heavy crude oils have high activation energy values both in the low and high temperature oxidation regions.

CHAPTER 3

STATEMENT OF THE PROBLEM

This study intends to investigate the combustion behavior and kinetic analysis of crude oils and their fractions and also the effect of heating rate on all samples.

Four different crude oils and saturate, aromatic, resin constituents of these crude oils were studied using two different thermoanalytical techniques that are thermogravimetry (TG/DTG) and differential scanning calorimetry (DSC). Separating the crude oil into their SARA fractions were performed by using column chromatography technique; however, at the end of the column chromatography asphaltene content could not be obtained.

The experiments were performed at three different heating rates (5, 10 and 15 °C/min) under air atmosphere. Same gas flow rate and pressure were used throughout all the experiments. The TGA and DSC experiments continued up to 900 K.

The reaction intervals were determined using both the TG/DTG and DSC curves. The TG/DTG curves were used to find the mass loss amounts in the reaction regions. The heat flow to the samples in reaction regions were determined by DSC curve. Moreover, different model fitting and isoconversional methods were applied for the determination of kinetic parameters. The effect of heating rate on combustion behavior and kinetic parameters were examined.

CHAPTER 4

EXPERIMENTAL EQUIPMENT AND PROCEDURE

In this study, TGA Q500 and DSC Q200 instruments were used to perform the experiments. The mechanical properties of these instruments were given in this section.

4.1. Experimental Equipment

4.1.1. Thermogravimetric Analyzer (TGA)

The Thermogravimetric Analyzer used with thermal analysis controller and associated software is a thermal weight-change instrument. The Thermogravimetric Analyzer measures the rate and amount of weight change as a function of temperature or isothermally as a function of time. Moreover, phase changes can also be detected as a consequence of oxidation, decomposition or dehydration.

TGA consists of six main parts which are the balance, furnace, sample platform, cabinet, heat exchangers and mass flow controllers. The functions of them are as follows [23];

- *furnace* controls the sample temperature and atmosphere.
- *balance*, key element in TGA, measures the sample weight precisely.
- *sample platform* loads and unloads the sample to or through the balance.
- *cabinet* houses the system electronics and mechanics.

- *heat exchanger* dissipates heat from the furnace.
- *mass flow controllers* controls the purge gas to the furnace and balance. TGA Q500 has two mass flow controllers.

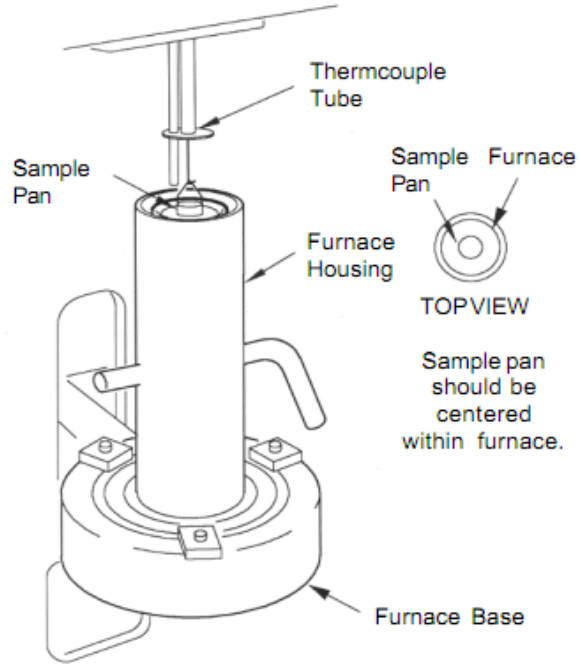

Figure 4.1 - The furnace assembly of TGA Instrument [23]

4.1.2. Differential Scanning Calorimeter (DSC)

Differential Scanning Calorimeter is used with thermal analysis controller and associated software. The DSC measures the amount of heat change associated with material transitions as a function of time or temperature. DSC gives qualitative and quantitative data on exothermic (heat evolution) and endothermic (heat absorption) reactions of a material as a consequence of phase changes, oxidation and other heat-related changes.

4.1.2.1. DSC Components

DSC consists of three main parts which are [24],

- *the instrument* itself containing the system electronics,
- *the DSC cell* measuring the change of temperature and heat flow
    - The sample material in a pan and the empty reference pan sit on the thermoelectric disk surrounded by the furnace in the DSC cell. As heating usually at linear rate the temperature of the cell is changed, the heat is transferred to the sample pan and reference pan through the thermoelectric disk. In general the DSCs measure the differential heat flow between the sample and the reference pan by the area of thermocouples using the thermal equivalent of Ohm's Law. However, this simple relationship does not take into account the extraneous heat flow between the sensor and the sample pan. This extraneous heat flow is taken into account in the DSC Q200.
- *the cooling accessory* the selection of which depends on the temperature range of the experiment.
    - There are two different cooling systems available with TA Instruments that are the Finned Air Cooling System (FACS) and Refrigerated Cooling System (RCS). The FACS permits the operation from ambient up to the 725 °C, using flowing air as a coolant. The RCS is used to perform DSC cooling experiments. In this study, the FACS is used as a cooling accessory since these experiments are run within the temperature range of 25 - 600 °C suitable for FACS.

4.1.3. Universal Analysis 2000 Program and Computer Controller

The common section for both the TGA and DSC is the universal analysis software and the computer controller. The TGA and DSC are controlled by a computer. This computer controller provides an interface between the experimenter and the analysis instrument. The computer stores experimental data runs in data analysis program and

enables experimenter to set up the experiment and enter the constants. The *TA Instruments' Universal Analysis 2000* program allows experimenter to analyze the data obtained from various thermal analysis instruments. Using this software user choose any combination of signals for plotting and analyzing the experimental data including first and second derivative [25]. The data file that is obtained at the end of the experiment is analyzed by the help of the Analyze menu in the software. The analyze menu allows user to integrate peak, finding peak max, onset point and finding the slope.

4.2. Experimental Procedure

In order to obtain accurate results, the experiments were conducted according to the written standards in TA Instruments Manual. For the experiments, all except very corrosive gases can be utilized with the instrument; in practice the inert gases nitrogen, helium, argon and the reactive gases air, oxygen and hydrogen can be used. In this study, the thermal analysis of the samples was conducted in oxidizing atmosphere. These oxidation experiments were run in air since the reactions are too fast in oxygen.

4.2.1. TGA Instrument Experimental Procedure

All the TGA experiments were run with platinum pan and sample weight approximately 2 mg with constant heating rate 5, 10 and 15 °C/min in a temperature range 25-600 °C. The balance purge gas and sample purge gas flow rates are adjusted to 80 and 120 ml/min, respectively.

The steps followed while running a TGA are as follows [23];

- selecting the pan type and material
    - In all the TGA experiments, platinum pan was used since the platinum pans are durable to temperatures as high as 900 °C, not reactive with most of the organic matter and easy to clean.

- creating or choosing the test procedure and entering experiment information through the TA instrument control software
- taring of the empty sample pan
    - Taring of the pan is performed to measure the weight of the empty pan and store it as an offset that is subtracted from the subsequent measurement to find the weight change of the sample.
- loading the sample into pan
    - TGA has high sensitivity to weight changes; therefore, small amounts of masses should be used during the experiments. Moreover, the sample should cover the pan base perfectly in order to allow purge gas to interact with sample surface evenly.
- attaching and setting up external accessories as required such as purge gas
    - Purge gas selection depends on the type of the experiment. Purge gas is distributed separately to two parts of the TGA: the balance chamber and the furnace. The balance purge maintains a positive pressure in the balance chamber to prevent decomposition products from contaminating the sensitive balance mechanism. The furnace purge permits rapid removal of decomposition products from the sample environment. The balance purge is always an inert gas independent of the experiment. The furnace gas can be an inert gas or oxidative gas depends on the experiment type.
- starting the experiment
- unloading the sample at the end of the experiment
- cleaning the pan
    - The pan was cleaned periodically between experiments with propane torch. In this way, any residue that was remained from the previous experiment was burned and cleaned.

4.2.1.1. Calibration of TGA

TGA calibration consists from two steps weight and temperature calibration performed through the instrument control software. The calibration results of TGA were given in Appendix A.I.

4.2.1.1.1. Weight Calibration

The mass calibration of TGA is done using the standard weights. The standard weights are placed to the sample pan and wait until the deviations are eliminated. In this study, 200 mg and 1 g weights were used for the mass calibration. The tare weight is measured and kept in the memory by the instrument for the appropriate weight range. In these experiments, the sample weights were approximately 2 mg; therefore, after calibration 200 mg range was selected as the weight range.

4.2.1.1.2. Temperature Calibration

The temperature calibration of TGA is done by using the Curie point method. This is done by placing a permanent magnet below the furnace close to the ferromagnetic sample. The sample experiences the magnetic force and higher mass is recorded. The sample is heated as usual. At Curie point, the sample loses its ferromagnetic property and is no longer attracted by the magnet, resulting in a sudden decrease in apparent mass. In this study, nickel was used as Curie standard. The Curie temperature of nickel is 354 °C. At Curie point, transition occurs over a relatively narrow temperature range and produces a step in the TGA curve. The temperature is recorded at the point of inflection or the end set of the step and compared with the Curie temperature of the reference material. The observed and actual temperatures were recorded to the temperature calibration table.

4.2.2. DSC Instrument Experimental Procedure

All the DSC experiments were run with open copper pan and sample weight approximately 2 mg with constant heating rate 5, 10 and 15 °C/min in a temperature range 25-600 °C. The balance purge gas and sample purge gas flow rates are adjusted to 80 and 129 ml/min, respectively.

The basic steps for running a DSC experiment given in the TA Instrument Manual are listed as follow [24];

- Selecting the pan type and material
    - In all DSC experiments, open copper pans were used since the copper is not reactive with the sample material and durable to temperatures as high as 600 °C. The pan type selection depends on the temperature and pressure range, composition, and reactivity requirements of the experiment.
- Preparing the sample
- Creating or choosing the test procedure and entering sample and instrument information through TA instrument control software
- Setting the purge gas flow rate
- Loading the sample and closing the cell lid
    - The sample pan is placed to the front platform and the reference empty pan is placed to the back platform. The pans are centered on the platforms.
- Starting the experiment

4.2.2.1. Calibration of DSC

The calibration procedure of DSC depends on the instrument model and heat flow selection. The model of the DSC instrument used during the experiments in this study requires only two calibrations that are the Tzero calibration and cell constant and temperature calibration. The calibration is needed when the cell, purge gas or

cooling accessory is changed. The results of DSC calibration were given in Appendix A.II.

4.2.2.1.1. Tzero Calibration

The DSC Tzero calibration requires two experiments. The first experiment is done without samples and pans (baseline); the second is performed with large approximately 95 mg sapphire disks without pans on both the sample and reference position. Both experiments use the same method beginning with a cell preheat followed by an equilibration at an initial temperature, holding isothermal for five minutes, heating at constant rate to a final temperature and holding isothermal for 5 minutes. The range of temperatures should be at least as broad as the desired experimental range. Tzero calibration should be done at relatively high heating rates such as 20°C/min in order to obtain the most accurate calibration of the sensor thermal capacitance and resistance values [24].

4.2.2.1.2. Cell Constant and Temperature Calibration

The cell constant calibration is done by heating a standard metal through its melting transition. The standard metal was selected as indium in this study. Cell constant is the ratio between the theoretical and calculated melting point of indium. Theoretically, when a standard sample melts, it draws more heat; as a result, a temperature difference develops between the sample and the sample thermocouple. The onset slope is the thermal resistance between these two points. The onset slope is used for the kinetic calculations to correct the thermal resistance [24].

The temperature calibration is done again by using standard metal (e.g. indium). Indium is heated thorough its melting transition. The extrapolated onset of the melting point of indium is compared with the known melting point of indium (156.6 °C). This difference is used for the temperature calibration [24].

4.3. Samples Properties Used during Experiments

In the scope of this thesis, four different crude oils taken from southeastern part of Turkey and their SARA fractions were used as samples for the thermal analysis experiments. The crude oils separated to their SARA fractions by column chromatography technique. However, after column chromatography since the asphaltene content of all the crude oil samples were low, no asphaltene were obtained from crude oils. The properties of the crude oils were given in Table 4.1. Moreover, the SARA fractions percentages were given in Table 4.2. All the sample properties were determined at Turkish Petroleum Corporation (TPAO) Research Center.

Table 4.1 - Properties of the Crude Oil samples

Measured Property	Analysis Method	Crude Oil 1	Crude Oil 2	Crude Oil 3	Crude Oil 4
API Gravity (°/60F)	ASTM D 4052	32.8	34.1	34.8	31.5
Viscosity (cst)	ASTM D 445				
40 °C		7.62	6.75	5.83	8.92
50 °C		5.77	5.18	4.73	6.83
60 °C		4.65	3.90	3.82	5.45
Total Sulphur (%)	IP 336	0.63	1.11	0.99	0.44
Asphaltene (%)	IP 143	1.96	1.58	2.27	2.24
Pour Point (°C)	ASTM D 97	-12	9	-15	-15

Table 4.2 - Percentages of SARA fractions of crude oils

Sample Name	Saturate (%)	Aromatic (%)	Resin (%)	Asphaltene (%)
Crude Oil 1	33.28	54.49	9.42	2.81
Crude Oil 2	33.20	58.58	6.04	2.18
Crude Oil 3	37.14	51.37	7.89	3.60
Crude Oil 4	41.64	46.04	8.27	4.04

CHAPTER 5

THERMAL ANALYSIS AND KINETICS

5.1. Thermal Analysis

Thermal analysis (TA) is a series of analytical experimental techniques to monitor the sample behavior against time or temperature while the temperature is programmed in a chosen gas atmosphere. The obtained results at the end of thermal analysis techniques depends on the operational (heating rate, atmosphere, pressure) and sample parameters (mass, geometrical shapes, structure) [26]. The advantages of TA over other analytical techniques are as follows [27];

- wide temperature can be used over the sample
- sample can be used almost any physical form (solid, liquid, gel)
- small amount of sample (0.1 μg – 10 mg) can be used
- the atmosphere in the vicinity of the sample can be standardized
- TA instruments are fairly priced
- time needed for an experiment is from several minutes to several hours.

5.1.1. Thermogravimetry (TG) / Thermogravimetric Analysis (TGA)

Thermogravimetry is a thermoanalytical technique in which the mass change of a sample as a function of temperature or as a function of time is determined in a controlled temperature program in a chosen gas atmosphere. The results of TGA experiments are shown in a TGA curve in mass or mass percent against time or

temperature [27]. Thermal changes that bring a change in the mass of the sample such as decomposition, sublimation, reduction, desorption, absorption and vaporization can be measured by TGA [26]. In TGA experiments, the temperature program can be adjusted according to the information required from the sample and the atmosphere is also important and can be reactive and inert.

5.1.1.1. Differential Thermogravimetry (DTG)

In DTG, the first derivative of the mass signal with respect to time (dm/dt) is plotted against time or temperature. This shows the rate of mass change and is a criterion for the rate of the reaction. For an interval of constant mass change dm/dt is zero. The DTG curve creates peak when the rate of mass change is maximum. The DTG peak is characterized by peak maximum temperature and the onset temperature. The peak maximum temperature is the peak temperature in the DTG curve and the onset temperature is the temperature that is the first mass change detected by the thermobalance. However, the DTG curve does not contain more information than the TGA curve [27].

5.1.2. Differential Scanning Calorimetry (DSC)

Differential scanning calorimetry is a thermoanalytical technique in which heat flow rate to the sample and the reference sample is measured as a function of temperature or time in a specified temperature program in a chosen gas atmosphere [26]. The energy change of the sample material is analyzed and the temperature at which these changes will occur will be determined. However, the main property that is measured by DSC is the heat flow rate to the sample. The specific heat or heat capacity (C_p) of a material can be determined using DSC. The heat capacity can be determined by subtracting the baseline from the heat capacity curve. Moreover, the enthalpy, energy required to heat the material to a specific temperature, can also be obtained by integrating the heat flow curve [28].

5.2. Kinetic Analysis

These thermoanalytical techniques can be further analyzed using kinetic analysis methods. The reaction rate kinetic parameters can be determined by two approaches isothermal and non-isothermal (dynamic) methods. In isothermal methods, the sample is quickly brought to the predetermined temperature and the sample response is recorded as a function of time. In non-isothermal experiments, generally the changed at constant heating rate and the sample behavior is monitored [27]. In the course of this work, non-isothermal method at different constant heating rates is applied to the samples.

Generally non-isothermal methods are selected for the analysis. The reasons can be classified as [27];

- these experiments are quicker,
- interpretation of the results is easier,
- the process of the reaction can be observed in a wide range of temperature intervals,
- several reaction steps can be observed in a single reaction,
- for the data evaluation a number of methods are available.

The non-isothermal reaction process can be considered as an isothermal reaction in an infinite small time interval and the reaction rate is expressed as [29];

$$\frac{d\alpha}{dt} = k(T)f(\alpha) \tag{5.1}$$

where

$d\alpha/dt$ = Reaction rate = Conversion rate of reaction

$k(T)$ = Specific rate constant = Reaction rate constant = Rate coefficient

$f(\alpha)$ = Conversion function = Reaction model

The starting point of the kinetic data is writing the differential rate equation. The reaction rate equation depends on the temperature represented by rate constant, k(T) and the conversion degree, α represented by reaction model, f(α) [28]. The conversion degree shows the changes progressively from reactants (α=0) to products (α=1) [26]. For example, for TGA, α values can be calculated from the mass loss up time t, $m_0 - m_t$, related to the overall mass loss corresponding to the completion of reaction $m_0 - m_f$, by $\alpha = (m_0-m_t) / (m_0-m_f)$. Similar expressions are available for other techniques.

The rate coefficient, k is a function of temperature and expressed by the Arrhenius equation [30];

$$k = Aexp(-\frac{E}{RT}) \tag{5.2}$$

where

k = Rate coefficient (min^{-1})

A = Pre-exponential factor = Arrhenius constant = Frequency factor (min^{-1})

E = Activation energy (J/mol)

R = Universal gas constant (J/molK)

T = Temperature (K)

The activation energy, E and the pre-exponential factor, A are the Arrhenius parameters. The activation energy is the minimum amount of energy that is required for the reaction to start. The pre-exponential factor is the frequency of the occurrence of the reaction situation that may lead to product formation [26].

For non-isothermal conditions, the temperature varies linearly with time at constant heating rate and this variation can be shown by;

$$T = T_0 + \beta t \tag{5.3}$$

where

T = Temperature

T_0 = Initial temperature

β = Heating rate (°C/min)

t = Time

The time dependence of temperature can be expressed as by taking the derivative of the temperature with respect to time;

$$\frac{dT}{dt} = \beta \tag{5.4}$$

By combining the equations (5.1) and (5.2) the following equation is obtained;

$$\frac{d\alpha}{dt} = Aexp(-\frac{E}{RT})f(\alpha) \tag{5.5}$$

By combining equations (5.4) and (5.5) the following is obtained;

$$\frac{d\alpha}{dT} = \frac{A}{\beta}\exp(-\frac{E}{RT})f(\alpha) \tag{5.6}$$

Separating variables;

$$\frac{d\alpha}{f(\alpha)} = \frac{A}{\beta}\exp\left(-\frac{E}{RT}\right)dT \tag{5.7}$$

By taking the integral of both sides;

$$\int_0^{\alpha} \frac{1}{f(\alpha)}d\alpha = \int_{T_0}^{T} \frac{A}{\beta}\exp(-\frac{E}{RT})dT \tag{5.8}$$

The term $\int_0^{\alpha} \frac{1}{f(\alpha)} d\alpha$ can be taken as g(α). Then, the equation (5.8) becomes;

$$g(\alpha) = \int_{T_0}^{T} \frac{A}{\beta} exp\left(-\frac{E}{RT}\right) dT \tag{5.9}$$

The $\int_{T_0}^{T} \frac{A}{\beta} \exp\left(-\frac{E}{RT}\right) dT$ term can be taken as $\int_0^{T} \frac{A}{\beta} \exp(-\frac{E}{RT}) dT$ since $\int_0^{T_0} \frac{A}{\beta} \exp(-\frac{E}{RT}) dT = 0$. Then, the equation can be written as;

$$g(\alpha) = \int_0^{T} \frac{A}{\beta} \exp(-\frac{E}{RT}) dT \tag{5.10}$$

Use of equation (5.10) involves the evaluation of the temperature integral $\int_0^{T} \exp(-\frac{E}{RT}) dT$.

The problem is simplified by introducing a variable, x. x can be taken as $E/_{RT}$. The boundary conditions also change. Finally, the equation (5.10) can be written as;

$$g(\alpha) = \frac{AE}{R\beta} p(x) \qquad where \qquad p(x) = \int_x^{\infty} \frac{\exp(-x)}{x^2} dx \tag{5.11}$$

The integral of the exponential term, p(x) has no analytical solution but has many linear approximations. The kinetic methods for calculating the kinetic parameters are relied on the exponential integral p(x).

Kinetic parameters can be calculated by different methods. The traditional classification of methods is distinguishing differential methods from integral methods. However, this classification is not of practical use since the data can be transformed from one form to other by the numerical methods of differentiation and integration. The classification based on method of calculation of kinetic parameters which involves either discrimination; that is, identification of the kinetic model f(α)

or a non-discriminatory method [30] is more practical. In other words, the two ways to calculate the kinetic parameters from the TGA are;

- model free (independent) methods or non-discriminatory or isoconversional methods

- reaction models or discriminatory or model fitting

Isoconversional methods can be used when the data from experiments at different heating rates are available, the unknown form of conversion function f(α) can be eliminated by comparing the measurements at a common value of α under different heating rates. Thus, these isoconversional methods can also be abbreviated as model independent or non-discriminating techniques for calculating the kinetic parameters. The isoconversional methods are based on the assumption the constant extent of the reaction, α is only a function of temperature and this dependence is generally shown by the general equation [26];

$$\ln\left(\frac{d\alpha}{dT}\right)\beta = \ln\left(\frac{A}{f(\alpha)}\right) - \frac{E}{RT} \tag{5.12}$$

The numerical value of activation energy can be determined by using different methods. However, the value of Arrhenius constant can be determined with the knowledge of the model f(α).

The model fitting methods are preferable in fossil fuel kinetics since their use of simplicity. For model fitting methods, single heating rate is enough. By using single heating rate data, the activation energy and the Arrhenius constant parameters is obtained simultaneously.

5.2.1. TG/DTG Kinetic Analysis

The data obtained from TGA can be subjected to different kinetic methods for the determination of kinetic parameters. The selected kinetic methods for the TGA experiments were the Ozawa – Flynn – Wall (OFW), Kissinger – Ahahira – Sunose (KAS) as the isoconversional methods and the Arrhenius, Coats and Redfern as the model fitting methods.

5.2.1.1. Isoconversional Methods

The two isoconversional methods were used in this thesis were the Ozawa – Flynn – Wall and Kissinger – Akahira – Sunose methods for the thermogravimetry analysis.

5.2.1.1.1. Ozawa -Flynn-Wall (OFW) Method

Ozawa [31], Flynn and Wall [32] developed an integral method that can determine the activation energy as a function of α without choosing the reaction model by using the Doyle's linear approximation [33] for the temperature integral p(x) where x=E/RT is valid only the range 20<x<60.

$$\ln p(x) = -5.331 - 1.052x \tag{5.13}$$

By changing the structure and taking the logarithm of both sides of the equation (5.11);

$$\ln \beta = \ln(\frac{AE}{Rg(\alpha)}) + \ln p(x) \tag{5.14}$$

Finally, by inserting equation (5.13) into equation (5.14), the following formula is obtained to determine activation energy, E at any particular value of conversion degree, α at different heating rates, β;

$$\ln \beta = \ln(\frac{AE}{Rg(\alpha)}) - 5.331 - 1.052\frac{E}{RT} \quad (5.15)$$

Thus, the ln β versus 1/T plot, obtained from experiments at different heating rates, should give a straight line whose slope ($slope = {}^{-1.052E}/_{R}$) gives the opportunity to calculate activation energy independently from kinetic model, f(α) at constant conversion (α=constant).

5.2.1.1.2. Kissinger-Akahira-Sunose (KAS) Method

Kissinger – Akahira – Sunose [34] neglect the term $\left(1 - {}^{2}/_{x}\right)/\left(1 - {}^{m}/_{x^2}\right)$ of the p(x) approximation;

$$p(x) = \frac{\exp(-x)}{x^2}\left[(1 - \frac{2}{x})/(1 - \frac{m}{x^2})\right] \quad (5.16)$$

and the approximation becomes,

$$p(x) = \frac{\exp(-x)}{x^2} \quad (5.17)$$

Insert the above equation into the equation (5.11) and obtain;

$$g(\alpha) = \frac{AE}{\beta R}\frac{\exp(-x)}{x^2} \quad (5.18)$$

Insert the x relation to the above equation;

$$g(\alpha) = \frac{ART^2}{\beta E}\exp(-\frac{E}{RT}) \quad (5.19)$$

Finally, by changing the form and taking the logarithm of both sides of the equation (5.19**)**, the following equation is obtained;

$$\ln\left(\frac{\beta}{T^2}\right) = \ln(\frac{AR}{Eg(\alpha)}) - \frac{E}{RT} \tag{5.20}$$

The activation energy is calculated from the slope of the $\ln({}^{\beta}/_{T^2})$ versus ${}^{1}/_{T}$ plot for constant conversion degree obtained from different heating rates, β.

5.2.1.2. Model Fitting Methods

The two model fitting models were used in this thesis were the differential model Arrhenius and the integral model Coats and Redfern for the thermogravimetry analysis.

5.2.1.2.1. Arrhenius Method

The Arrhenius method [22] assumes that the total rate of mass loss of the total sample is only dependent on the rate constant, the temperature and the remaining sample mass. Moreover, the reaction order, n is assumed to be unity. The kinetic model gets the form;

$$\frac{dw}{dt} = kw^n \qquad where \quad k = A\exp\left(-\frac{E}{RT}\right) \tag{5.21}$$

with the assumption of the first order kinetics;

$$\frac{dw}{dt} = A\exp\left(-\frac{E}{RT}\right)w \tag{5.22}$$

by taking the logarithm of both sides the Arrhenius model equation is obtained;

$$\log\left(\frac{dw/dt}{w}\right) = \log A - \frac{E}{2.303RT} \tag{5.23}$$

When $\log({}^{(dw/dt)}/_{w})$ versus $1/T$ graph is plotted, the linear regions should be selected for the analysis. From the slope of graph, equal to ${}^{E}/_{2.303R}$., the activation energy can be calculated. The Arrhenius constant can be calculated from the intercept ($\log A$).

5.2.1.2.2. Coats and Redfern Method

The Coats and Redfern method [35] is one of the most preferred methods. It can be used when the reaction order, n is believed to be different than unity. The p(x) approximation is similar to the KAS method. Coats and Redfern neglect the term $\left(1 - {}^{m}/_{x^2}\right)$ in the p(x) approximation.

$$p(x) = \frac{\exp(-x)}{x^2}\left[(1 - \frac{2}{x})/(1 - \frac{m}{x^2})\right] \tag{5.24}$$

and the p(x) becomes;

$$p(x) = \frac{\exp(-x)}{x^2}\left(1 - \frac{2}{x}\right) \tag{5.25}$$

and f(α) is assumed as;

$$f(\alpha) = (1 - \alpha)^n \tag{5.26}$$

By substituting equations (5.25) and (5.26) into the equation (5.11);

$$\ln\left(\frac{1-(1-\alpha)^n}{T^2(1-n)}\right) = \ln\left[\frac{AR}{\beta E}\left(1-\frac{2RT}{E}\right)\right] - \frac{E}{RT} \qquad for \;\; n \neq 1 \tag{5.27}$$

$$\ln\left(-\frac{\ln(1-\alpha)}{T^2}\right) = \ln\left[\frac{AR}{\beta E}\left(1-\frac{2RT}{E}\right)\right] - \frac{E}{RT} \qquad for \;\; n = 1 \tag{5.28}$$

The slopes of; $\ln\left(1-\ {(1-\alpha)^n}/{T^2(1-n)}\right)$ versus ${1}/{T}$ for n≠1 or $\ln(-{\ln(1-\alpha)}/{T^2})$ versus ${1}/{T}$ for n=1 curves gives ${E}/{R}$ from this the activation energy can be calculated. The order of the reaction, n is the value that gives the best linear plot.

5.2.2. DSC Kinetic Analysis

The data obtained from DSC can be subjected to different kinetic methods for the determination of kinetic parameters. The selected kinetic methods for the DSC experiments were Borchardt & Daniels and ASTM E698.

5.2.2.1. Borchardt & Daniels Method

The Borchardt & Daniels method [36] allows the calculation of activation energy, E, heat of reaction, ΔH and the pre-exponential factor, A. The principal that the method relies on is the ratio of the partial area to the total area of the exothermic curve. The disadvantage of the method is that it does not work in the endothermic pyrolysis peaks; however, this problem is solved by replacing the sample and the reference pans. The method assumes reaction follows nth order kinetics and based on the equation,

$$\frac{d\alpha}{dt} = k\exp(-\frac{E}{RT})\ (1-\alpha)^n \tag{5.29}$$

The temperature dependence is indicated by the Arrhenius equation. By taking the logarithm of the Equation (5.29),

$$\ln(\frac{d\alpha}{dt}) = \ln A - \frac{E}{RT} + n\ln(1-\alpha) \tag{5.30}$$

To solve the equation (5.30), dα/dt and α values are required. The dα/dt is obtained by dividing the peak height (dH/dt) at the temperature T to the total heat of reaction ΔH_0;

$$\frac{d\alpha}{dt} = \frac{dH/dt}{\Delta H_0} \tag{5.31}$$

where

ΔH_0 = Total peak area

The conversion degree, α is the ratio of the partial area ΔH_T at temperature T to the total peak area ΔH_0,

$$\alpha = \frac{\Delta H_T}{\Delta H_0} \tag{5.32}$$

5.2.2.2. ASTM E698 Method

In this method, the activation energy and the pre-exponential factor can be determined. The iterative procedure for finding the kinetic parameters are given below [37],

1. log β versus $1/T_m$ is plotted. T_m is the peak maximum temperature at each heating rate in Kelvin.
2. The slope of the graph is determined and recorded as $^{d\log\beta}/_{d\ 1/T_m}$.

3. An approximate activation energy value is determined from;

$$E = -2.19\,R\,(\frac{d\log\beta}{d\;1/T_m}) \tag{5.33}$$

4. The E value is refined,
    a. The E/RT value is calculated.
    b. The D value is found from the table given in Table 5.1.
    c. New value for E is calculated as follows,

$$E = (-\frac{2.303\,R}{D})(\frac{d\log\beta}{d\;1/T_m}) \tag{5.34}$$

5. These steps are repeated until the two E values are close to each other.
6. The Arrhenius pre-exponential factor is calculated as follows,

$$A = \frac{\beta E}{RT_m^2}\left(e^{\frac{E}{RT_m}}\right) \tag{5.35}$$

where β is the heating rate in the middle of the range.

Table 5.1 - x=E/RT versus D values for ASTM E698 [37]

x = E/(RT)	*D*	x = E/(RT)	*D*
5	1,3429	20,5	1,0932
5,5	1,3152	21	1,0911
6	1,2917	21,5	1,0891
6,5	1,2715	22	1,0871
7	1,2540	22,5	1,0853
7,5	1,2386	23	1,0835
8	1,2250	23,5	1,0818
8,5	1,2129	24	1,0801
9	1,2020	24,5	1,0786
9,5	1,1922	25	1,0770
10	1,1833	25,5	1,0756
10,5	1,1752	26	1,0742
11	1,1678	26,5	1,0728
11,5	1,1610	27	1,0715
12	1,1548	27,5	1,0703
12,5	1,1490	28	1,0690
13	1,1436	28,5	1,0679
13,5	1,1386	29	1,0667
14	1,1339	29,5	1,0656
14,5	1,1296	30	1,0646
15	1,1255	30,5	1,0636
15,5	1,1217	31	1,0626
16	1,1181	31,5	1,0616
16,5	1,1147	32	1,0607
17	1,1115	32,5	1,0598
17,5	1,1084	33	1,0589
18	1,1056	33,5	1,0580
18,5	1,1028	34	1,0572
19	1,1003	34,5	1,0564
19,5	1,0978	35	1,0556
20	1,0955		

CHAPTER 6

RESULTS AND DISCUSSION

Crude oils are complex mixtures of many hydrocarbons and when they are subjected to extreme heat, they follow parallel and consecutive reactions and undergo permanent molecular change. The extent of this change depends on the complexity of the molecular structure of the reaction environment [8]. Although the crude oils are complex mixtures with different physical properties, when heated, all of them have the same reactions. To reduce the effect of this complexity, it is more meaningful to separate the oil into less complex, more chemically representative constituents that are saturate, aromatic, resin and asphaltene (SARA) fractions. These fractions form the major portion of the oil.

6.1. Results of TG/DTG Experiments

In this study, during the TGA combustion experiments, two different reaction regions were observed. In the first reaction region, distillation and low-temperature oxidation (LTO) reactions occurred while in the second reaction region high temperature oxidation (HTO) reactions or combustion of solid carbonaceous residue (coke) occurred. The TG/DTG curves of the crude oils and their SARA fraction were given in Appendix B.I.

The TG/DTG curve of Crude Oil 3 at 5 °C/min was shown in Figure 6.1 as an example for the determination of the reaction intervals, mass loss rates and peak temperatures. The reaction regions were found out looking at a slope change in TG

curve and a hump trace in DTG curve. The DTG curves are very helpful for recognizing the temperature intervals since sometimes the finding the slope change in TG curve is not easy. After determining the reaction intervals, the mass loss amounts in these intervals were found out. The peak temperatures are the peak points in DTG hump. The peak temperatures show the maximum rate of decomposition.

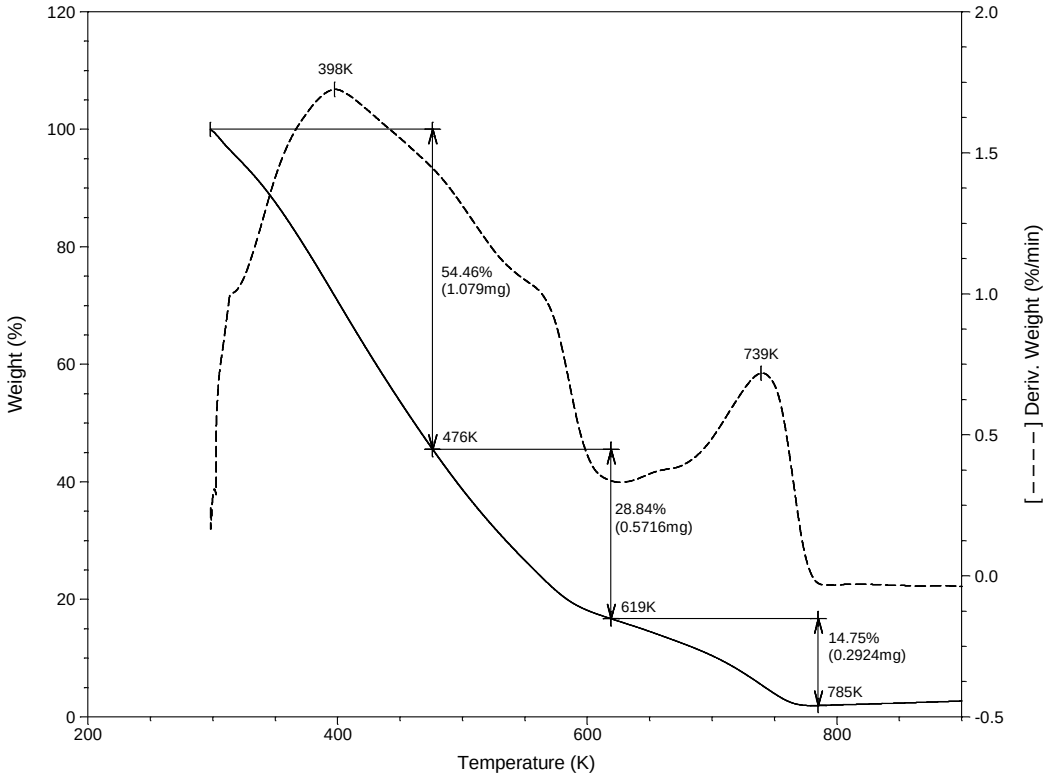

Figure 6.1 - TG/DTG curve of Crude Oil 3 at 5 °C/min

By examining the TG/DTG combustion curve of the Crude Oil 3 shown in Figure 6.1, the reaction regions could be determined. Up to around 476 K, the TG curve had a constant slope. This interval was identified as the distillation. No oxidation reactions occurred in this step. Distillation interval was responsible from the evaporation of volatile matter and free moisture from the sample. The LTO reaction was between 476 K and 619 K and the mass loss amount in this reaction interval was 28.84% of the initial mass of the sample. The last reaction region between 619 and 785 K was responsible from HTO reactions, main combustion region, which

contributes to the most of the heat of reaction and the mass loss in this region was 14.75%.

LTO reactions are the formation of higher molecular weight and more complex materials and combustion of light components [38]. LTO is responsible from the formation of the byproducts that introduce oxygen in the form of aldehydes, ketones, alcohols, hydrogen peroxides called as oxygenated compounds and production of little or no carbon oxides [38] [39]. The oxygenated compounds are believed to be less volatile, more viscous and denser than the original oil that they are formed [40]. LTO reactions are especially important in in situ combustion process since during these reactions the fuel is formed for the continuity of the in situ combustion.

The combustion of the fuel deposited in the thermal decomposition process is known as the HTO. The HTO reaction region is mainly responsible from the exothermic heat of reaction. This process is characterized by the oxidative degradation of different types of crude oils. During these reactions, there is a continuous conversion of the hydrocarbons to the other types of hydrocarbons that make the combustion process more complicated [10]. HTO is also a heterogeneous reaction responsible from the reaction of oxygen with fuel, unoxidized oil and the oxygenated compounds to give water and carbon oxides [39]. This region is identified from the TGA curve with rapid mass loss and also from DTG curve with a hump trace.

For the whole crude oils, the mass loss rates, the peak temperatures and the temperature intervals of the reaction regions were demonstrated in Table 6.1. Although the °API gravities of the crude oils were close to each other, the heavier the crude oil the lesser the amount of the initial mass was lost in the first reaction region and the higher amount of its initial mass was lost in the second reaction region. As the heating rate increased the reaction, completing temperatures were also increased. Moreover, the peak temperatures of the crude oils were shifted to the high temperatures with increasing heating rate.

Table 6.1 - TG/DTG reaction intervals, mass losses and peak temperatures of the Crude Oils at different heating rates under combustion

		I. Region					II. Region		
		Distillation		LTO			HTO		
	β (°C/min)	T (K)	Loss (%)	T (K)	Loss (%)	T_p (K)	T (K)	Loss (%)	T_p (K)
Crude Oil 1	5	298-467	53.65	467-631	28.57	380	631-789	13.04	738
	10	298-503	56.37	503-647	22.31	397	627-820	13.73	756
	15	298-485	51.69	485-656	31.32	408	656-854	12.95	756
Crude Oil 2	5	298-470	54.15	470-629	29.1	389	629-790	8.819	737
	10	298-527	58.34	527-690	20.35	400	689-811	7.065	746
	15	298-537	64.34	537-666	22.27	411	666-847	9.69	757
Crude Oil 3	5	298-476	54.46	476-619	28.84	398	619-785	14.75	739
	10	298-497	53.43	497-643	28.67	412	643-829	15.41	756
	15	298-493	46.2	493-657	29.17	423	657-858	13.63	763
Crude Oil 4	5	298-466	52.56	466-585	28.1	375	585-792	18.8	739
	10	298-470	48.6	470-604	30.32	404	604-834	17.65	767
	15	298-493	45.24	493-663	30.05	421	663-863	14.45	773

It is recognized that the crude oils are composed of four main components, saturates, aromatics, resins and asphaltenes. Among them, the asphaltenes is the most resistant part of the crude oil and affected from oxygen at relatively high temperatures. Asphaltenes contribution is negligible in distillation and LTO. They lose high amounts of their mass in HTO reactions since they are the heaviest part of the crude oils. The other side of the asphaltenes is saturates. They are highly affected from oxygen at relatively low temperatures. They lose almost all of their mass in distillation and LTO reactions [41].

As an example, Crude Oil 1 and its SARA constituents were demonstrated in Figure 6.2. As can clearly be seen from the figure, saturates were highly reactive and lost most of their mass in the first reaction region since they are forming the lightest part of the crude oils. However, it had the lowest peak in the second reaction region and almost lost none of its mass in this region. The other extreme point, in this thesis, work was resins, as again can be seen from the Figure 6.2, resin lost less amount of their initial mass in the first reaction region; though, they were highly active in HTO

and lost most of their mass in HTO. The aromatic contribution to first reaction region was considerable.

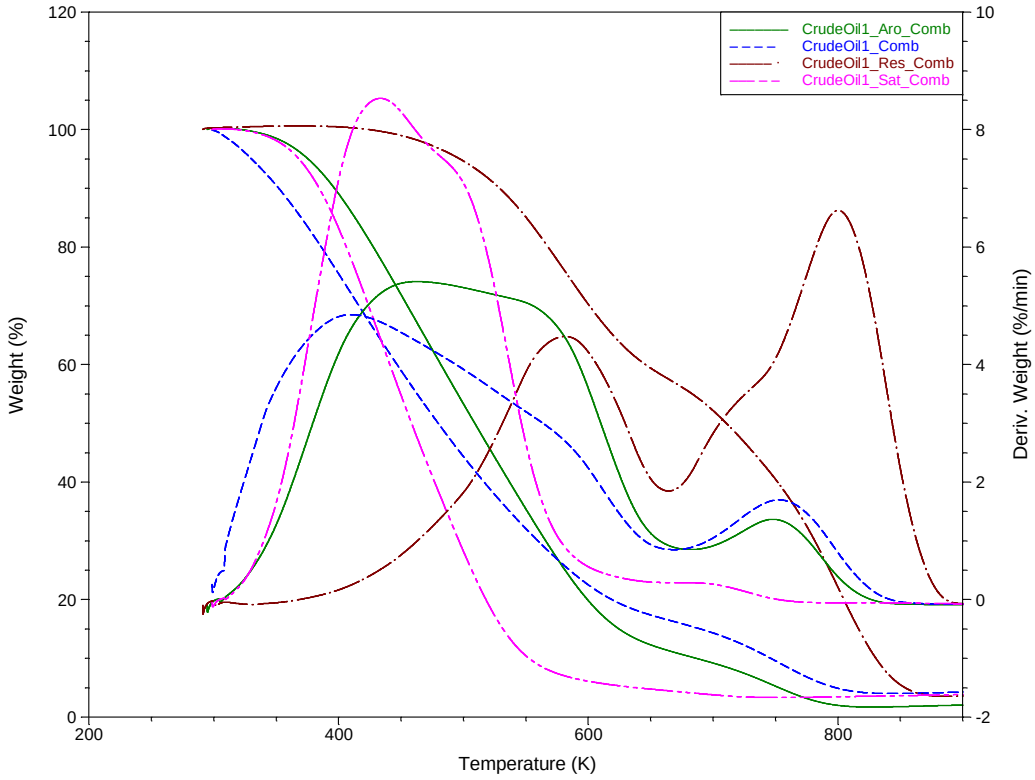

Figure 6.2 - Crude Oil 1 and its SARA fractions at 15°C/min under combustion

The Table 6.2 shows the reaction intervals, peak temperatures and mass loss amounts of the Crude Oil 1 and its SARA fractions at three different heating rates. From the table, it can be deduced that saturates total mass loss in the first reaction region is comparatively high and fast than the other fractions. Its LTO and HTO starting temperatures were also lower since they are the lightest part in crude oils. On the other hand, the resin was the almost the opposite of saturate. Its mass loss rate was lower than saturate in first reaction region and higher in HTO reaction region. The LTO and HTO starting temperatures for resins were higher than the aromatics and saturates and completion temperature of the oxidation reactions was highest.

Moreover, the temperature interval extent of resin in HTO was higher than others. Aromatic was between these two ends.

Table 6.2 - TG/DTG reaction intervals, mass losses and peak temperatures of the Crude Oil 1 and its SARA fractions at different heating rates under combustion

		I. Region					II. Region		
		Distillation		LTO			HTO		
	β (°C/min)	T (K)	Loss (%)	T (K)	Loss (%)	T_p (K)	T (K)	Loss (%)	T_p (K)
Crude Oil 1	5	298-467	53.65	467-631	28.57	380	631-789	13.04	738
	10	298-503	56.37	503-647	22.31	397	627-820	13.73	756
	15	298-485	51.69	485-656	31.32	408	656-854	12.95	756
Saturate	5	298-474	68.84	474-552	21.87	405	552-707	2.80	669
	10	298-467	55.57	467-571	29.49	416	601-750	3.85	692
	15	298-480	61.84	480-589	31.61	435	589-699	3.20	699
Aromatic	5	198-484	48.31	484-628	39.72	424	628-779	10.79	724
	10	298-505	50.28	505-630	33.9	456	630-828	10.09	758
	15	298-547	63.61	547-662	24.95	444	662-834	9.72	751
Resin	5	298-608	31.53	608-719	17.64	554	719-826	37.53	771
	10	298-624	33.79	624-742	18.84	551	742-875	38.99	789
	15	298-631	37.49	631-750	21.97	583	750-892	36.99	799

The peak and burn-out temperatures for all components were shifted to the high temperatures with increasing heating rates. The peak temperatures for saturates were lower whereas they were higher in resins. Moreover, as the heating rate was increased, the reaction temperature intervals for all samples were increased.

The burn-out temperature is the temperature at which the oxidation reactions are completed [22]. From Table 6.3, it is noted that the heavier fractions complete their oxidation at high temperatures.

Table 6.3 - TG/DTG burn-out temperature for Crude Oil 1

	I. Region			II. Region		
	5 °C/min	10 °C/min	15 °C/min	5 °C/min	10 °C/min	15 °C/min
Crude Oil 1	631	647	656	789	820	854
Saturate	552	571	589	707	750	699
Aromatic	628	630	662	779	828	834
Resin	719	742	750	826	875	892

6.2. Results of DSC Experiments

The DSC combustion curves of the crude oils and their SARA fraction were given in Appendix B.II. Under an oxidizing environment, the system undergoes exothermic reactions and as a result exothermic peaks occur in DSC curves with the exception of distillation process which is an endothermic process.

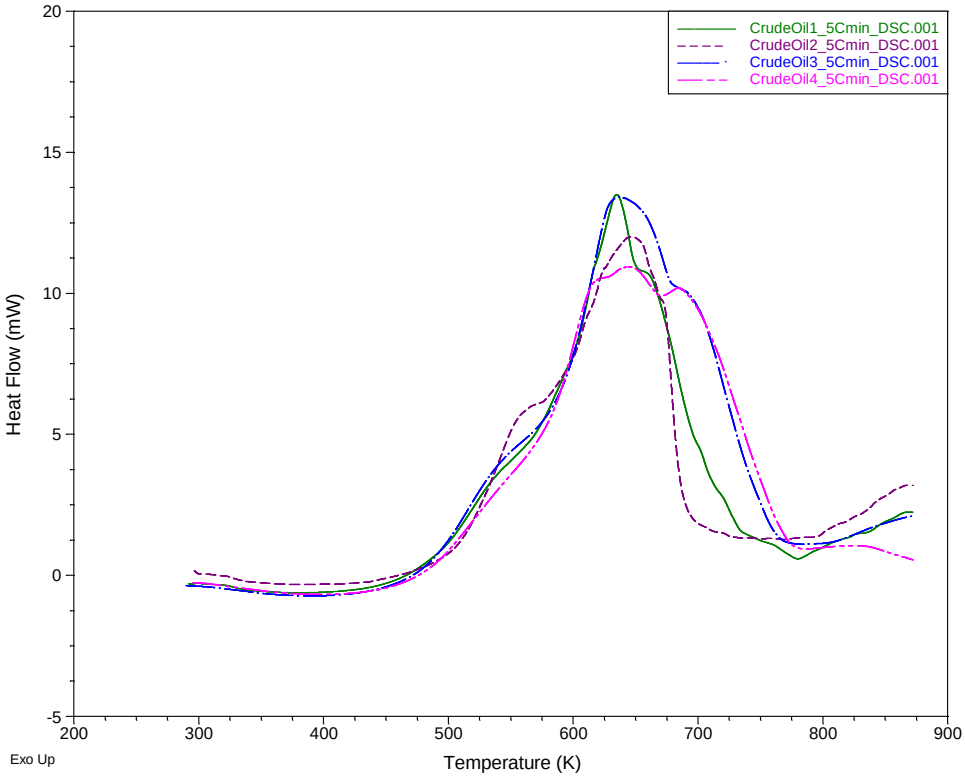

Figure 6.3 - DSC curve of Crude Oils at 5 °C/min

As shown in Figure 6.3, in air atmosphere two distinct reaction zones were identified, LTO and HTO. The first peak corresponded to LTO reactions that are heterogeneous reactions between liquid and gas. These reactions consume significant amounts of oxygen since during these reactions hydrocarbons are oxygenated. In LTO reaction region, volatile hydrocarbons are vaporized and the light hydrocarbons are oxidized. HTO reaction regions are again heterogeneous reactions between liquid and gas and produce carbon oxides and water [12].

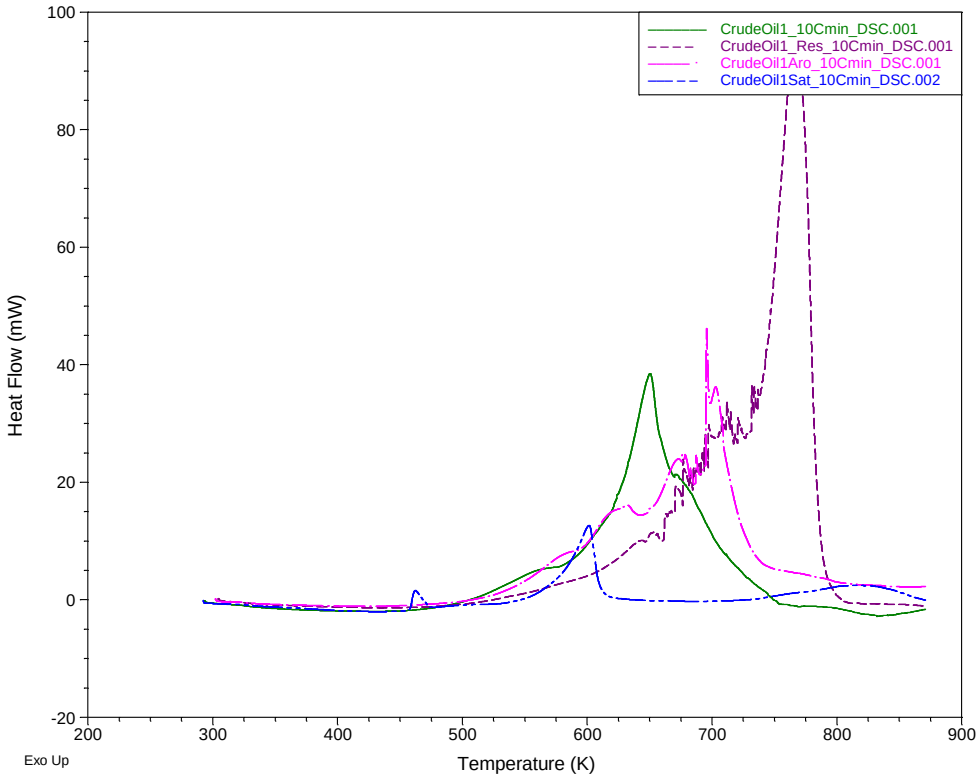

Figure 6.4 - DSC combustion curve of Crude Oil 1 and its SARA fractions at 10 °C/min

In literature, it is the known fact that the heavier oils release high amount of heat in HTO reaction region. This high heat release in HTO is attributed to the asphaltene content of the crude oil. Hence, the role of asphaltene in the combustion process is sustaining the combustion. In other words, asphaltene is needed for the continuity of the combustion. The effect of asphaltene content on the °API gravity is considerable.

As the concentration of the asphaltene content increase, the °API gravity of the crude oils decreases. Therefore, the low °API gravity crude oils oxidation behavior can be understood by the asphaltene oxidation behavior [10].

Table 6.4 - DSC Combustion Reaction Intervals, Peak Temperatures, Heat of Reaction, Peak Temperatures and Heat Flow of Crude Oil and Its SARA Fractions

		Reaction Intervals (K)				
	β (°C/min)	I. Region	II. Region	Heat of Reaction (J/g)	T_p (K)	Heat Flow (mW)
Crude Oil 1	5	466-565	565-739	4606	634	13.55
	10	508-578	578-759	6103	650	38.54
	15	497-595	595-782	6694	682	46.18
Saturate	5	416-468	468-667	1721	585	7.016
	10	445-494	494-660	1132	601	12.63
	15	423-496	496-673	1567	607	19.24
Aromatic	5	489-586	586-752	5086	666	30.03
	10	509-646	646-752	2758	696	41.53
	15	548-645	645-775	3151	693	42.45
Resin	5	492-704	704-757	8398	734	75.85
	10	531-737	737-802	7212	766	90.23
	15	550-732	732-826	7369	778	167.1

The Figure 6.4 and Table 4.1 showed that saturates LTO stating temperatures were low compared to the other constituents. From that point, it could be deduced that saturates can activate the combustion process at lower temperatures. Moreover, the stability of the combustion front in in situ combustion may be affected from the existence of saturates since saturates may form a secondary front at low temperatures behind the combustion front. Saturates were followed by aromatics and resins. In this work, the resins were responsible from the formation of the high amount of heat in HTO reactions. The temperature interval extent of the heavier samples was higher than the other samples.

The peak temperature of the all the crude oils and their SARA fraction were shifted to high temperatures with increase in heating rate. The heat flows from the samples were increased with an increase in the heating rate and highest for the resins.

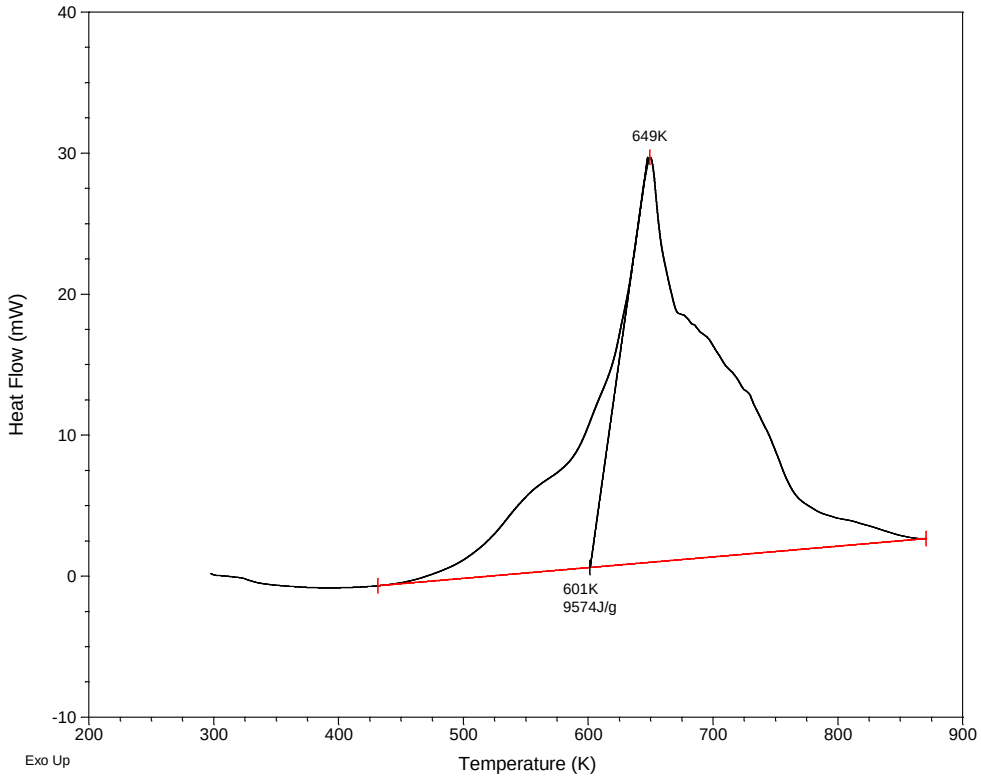

Figure 6.5 - Area under the DSC Combustion Curve of Crude Oil 4 at 10 °C/min

Figure 6.5 was shown as an example for the calculation of heat released during combustion reaction in DSC analysis. The enthalpy change, ΔH of the reaction was calculated by integration the area under the DSC curve. This integration was performed by using the *Universal Analysis* integration function.

6.3. Results of Kinetic Analysis

Thermoanalytical techniques are used for the determination of kinetics of reaction during the heating of samples. Non-isothermal kinetic study of crude oils is very complex since they follow numerous complex parallel and consecutive reactions. Many methods of kinetic analysis were developed by different assumptions. The

determined kinetic parameters are only representative values for the complex reactions. In this work, THERA-Kinetics software [42] was used for the determination of kinetic parameters.

6.3.1. TG/DTG Kinetic Analysis

The kinetic parameters for the crude oils and their SARA fractions were calculated by using both the isoconversional and model fitting methods. Two reaction regions, HTO and LTO were observed both in the crude oils and their SARA fractions. These two reaction regions were subjected to kinetic analysis and activation energy, E, the Arrhenius constant, A were determined for all samples.

6.3.1.1. Results of Isoconversional Methods

The use of the isoconversional methods requires the data at different heating rates. At least three heating rates are required. All the isoconversional methods based on the same assumption the reaction rate at constant degree of conversion is only a function of temperature. The activation energy can be found by without assuming of finding any particular form of reaction model [43]. For the TG/DTG data, Ozawa-Flynn-Wall (OFW) and Kissinger-Akahira-Sunose (KAS) isoconversional methods were selected. The plots of isoconversional methods were given in Appendix C.

6.3.1.1.1. OFW and KAS Methods

For OFW method, the activation energies were determined from the slope of ln β versus 1/T graph using the data at three different heating rates (5, 10 and 15 °C/min) at constant degree of conversion. The activation energy values for Crude Oil 4 at each conversion degrees, α were shown in Table 6.5 as an example.

The mean activation energy values of each sample were calculated and the results were tabulated in Table 6.6.

Table 6.5 – E (kJ/mol) of Crude Oil 4 and its SARA fractions at constant conversion degrees by OFW method

		α								
		0.1	**0.2**	**0.3**	**0.4**	**0.5**	**0.6**	**0.7**	**0.8**	**0.9**
Crude Oil 4	**I. Region**	38	41	45	49	54	59	65	74	86
	II. Region	90	94	102	108	109	108	105	101	96
Saturate	**I. Region**	36	40	47	57	66	72	75	76	69
	II. Region	-	-	-	-	-	-	-	-	-
Aromatic	**I. Region**	95	86	83	83	84	85	91	91	86
	II. Region	89	96	100	98	94	90	87	85	83
Resin	**I. Region**	91	97	105	112	120	130	87	112	152
	II. Region	269	247	226	208	193	181	169	157	142

Table 6.6 – E_{mean} (kJ/mol) values for Crude Oils and their SARA fractions by OFW method

	E_{mean} (kJ/mol)	
	I. Region	**II. Region**
Crude Oil 1	61	134
Saturate	77	-
Aromatic	90	120
Resin	97	137
Crude Oil 2	61	119
Saturate	54	-
Aromatic	67	120
Resin	85	144

	E_{mean} (kJ/mol)	
	I. Region	**II. Region**
Crude Oil 3	65	119
Saturate	77	-
Aromatic	82	128
Resin	96	139
Crude Oil 4	57	101
Saturate	60	-
Aromatic	87	91
Resin	112	199

For KAS method, the activation energies were determined from the slope of ln (β/T^2) versus 1/T graph using the data at three different heating rates (5, 10 and 15 °C/min) at constant degree of conversion. The activation energies values for Crude Oil 4 at conversion degrees, α were shown in Table 6.7.

Table 6.7 - Activation energies of Crude Oil 4 and its SARA fractions at constant conversion degrees by KAS method

		α								
		0.1	**0.2**	**0.3**	**0.4**	**0.5**	**0.6**	**0.7**	**0.8**	**0.9**
Crude Oil 4	**I. Region**	30	35	39	43	47	52	58	66	78
	II. Region	86	88	96	102	103	101	98	93	88
Saturate	**I. Region**	34	38	46	56	64	70	73	74	66
	II. Region	-	-	-	-	-	-	-	-	-
Aromatic	**I. Region**	85	82	80	77	78	81	80	80	76
	II. Region	84	91	95	94	90	88	86	80	84
Resin	**I. Region**	88	95	101	109	117	126	81	106	148
	II. Region	270	247	225	206	190	176	164	152	136

The mean activation energy values of each sample were calculated and the results were tabulated in Table 6.8.

Table 6.8 - Average activation energy values for Crude Oils and their SARA fractions by KAS method

	E_{mean} (kJ/mol)	
	I. Region	**II. Region**
Crude Oil 1	57	127
Saturate	74	-
Aromatic	87	114
Resin	92	131
Crude Oil 2	57	113
Saturate	50	-
Aromatic	62	114
Resin	80	138

	E_{mean} (kJ/mol)	
	I. Region	**II. Region**
Crude Oil 3	61	113
Saturate	74	-
Aromatic	78	122
Resin	91	134
Crude Oil 4	50	95
Saturate	58	-
Aromatic	80	88
Resin	108	196

The results indicate that the activation energies were significantly changing with the degree of conversion as can be seen from Figure 6.6 and Figure 6.7. This is an indication of complex reaction mechanism for crude oil combustion. One cannot apply the single rate equation to describe the kinetics of such a process. However, this does not invalidate the use of isoconversional methods since they use the certain

degree of conversion and a narrow temperature range related to this conversion degree [43].

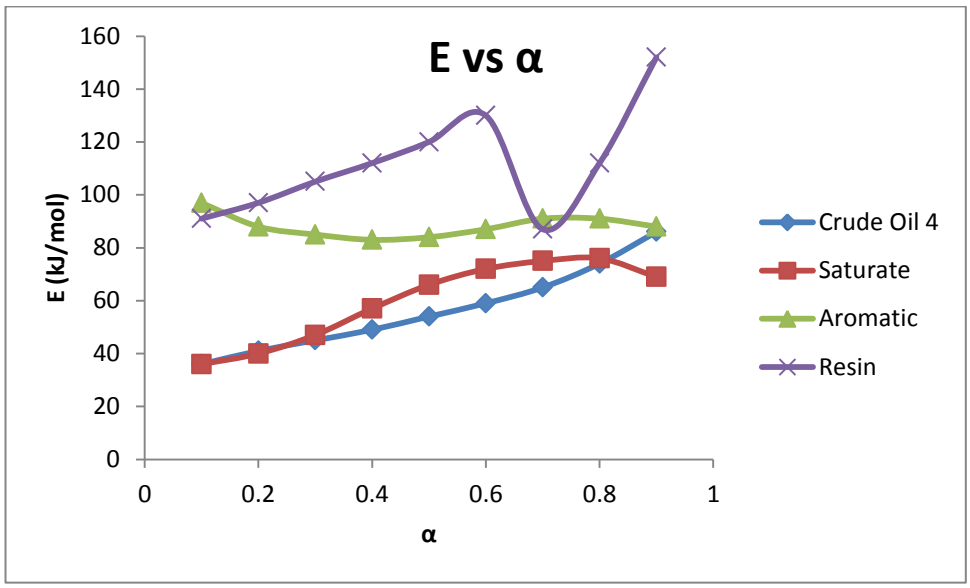

Figure 6.6 - Change of E with α for Crude Oil 4 and its constituents in I. Region by OFW method

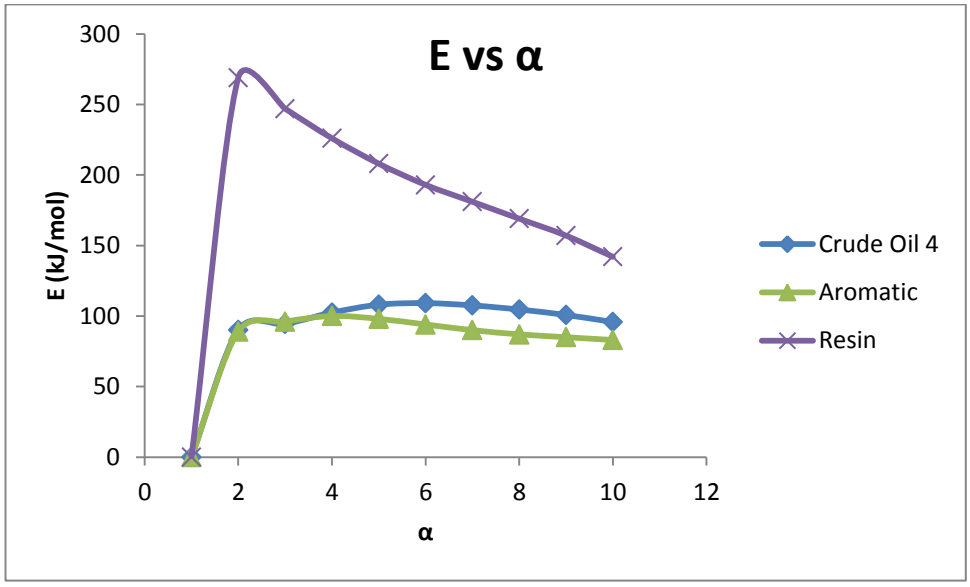

Figure 6.7 - Change of E with α for Crude Oil 4 and its constituents in II. Region by OFW method

6.3.1.2. Results of Model Fitting Methods

The use of the model fitting methods requires the data at single heating rate. Single activation energy is obtained for the overall reaction. For the TG/DTG data, Arrhenius and Coats and Redfern methods were selected. For the determination of kinetic parameters, 10 °C/min heating rate data were used for all samples. The plots of model fitting methods were given in Appendix D.

6.3.1.2.1. Arrhenius & Coats and Redfern Methods

The Arrhenius method assumes that the total rate of mass loss of the total sample is only dependent on the rate constant, the temperature and the remaining sample mass. The reaction order is assumed to be unity. The graph of $\log({}^{(dw/dt)}/_{w})$ versus $1/T$

was plotted and the linear parts were selected for the analysis. The activation energies were calculated from the slope of the linear parts. The activation energies and Arrhenius constant parameters were given in Table 6.9 for crude oils and their fractions.

Table 6.9 – E (kJ/mol) and Arrhenius constants (1/min) according to Arrhenius method

		I. Region	II. Region
Crude Oil 1	**E**	6	84
	A	0.20225	7.44E+04
	R^2	0.99620	0.99718
Saturate	**E**	5	-
	A	0.37730	-
	R^2	0.99915	-
Aromatic	**E**	20	70
	A	7.53128	7.65E+03
	R^2	0.99732	0.99958
Resin	**E**	70	159
	A	6196	6.99E+09
	R^2	0.99640	0.99945
Crude Oil 2	**E**	12	73
	A	0.67793	7651.58
	R^2	0.997712	0.99843
Saturate	**E**	15	-
	A	4.99294	-
	R^2	0.99929	-
Aromatic	**E**	31	116
	A	59.02180	8.05E+06
	R^2	0.99968	0.99872
Resin	**E**	87	133
	A	1.15E+05	7.47E+07
	R^2	0.99452	0.99917

		I. Region	II. Region
Crude Oil 3	**E**	6	110
	A	0.27141	7.78E+06
	R^2	0.99604	0.99164
Saturate	**E**	11	-
	A	2.19658	-
	R^2	0.99742	-
Aromatic	**E**	12	120
	A	0.96144	4.15E+07
	R^2	0.99886	0.99962
Resin	**E**	28	138
	A	10.82040	1.11E+08
	R^2	0.99780	0.99898
Crude Oil 4	**E**	5	93
	A	0.21247	4.05E+05
	R^2	0.99815	0.99588
Saturate	**E**	5	-
	A	0.55363	-
	R^2	0.98388	-
Aromatic	**E**	25	98
	A	23.44180	1.35E+06
	R^2	0.99836	0.98440
Resin	**E**	93	125
	A	9.21E+08	1.94E+07
	R^2	0.99589	0.99926

The graph of $\ln(^{-\ln(1-\alpha)}/_{T^2})$ versus $1/T$ was plotted and the linear parts were selected for the analysis. The activation energies were calculated from the slope of the linear part. The activation energies and Arrhenius constants were given in Table 6.10.

Table 6.10 - Activation energies and Arrhenius constants according to Coats and Redfern method

		I. Region	II. Region
Crude Oil 1	**E**	26	69
	A	2.81E-03	0.12046
	R^2	0.99592	0.991949
Saturate	**E**	17	-
	A	0.00014	-
	R^2	0.99698	-
Aromatic	**E**	36	69
	A	0.02001	0.14775
	R^2	0.99730	0.99282
Resin	**E**	40	104
	A	0.00201	7.32408
	R^2	0.998726	0.993532
Crude Oil 2	**E**	15	65
	A	7.63E-05	0.08412
	R^2	0.993191	0.995178
Saturate	**E**	21	-
	A	0.00046	-
	R^2	0.99980	-
Aromatic	**E**	19	71
	A	9.14E-05	0.12510
	R^2	0.99942	0.99095
Resin	**E**	27	90
	A	0.00031	0.89833
	R^2	0.997696	0.994813

		I. Region	II. Region
Crude Oil 3	**E**	8	83
	A	0.00001	0.99640
	R^2	0.99954	0.99362
Saturate	**E**	19	-
	A	0.00034	-
	R^2	0.99884	-
Aromatic	**E**	20	98
	A	0.00009	8.14063
	R^2	0.99891	0.99471
Resin	**E**	30	120
	A	0.00023	1.05E+02
	R^2	0.99734	0.99832
Crude Oil 4	**E**	28	67
	A	0.00557	0.08431
	R^2	0.99502	0.99139
Saturate	**E**	22	-
	A	0.00067	-
	R^2	0.99943	-
Aromatic	**E**	26	72
	A	7.14E-04	0.19765
	R^2	0.99728	0.99443
Resin	**E**	28	111
	A	0.00014	2.03E+01
	R^2	0.99808	0.99447

In order to determine heating rate effect on activation energy and pre-exponential factor the Coats and Redfern model was applied to the Crude Oil 3 and its fraction for demonstration purposes. The results can be seen in Table 6.11. It was observed from Table 6.11 that heating rate had no effect on activation energy values.

For the Coats and Redfern method, the reaction order, n was assumed to be unity. Although the complex reactions are followed during the crude oil combustion, when some simple generalizations are made, it seems reasonable to assume reaction order

as unity. These were the sample size was too small, there is an excess supply of air, the progress of the reaction is independent of the air concentration.

Table 6.11 - E and A values at three different heating rates for Crude Oil 3 and its fractions

		5 °C/min		10 °C/min		15 °C/min	
		I. Region	II. Region	I. Region	II. Region	I. Region	II. Region
Crude Oil 3	E	7	82	8	83	8	83
	A	1.29E-05	1.84465	1.03E-05	0.99640	9.17E-06	0.82239
	R^2	0.99682	0.98284	0.99954	0.99362	0.99978	0.99730
Saturate	E	19	-	19	-	17	-
	A	3.72E-04	-	0.00034	-	2.63E-04	-
	R^2	0.99291	-	0.99884	-	0.99489	-
Aromatic	E	20	99	20	98	20	98
	A	1.54E-04	14.50500	8.77E-05	8.14063	1.15E-04	6.83088
	R^2	0.99109	0.99290	0.99891	0.99471	0.99382	0.98857
Resin	E	30	120	30	120	30	121
	A	1.85E-04	884.17200	2.35E-04	105.4800	2.06E-04	63.52800
	R^2	0.99262	0.98814	0.99734	0.99832	0.99802	0.99646

6.3.1.3. Comparison of the Kinetic Parameter Obtained from TG/DTG

From the activation energy results of isoconversional methods, it was seen that saturates gave almost the lower activation energy at each conversion degree, α for both OFW and KAS methods and lower activation energies in model fitting methods. Reasonable activation energy values could not be calculated for saturates in the second region. This behavior can be attributed to the fact that since saturates were the lightest part of the crude oils; therefore, the mass loss amounts in the second region were small and so negligible. For this reason, the activation energies of saturates in the second region were not evaluated. On the other hand, since resins were the heaviest part of the fractions, their activation energies were the highest almost at each degree of conversion in both reaction regions. The activation energies for aromatics were in between saturates and resins. For all samples, except saturates, the

second reaction regions gave high values compared to the first reaction region. In addition, the Arrhenius constants, evaluated in model fitting methods, were generally higher for the heavier samples.

The crude oil combustion is a complex reaction mechanism that follows parallel and consecutive reactions. The isoconversional methods, OFW and KAS, assume constant activation energy from the beginning to the considered conversion degree, α. Moreover, single average value of activation energy is obtained from the model fitting methods for the overall reaction. These deficiencies in the methods do not reveal the complexity in combustion. The activation energy values of the crude oils should be expected between the activation energies of saturates aromatics and resins; however, the expectations should not satisfied. This could be due to the experimental errors.

6.3.2. DSC Kinetic Analysis

The kinetic parameters for the crude oils and their SARA fractions were calculated by using the two different methods Borchardt & Daniels and ASTM E698 methods. Second reaction region was subjected to kinetic analysis and activation energy, E, and the Arrhenius constant, A were determined for all samples.

6.3.2.1. Borchardt & Daniels Method

For the Borchardt and Daniels method, *TA Instruments* software package *TA Specialty Library* was used different from other methods. The activation energy, Arrhenius constant and heat of reaction were determined for each sample at different heating rates. The sample calculation for Crude Oil 4 was demonstrated in Figure 6.8.

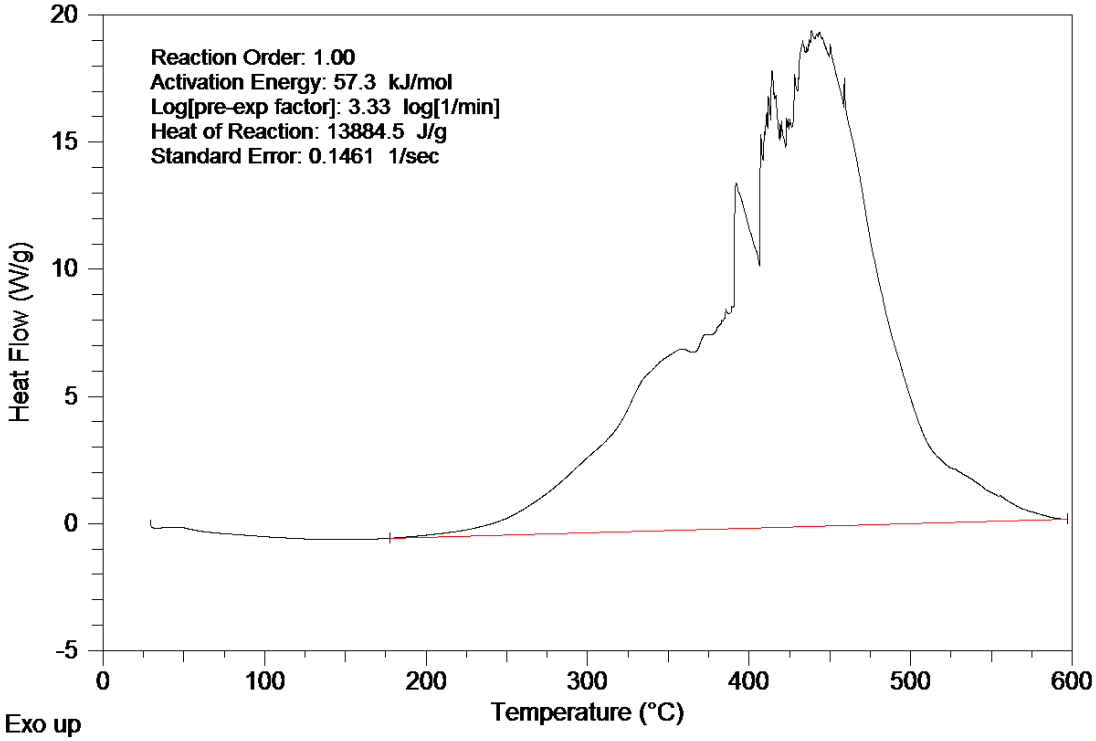

Figure 6.8 - Determination of kinetic parameters according to B&D for Crude Oil 4 Aromatic at 10 °C/min

From Table 6.12, it was observed that the activation energies and the pre-exponential factor were increased with increased heating rate. The activation energies and the pre-exponential factors were highest for resin fractions. The activation energy values of crude oils were again higher than the saturate. This could be due to the experimental errors.

Table 6.12 - Activation energies and Arrhenius constants by B&D method

	β (°C/min)	E (kJ/mol)	log A (log (1/min))	A (1/min)		β (°C/min)	E (kJ/mol)	log A (log (1/min))	A (1/min)
Crude Oil 1	5	52.2	3.15	1.41E+03	**Crude Oil 3**	5	49.7	2.83	6.76E+02
	10	62.8	4.21	1.62E+04		10	55.6	3.46	2.88E+03
	15	63.5	4.19	1.55E+04		15	59.8	3.88	7.59E+03
Saturate	5	35.1	1.87	7.41E+01	**Saturate**	5	35.8	2.01	1.02E+02
	10	44.9	2.99	9.77E+02		10	40.1	2.54	3.47E+02
	15	46.2	3.24	1.74E+03		15	44.5	3.06	1.15E+03
Aromatic	5	43.2	2.2	1.58E+02	**Aromatic**	5	42	2.02	1.05E+02
	10	55.9	3.44	2.75E+03		10	43.1	2.19	1.55E+02
	15	74.4	5.09	1.23E+05		15	53.4	3.12	1.32E+03
Resin	5	95.4	5.84	6.92E+05	**Resin**	5	100.4	6.12	1.32E+06
	10	104.2	8.36	2.29E+08		10	101.7	6.21	1.62E+06
	15	157.1	10.24	1.74E+10		15	103.3	6.54	3.47E+06
Crude Oil 2	5	58	3.73	5.37E+03	**Crude Oil 4**	5	54.1	3.16	1.45E+03
	10	61.6	4.17	1.48E+04		10	57.3	3.64	4.37E+03
	15	68.6	4.65	4.47E+04		15	60.7	3.92	8.32E+03
Saturate	5	43.3	2.71	5.13E+02	**Saturate**	5	50.5	3.31	2.04E+03
	10	51.6	3.8	6.31E+03		10	54.9	3.64	4.37E+03
	15	59	4.32	2.09E+04		15	60.7	4.53	3.39E+04
Aromatic	5	44.8	2.21	1.62E+02	**Aromatic**	5	52.8	2.85	7.08E+02
	10	48.7	2.65	4.47E+02		10	57.3	3.33	2.14E+03
	15	48.8	2.7	5.01E+02		15	71	4.69	4.90E+04
Resin	5	101.6	5.8	6.31E+05	**Resin**	5	93.4	5.59	3.89E+05
	10	108.6	6.77	5.89E+06		10	104.5	6.54	3.47E+06
	15	113.2	7.33	2.14E+07		15	122.5	7.82	6.61E+07

6.3.2.2. ASTM E698 Method

The peak temperatures were determined for each sample at each heating rate. The procedures explained in Chapter 5 were followed and the activation energies were calculated by the help of the software [42]. The plots of ASTM E698 were given in Appendix E.

Table 6.13 - Activation energy and Arrhenius constant values for Crude Oils and SARA fractions by ASTM E 698 method

	E (kJ/mol)	A (1/min)		E (kJ/mol)	A (1/min)
Crude Oil 1	67	4.62E+04	**Crue Oil 3**	91	3.48E+06
Saturate	133	1.61E+11	**Saturate**	88	1.35E+07
Aromatic	97	4.59E+06	**Aromatic**	45	1.60E+02
Resin	102	1.89E+06	**Resin**	92	3.62E+05
Crude Oil 2	80	4.29E+05	**Crude Oil 4**	77	3.47E+05
Saturate	103	3.31E+08	**Saturate**	95	5.52E+07
Aromatic	44	1.36E+02	**Aromatic**	47	3.09E+02
Resin	84	1.20E+05	**Resin**	99	1.02E+06

From the Table 6.13, it was observed that although saturates activation energy expected to be lowest this method, this method did not meet the expectations. This conflict could be attributed to the close peak temperatures of saturates at each heating rate. Aromatics and resins behaved in a same manner; that is; the activation energies of aromatic were lower than resins.

CHAPTER 7

CONCLUSIONS

This research was carried out using four different crude oils and their saturate, aromatic and resin fractions. The asphaltene content of the crude oils were not obtained after the column chromatography. TG/DTG and DSC techniques were applied to the samples. The experiments were performed at three different heating rates (5, 10 and 15 °C/min). The combustion experiments were performed in air atmosphere.

In thermogravimetric analysis, two reaction regions were identified in crude oil and their SARA fractions. ın the first reaction region, distillation and low-temperature oxidation (LTO) reactions occurred and high-temperature oxidation (HTO) reactions occurred in the second reaction region. LTO reaction region is responsible from the formation of high molecular weight components and the combustion of light molecules. HTO reaction region is responsible from the burning of the coke. From the TG/DTG curves, it was analyzed that saturates, the lightest part of the crude oils, were highly reactive in LTO region whereas the resins, the heaviest part of the crude oil, were not that much reactive in the LTO region. The mass loss amount of the resins in HTO was the largest. Since saturates mainly composed of light molecules, the mass loss amount of them in the HTO region was low. The LTO and HTO starting and ending temperature were highest for resins than aromatics and saturates, respectively. Moreover, the temperature interval extents of resins were higher than the others.

The peak and burn-out temperatures of the crude oils and their fractions were shifted to higher temperatures with the increase in heating rate. The temperature extent of the LTO and HTO reactions were increased with increase in heating rate.

In differential scanning calorimetry (DSC), the two reaction regions were again identified, LTO and HTO. The resins, heavier part of the crude oils, released more heat during combustion. Their temperature extents were larger and reaction completing temperatures were higher.

As the heating rates increased in DSC experiments, the peak temperatures were shifted to high temperatures. The heat flow from the samples was increased for all samples and the temperature at which the reactions completes was increased.

For the calculation of kinetic parameters, several model fitting and isoconversional methods were applied. According to isoconversional methods, the activation energy, E values were changed with the degree of conversion, α. This was an indication of the parallel and complex reaction mechanism. Mean activation energy, E_{mean} values were calculated. It was observed that E_{mean} values were getting higher as the crude oil fraction was getting higher. By using the model fitting methods, the pre-exponential factor, A was calculated and from the results the A values like E_{mean} were higher for heavier constituents of crude oils. Moreover, the results showed that E was not affected from the heating rate change.

REFERENCES

[1] "BP Statistical Review of World Energy June 2011," June 2011.

[2] M. Prat, "Thermal Recovery," *Society of Petroleum Engineers of AIME,* 1982.

[3] N. Mahinpey, A. Ambalae and K. Asghari, "In Situ Combustion in Enhanced Oil Recovery: A Review," pp. 995-1021, 1 August 2007.

[4] H. J. Tadema, "Mechanism of Oil Production by Underground Combıstion," in *Proc. Fifth World Petroleum Congress,* New York, 1959.

[5] J. H. Bae, "Characterization of Crude Oil for Fireflooding Using Thermal Analysis Methods," *Society of Petroleum Engineers,* pp. 211-218, June 1977.

[6] S. Vossoughi and G. P. Willhite, "Development of a Kinetic Model for In-Situ Combustion and Prediction of the Process Variables using TGA/DSC Techniques," *Society of petroleum Engineers,* pp. 1-12, 1982.

[7] O. Karacan and M. V. Kok, "Pyrolysis Analysis of Crude oils and Their Fractions," *Energy & Fuels,* vol. 11, pp. 385-391, 1997.

[8] M. V. Kok and O. Karacan, "Pyrolysis Analysis and Kinetics of Crude Oils," *Journal of Thermal Analysis,* vol. 52, pp. 781-788, 19 September 1998.

[9] M. V. Kok and M. R. Pamir, "Non-Isothermal Pyrolysis and Kinetics of Oil Shales," vol. 56, pp. 953-958, 1999.

[10] M. V. Kok and C. O. Karacan, "Behavior and Effect of SARA Fractions of Oil During Combustion," vol. 3, pp. 380-385, October 2000.

[11] H. B. Al-Saffar, H. Hasanin, D. Price and R. Hughes, "Oxidation Reactions of a Light Crude Oil and Its SARA Fractions in Consolidated Cores," *Energy & Fuels,* vol. 15, no. 1, pp. 182-188, 2001.

[12] M. V. Kok and A. G. Iscan, "Catalytic Effects of Metallic Additives on the Combustion Properties of Crude Oils by Thermal Analysis Techniques," *Journal of Thermal Analysis and Calorimetry,* vol. 64, pp. 1311-1318, 2001.

[13] S. Li and C. Yue, "Study of Different Kinetic Models for Oil Shale Pyrolysis," *Fuel Processing Technology,* vol. 85, pp. 51-61, 31 March 2003.

[14] M. V. Kok and R. Pamir, "Pyrolysis Kinetics of Oil Shales Determined by DSC and TG/DTG," *Oil Shale,* vol. 20, pp. 57-68, 2003.

[15] J. Li, S. A. Mehta, R. G. Moore, M. G. Ursenbach, E. Zalewski, H. Ferguson and N. E. Okazawa, "Oxidation and Ignition Behavior of Saturated Hydrocarbon Samples with Crude Oils Using TG/DTG and DTA Thermal Analysis Techniques," *Journal of Canadian Petroleum Technology,* vol. 43, no. 7, pp. 45-51, July 2004.

[16] M. V. Kok, G. Pokol, C. Keskin, J. Madarasz and S. Bagci, "Light Crude Oil Combustion in the Presence of Limestone Matrix," *Journal of Thermal Analysis and Calorimetry,* vol. 75, pp. 781-786, 2004.

[17] S. Bagci and M. V. Kok, "Combustion Reaction Kinetics Studies of Turkish Crude Oils," *Energy & Fuels,* vol. 18, pp. 1472-1482, 2 June 2004.

[18] A. Ambalae, N. Mahinpey and N. Freitag, "Thermogravimetric Studies on Pyrolysis and Combustion Behavior of a Heavy Oil and Its Asphaltenes," *Energy & Fuel,* vol. 20, pp. 560-565, 2006.

[19] G. J. Mendez Kuppe, S. A. Metha, R. G. Moore, M. G. Ursenbach and E. Zalewski, "Heats of Combustion of Selected Crude Oils and Their SARA Fractions," *Journal of Canadian Petroleum Technology,* vol. 47, pp. 38-42, January 2008.

[20] P. Murugan, N. Mahinpey, T. Mani and N. Freitag, "Pyrolysis and Combusiton Kinetics of Fostern Oil Using Thermogravimetric Analysis," *Fuel,* vol. 88, pp. 1708-1713, 2009.

[21] L. V. Castro and F. Vazquez, "Fractionation and Characterization of Mexican Crude Oils," *Energy & Fuels,* pp. 1603-1609, 2009.

[22] M. V. Kok, "Characterization of Medium and Heavy Crude Oils Using Thermal Analysis Techniques," *Fuel Processing Technology,* vol. 92, pp. 1026-2031, 17 January 2011.

[23] Thermogravimetric Analyzer TGA, New Castle: TA Instruments, 2006.

[24] Differential Scanning Calorimeter, New Castle: TA Instruments, 2006.

[25] Universal Analysis 2000, New Castle: TA Instruments, 2003.

[26] M. E. Brown, Handbook of Thermal Analysis and Calorimetry, Amsterdam:

Elsevier Science B.V., 1998.

[27] T. Hatakeyama and F. X. Quinn, Thermal Analysis Fundamentals and Application to Polymer Science, West Sussex: John Wiley & Sons Ltd., 1999.

[28] P. Gabbott, Principle and Application of Thermal Analysis, New Delhi, India: Blackwell Publishing, 2008.

[29] T. Hatakeyama and Z. Liu, Handbook of Thermal Analysis, West Sussex: John Wiley & Sons Ltd, 1998.

[30] M. E. Brown, Introduction to Thermal Anlysis Techniques and Applications, Dordrecht: Kluwer Academic Publishers, 2001.

[31] T. Ozawa, "A New Method of Analyzing Thermogravimetric Data," *Bulletin of the Chemical Society of Japan*, vol. 38, no. 11, pp. 1881-1886, November 1965.

[32] J. H. Flynn and L. A. Wall, "General Threatment of the Thermogravimetry of Polymers," *Journal of Research of the National Bureau Standards*, vol. A Physics and Chemistry Volume 70A, no. 6, pp. 487-523, 1966.

[33] C. D. Doyle, "Estimating Isothermal Life from Thermogravimetric Data," *Journal of Applied Polymer Science*, vol. 6, 1962.

[34] T. Akahira and T. Sunose, "Method of Determining Activation Deterioration Constant of Electrical Insulating Materials," *Research Report of Chiba Institute of Technology*, vol. 16, pp. 22-31, 1971.

[35] A. Coats and J. Redfern, "Kinetic Parameters from Thermogravimetric Data," *Nature*, vol. 201, pp. 68-69, 1964.

[36] H. Borchardt and F. Daniels, "The Application of Differential Thermal Analysis to the Study of Reaction Kinetics," *Journal of American Chemical Society*, vol. 5, p. 41, 1957.

[37] ASTM, "Standard Test Method for Arrhenius Kinetic Constants for Thermally Unstable Materials Using Differential Scanning Calorimetry and the Flynn/Wall/Ozawa Method".

[38] P. M. Crnkovic, C. R. Leiva, A. M. Santos and F. E. Milioli, "Kinetic Study of the Degradation of Brazilian Fuel Oils," *Energy & Fuels*, vol. 21, no. 6, pp. 3415-3419, 2007.

[39] S. Razzaghi, R. Kharrat, V. Shapour and D. Rashtchian, "Feasibility Study of Auto Ignition in In Situ Combustion Process," *Journal of Petroleum Institute*, vol. 51, no. 5, pp. 287-297, 2008.

[40] R. G. Moore, D. W. Bennion and M. G. Ursenbach, "A Review of In Situ Combustion Mechanisms," vol. 5, 1998.

[41] M. V. Kok, O. Karacan and R. Pamir, "Kinetic Analysis of Oxidation Behavior of Crude Oil SARA Constituents," *Energy & Fuels,* vol. 12, no. 3, pp. 580-588, 1998.

[42] G. Ertunc, Development of a Software for Determination of Kinetic Parameters in Thermal Analysis, 2011.

[43] S. Vyazovkin, A. K. Burnham, J. M. Criado, L. A. Perez-Maqueda, C. Popescu and N. Sbirrazzuoli, "ICTAC Kinetics Committee Recomendations for Performing Kinetic Computations on Thermal Analysis Data," *Thermochimica Acta,* vol. 520, pp. 1-19, 2011.

[44] H. Kopsch, Thermal Methods In Petroleum Analysis, New York: VCH Publishers, 1995.

[45] Universal Analysis 2000, New Castle: TA Instruments, 2003 .

[46] A. Millington, D. Price and R. Hughes, "The Use of Thermal Analysis Techniques to Obtain Information Relevant to the In Situ Combustion Process for Enhanced Oil Recovery," *Journal of Thermal Analysis and Calorimetry,* vol. 40, pp. 225-238, 1993.

[47] S. Akin, M. V. Kok, S. Bagci and O. Karacan, "Oxidation of Heavy Oil and Their SARA Fractions: Its Role in Modeling In-Situ Combustion," *Society of Petroleum Engineers,* 2000.

APPENDIX A

CALIBRATION RESULTS

A.I. TGA Calibration Results

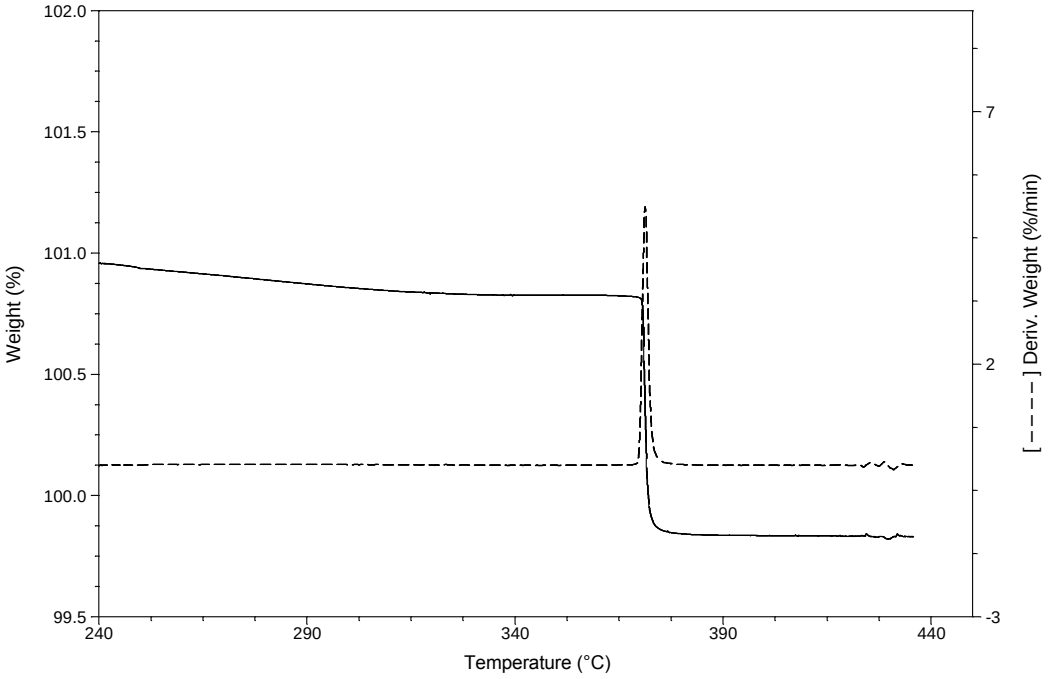

Figure A.I.1 – Temperature Calibration of TGA by Curie Point Determination

A.II. DSC T_{zero} Calibration Results

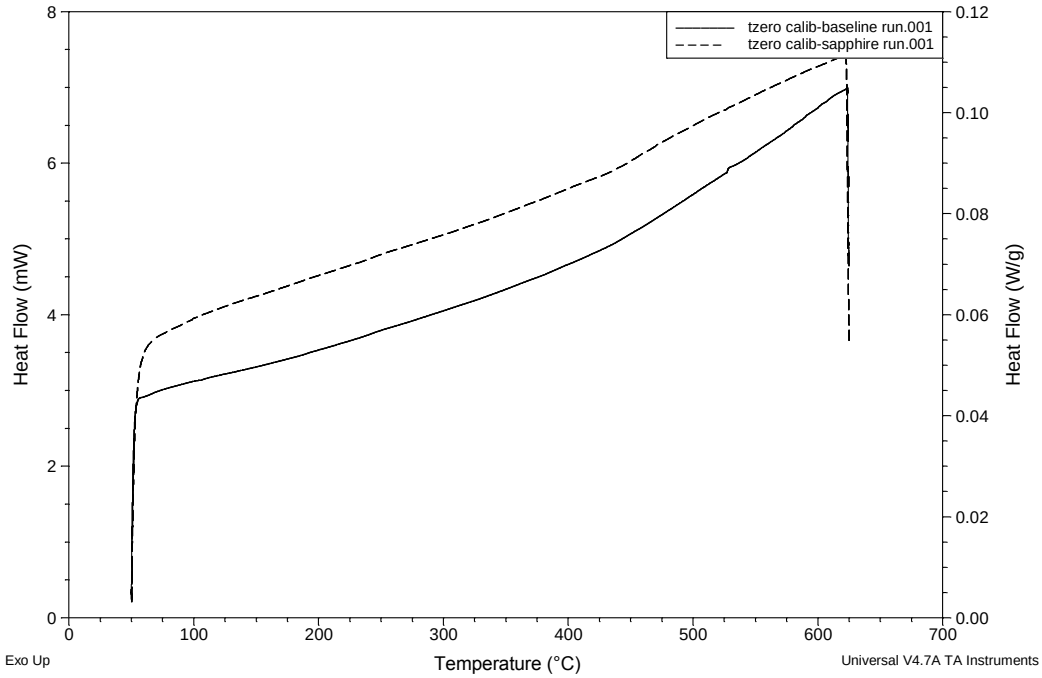

Figure A.II.1 – Baseline and Sapphire Curves T_{zero} Calibration of DSC

A.III. DSC Cell Constant and Temperature Calibration

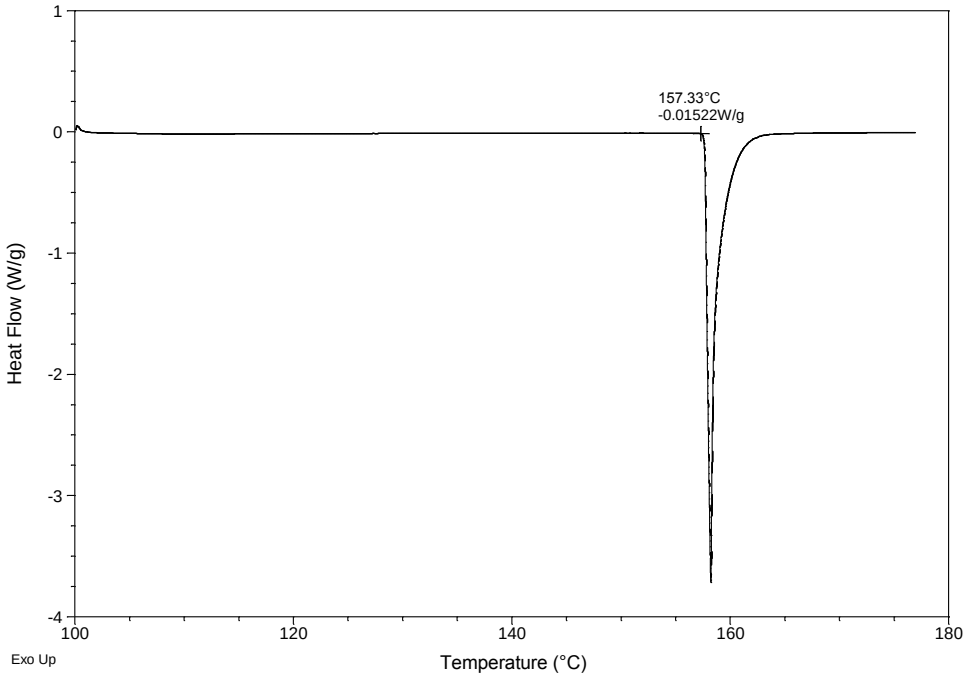

Figure A.III.1 – Melting Point of Indium for Cell Constant and Temperature Calibration

APPENDIX B

RESULTS OF EXPERIMENTS

B.I. Results of TG/DTG Experiments

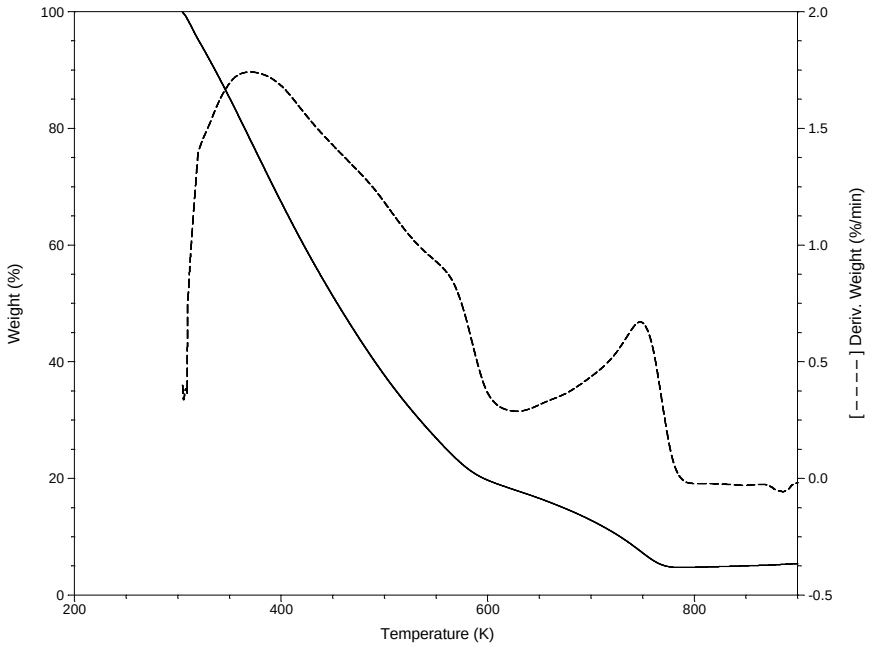

Figure B.I.1 - TG/DTG Curve of Crude Oil 1 at 5 °C/min

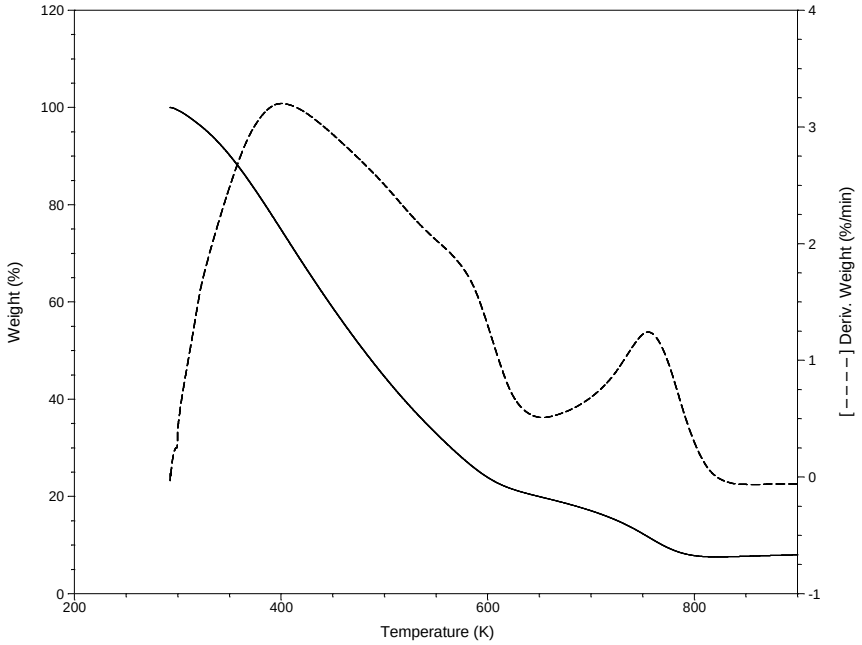

Figure B.I.2 - TG/DTG Curve of Crude Oil 1 at 10 °C/min

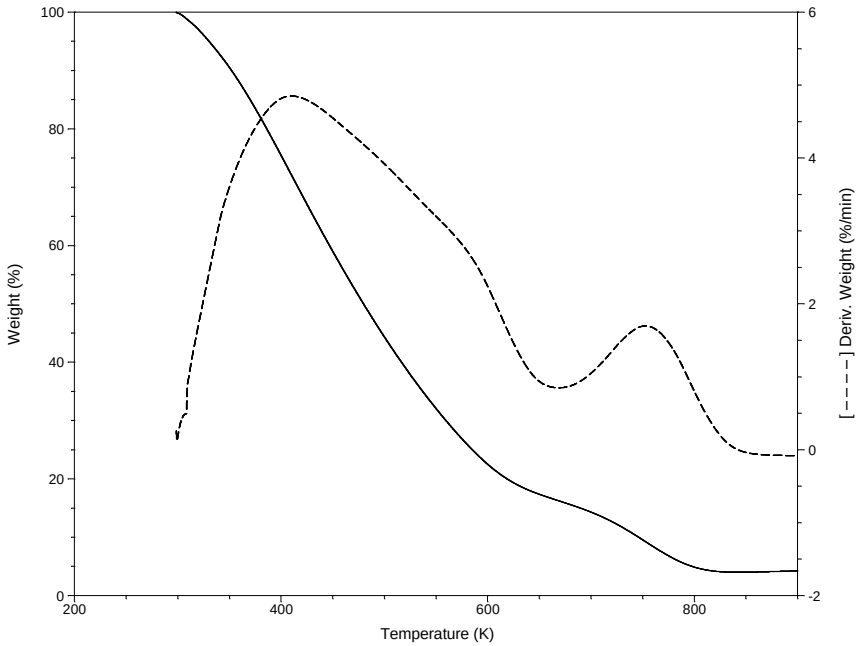

Figure B.I.3 - TG/DTG Curve of Crude Oil 1 at 15 °C/min

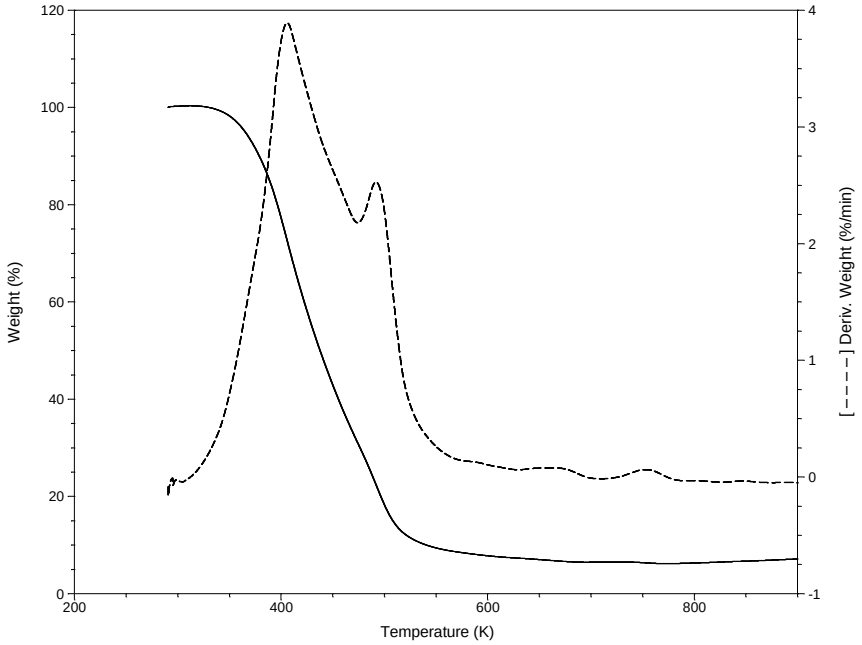

Figure B.I.4 - TG/DTG Curve of Crude Oil 1 Saturate at 5 °C/min

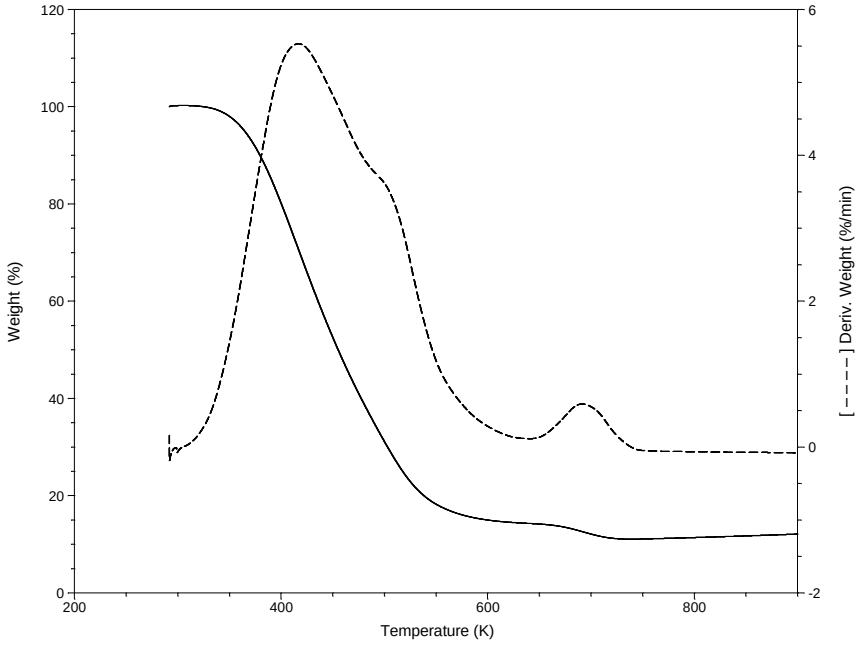

Figure B.I.5 - TG/DTG Curve of Crude Oil 1 Saturate at 10 °C/min

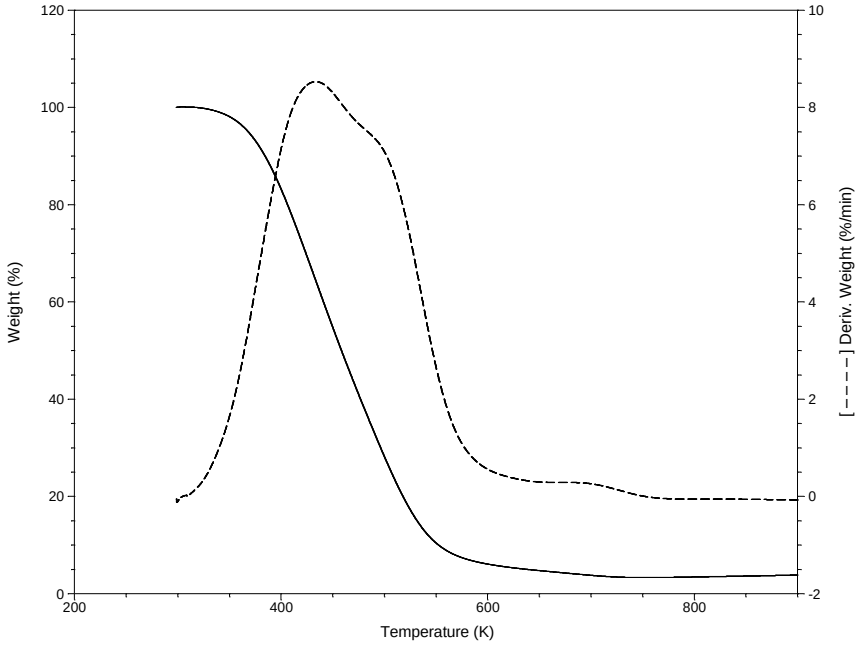

Figure B.I.6 - TG/DTG Curve of Crude Oil 1 Saturate at 15 °C/min

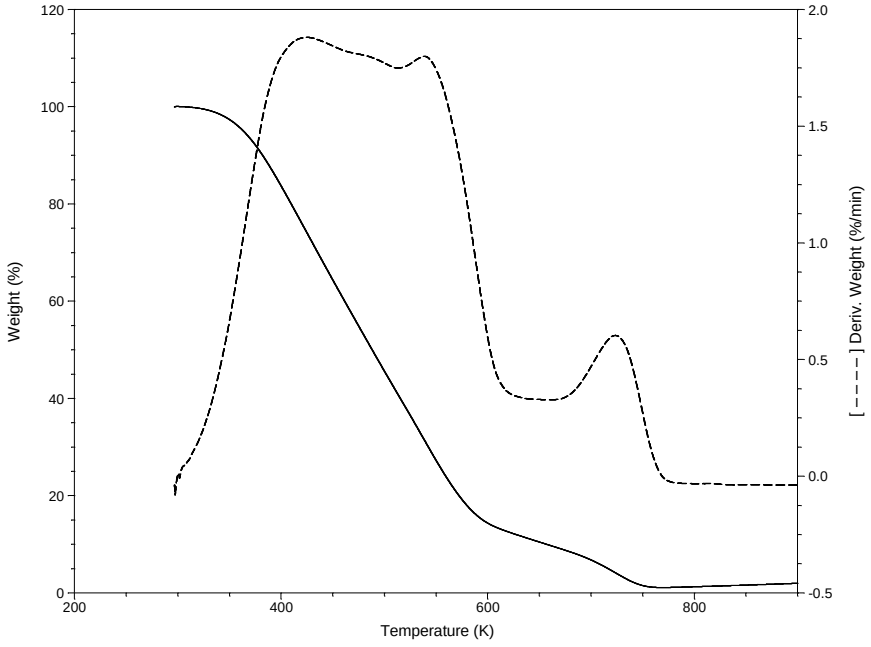

Figure B.I.7 - TG/DTG Curve of Crude Oil 1 Aromatic at 5 °C/min

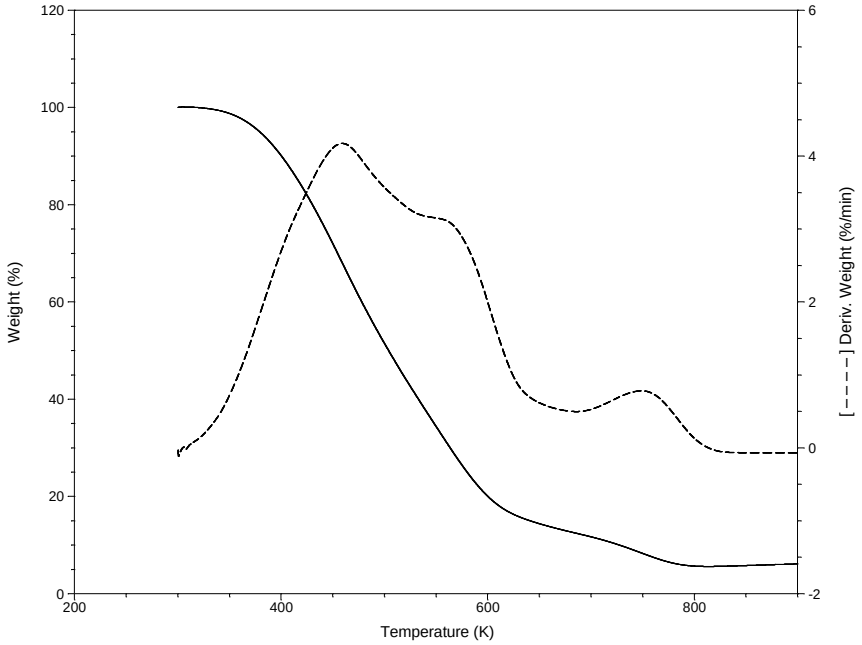

Figure B.I.8 - TG/DTG Curve of Crude Oil 1 Aromatic at 10 °C/min

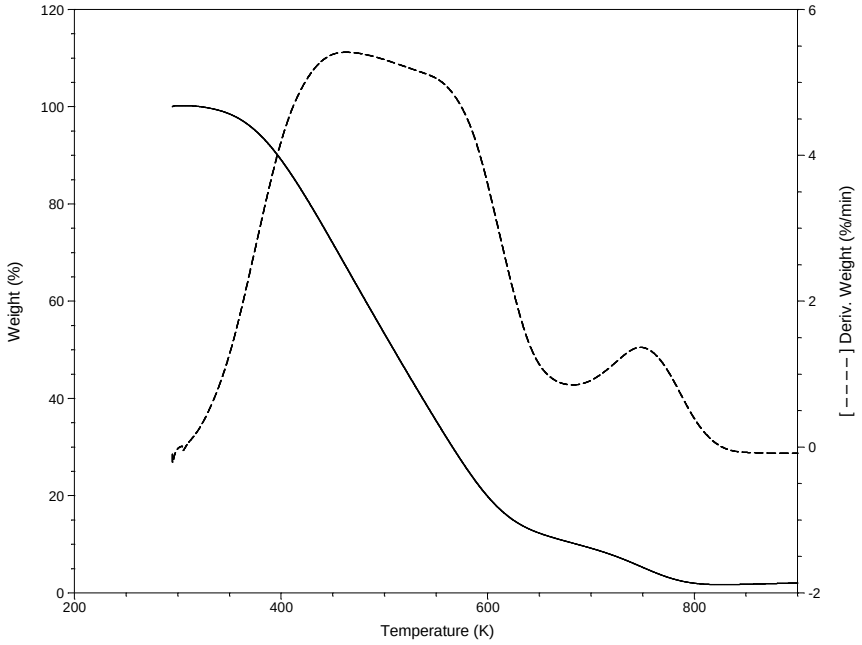

Figure B.I.9 - TG/DTG Curve of Crude Oil 1 Aromatic at 15 °C/min

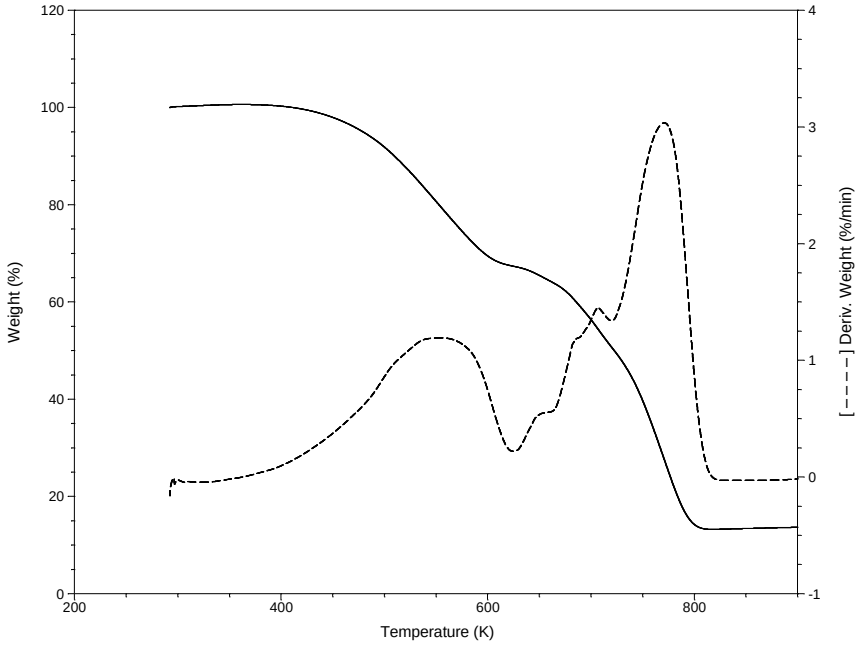

Figure B.I.10 - TG/DTG Curve of Crude Oil 1 Resin at 5 °C/min

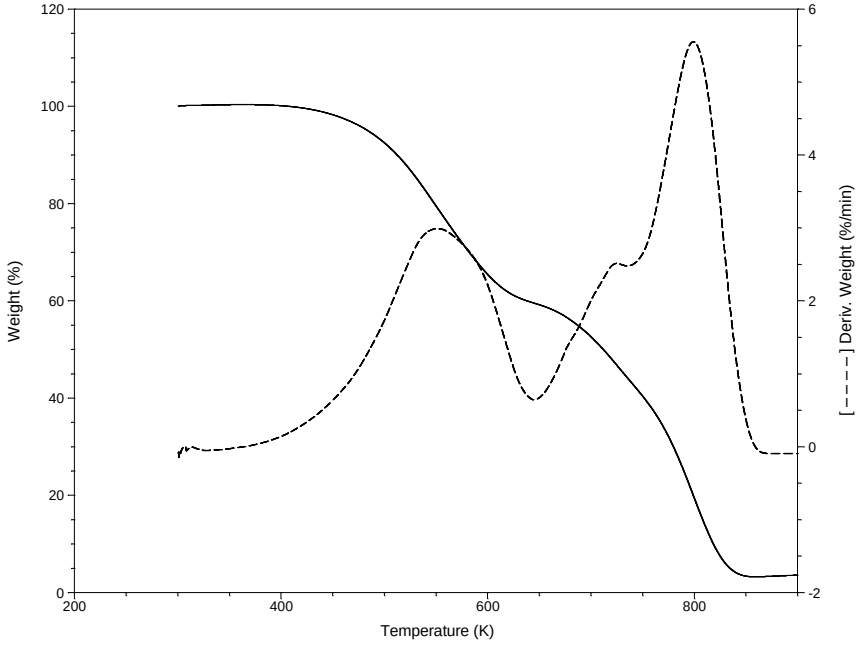

Figure B.I.11 - TG/DTG Curve of Crude Oil 1 Resin at 10 °C/min

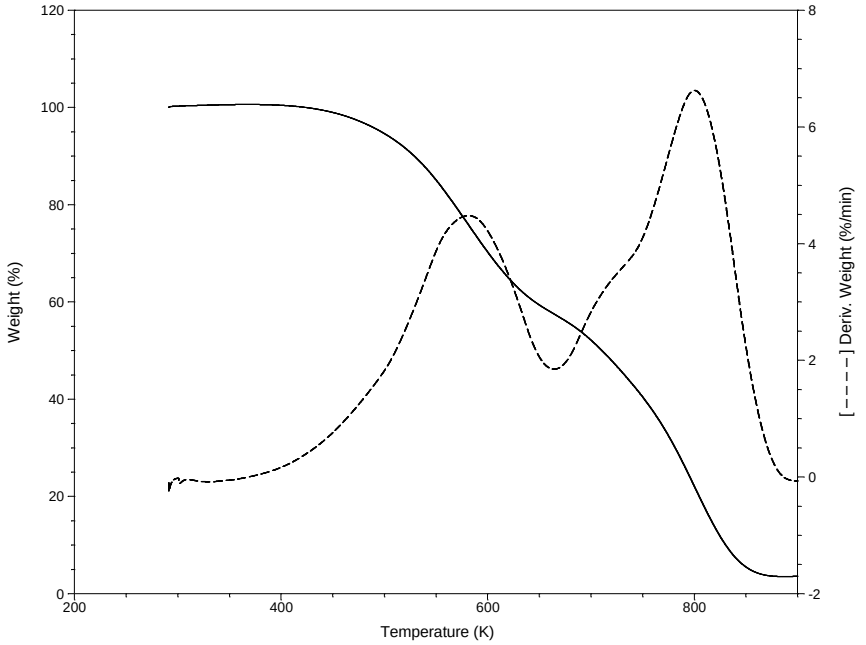

Figure B.I.12 - TG/DTG Curve of Crude Oil 1 Resin at 15 °C/min

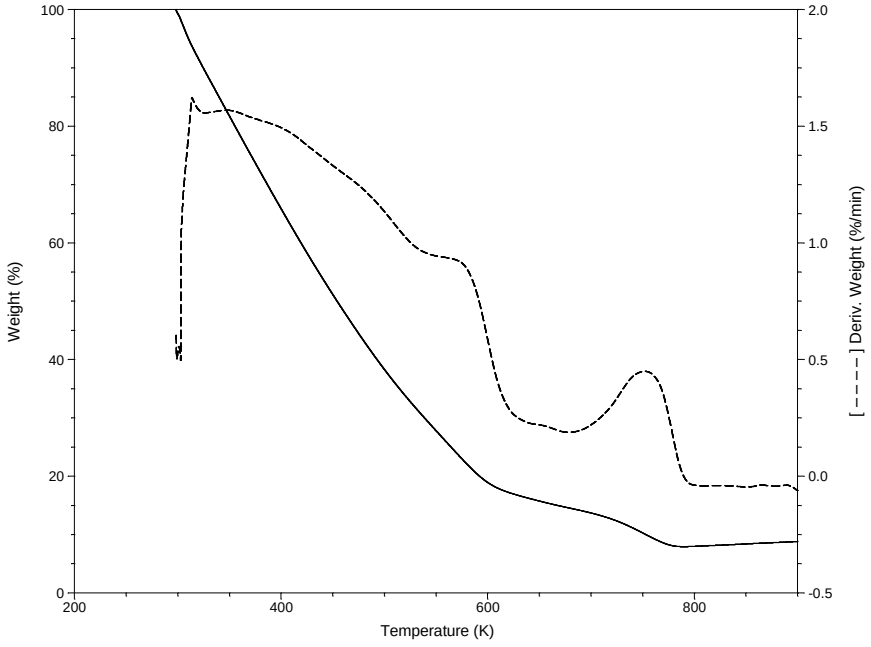

Figure B.I.13 - TG/DTG Curve of Crude Oil 2 at 5 °C/min

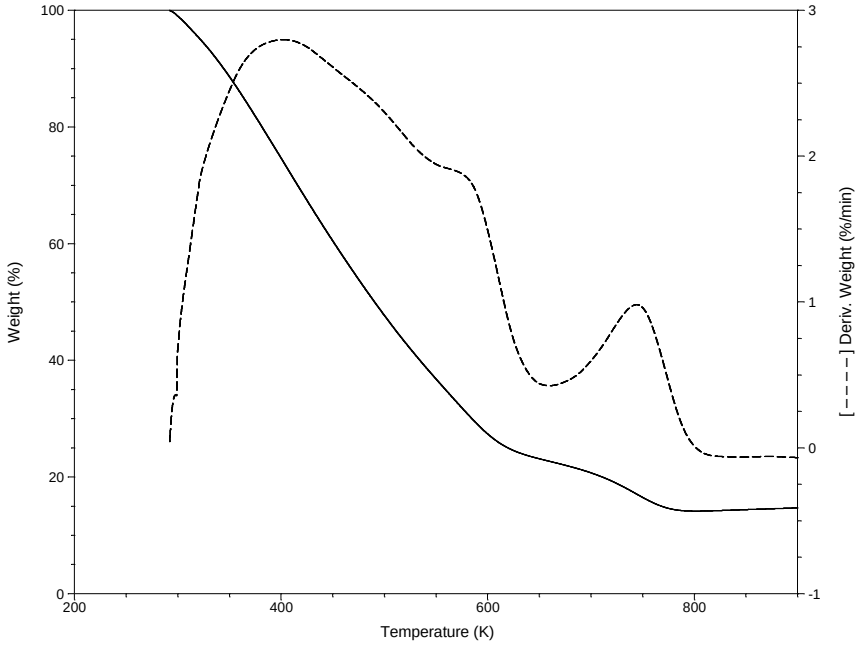

Figure B.I.14 - TG/DTG Curve of Crude Oil 2 at 10 °C/min

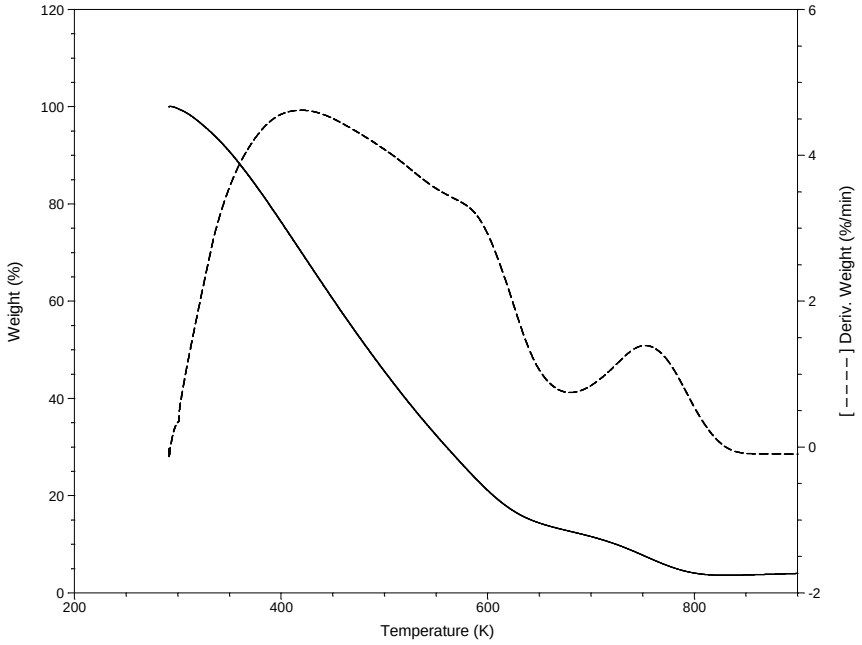

Figure B.I.15 - TG/DTG Curve of Crude Oil 2 at 15 °C/min

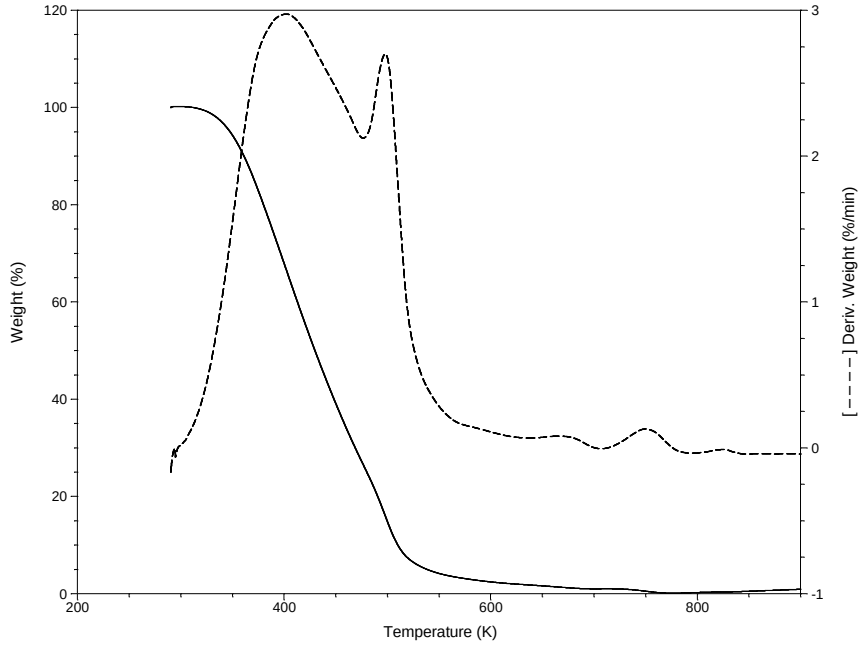

Figure B.I.16 - TG/DTG Curve of Crude Oil 2 Saturate at 5 °C/min

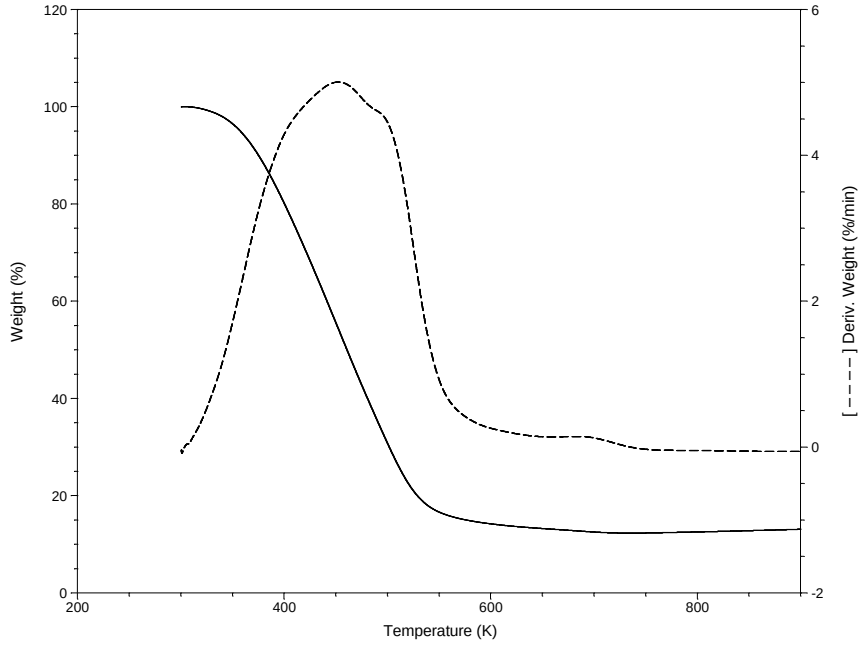

Figure B.I.17 - TG/DTG Curve of Crude Oil 2 Saturate at 10 °C/min

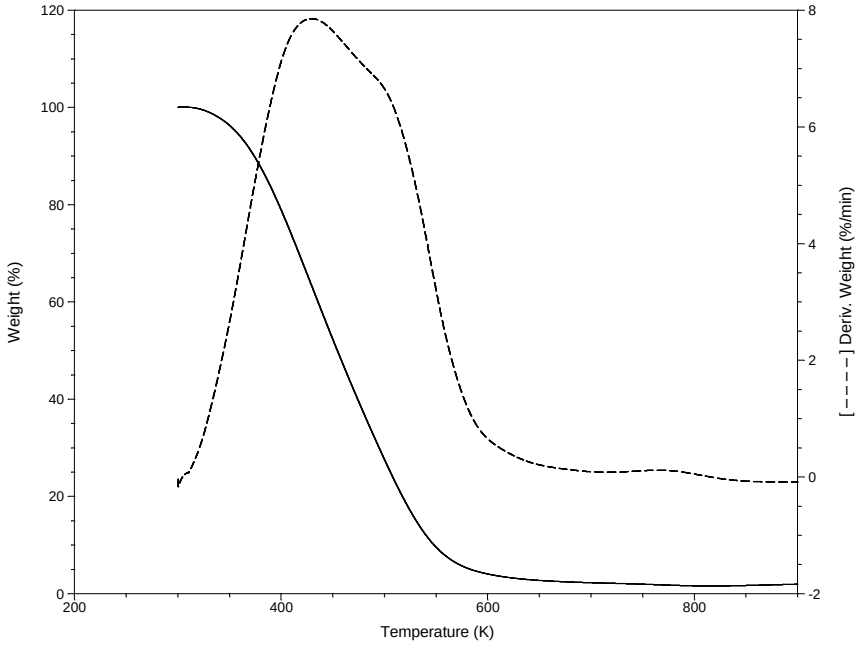

Figure B.I.18 - TG/DTG Curve of Crude Oil 2 Saturate at 15 °C/min

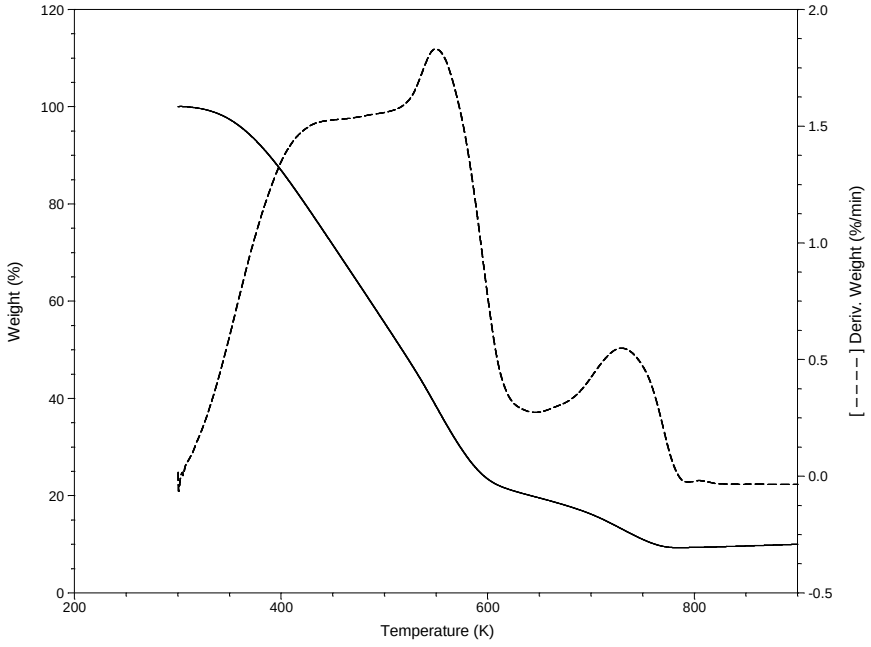

Figure B.I.19 - TG/DTG Curve of Crude Oil 2 Aromatic at 5 °C/min

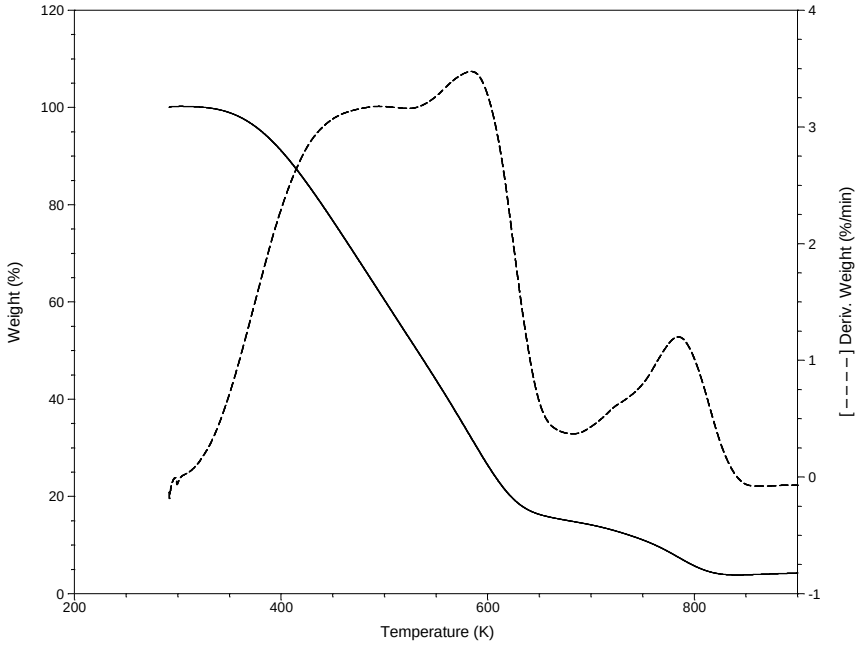

Figure B.I.20 - TG/DTG Curve of Crude Oil 2 Aromatic at 10 °C/min

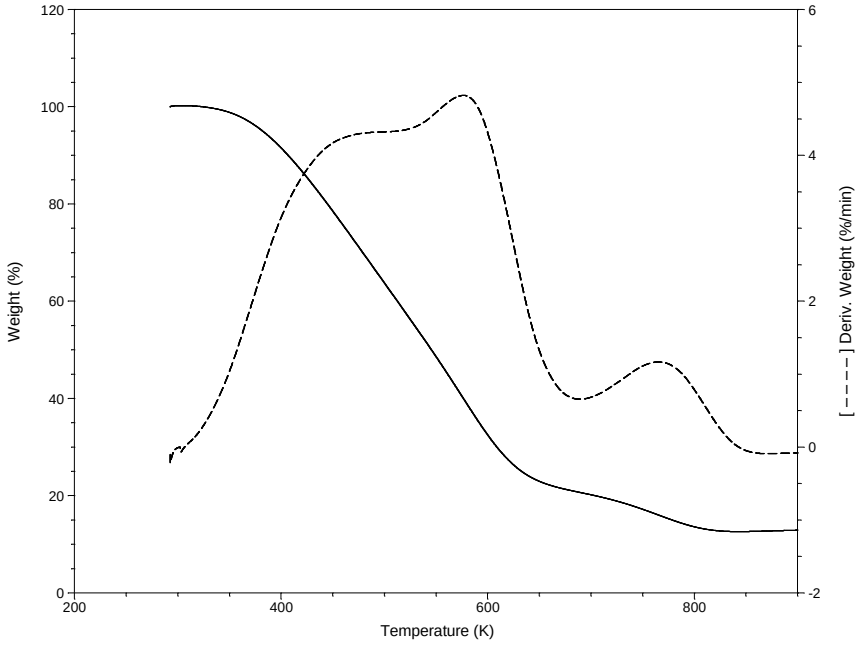

Figure B.I.21 - TG/DTG Curve of Crude Oil 2 Aromatic at 15 °C/min

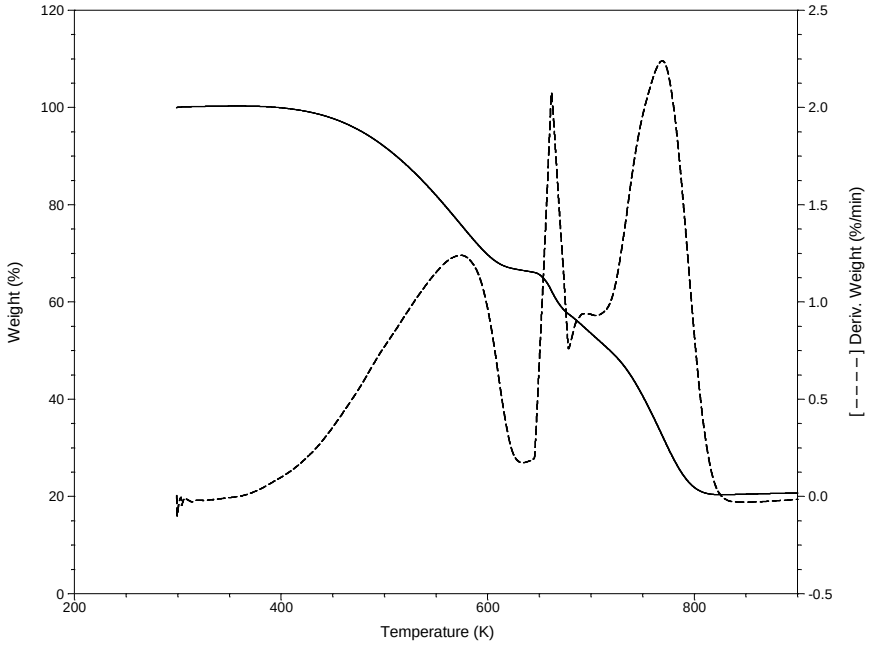

Figure B.I.22 - TG/DTG Curve of Crude Oil 2 Resin at 5 °C/min

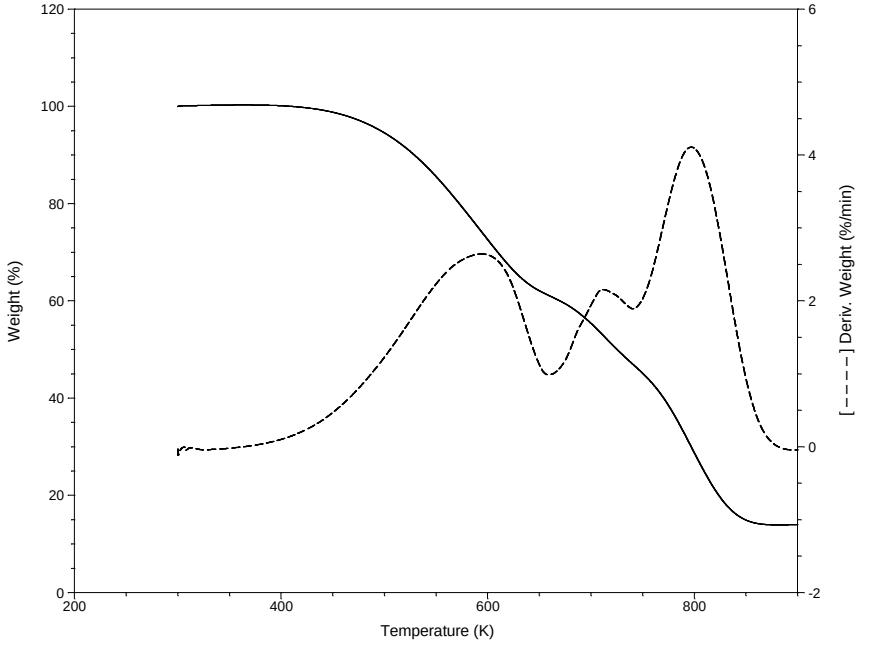

Figure B.I.23 - TG/DTG Curve of Crude Oil 2 Resin at 10 °C/min

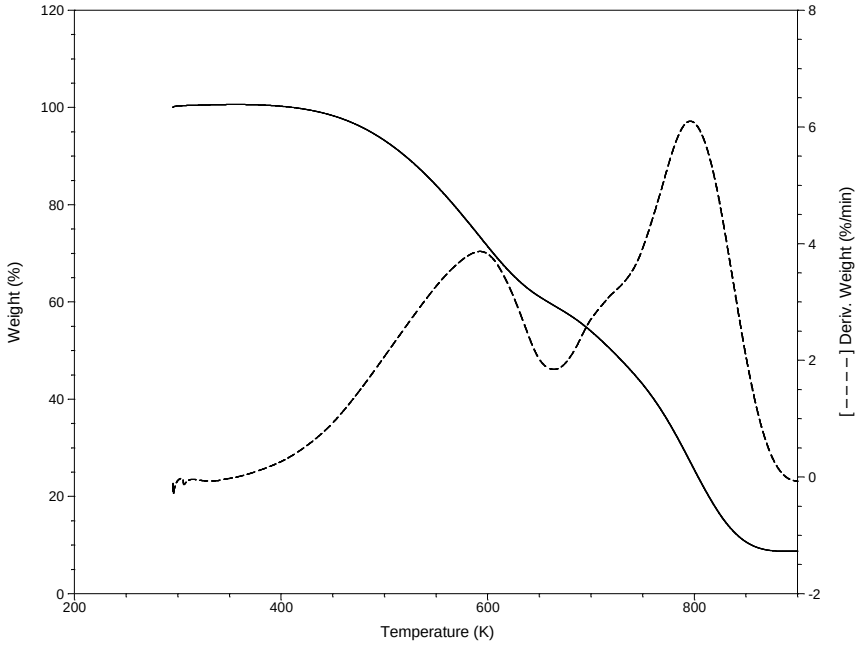

Figure B.I.24 - TG/DTG Curve of Crude Oil 2 Resin at 15 °C/min

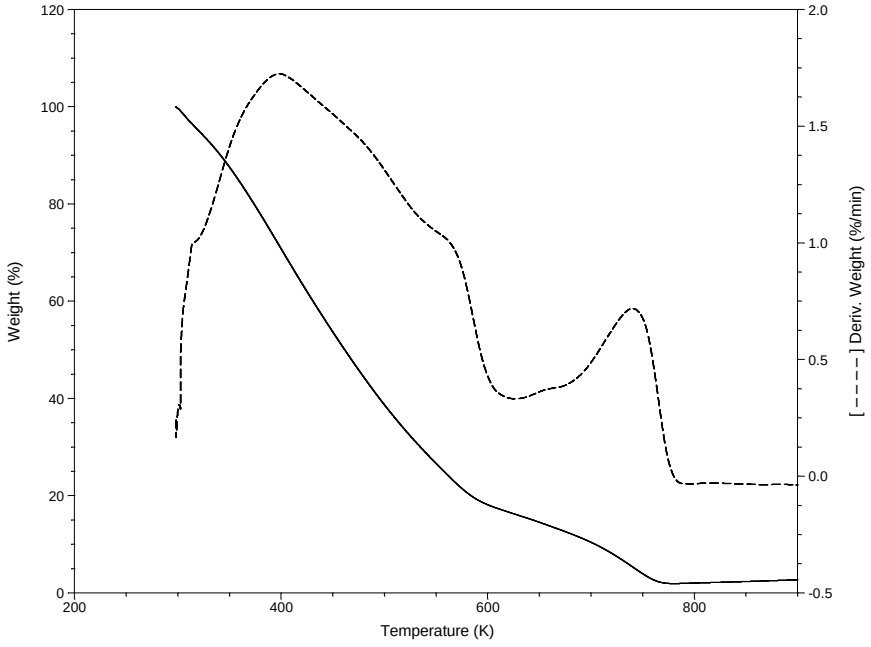

Figure B.I.25 - TG/DTG Curve of Crude Oil 3 at 5 °C/min

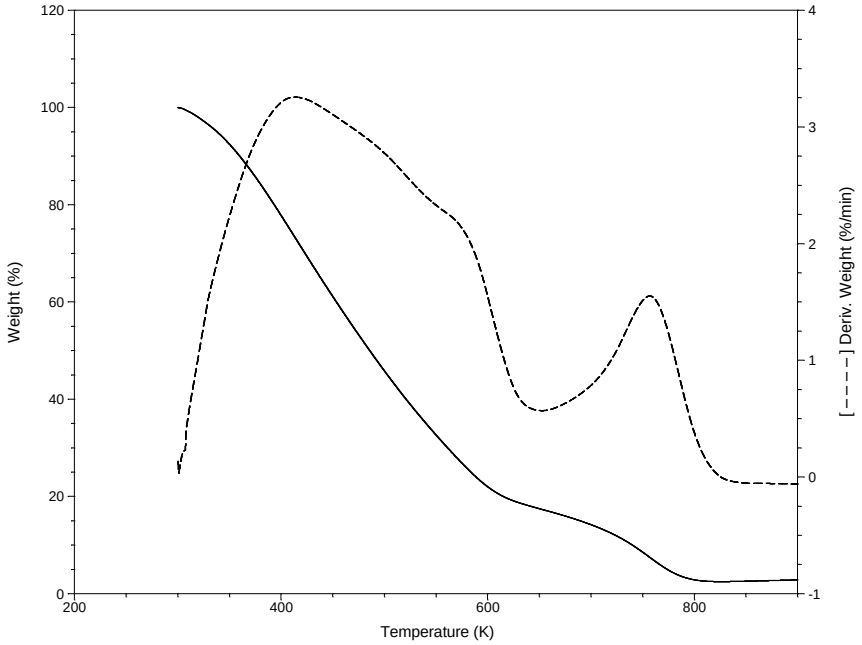

Figure B.I.26 - TG/DTG Curve of Crude Oil 3 at 10 °C/min

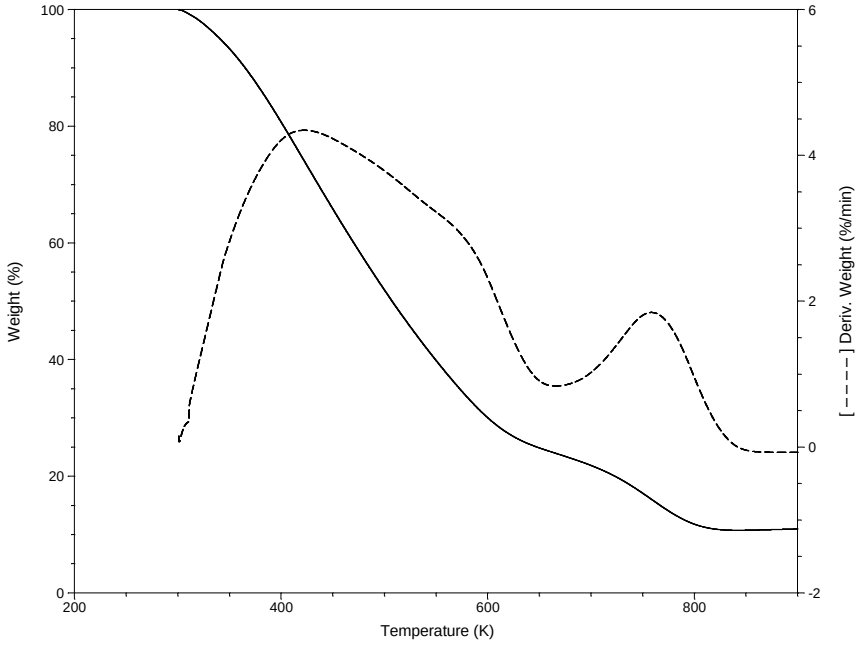

Figure B.I.27 - TG/DTG Curve of Crude Oil 3 at 15 °C/min

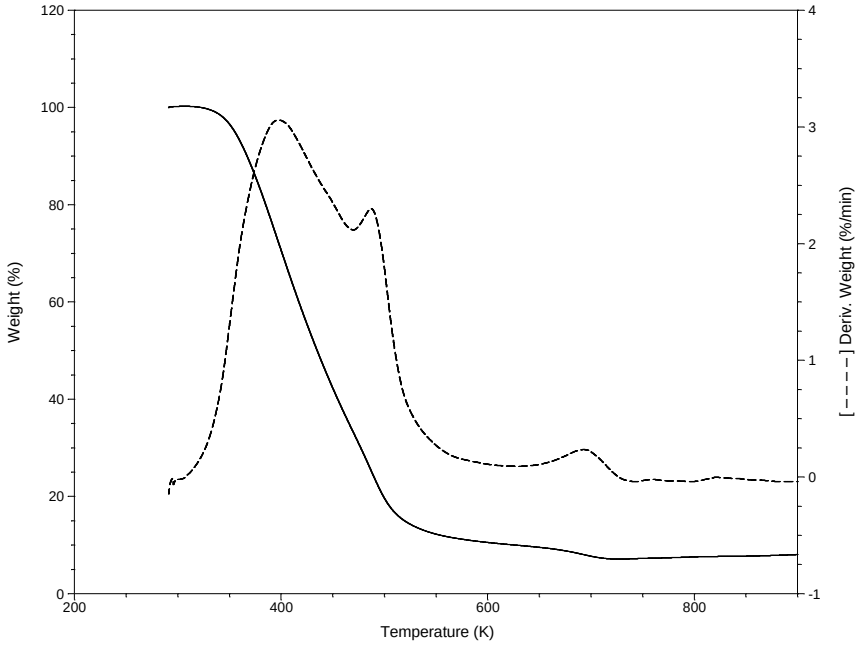

Figure B.I.28 - TG/DTG Curve of Crude Oil 3 Saturate at 5 °C/min

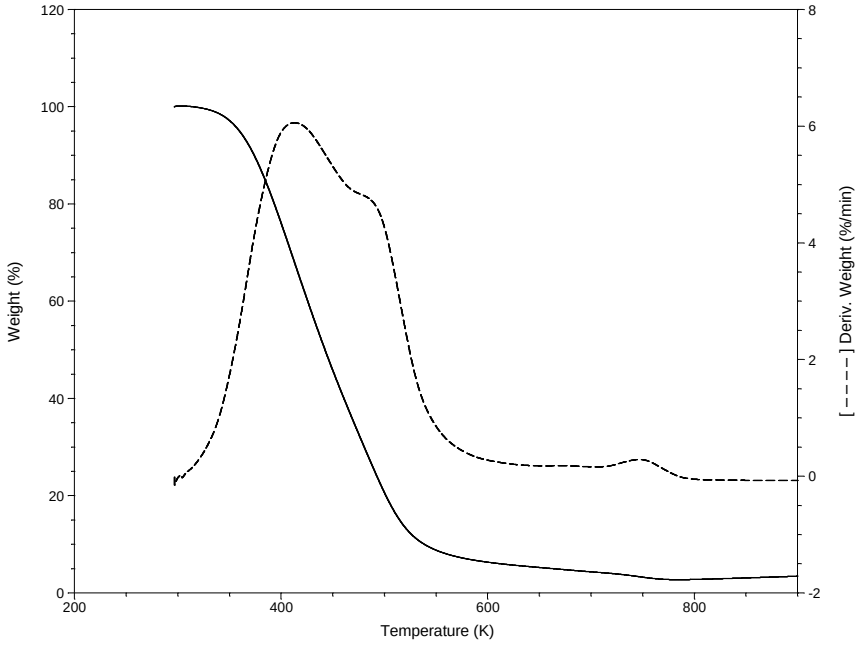

Figure B.I.29 - TG/DTG Curve of Crude Oil 3 Saturate at 10 °C/min

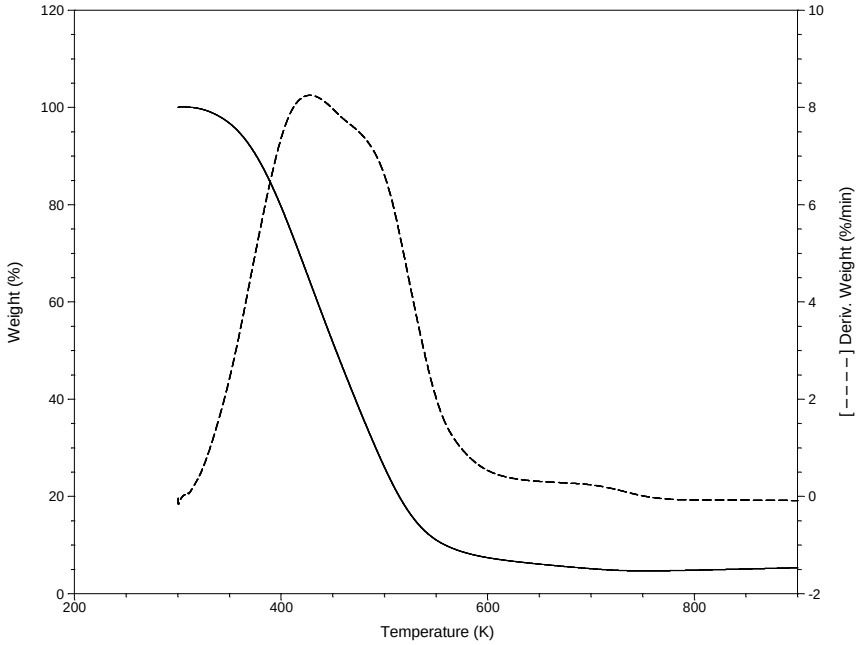

Figure B.I.30 - TG/DTG Curve of Crude Oil 3 Saturate at 15 °C/min

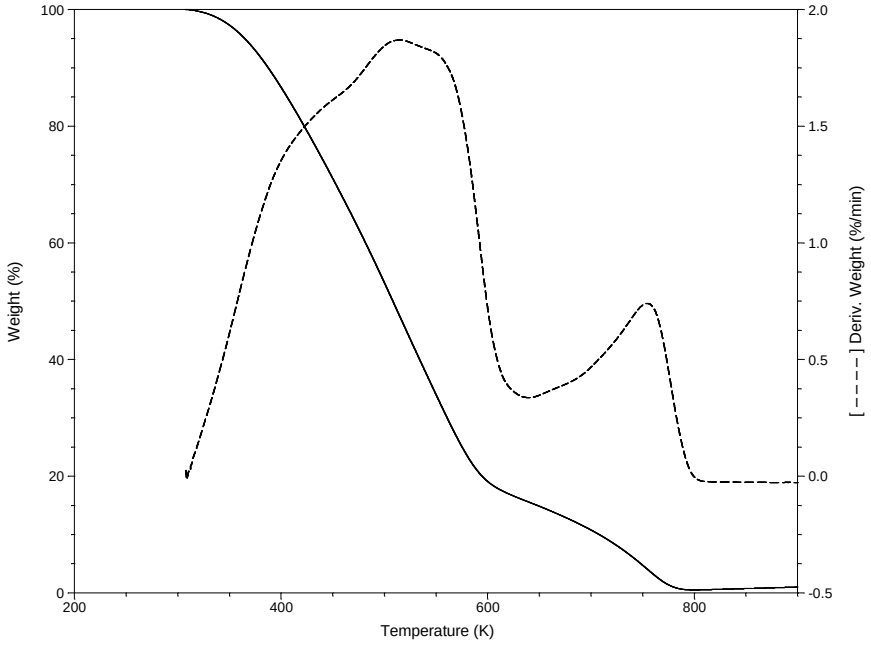

Figure B.I.31 - TG/DTG Curve of Crude Oil 3 Aromatic at 5 °C/min

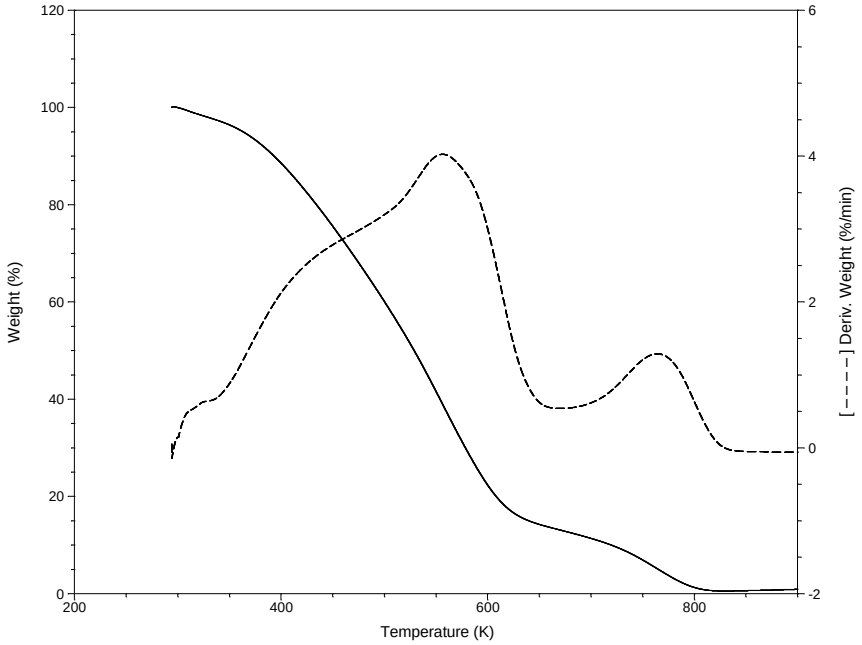

Figure B.I.32 - TG/DTG Curve of Crude Oil 3 Aromatic at 10 °C/min

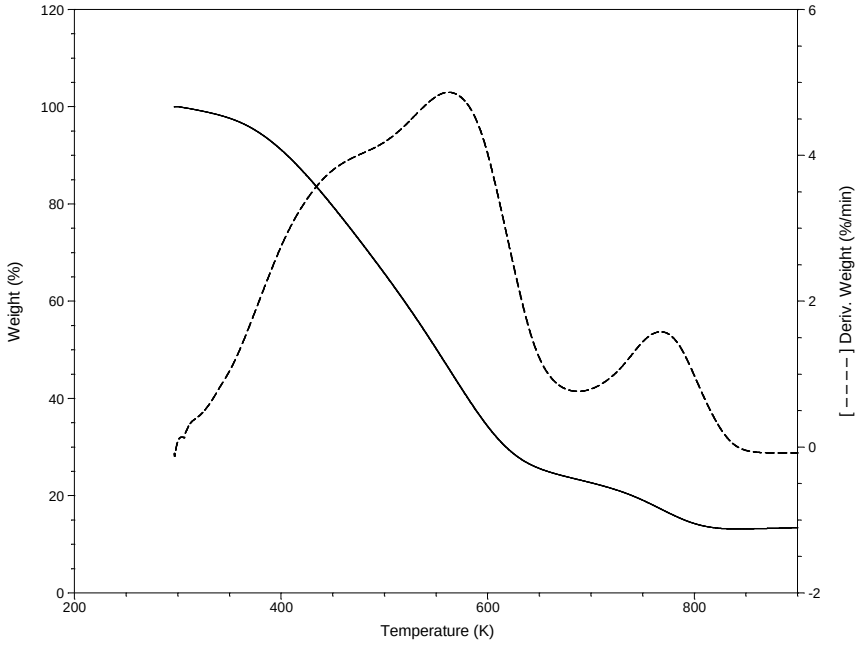

Figure B.I.33 - TG/DTG Curve of Crude Oil 3 Aromatic at 15 °C/min

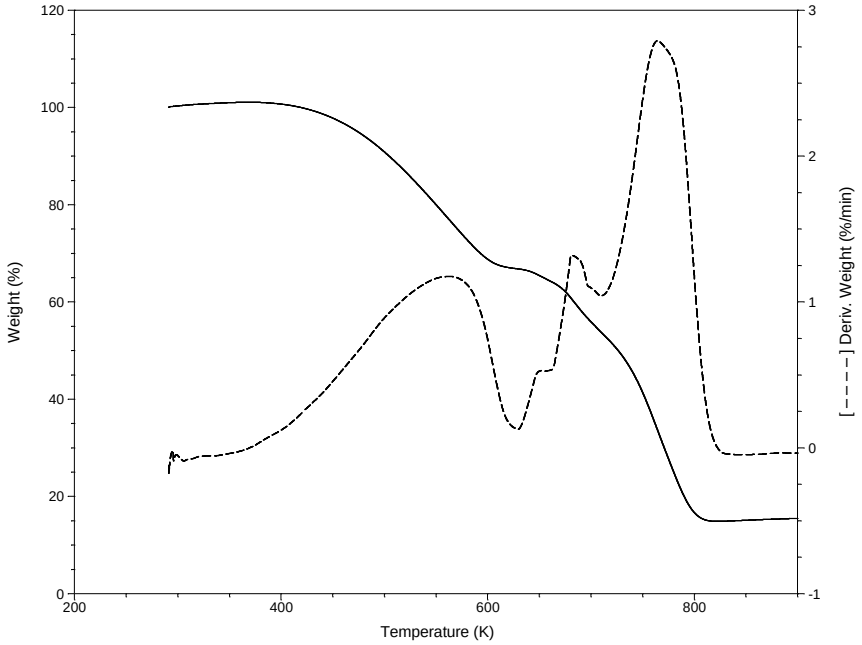

Figure B.I.34 - TG/DTG Curve of Crude Oil 3 Resin at 5 °C/min

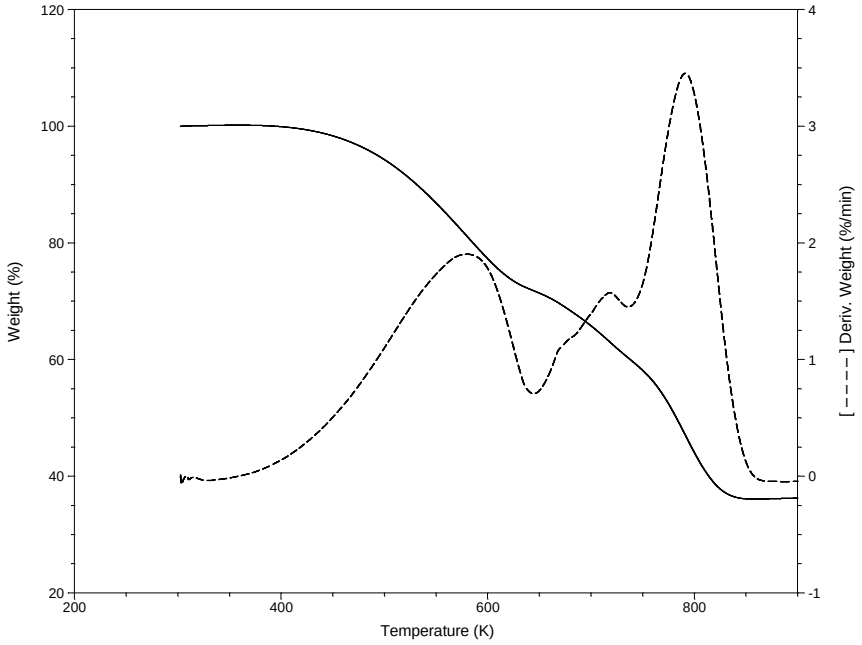

Figure B.I.35 - TG/DTG Curve of Crude Oil 3 Resin at 10 °C/min

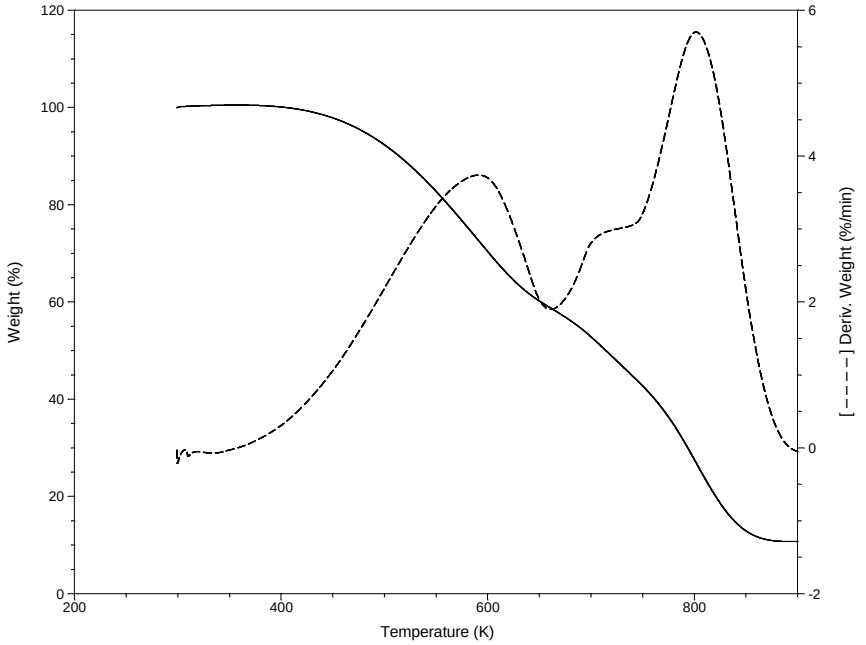

Figure B.I.36 - TG/DTG Curve of Crude Oil 3 Resin at 15 °C/min

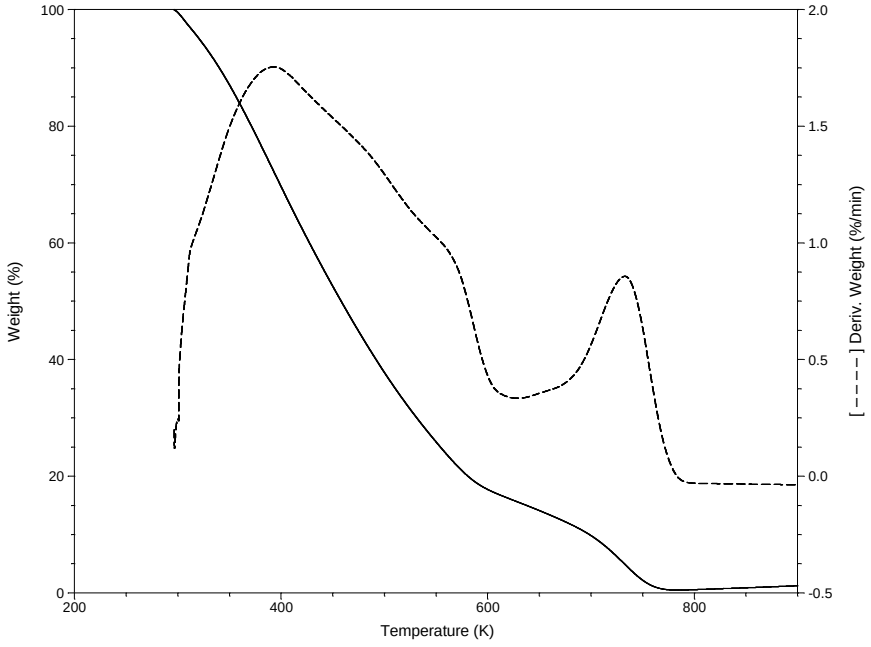

Figure B.I.37 - TG/DTG Curve of Crude Oil 4 at 5 °C/min

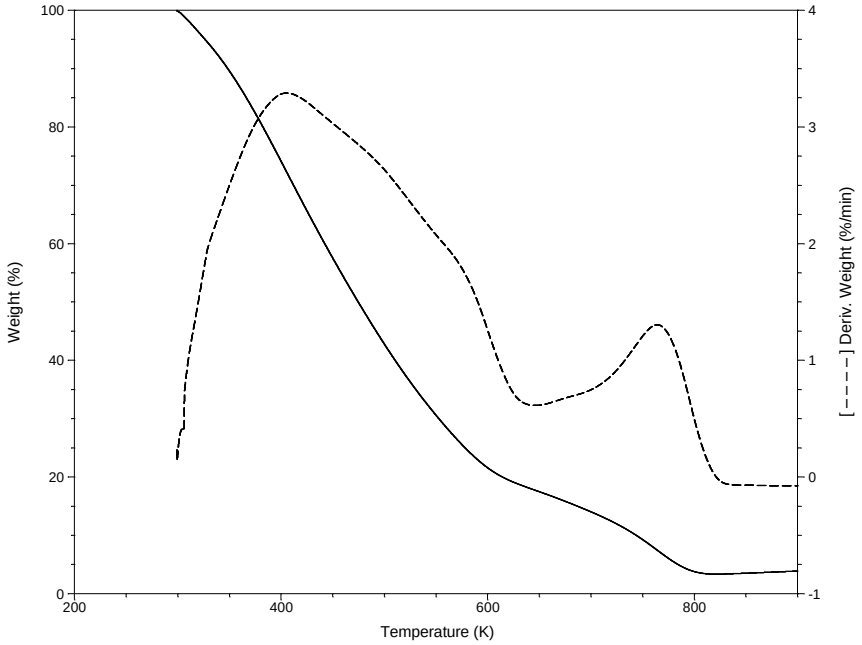

Figure B.I.38 - TG/DTG Combustion Curve of Crude Oil 4 at 10 °C/min

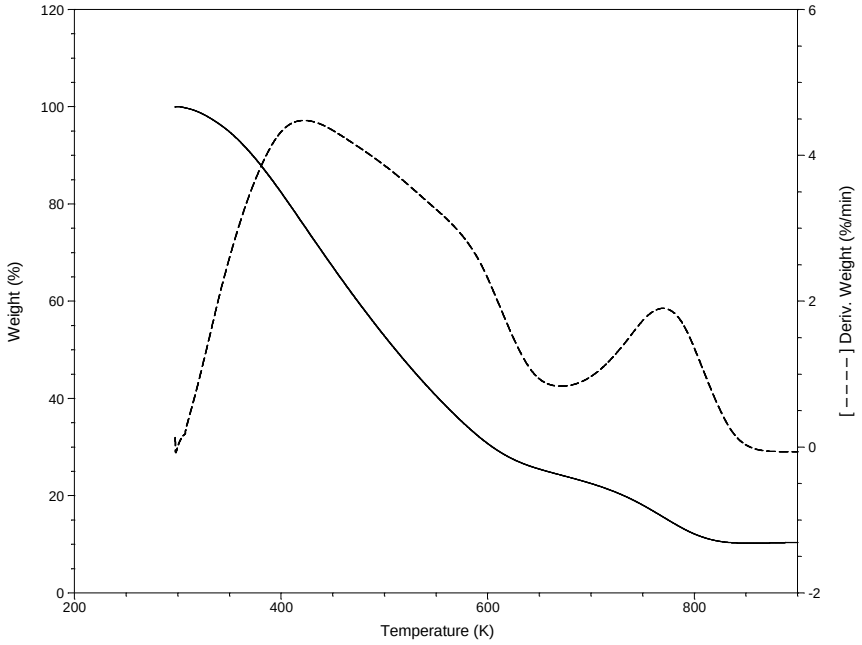

Figure B.I.39 - TG/DTG Curve of Crude Oil 4 at 15 °C/min

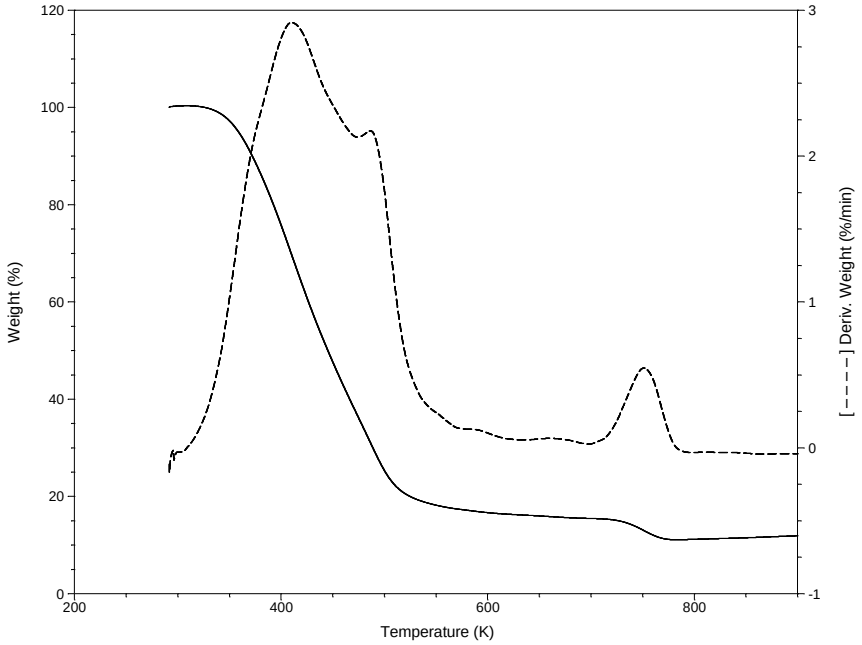

Figure B.I.40 - TG/DTG Curve of Crude Oil 4 Saturate at 5 °C/min

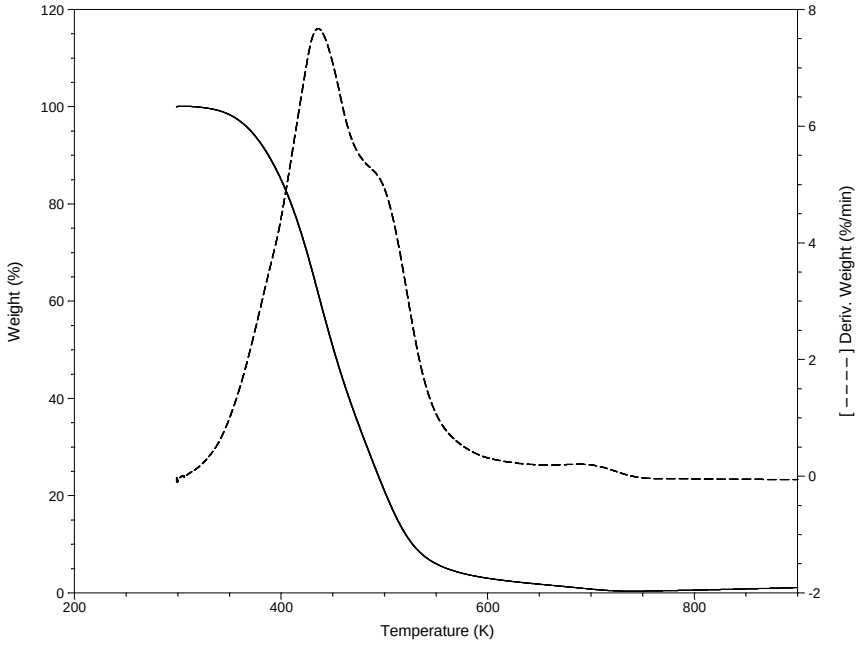

Figure B.I.41 - TG/DTG Curve of Crude Oil 4 Saturate at 10 °C/min

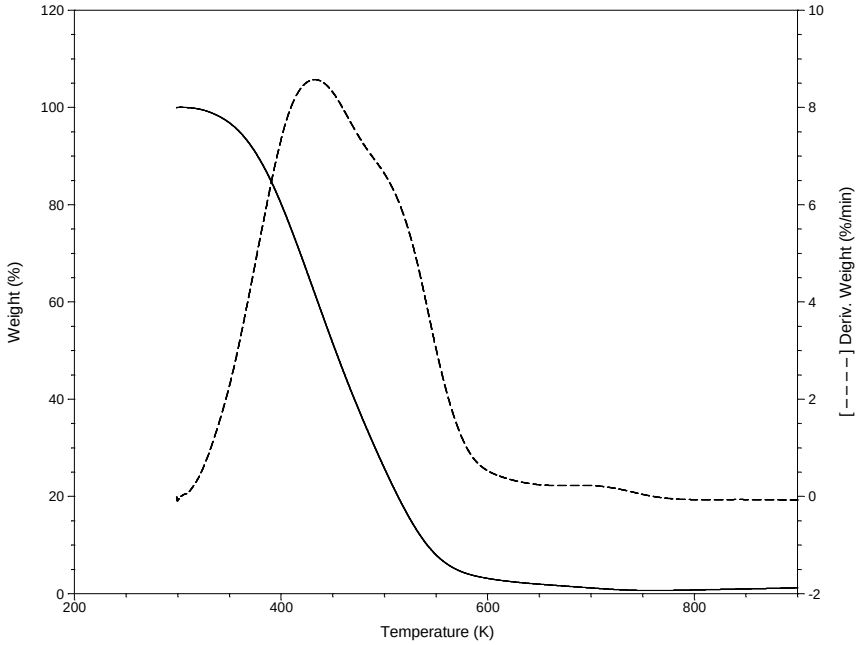

Figure B.I.42 - TG/DTG Combustion Curve of Crude Oil 4 Saturate at 15 °C/min

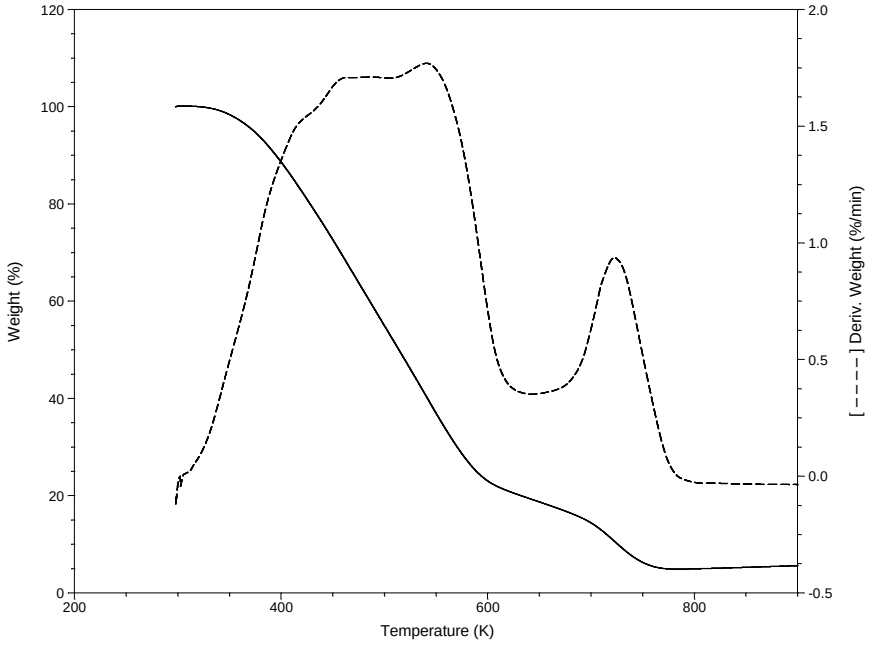

Figure B.I.43 - TG/DTG Curve of Crude Oil 4 Aromatic at 5 °C/min

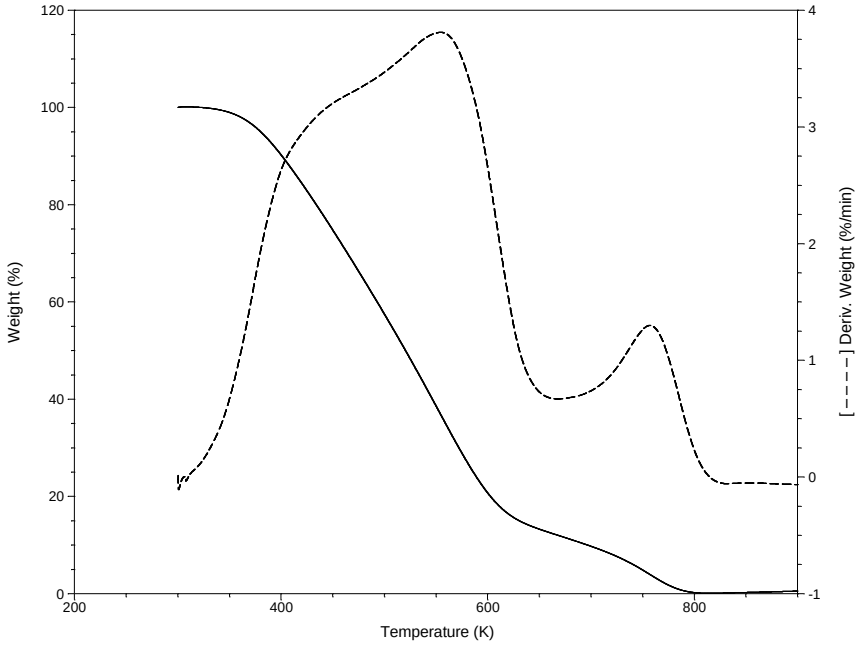

Figure B.I.44 - TG/DTG Curve of Crude Oil 4 Aromatic at 10 °C/min

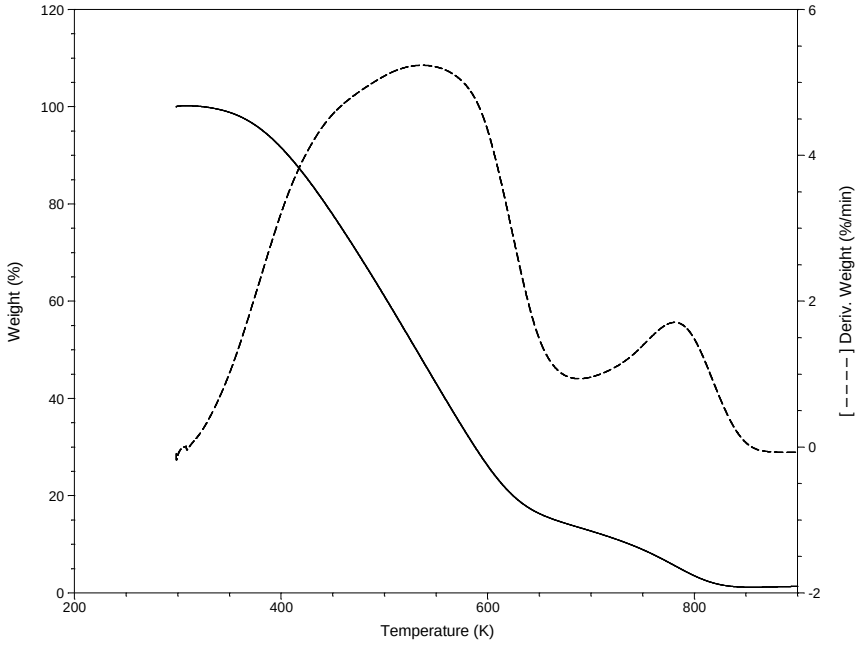

Figure B.I.45 - TG/DTG Curve of Crude Oil 4 Aromatic at 15 °C/min

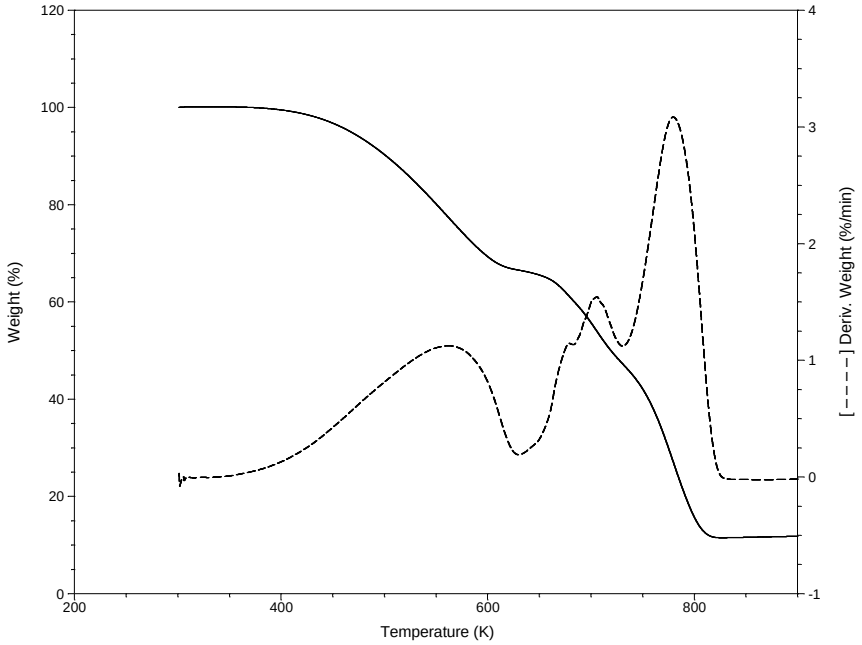

Figure B.I.46 - TG/DTG Curve of Crude Oil 4 Resin at 5 °C/min

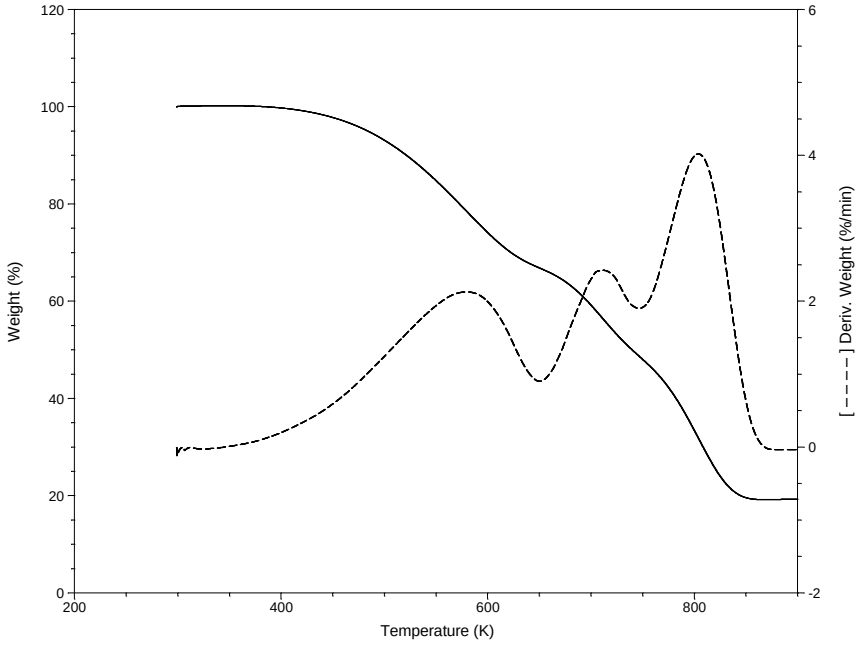

Figure B.I.47 - TG/DTG Curve of Crude Oil 4 Resin at 10 °C/min

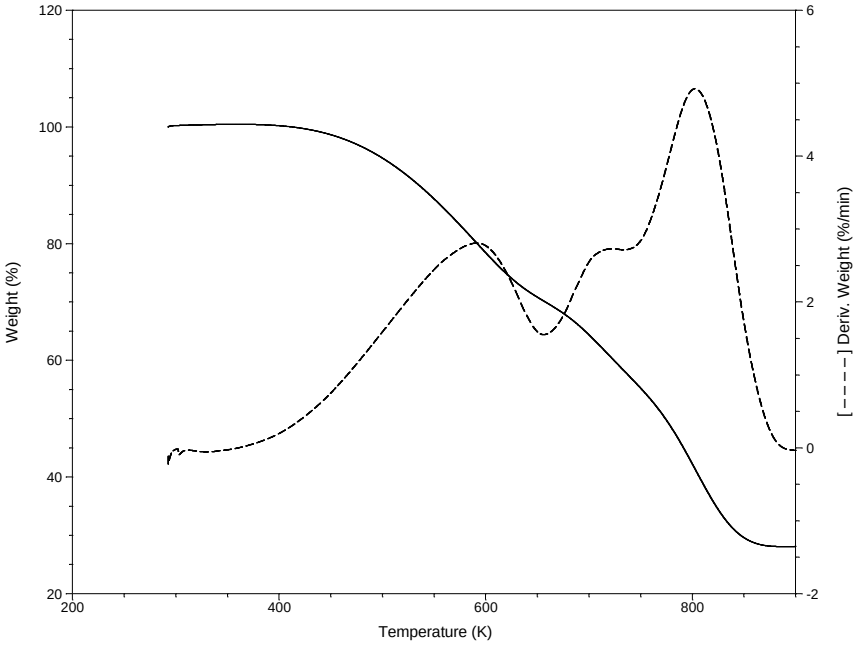

Figure B.I.48 - TG/DTG Curve of Crude Oil 4 Resin at 15 °C/min

B.II. Results of DSC Experiments

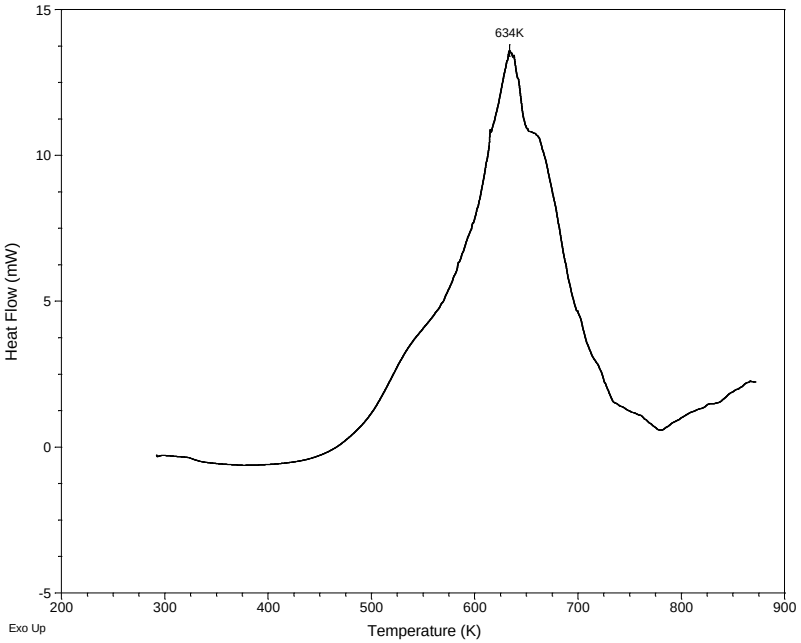

Figure B.II.1 - DSC Curve of Crude Oil 1 at 5 °C/min

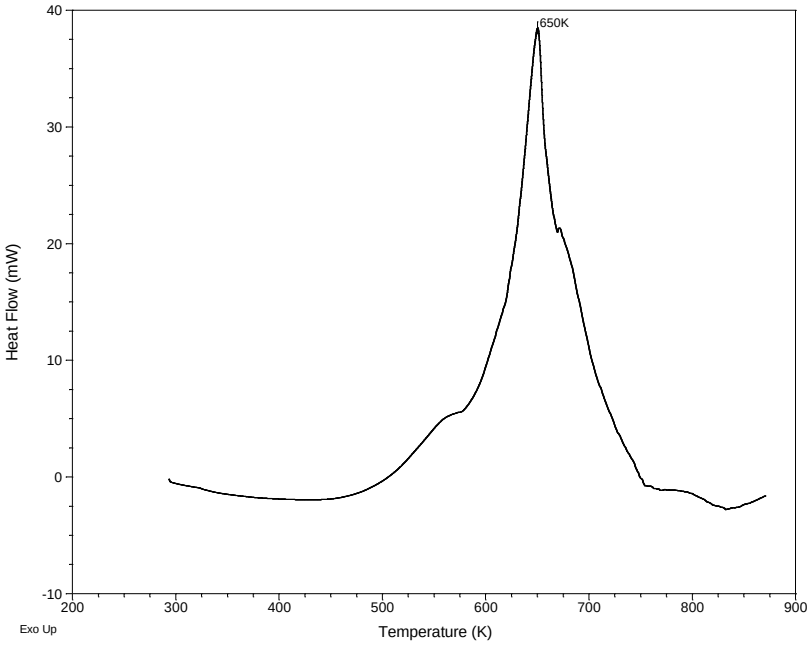

Figure B.II.2 - DSC Curve of Crude Oil 1 at 10 °C/min

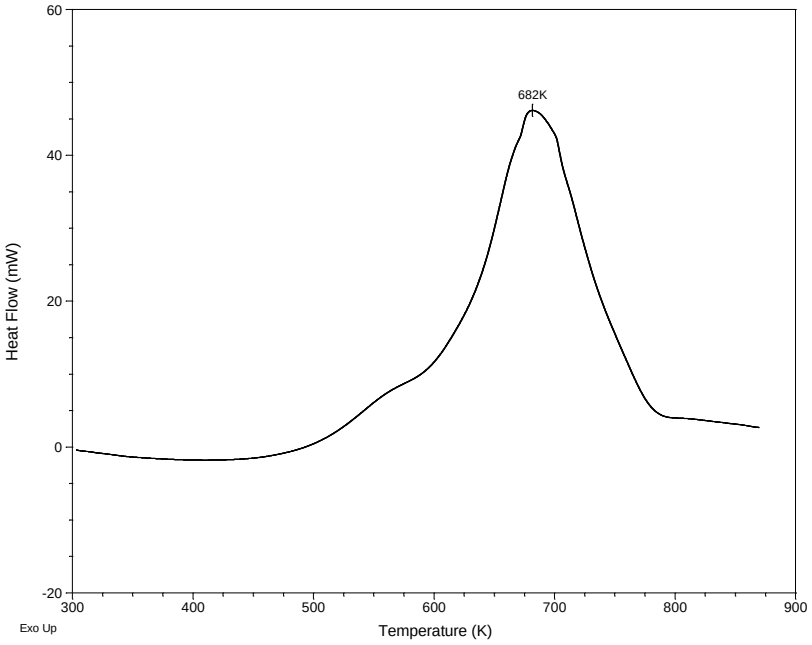

Figure B.II.3 - DSC Combustion Curve of Crude Oil 1 at 15 °C/min

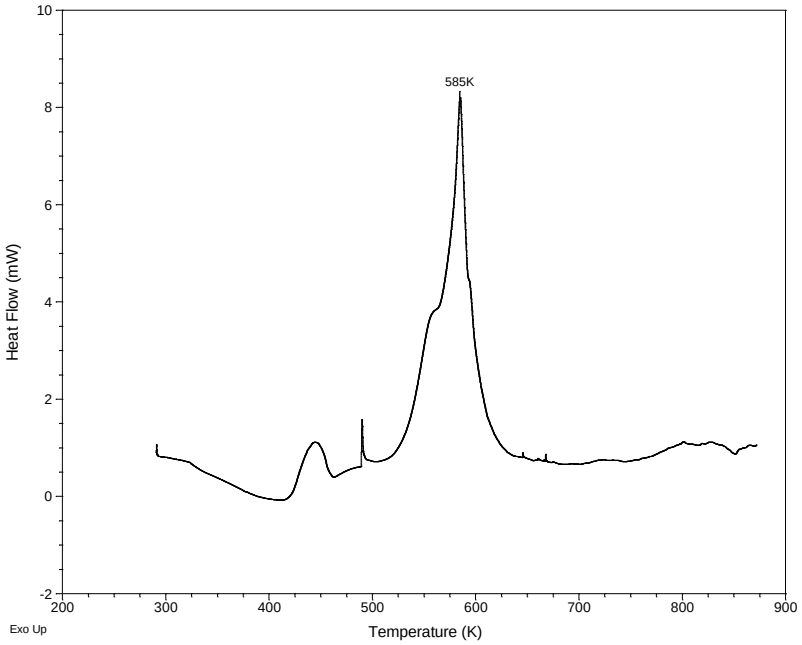

Figure B.II.4 - DSC Curve of Crude Oil 1 Saturate at 5 °C/min

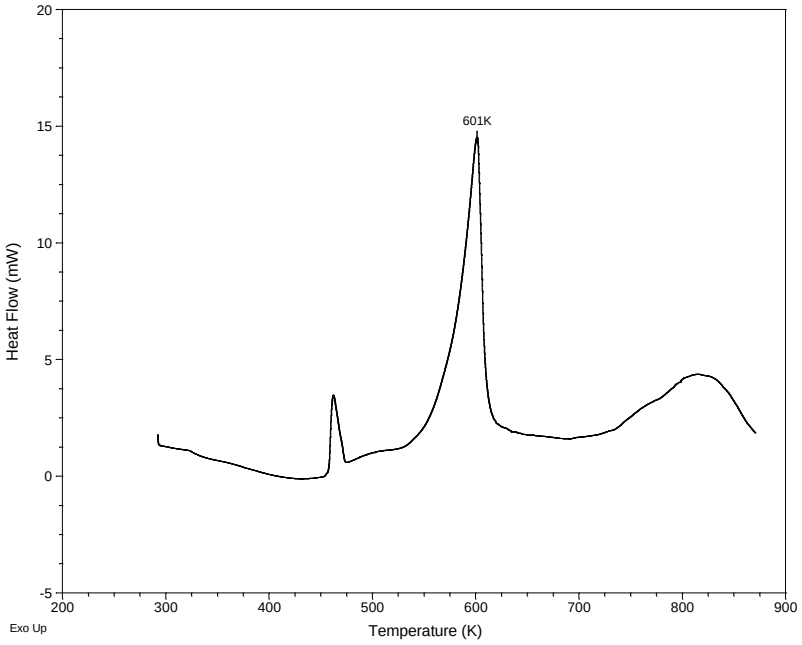

Figure B.II.5 - DSC Curve of Crude Oil 1 Saturate at 10 °C/min

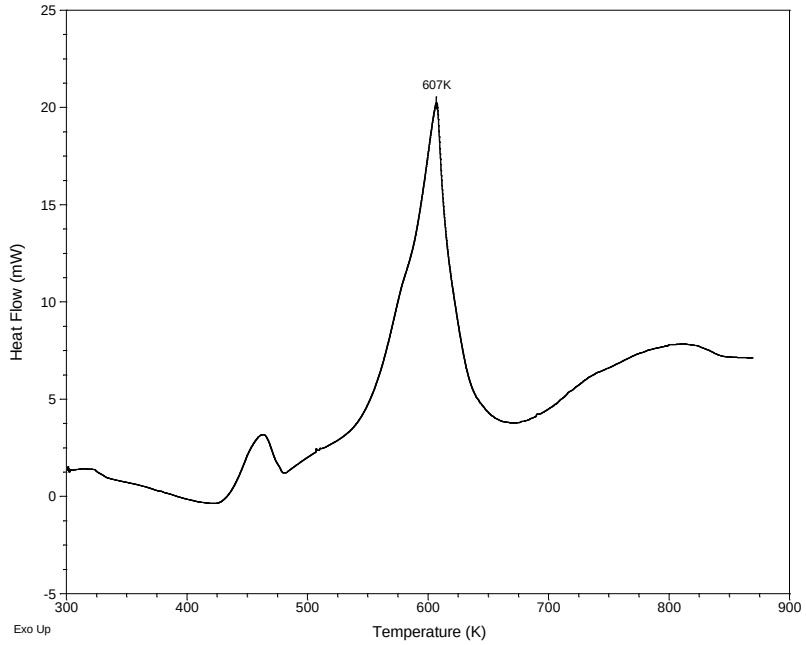

Figure B.II.6 - DSC Curve of Crude Oil 1 Saturate at 15 °C/min

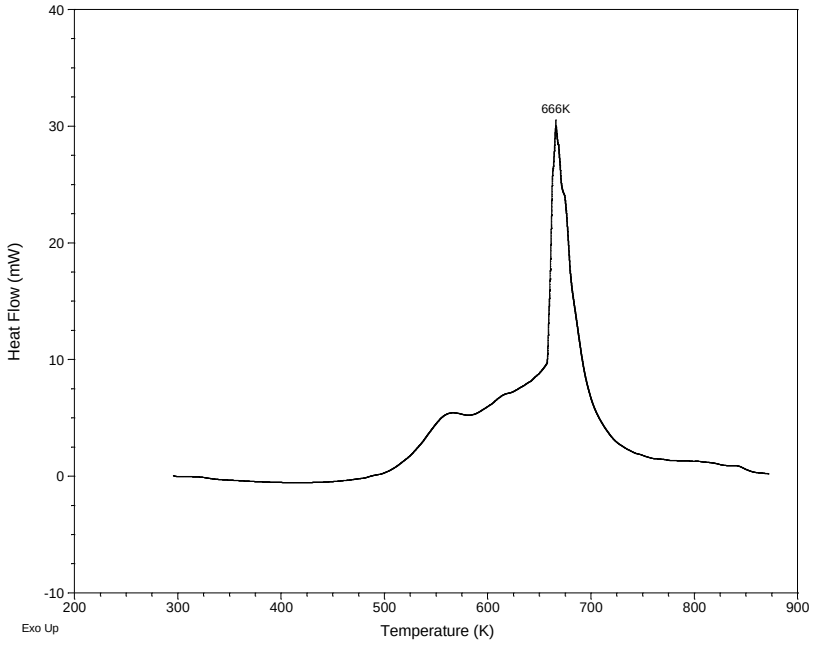

Figure B.II.7 - DSC Curve of Crude Oil 1 Aromatic at 5 °C/min

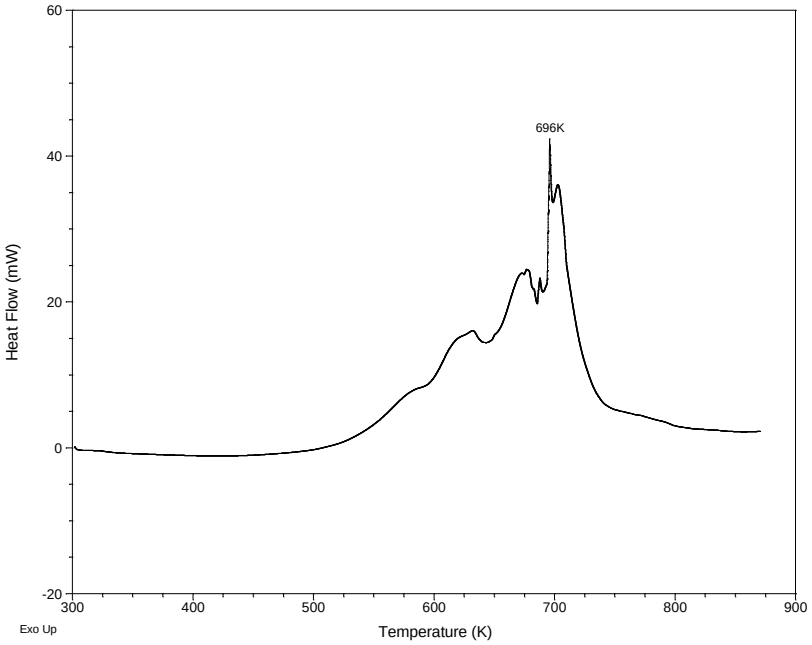

Figure B.II.8 - DSC Curve of Crude Oil 1 Aromatic at 10 °C/min

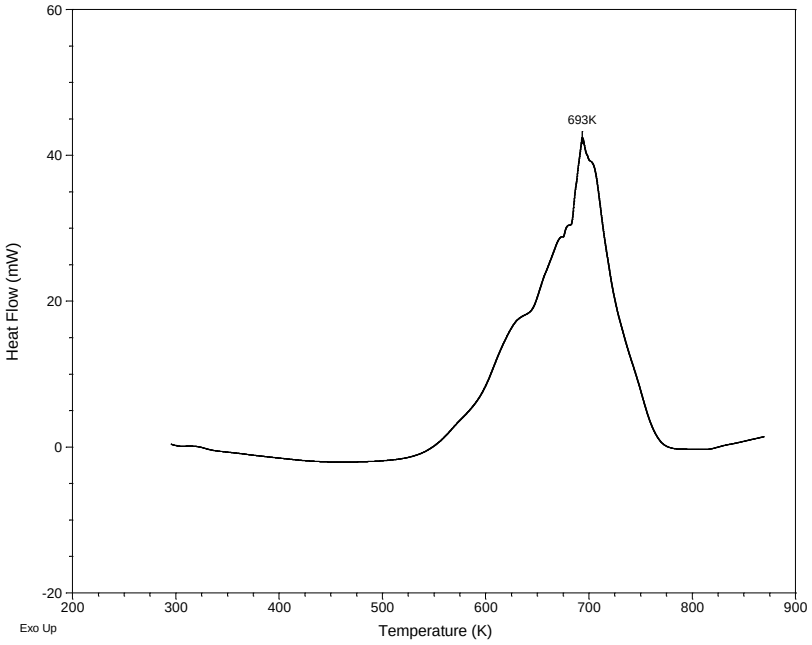

Figure B.II.9 - DSC Curve of Crude Oil 1 Aromatic at 15 °C/min

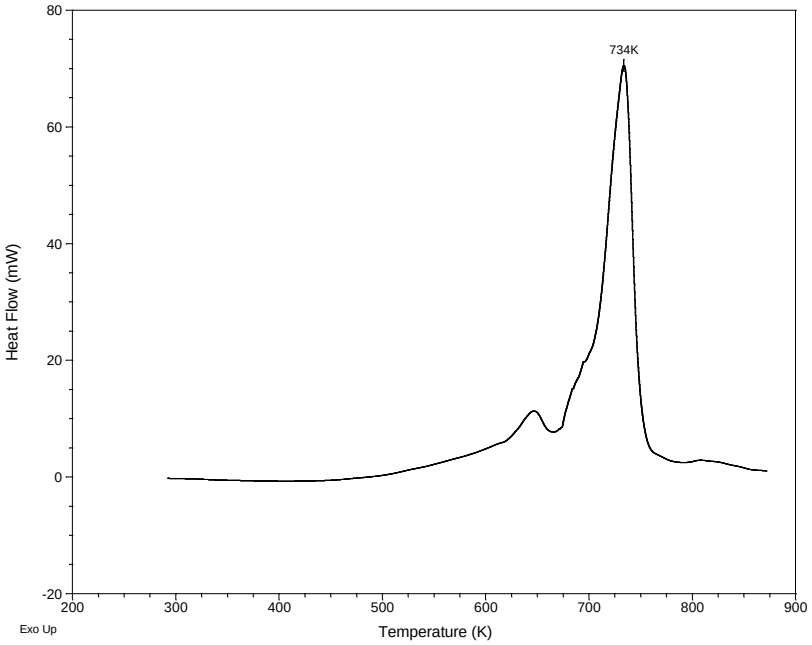

Figure B.II.10 - DSC Curve of Crude Oil 1 Resin at 5 °C/min

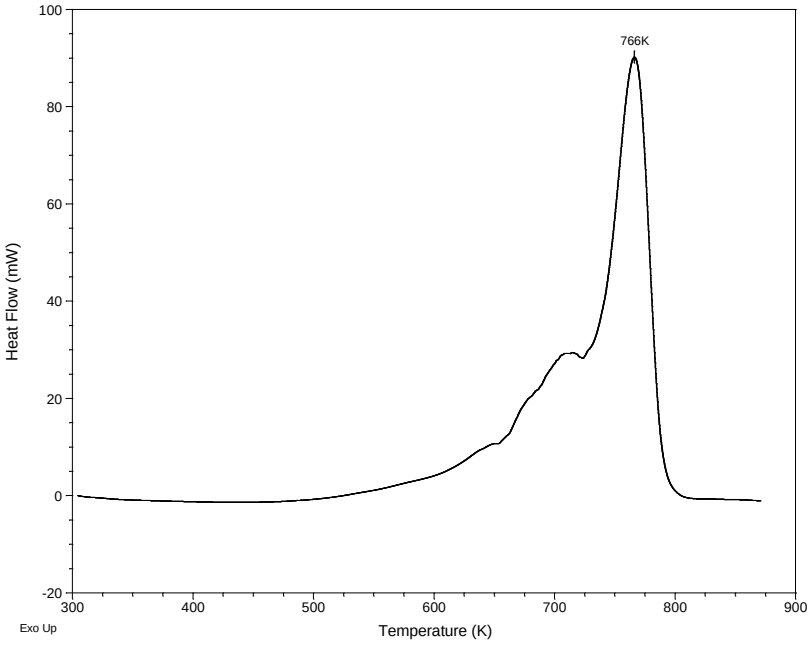

Figure B.II.11 - DSC Curve of Crude Oil 1 Resin at 10 °C/min

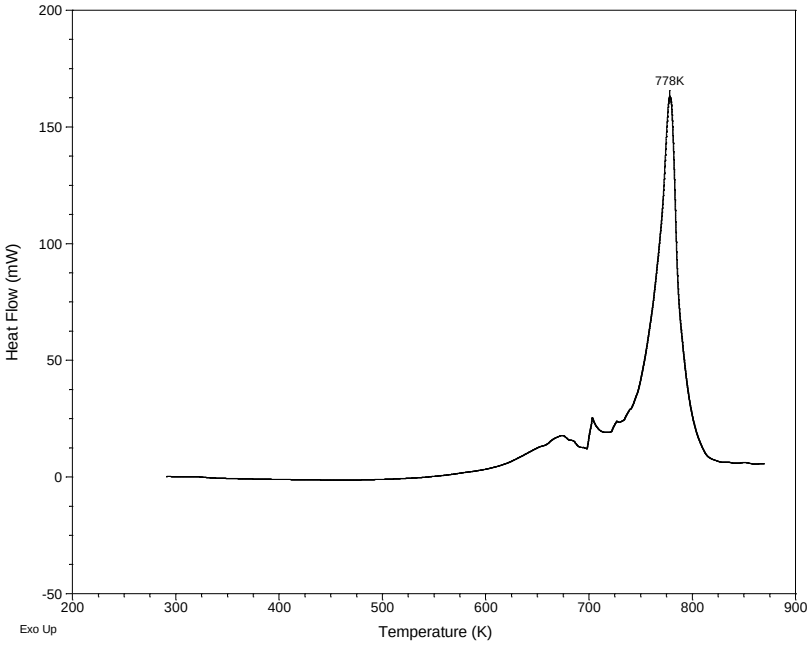

Figure B.II.12 - DSC Curve of Crude Oil 1 Resin at 15 °C/min

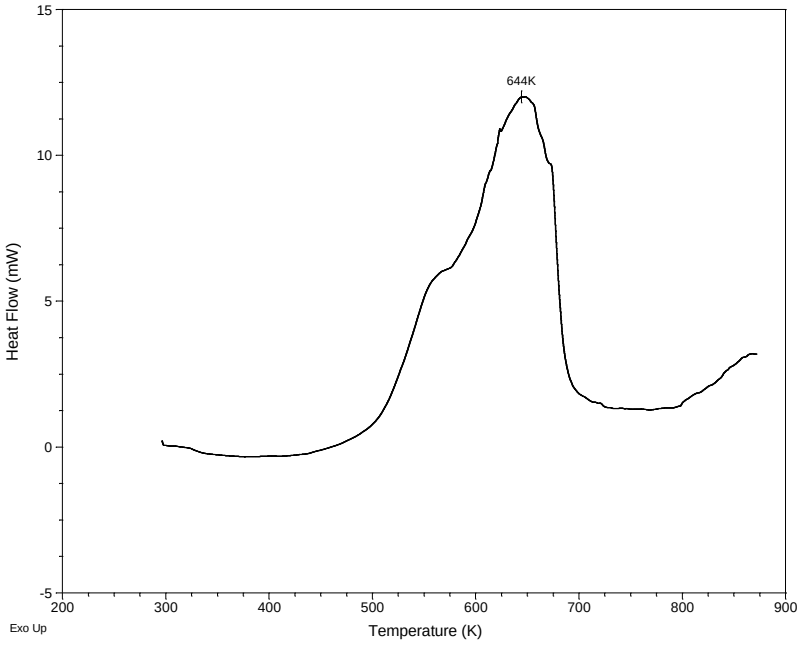

Figure B.II.13 - DSC Curve of Crude Oil 2 at 5 °C/min

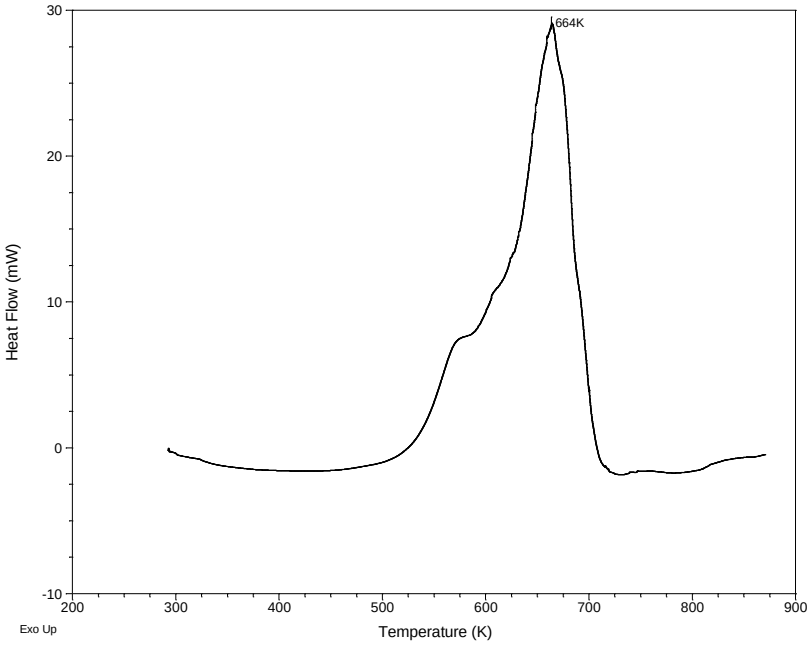

Figure B.II.14 - DSC Curve of Crude Oil 2 at 10 °C/min

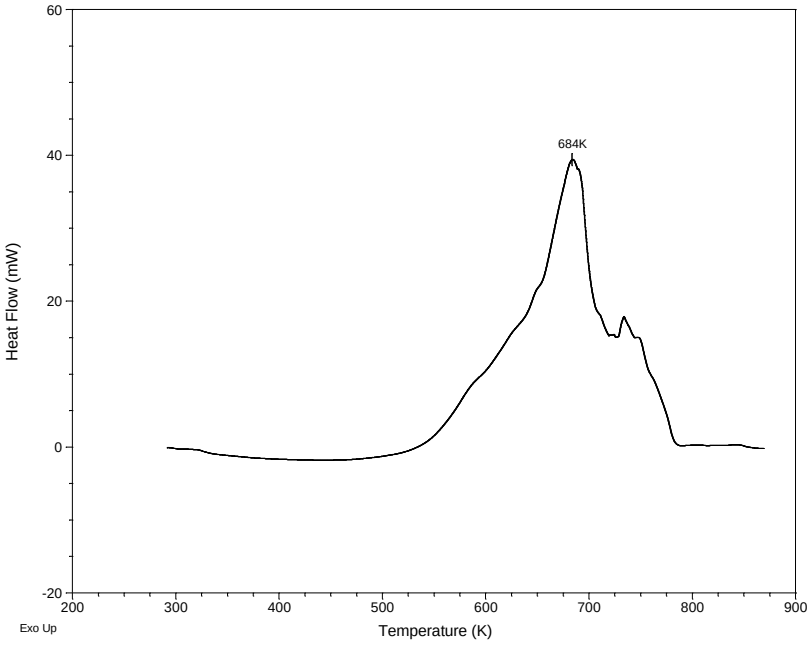

Figure B.II.15 - DSC Curve of Crude Oil 2 at 15 °C/min

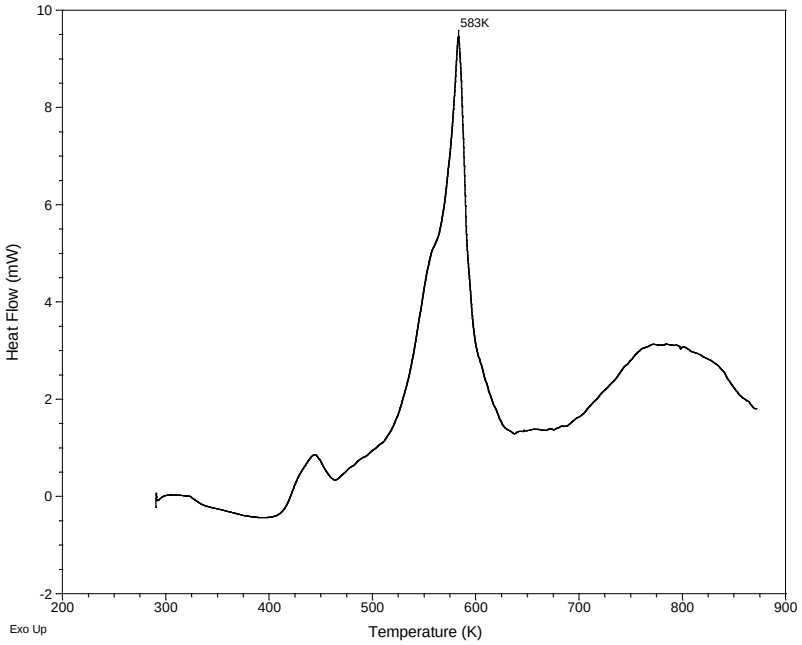

Figure B.II.16 - DSC Combustion Curve of Crude Oil 2 Saturate at 5 °C/min

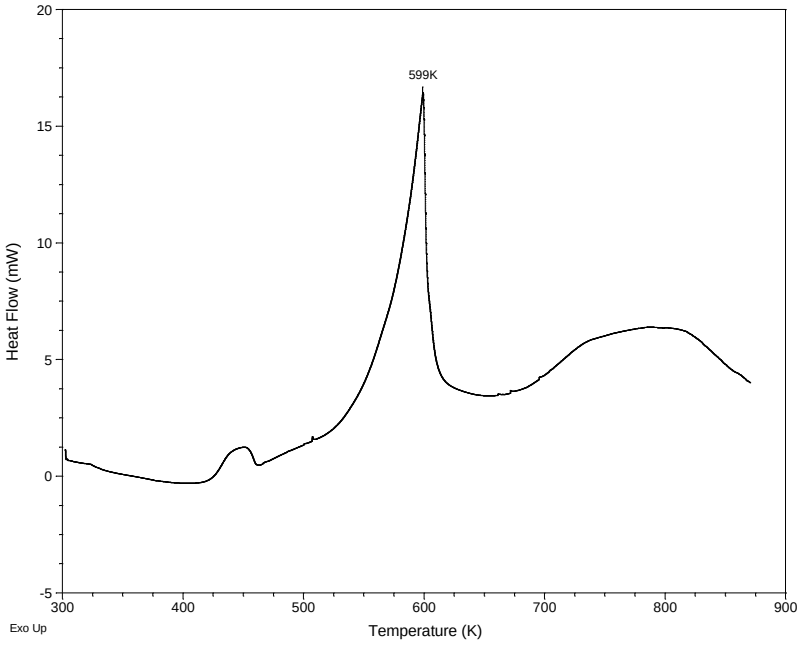

Figure B.II.17 - DSC Curve of Crude Oil 2 Saturate at 10 °C/min

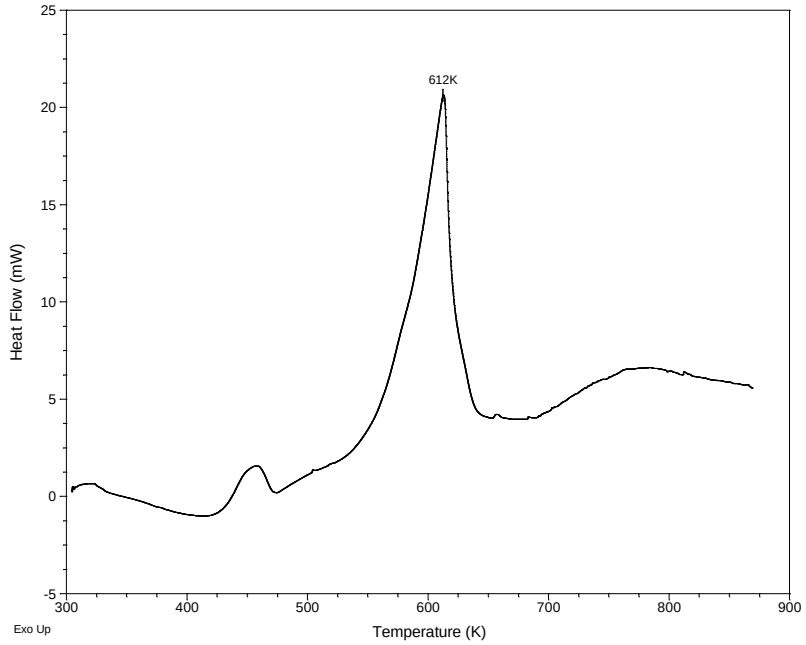

Figure B.II.18 - DSC Curve of Crude Oil 2 Saturate at 15 °C/min

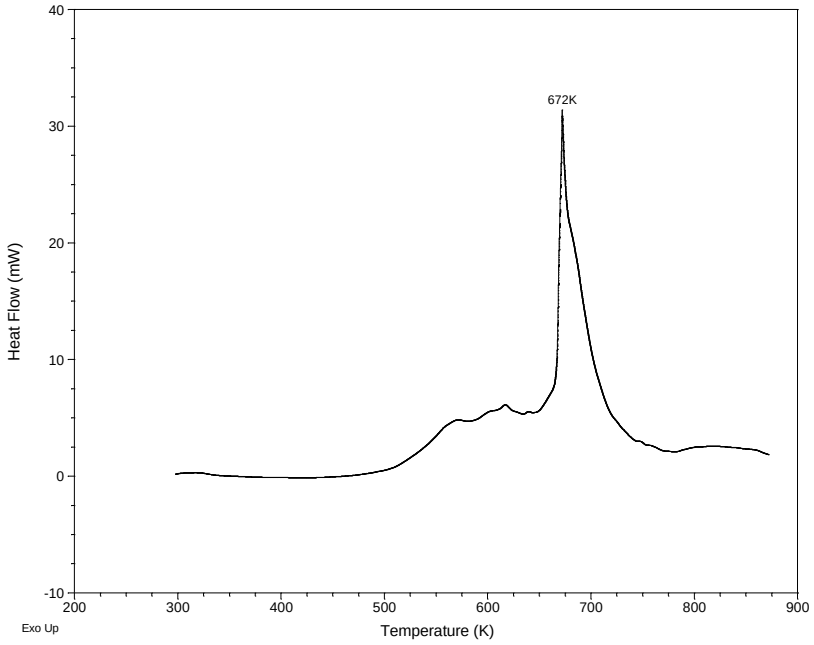

Figure B.II.19 - DSC Curve of Crude Oil 2 Aromatic at 5 °C/min

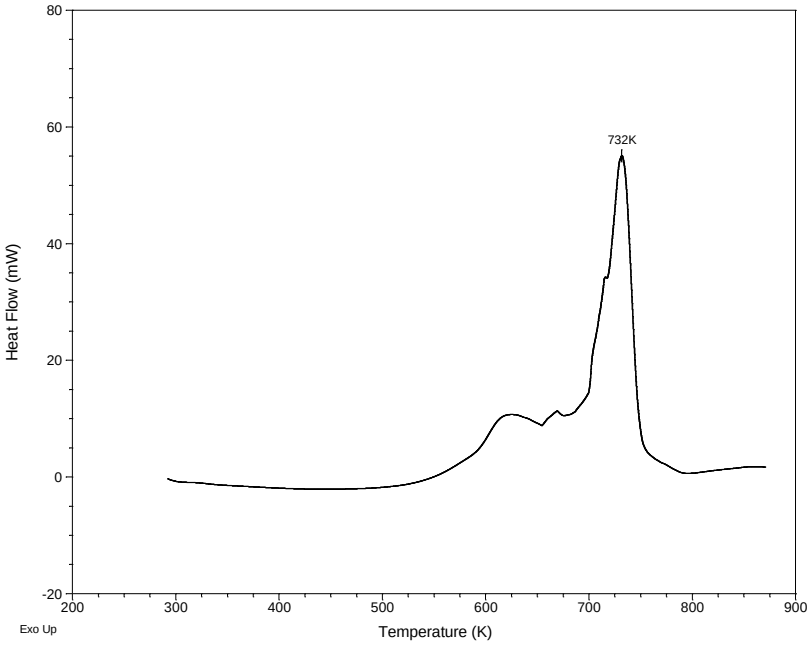

Figure B.II.20 - DSC Curve of Crude Oil 2 Aromatic at 10 °C/min

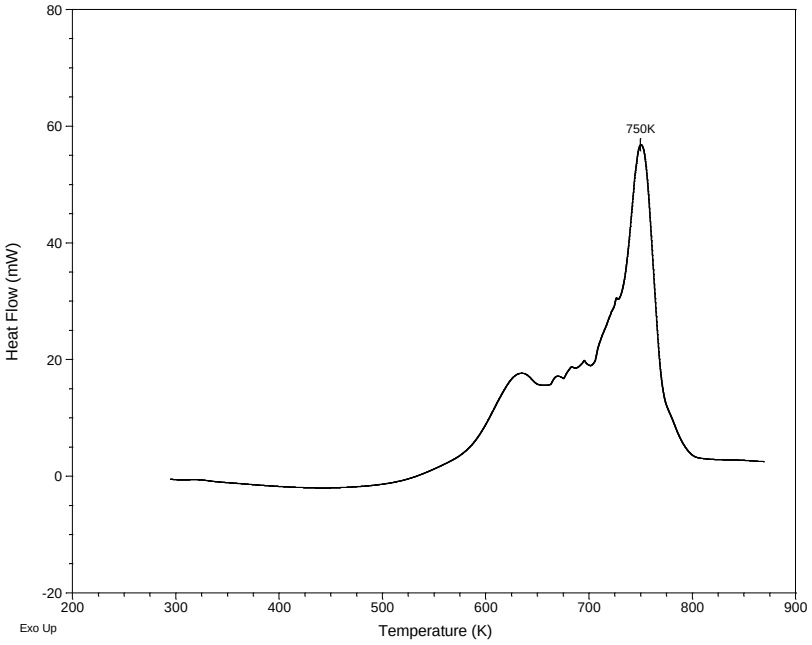

Figure B.II.21 - DSC Curve of Crude Oil 2 Aromatic at 15 °C/min

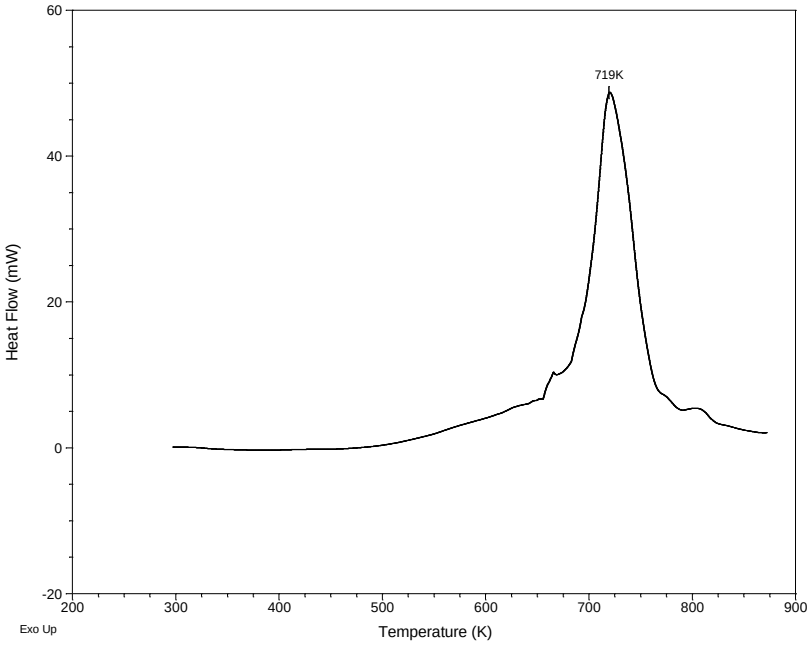

Figure B.II.22 - DSC Curve of Crude Oil 2 Resin at 5 °C/min

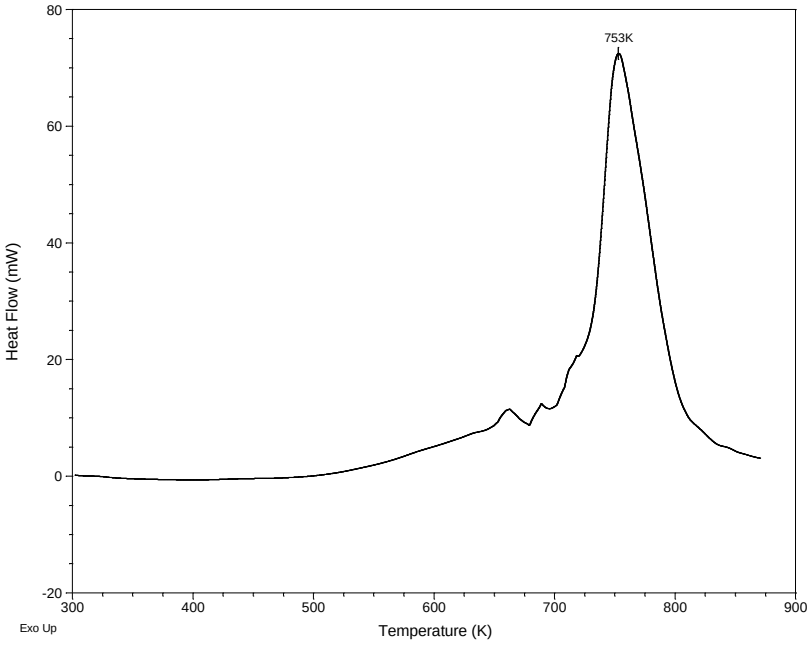

Figure B.II.23 - DSC Curve of Crude Oil 2 Resin at 10 °C/min

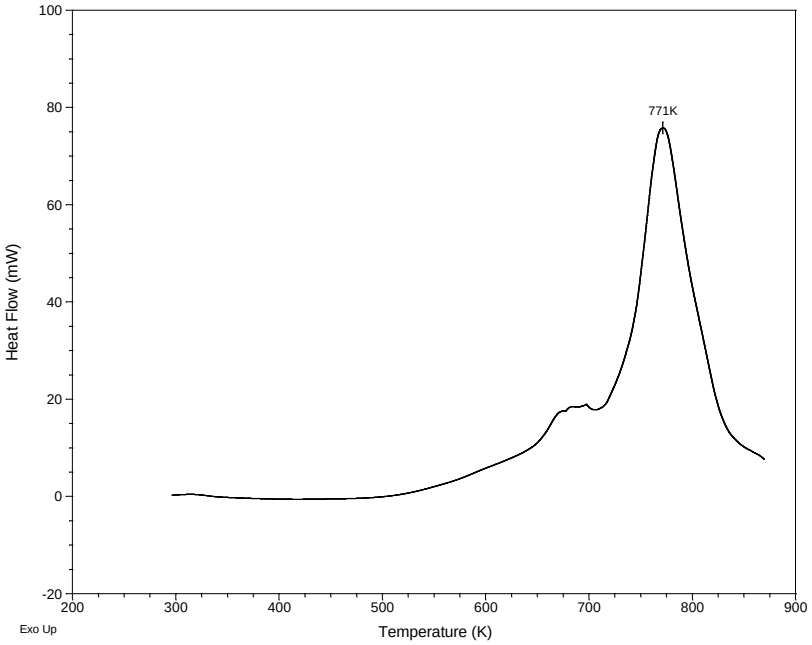

Figure B.II.24 - DSC Combustion Curve of Crude Oil 2 Resin at 15 °C/min

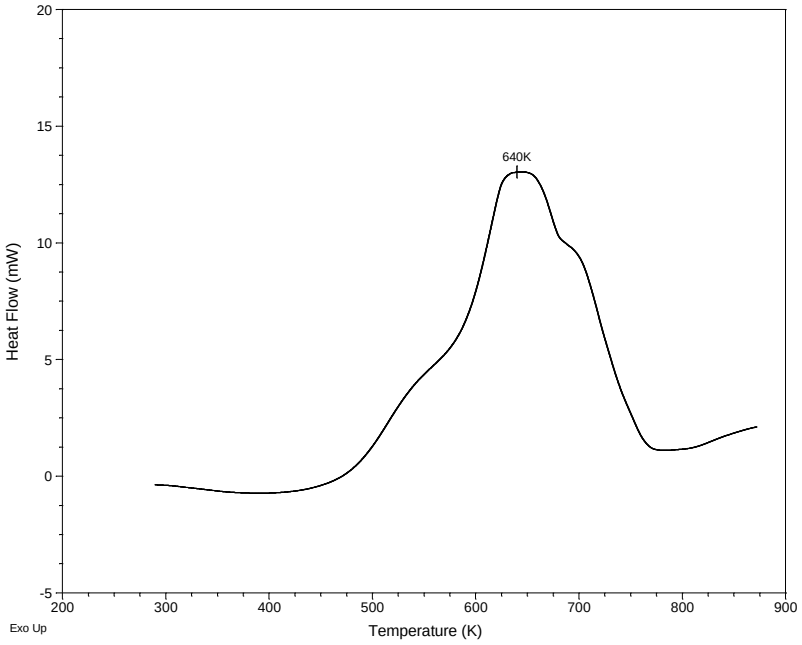

Figure B.II.25 - DSC Curve of Crude Oil 3 at 5 °C/min

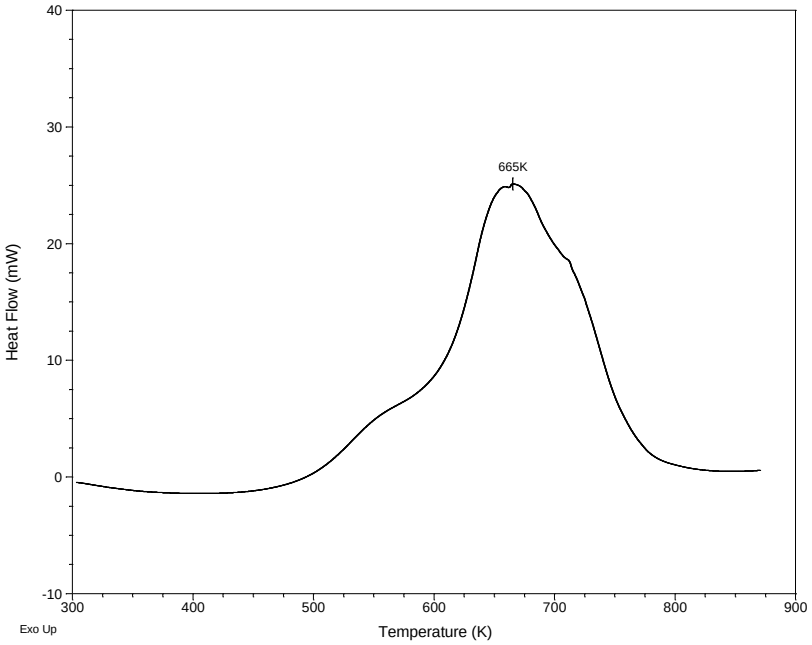

Figure B.II.26 - DSC Curve of Crude Oil 3 at 10 °C/min

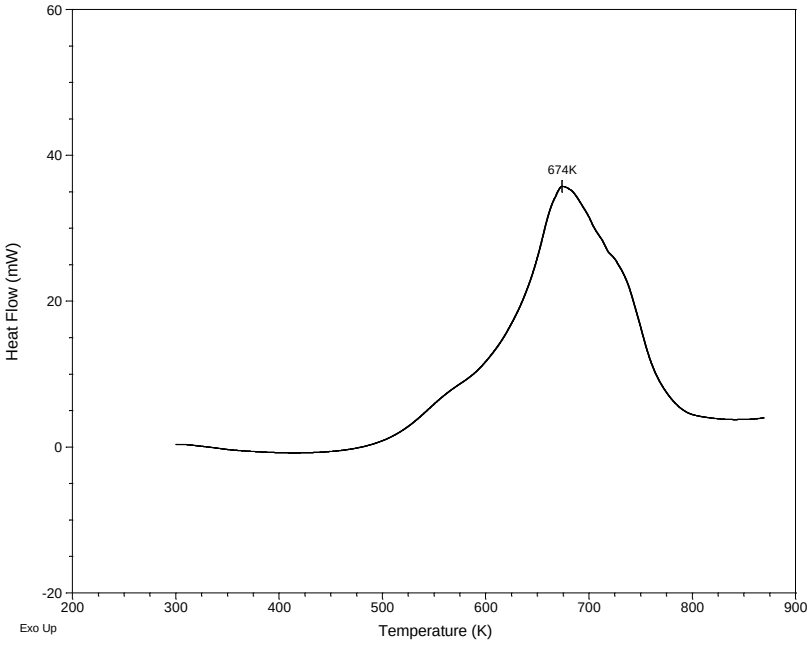

Figure B.II.27 - DSC Curve of Crude Oil 3 at 15 °C/min

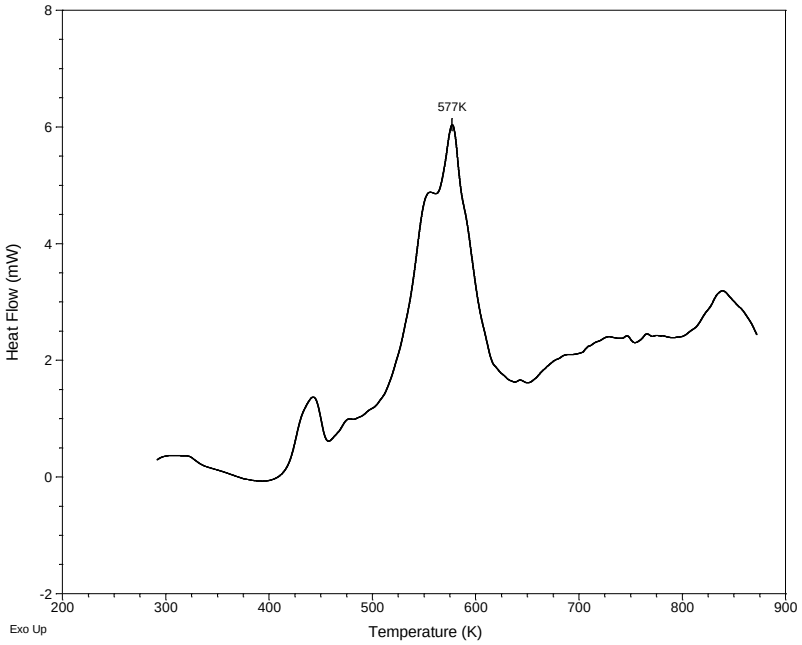

Figure B.II.28 - DSC Curve of Crude Oil 3 Saturate at 5 °C/min

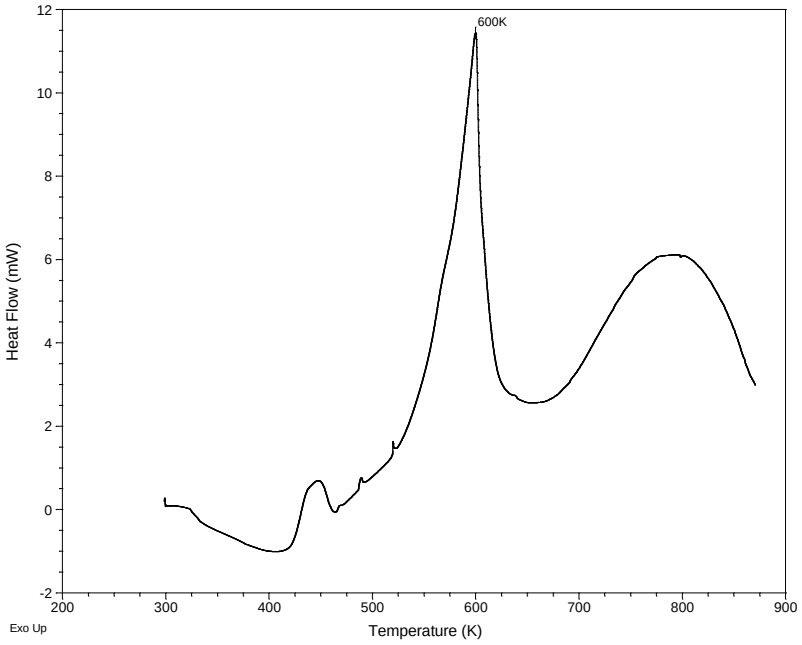

Figure B.II.29 - DSC Curve of Crude Oil 3 Saturate at 10 °C/min

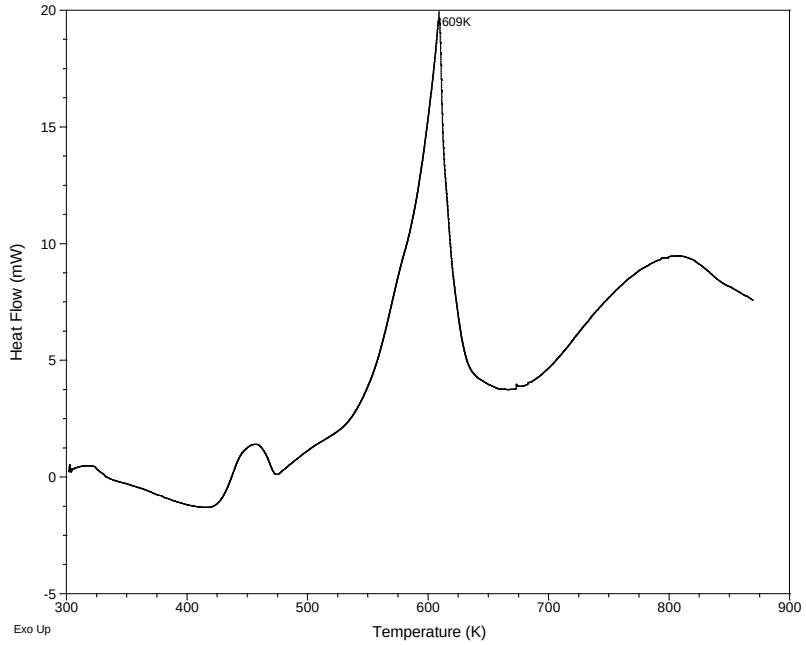

Figure B.II.30 - DSC Curve of Crude Oil 3 Saturate at 15 °C/min

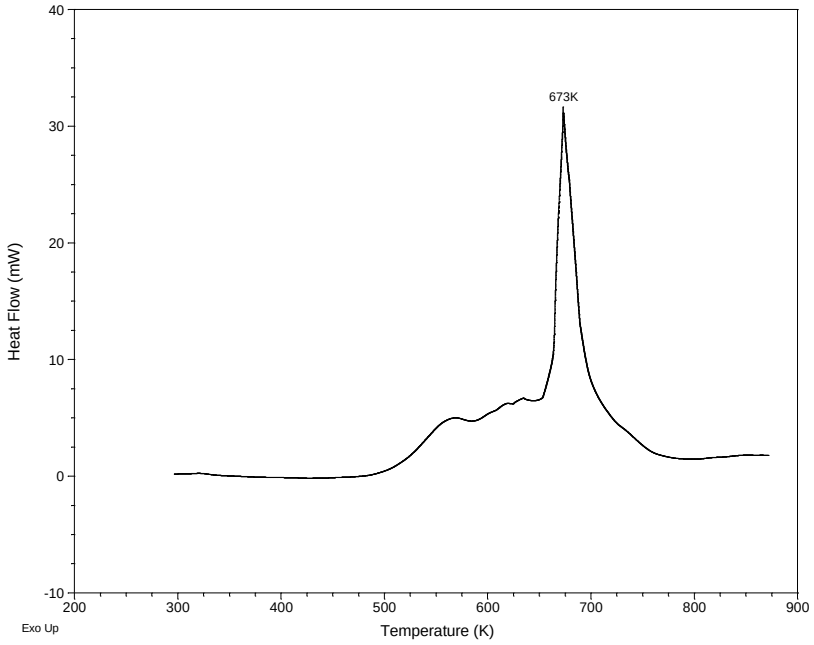

Figure B.II.31 - DSC Curve of Crude Oil 3 Aromatic at 5 °C/min

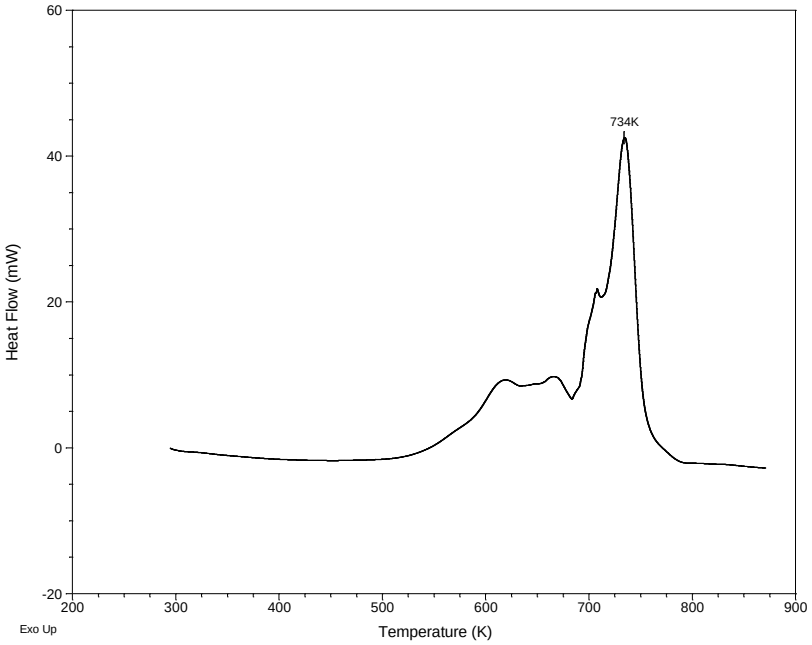

Figure B.II.32 - DSC Curve of Crude Oil 3 Aromatic at 10 °C/min

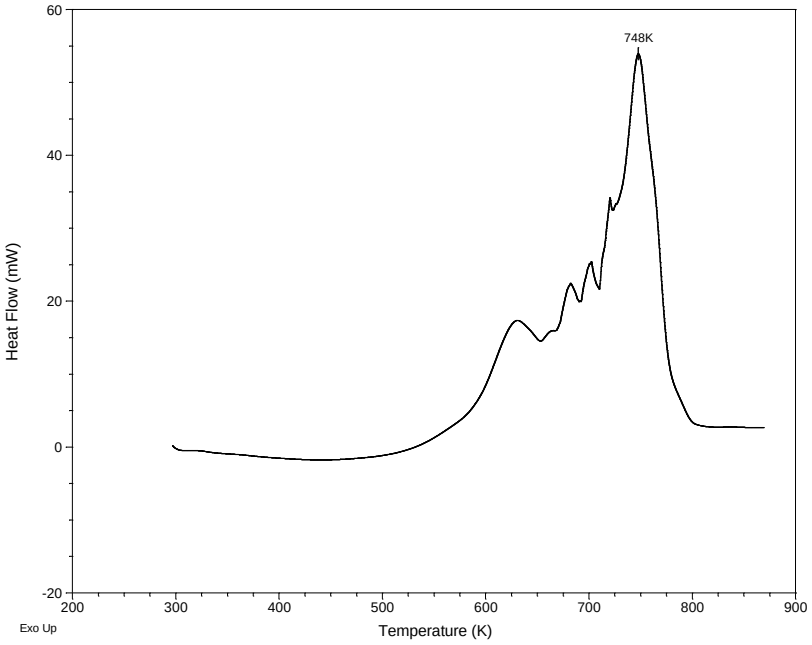

Figure B.II.33 - DSC Curve of Crude Oil 3 Aromatic at 15 °C/min

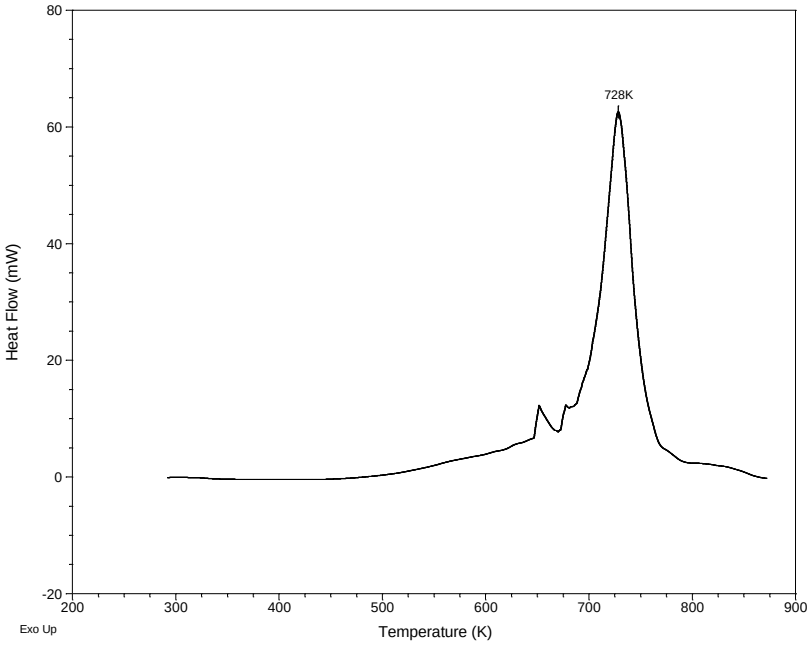

Figure B.II.34 - DSC Curve of Crude Oil 3 Resin at 5 °C/min

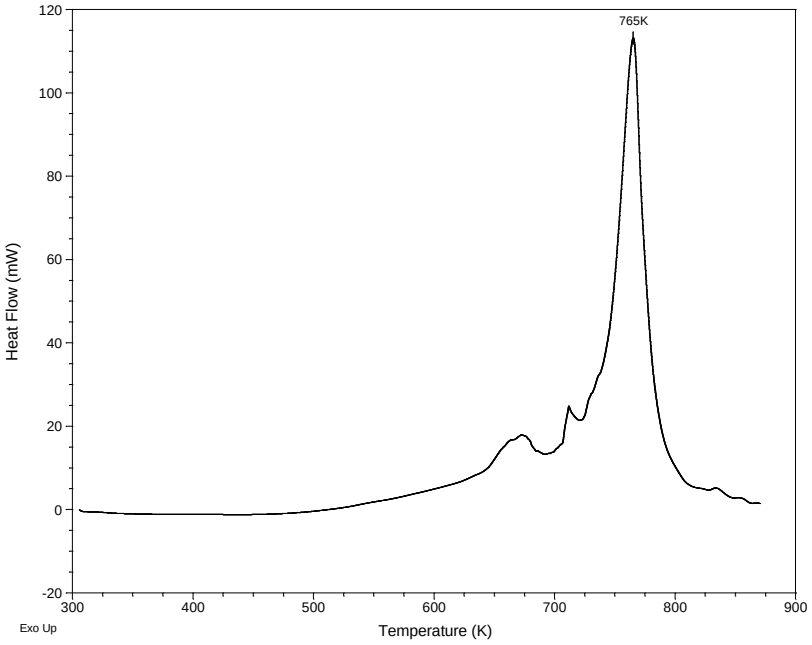

Figure B.II.35 - DSC Curve of Crude Oil 3 Resin at 10 °C/min

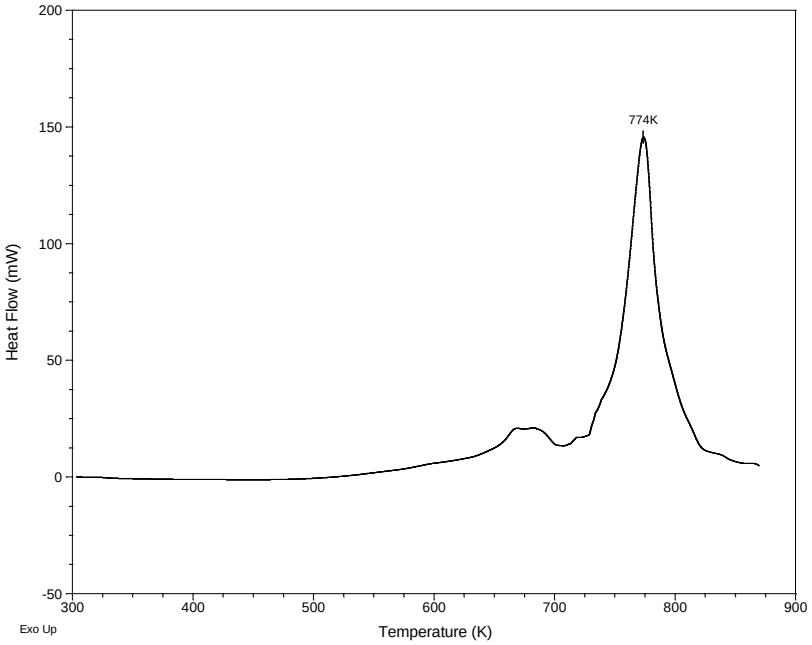

Figure B.II.36 - DSC Curve of Crude Oil 3 Resin at 15 °C/min

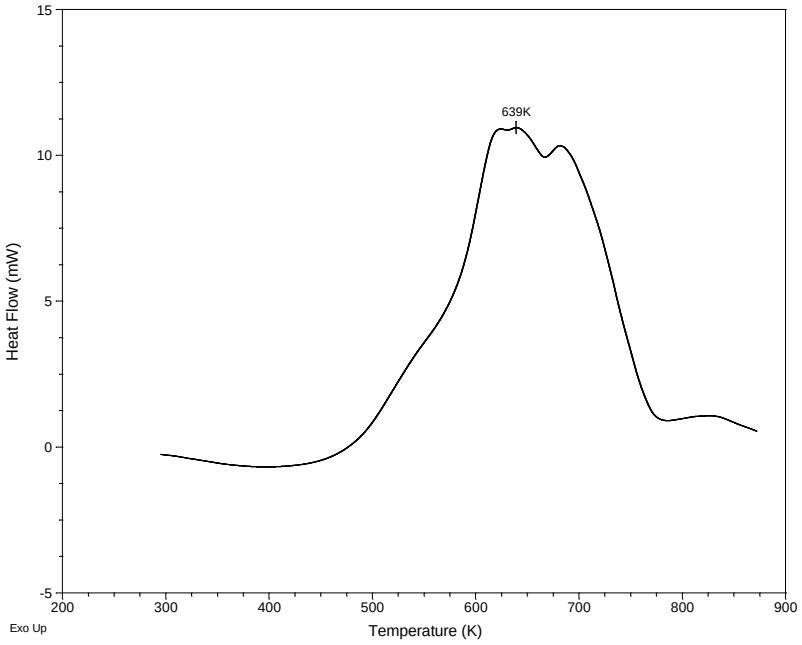

Figure B.II.37 - DSC Curve of Crude Oil 4 at 5 °C/min

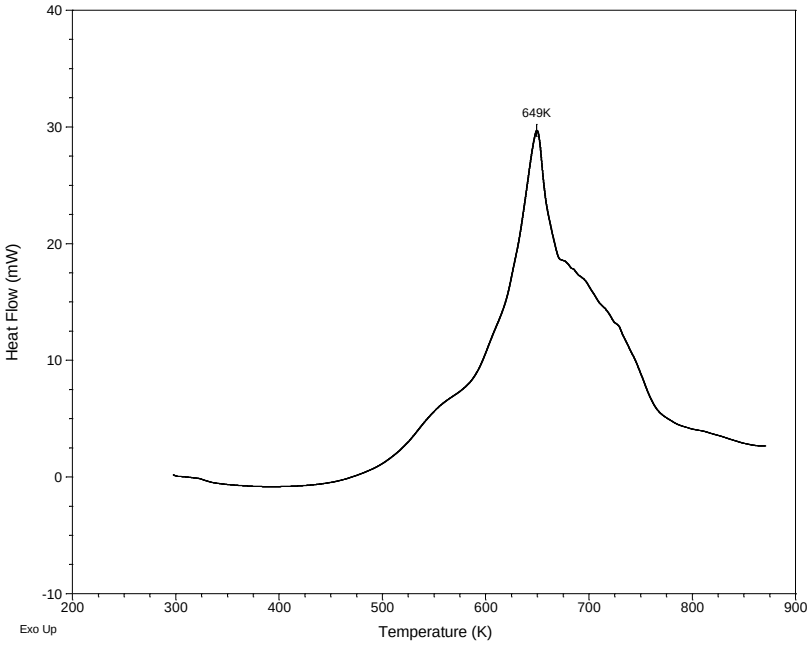

Figure B.II.38 - DSC Curve of Crude Oil 4 at 10 °C/min

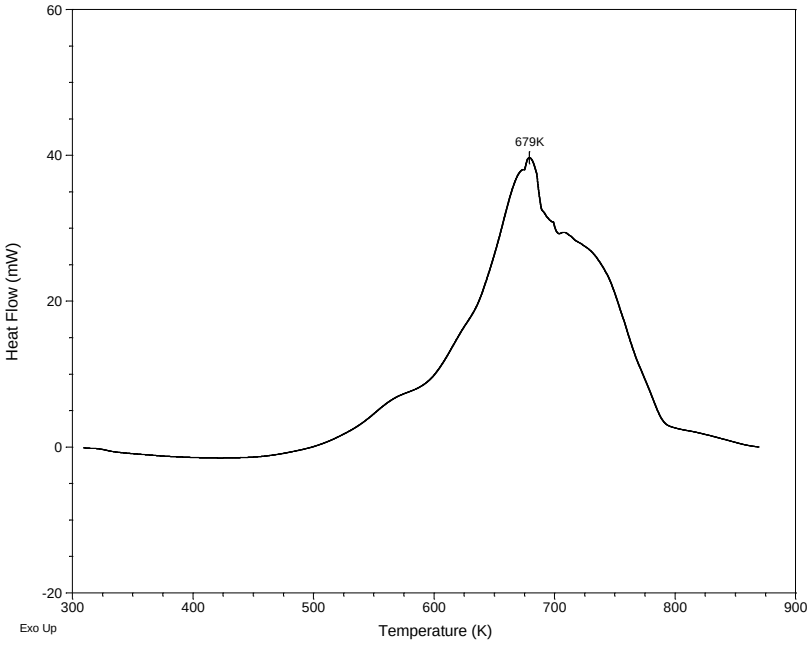

Figure B.II.39 - DSC Curve of Crude Oil 4 at 15 °C/min

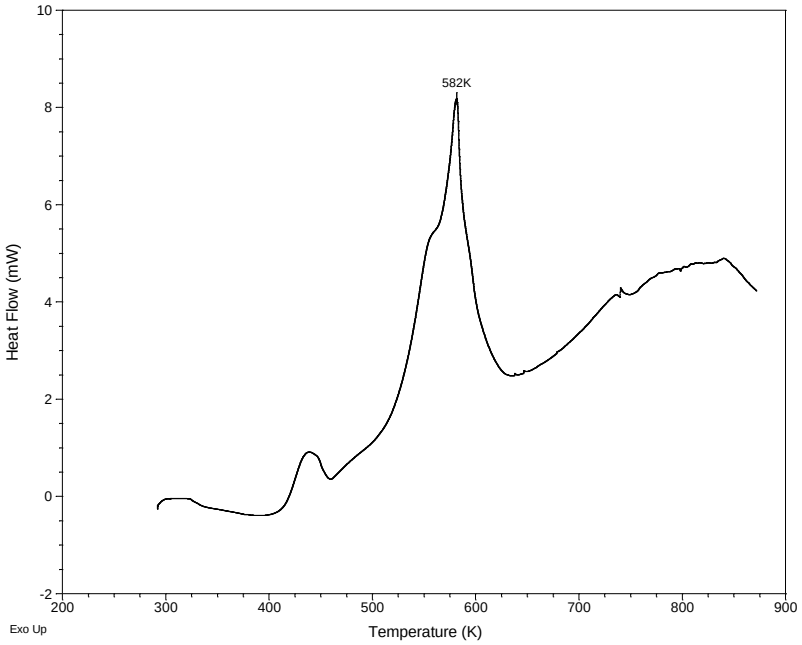

Figure B.II.40 - DSC Curve of Crude Oil 4 Saturate at 5 °C/min

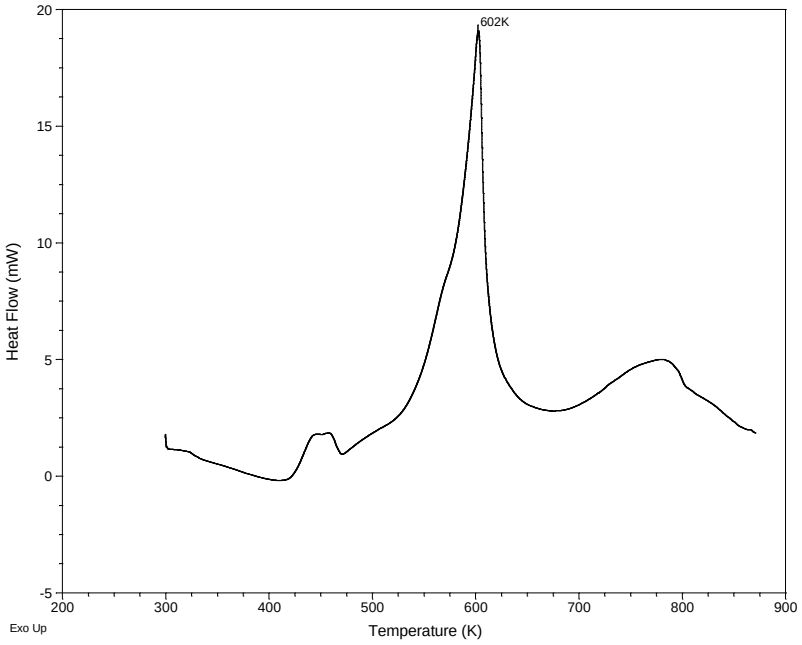

Figure B.II.41 - DSC Curve of Crude Oil 4 Saturate at 10 °C/min

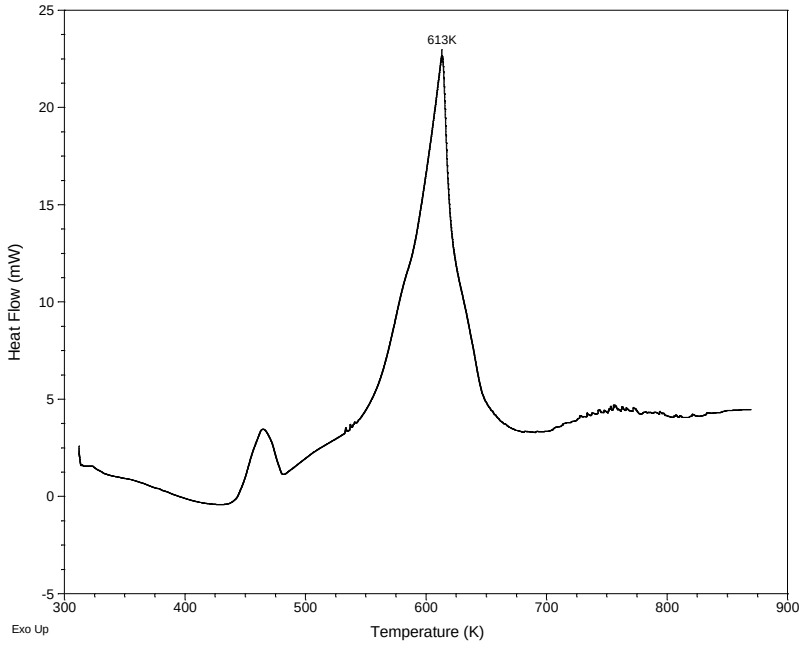

Figure B.II.42 - DSC Curve of Crude Oil 4 Saturate at 15 °C/min

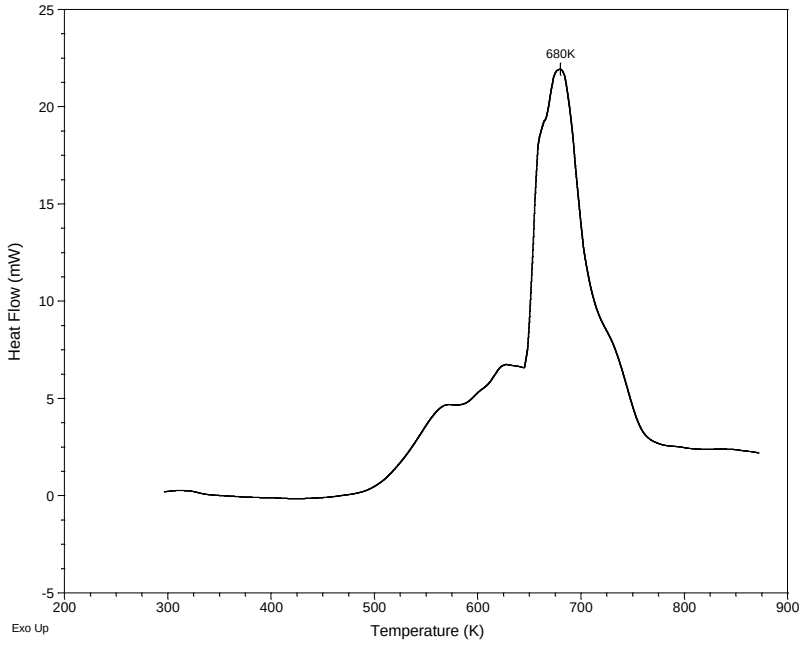

Figure B.II.43 - DSC Curve of Crude Oil 4 Aromatic at 5 °C/min

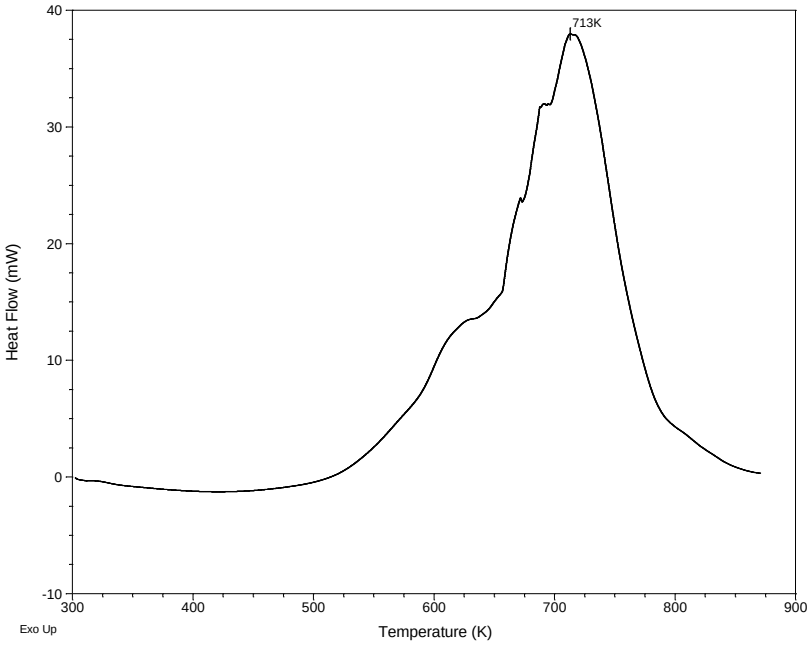

Figure B.II.44 - DSC Curve of Crude Oil 4 Aromatic at 10 °C/min

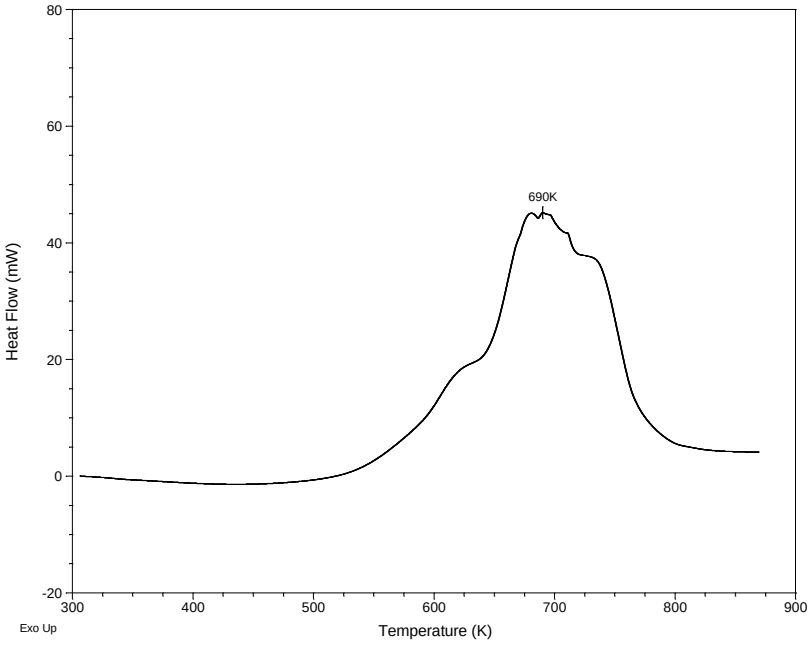

Figure B.II.45 - DSC Curve of Crude Oil 4 Aromatic at 15 °C/min

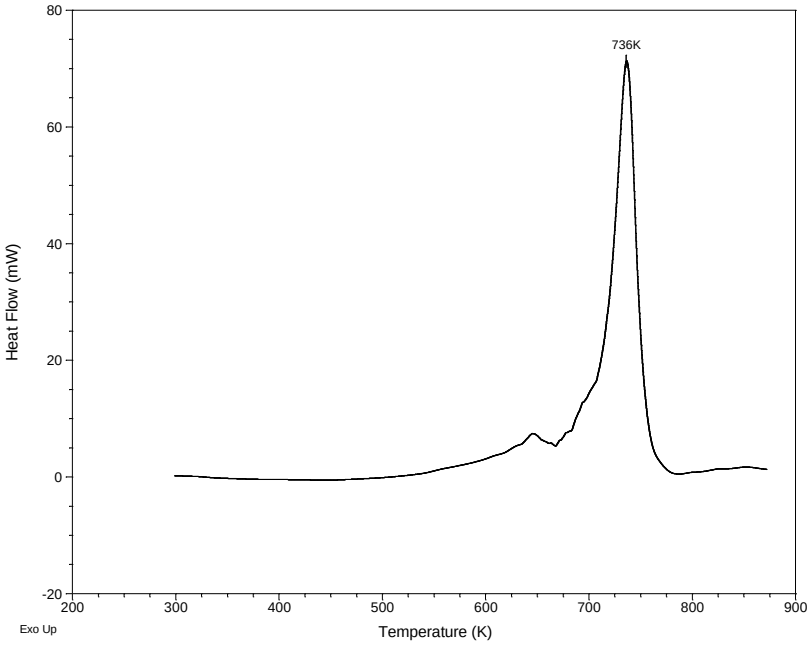

Figure B.II.46 - DSC Curve of Crude Oil 4 Resin at 5 °C/min

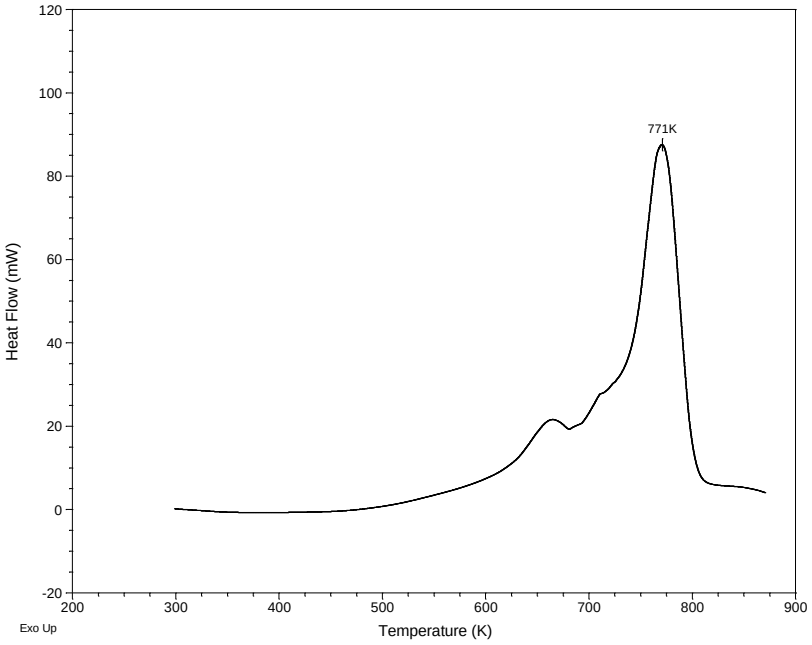

Figure B.II.47 - DSC Curve of Crude Oil 4 Resin at 10 °C/min

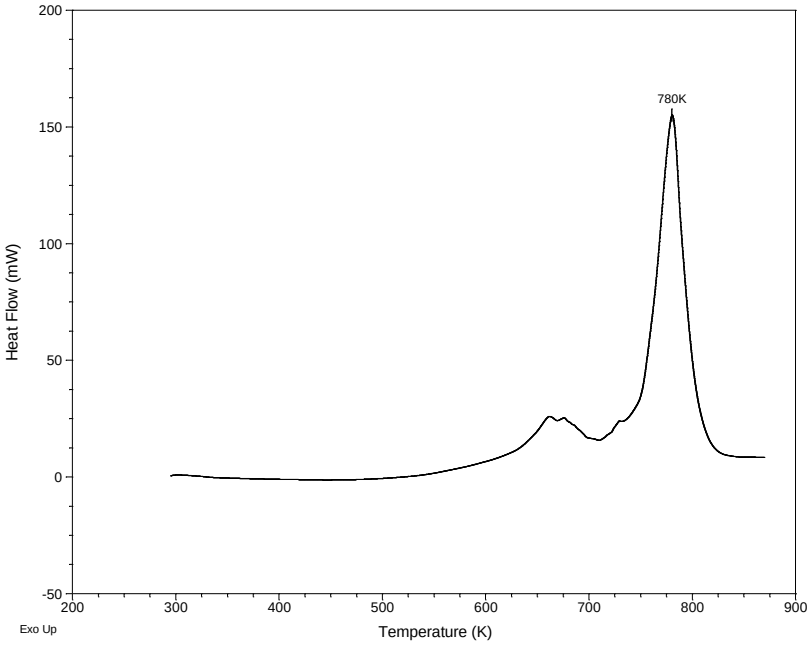

Figure B.II.48 - DSC Curve of Crude Oil 4 Resin at 15 °C/min

APPENDIX C

PLOTS OF ISOCONVERSIONAL METHODS

C.I. Plots of OFW Method

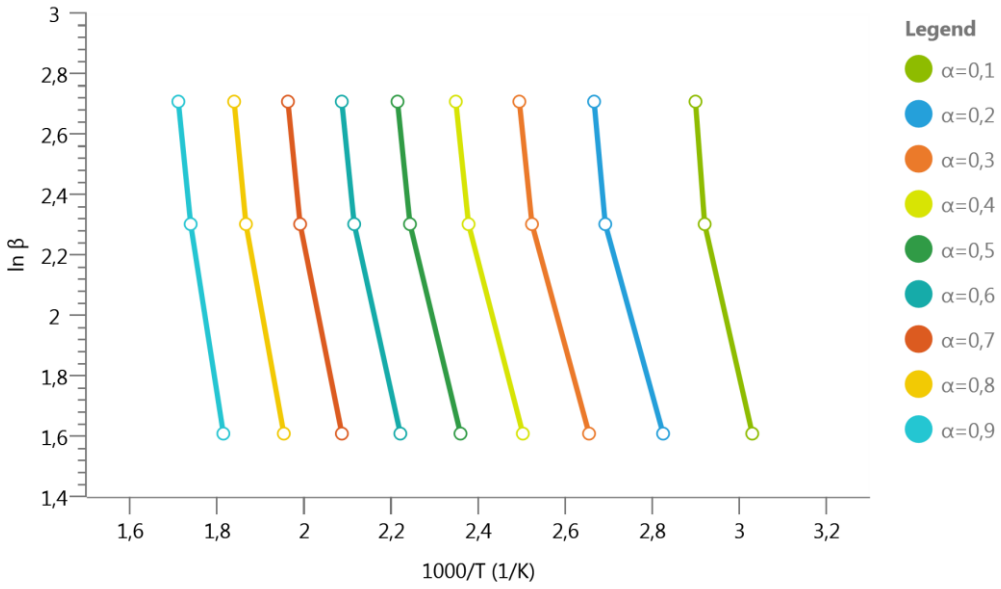

Figure C.I.1 - OFW plot of Crude Oil 1 for I. Region

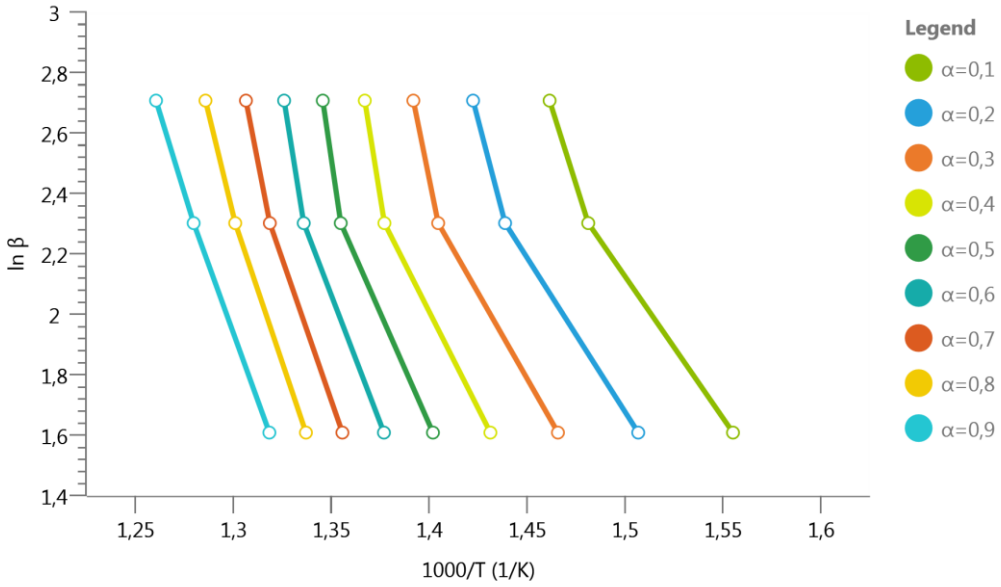

Figure C.I.2 - OFW plot of Crude Oil 1 for II. Region

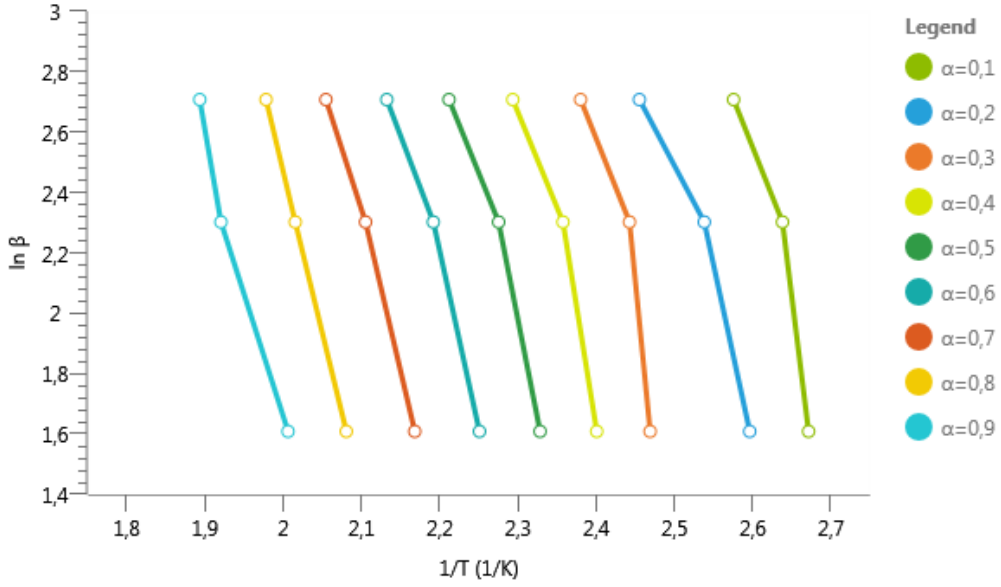

Figure C.I.3 - OFW plot of Crude Oil 1 Saturate for I. Region

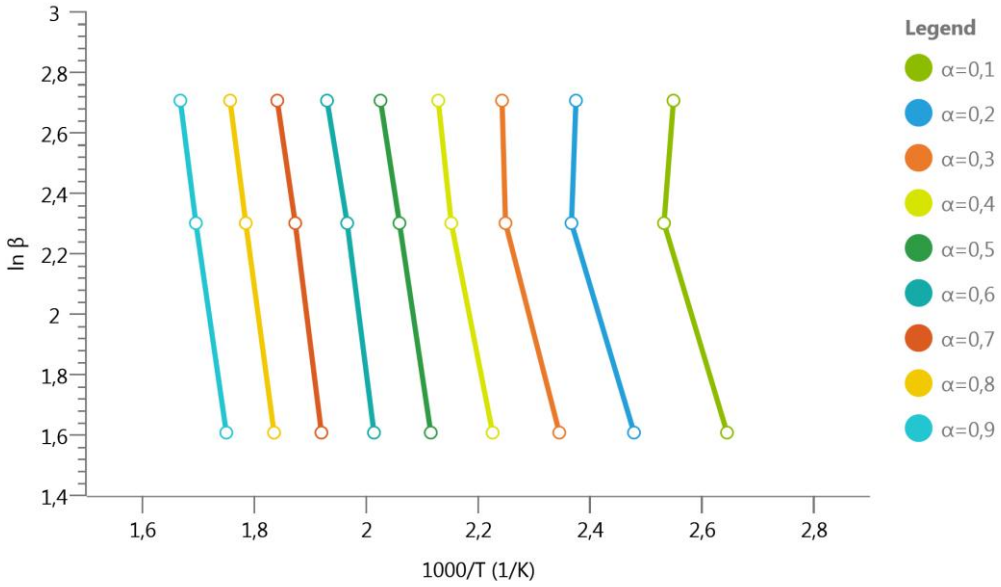

Figure C.I.4 - OFW plot of Crude Oil 1 Aromatic for I. Region

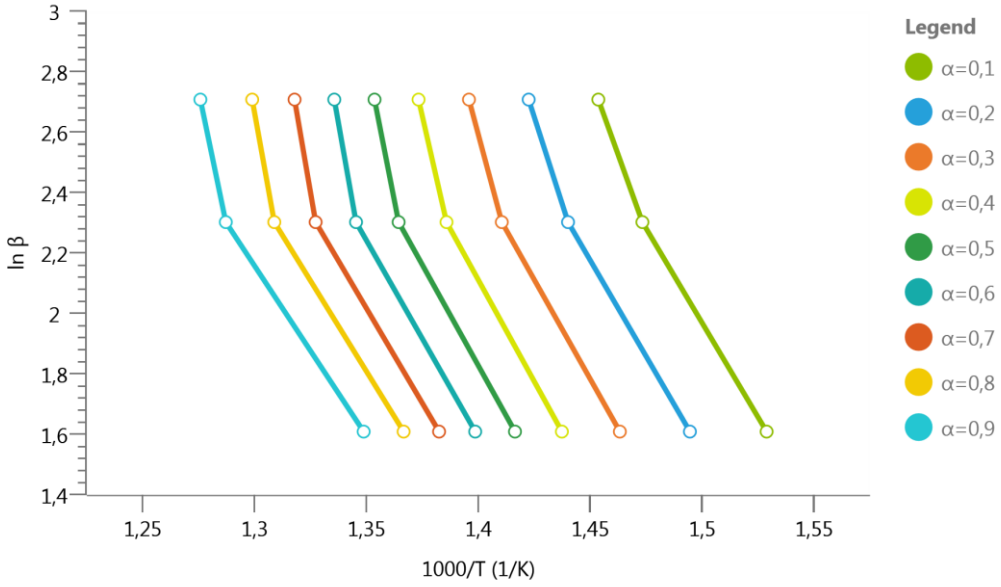

Figure C.I.5 - OFW plot of Crude Oil 1 Aromatic for II. Region

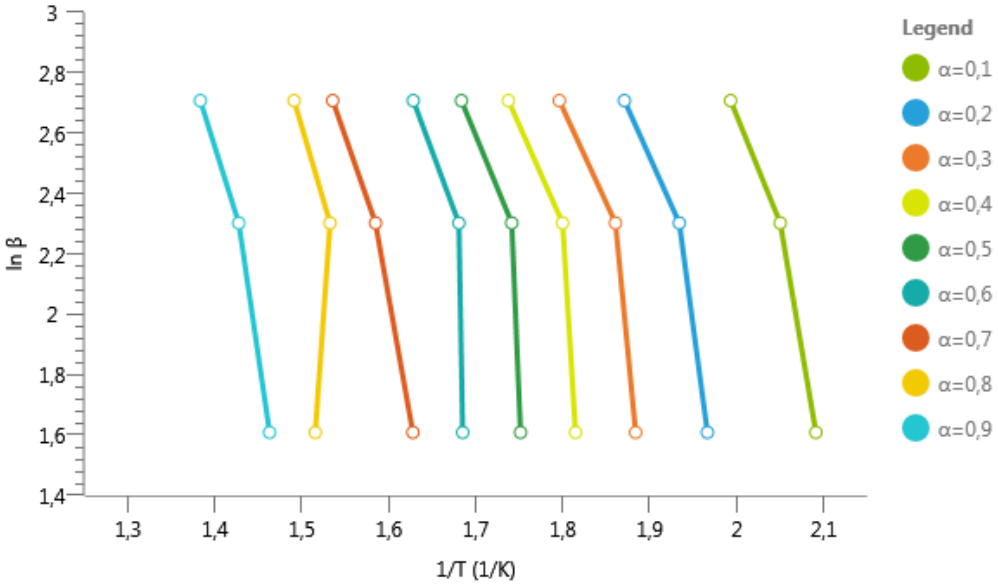

Figure C.I.6 - OFW plot of Crude Oil 1 Resin for I. Region

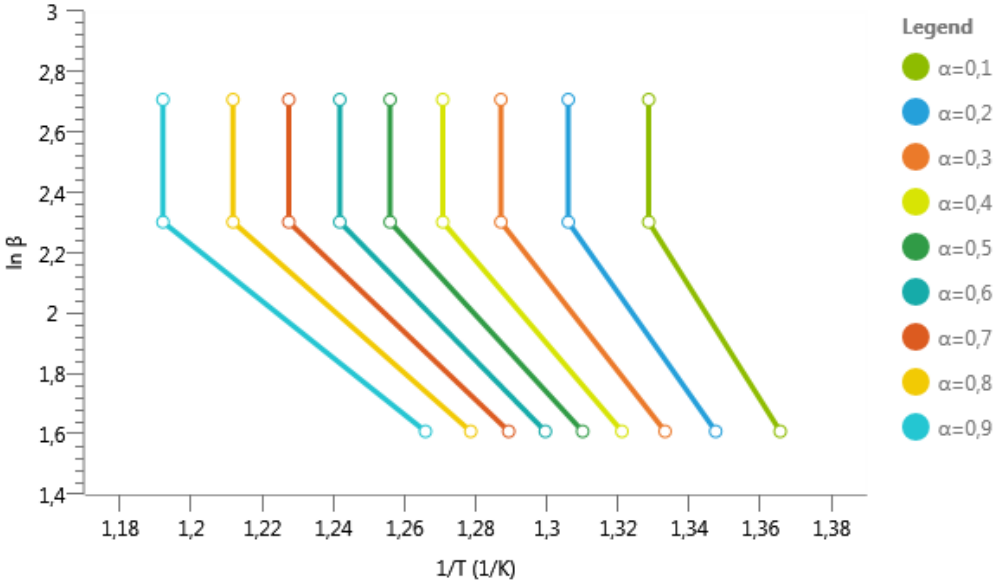

Figure C.I.7 - OFW plot of Crude Oil 1 Resin for II. Region

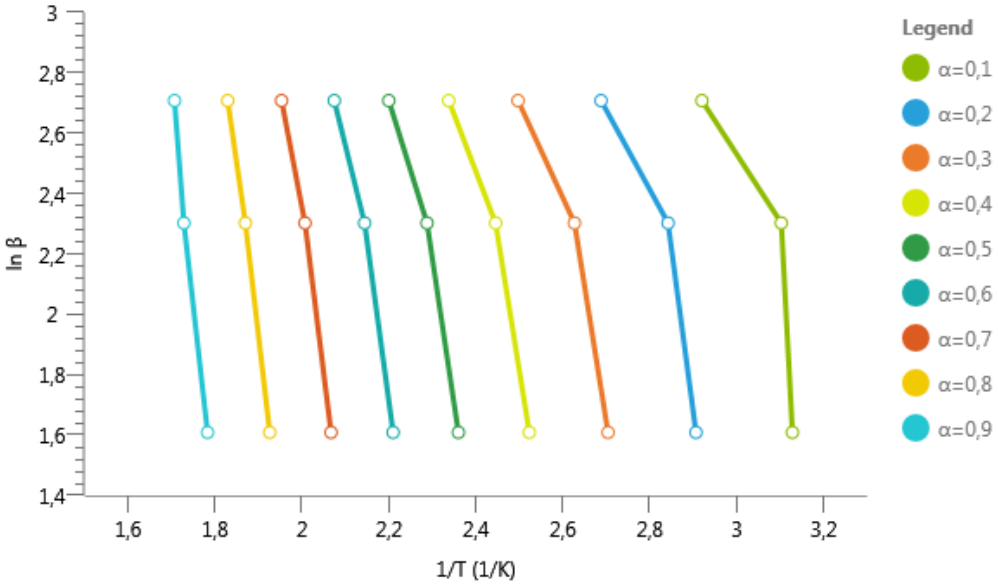

Figure C.I.8 - OFW plot of Crude Oil 2 for I. Region

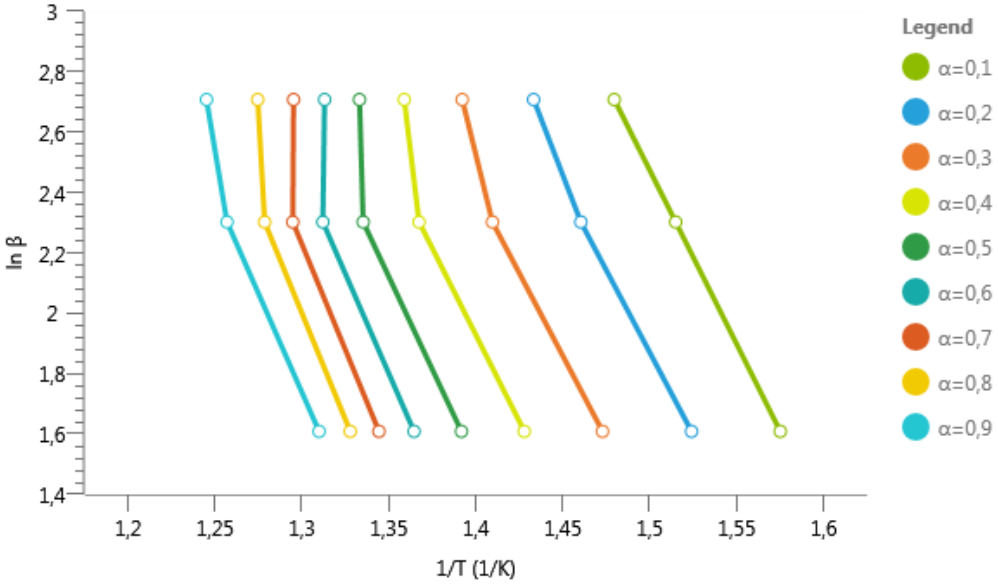

Figure C.I.9 - OFW plot of Crude Oil 2 for II. Region

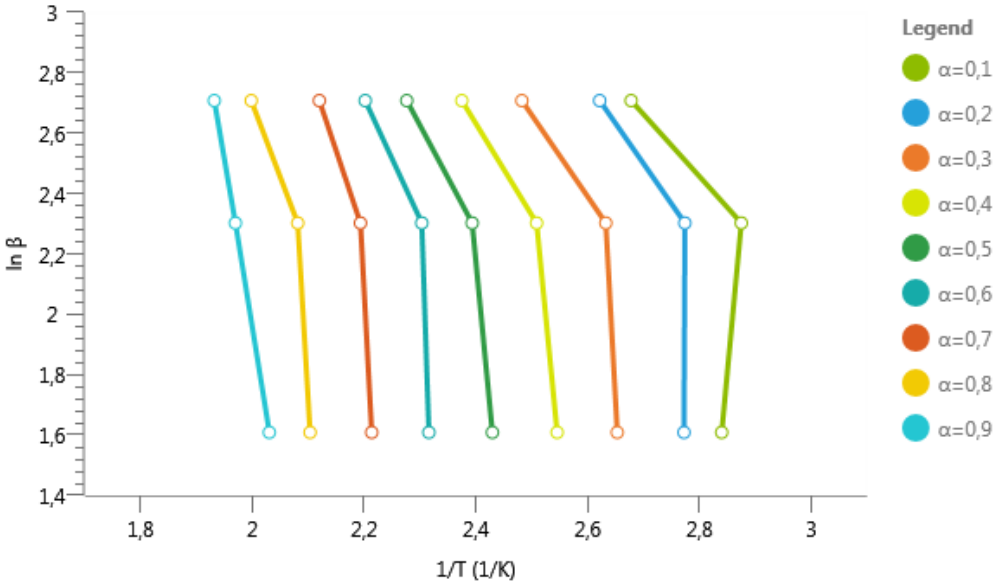

Figure C.I.10 - OFW plot of Crude Oil 2 Saturate for I. Region

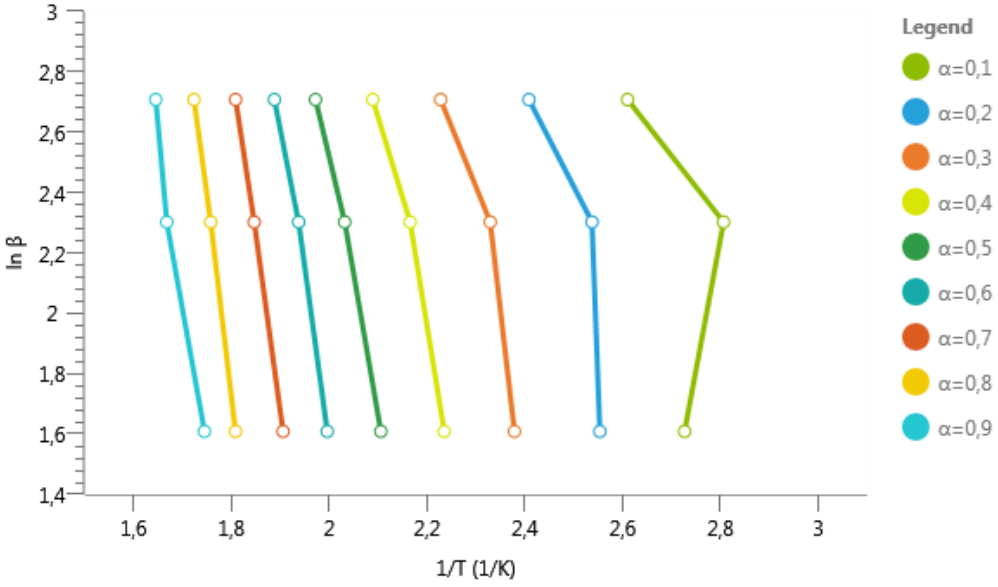

Figure C.I.11 - OFW plot of Crude Oil 2 Aromatic for I. Region

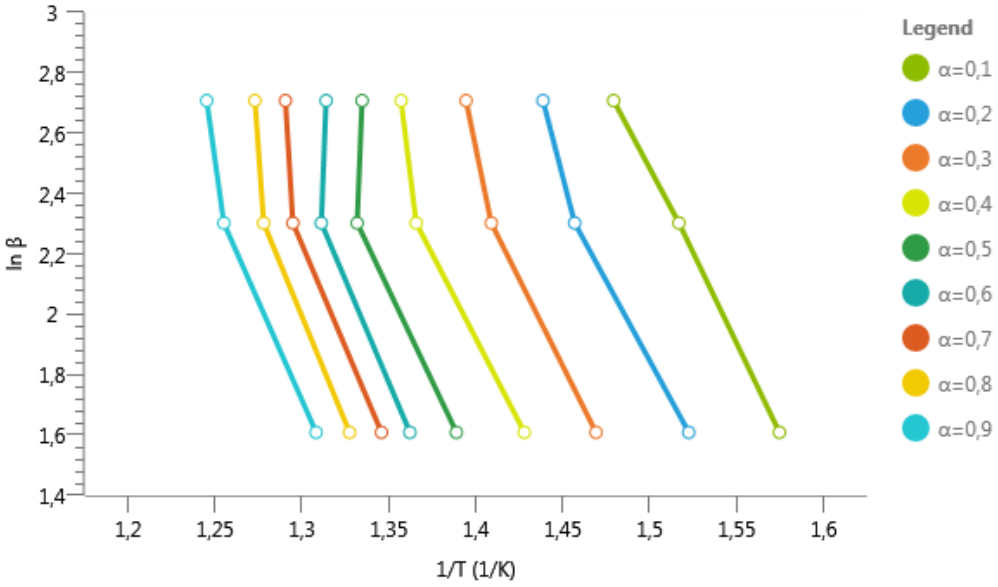

Figure C.I.12 - OFW plot of Crude Oil 2 Aromatic for II. Region

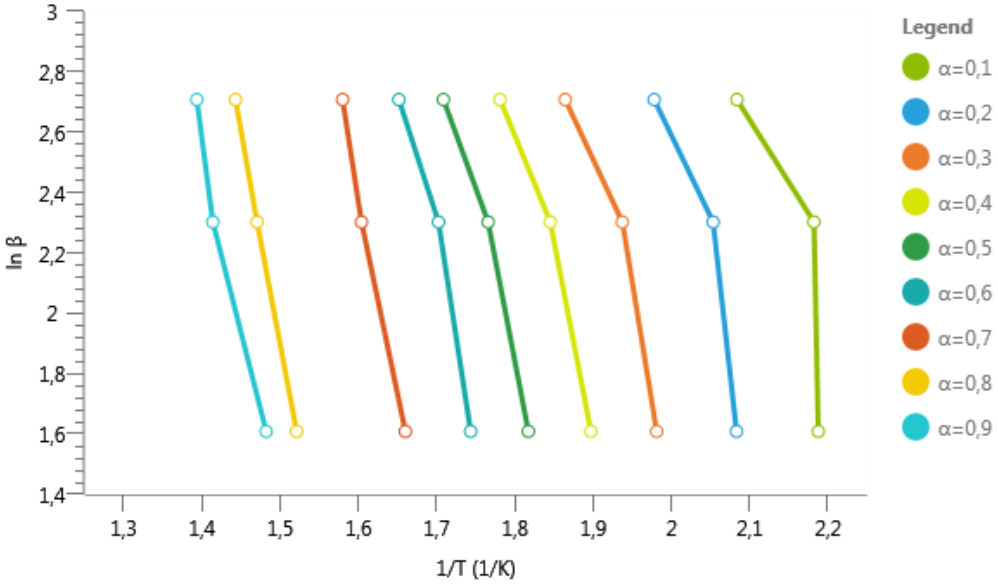

Figure C.I.13 - OFW plot of Crude Oil 2 Resin for I. Region

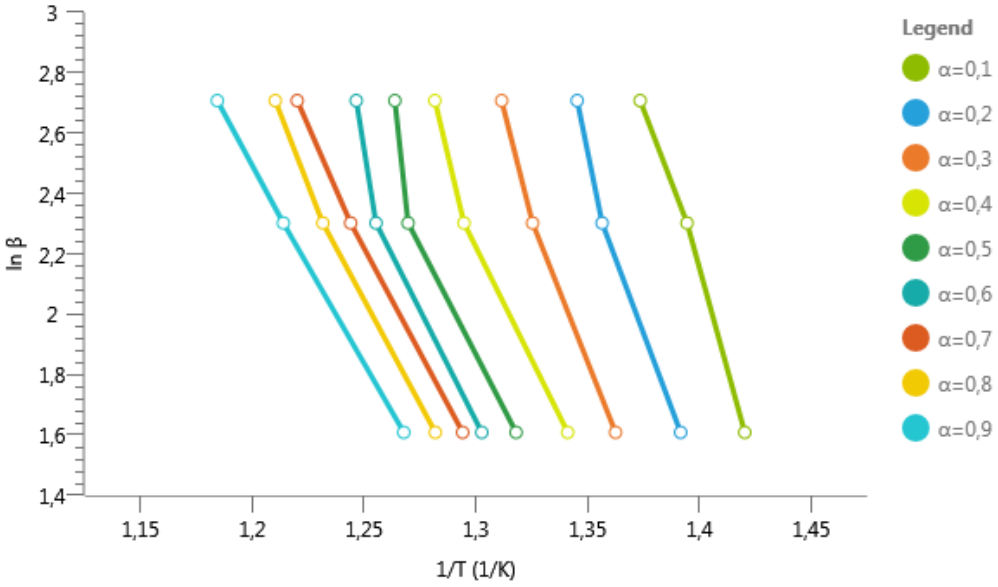

Figure C.I.14 - OFW plot of Crude Oil 2 Resin for II. Region

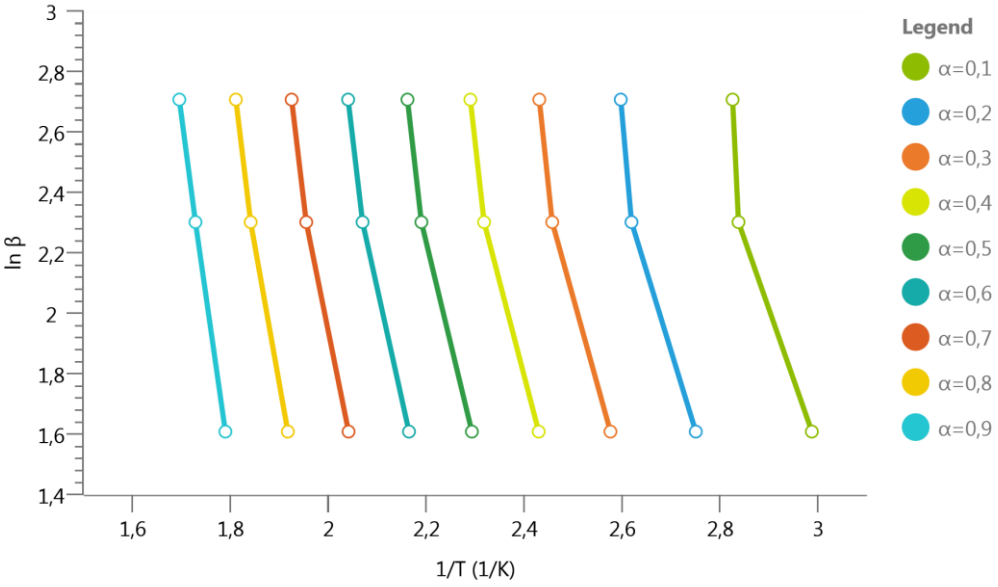

Figure C.I.15 - OFW plot of Crude Oil 3 for I. Region

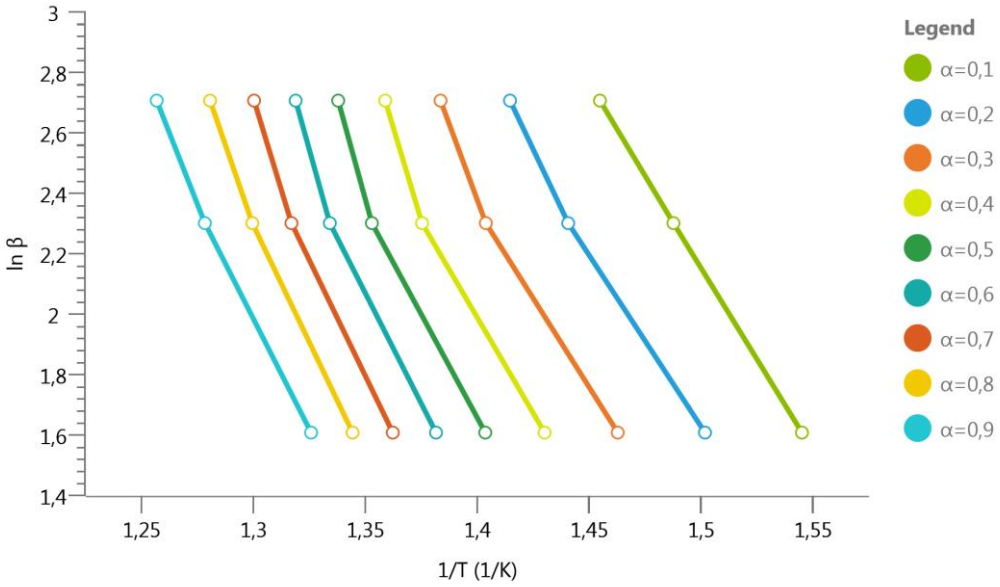

Figure C.I.16 - OFW plot of Crude Oil 3 for II. Region

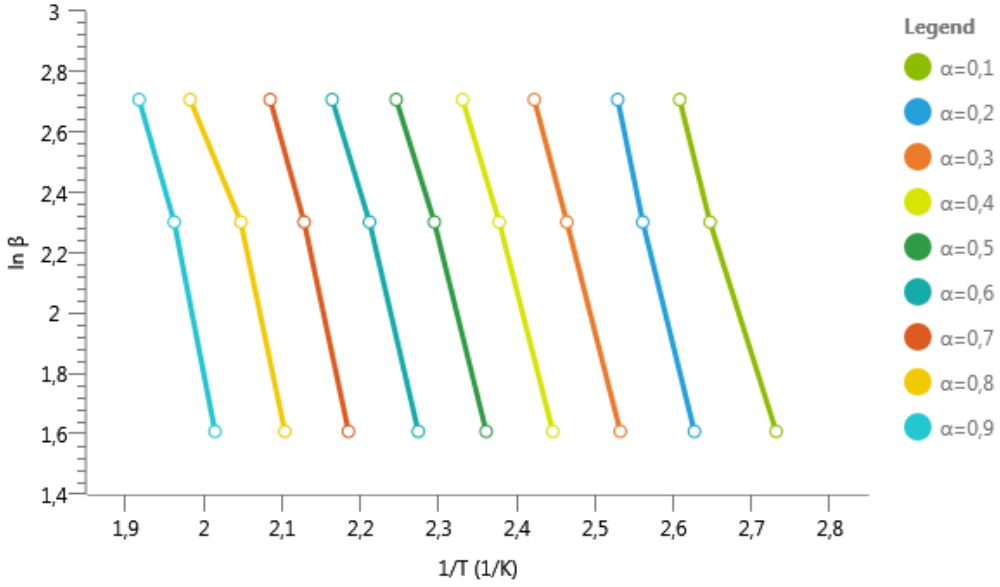

Figure C.I.17 - OFW plot of Crude Oil 3 Saturate for I. Region

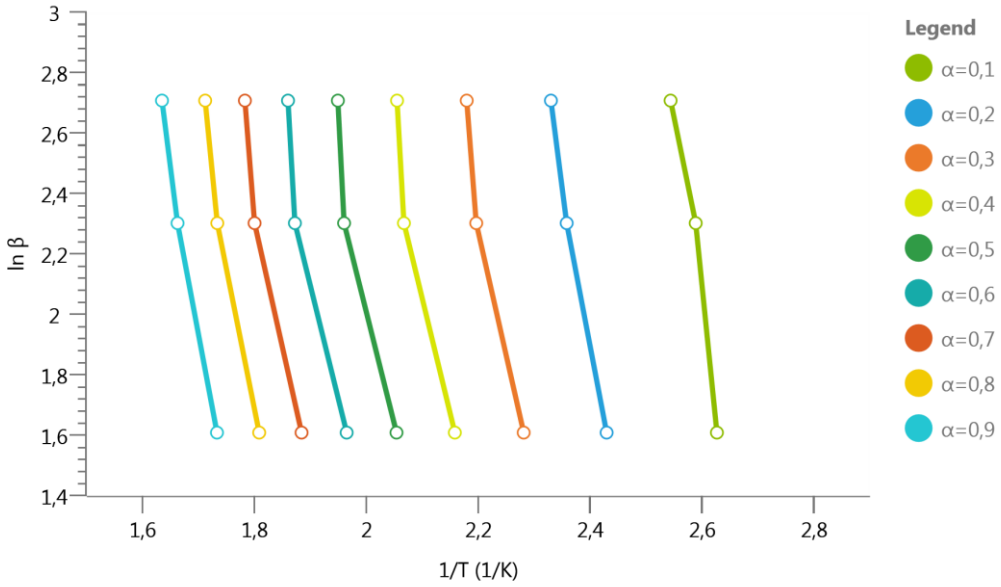

Figure C.I.18 - OFW plot of Crude Oil 3 Aromatic for I. Region

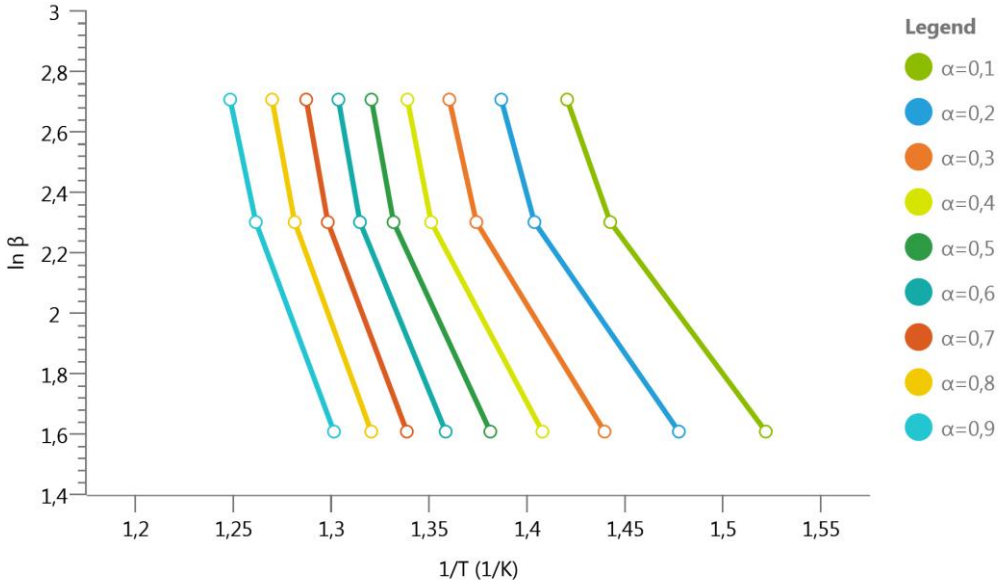

Figure C.I.19 - OFW plot of Crude Oil 3 Aromatic for II. Region

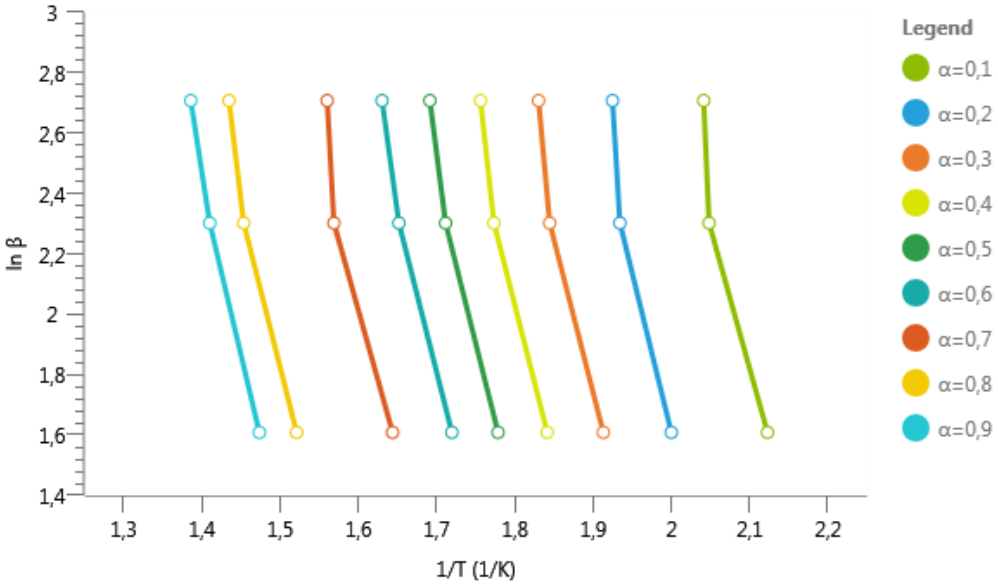

Figure C.I.20 - OFW plot of Crude Oil 3 Resin for I. Region

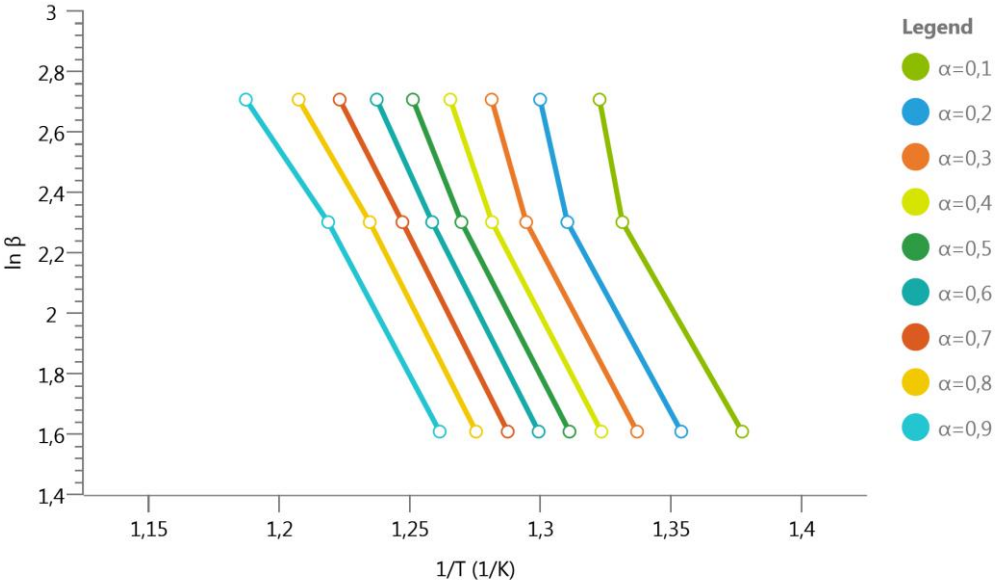

Figure C.I.21 - OFW plot of Crude Oil 3 Resin for II. Region

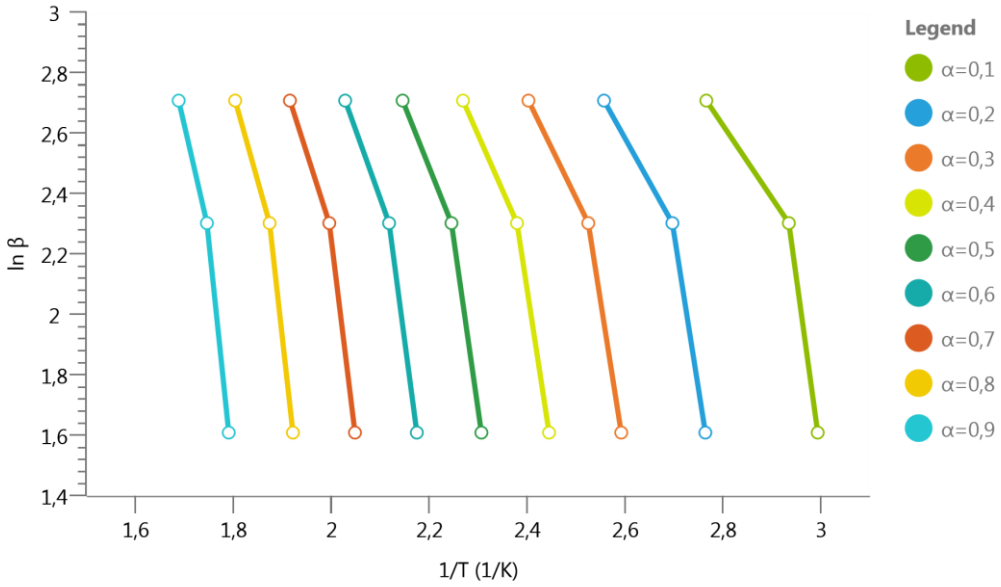

Figure C.I.22 - OFW plot of Crude Oil 4 for I. Region

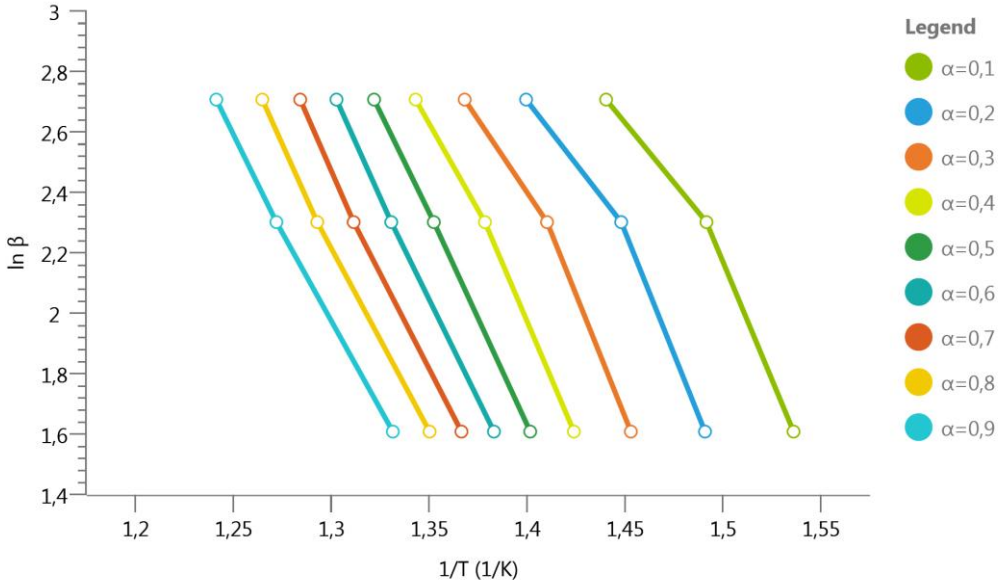

Figure C.I.23 - OFW plot of Crude Oil 4 for II. Region

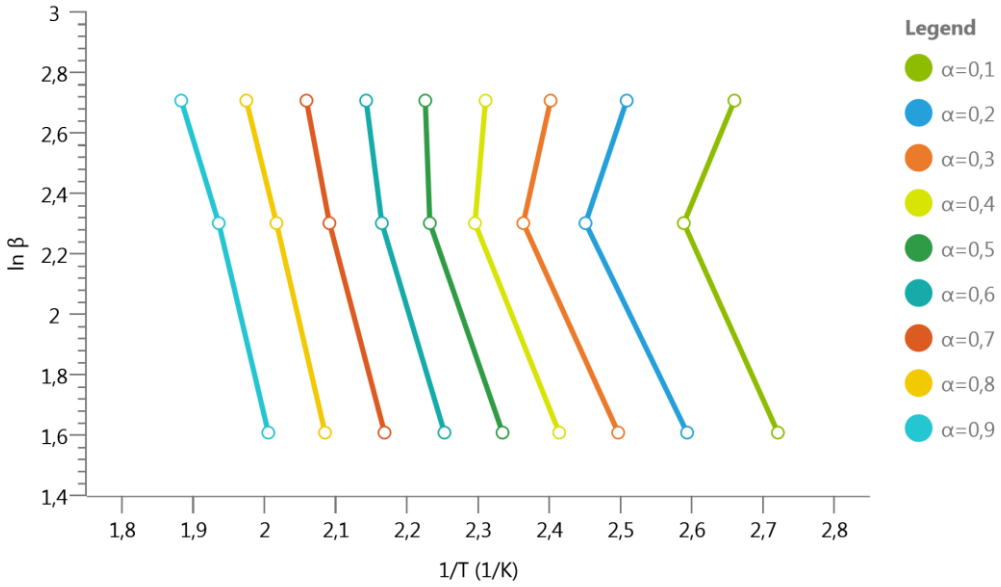

Figure C.I.24 - OFW plot of Crude Oil 4 Saturate for I. Region

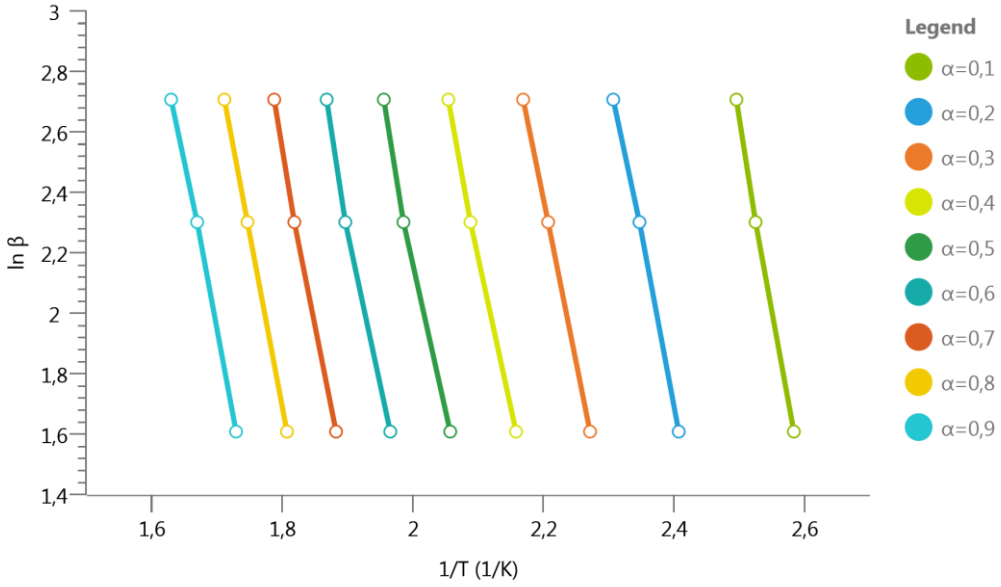

Figure C.I.25 - OFW plot of Crude Oil 4 Aromatic for I. Region

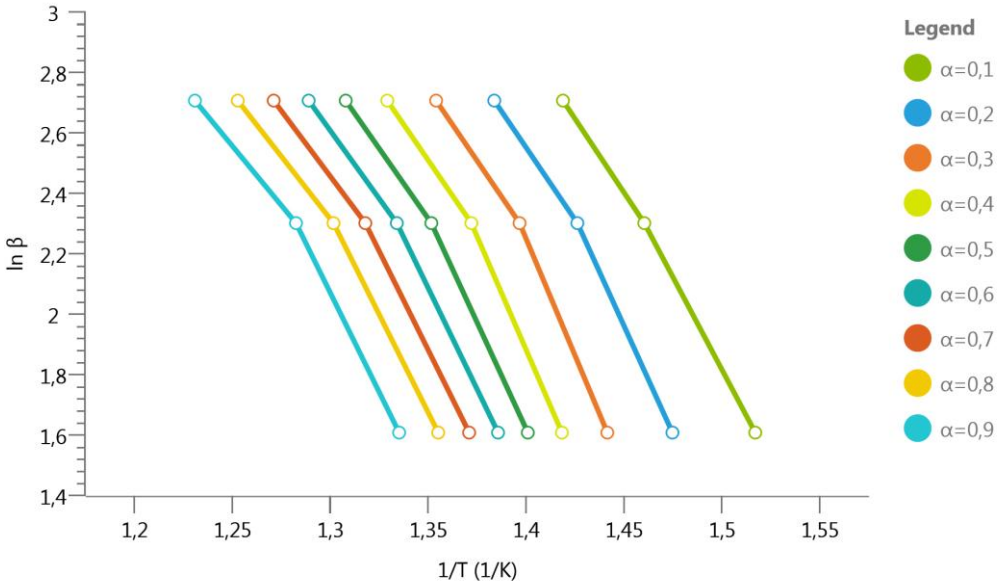

Figure C.I.26 - OFW plot of Crude Oil 4 Aromatic for II. Region

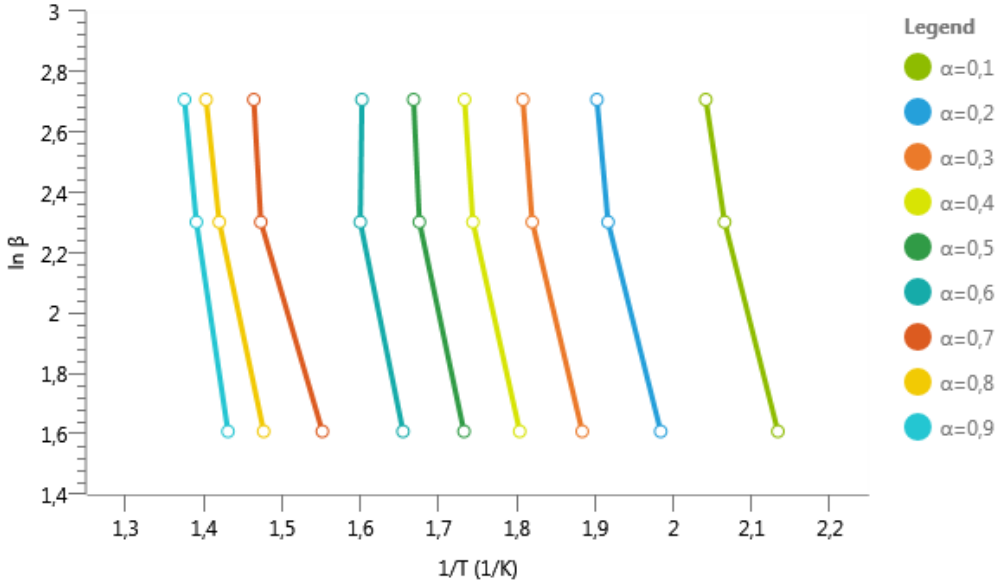

Figure C.I.27 - OFW plot of Crude Oil 4 Resin for I. Region

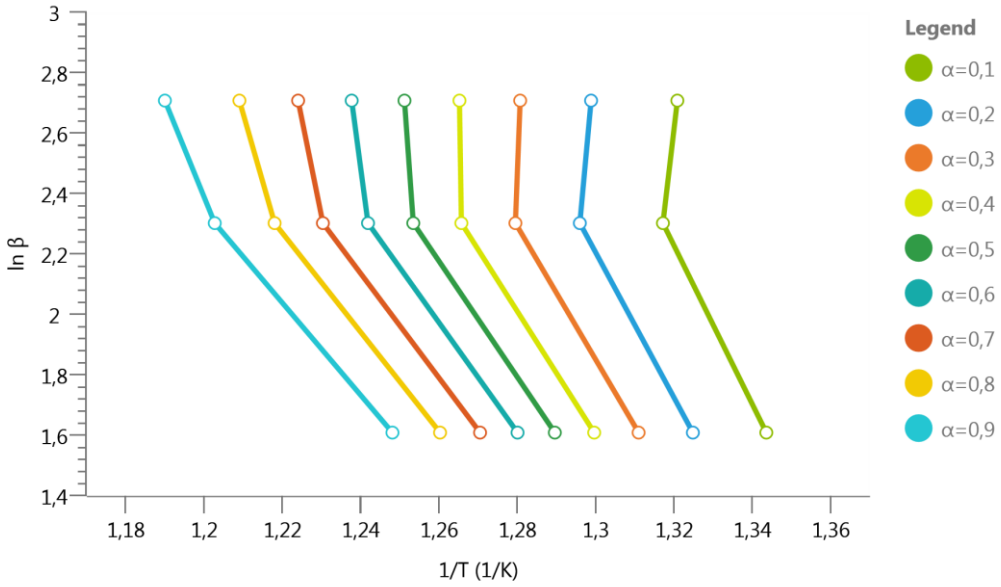

Figure C.I.28 - OFW plot of Crude Oil 4 Resin for II. Region

C.II. Plots of KAS Method

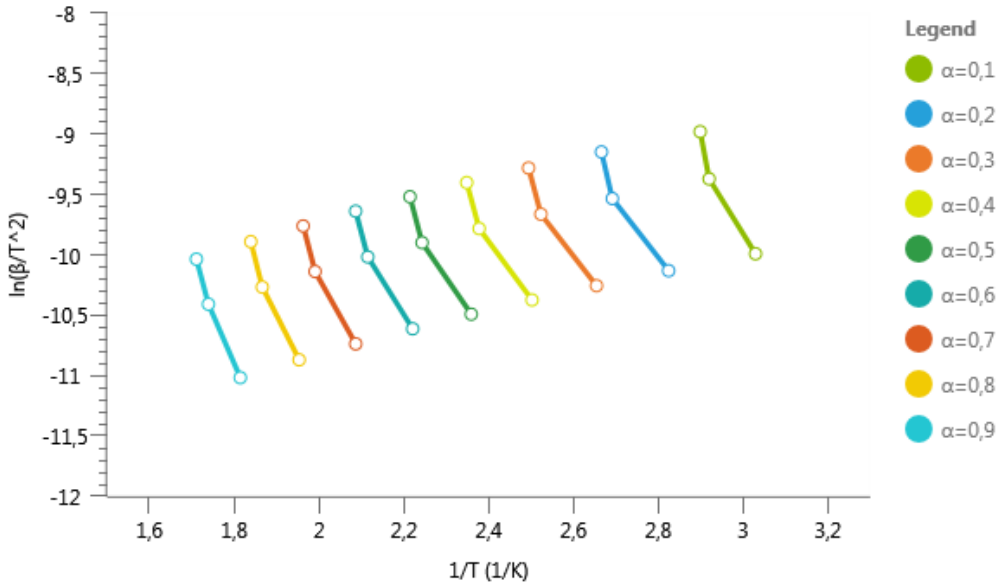

Figure C.II.1 - KAS plot of Crude Oil 1 for I. Region

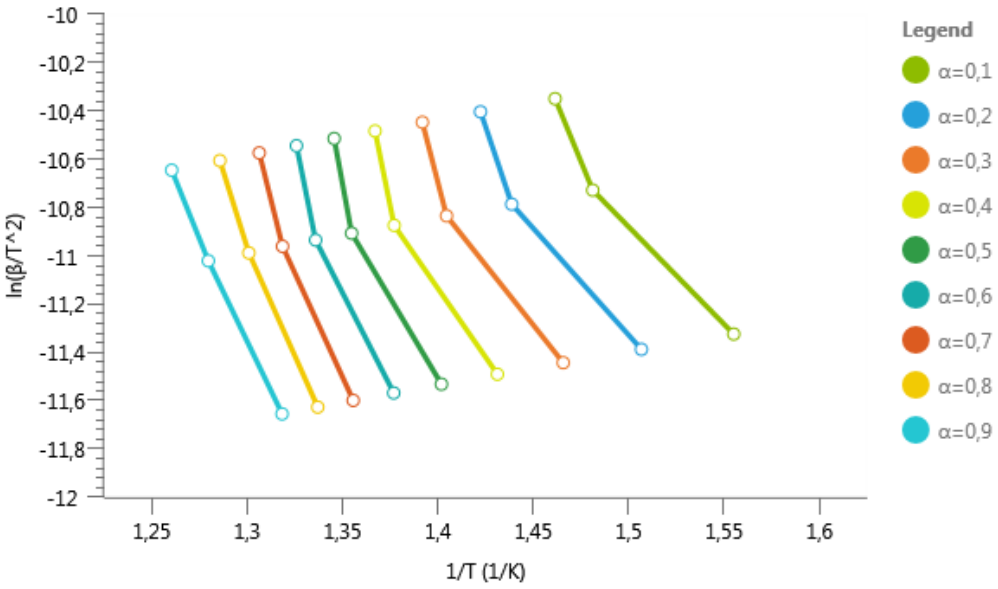

Figure C.II.2 - KAS plot of Crude Oil 1 for II. Region

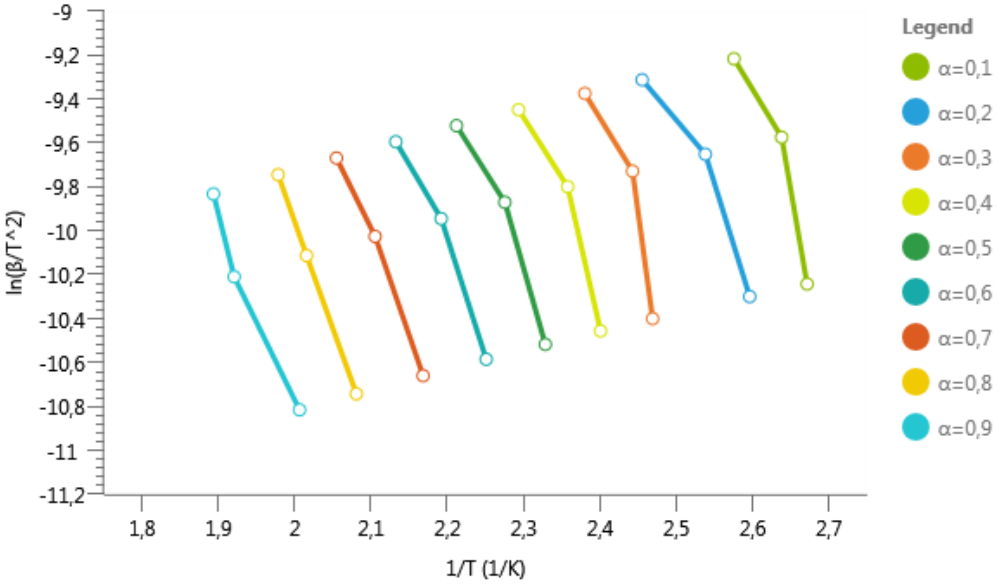

Figure C.II.3 - KAS plot of Crude Oil 1 Saturate for I. Region

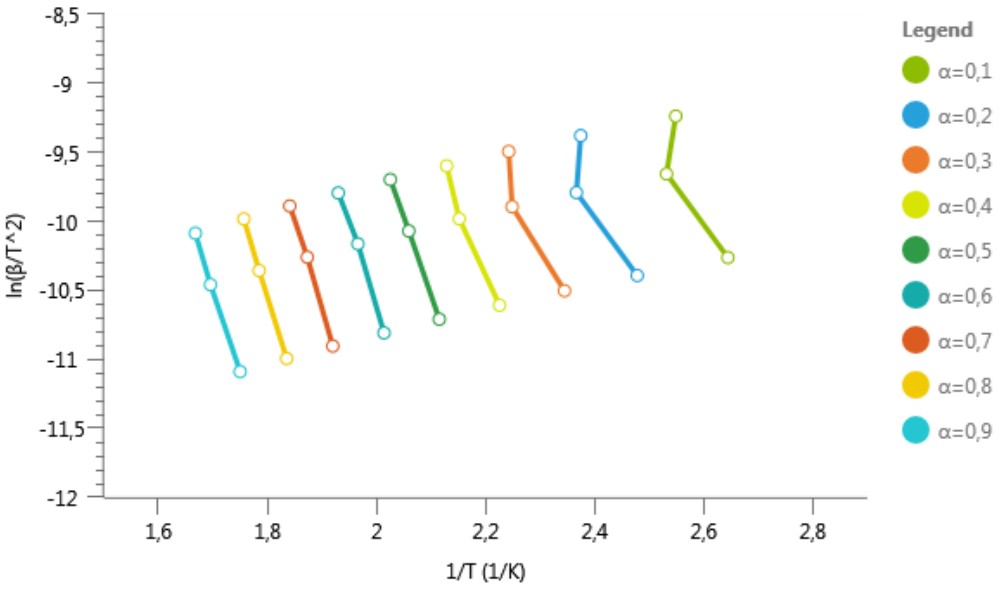

Figure C.II.4 - KAS plot of Crude Oil 1 Aromatic for I. Region

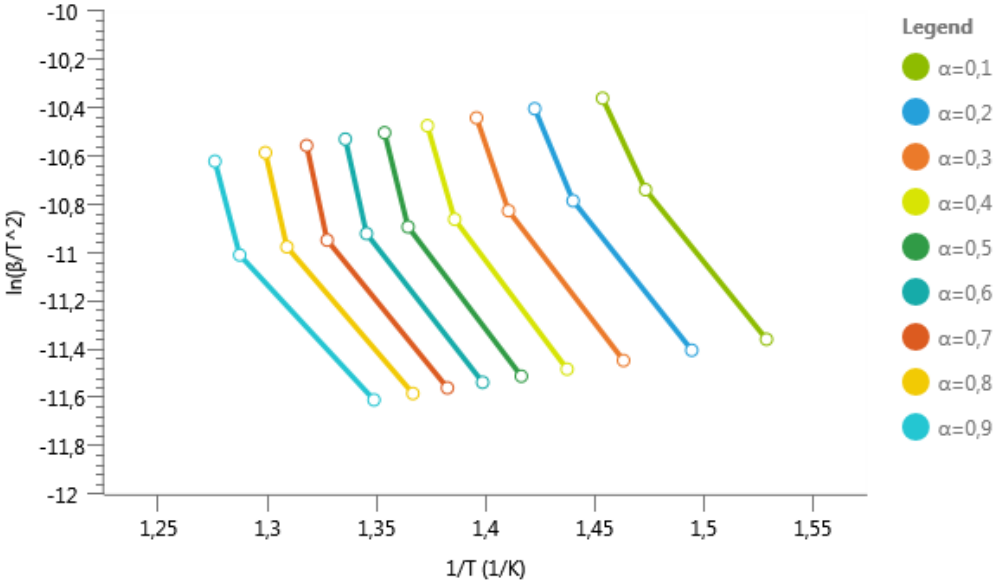

Figure C.II.5 - KAS plot of Crude Oil 1 Aromatic for II. Region

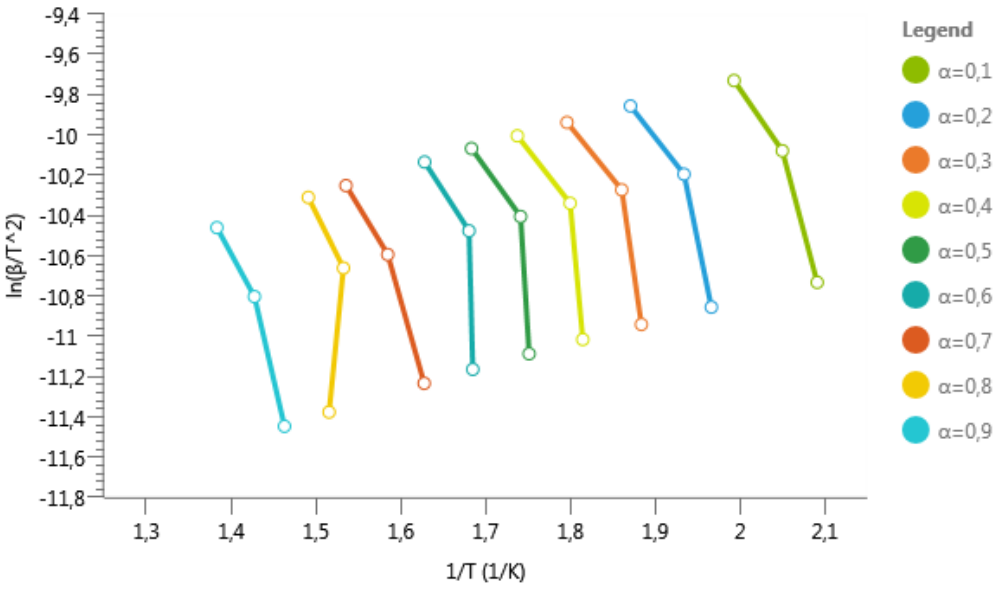

Figure C.II.6 - KAS plot of Crude Oil 1Resin for I. Region

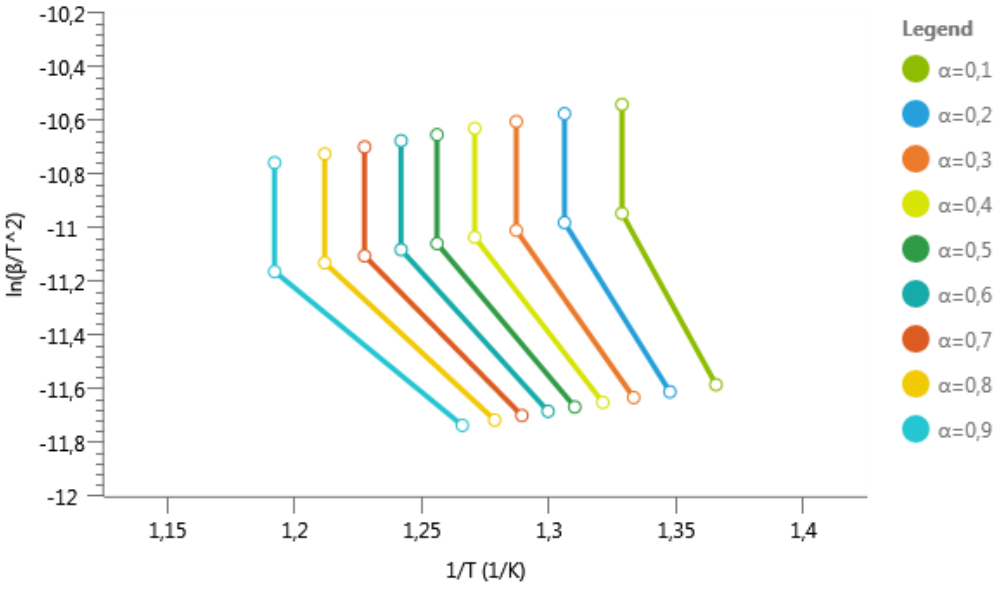

Figure C.II.7 - KAS plot of Crude Oil 1 Resin for II. Region

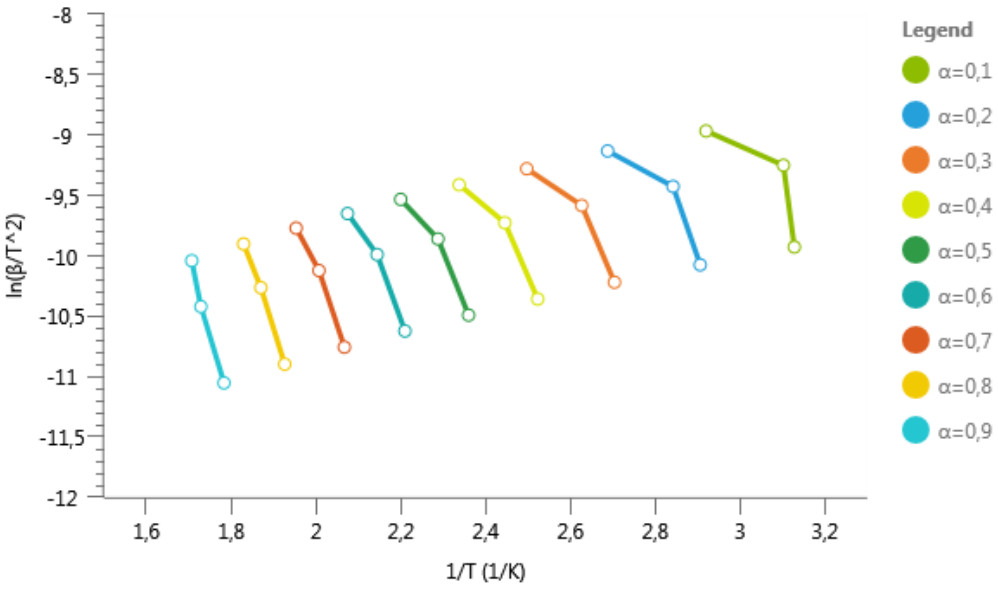

Figure C.II.8 - KAS plot of Crude Oil 2 for I. Region

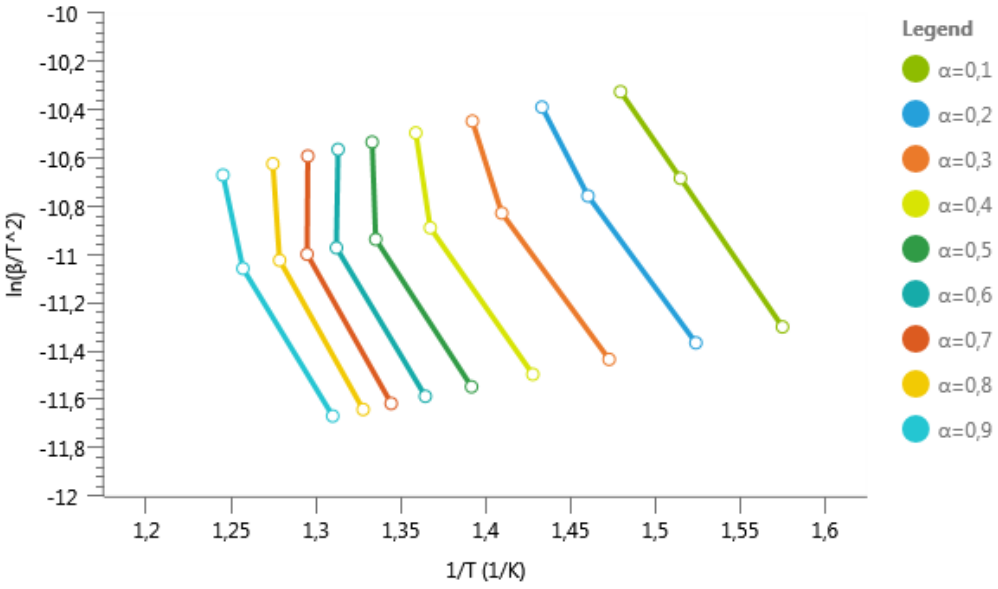

Figure C.II.9 - KAS plot of Crude Oil 2 for II. Region

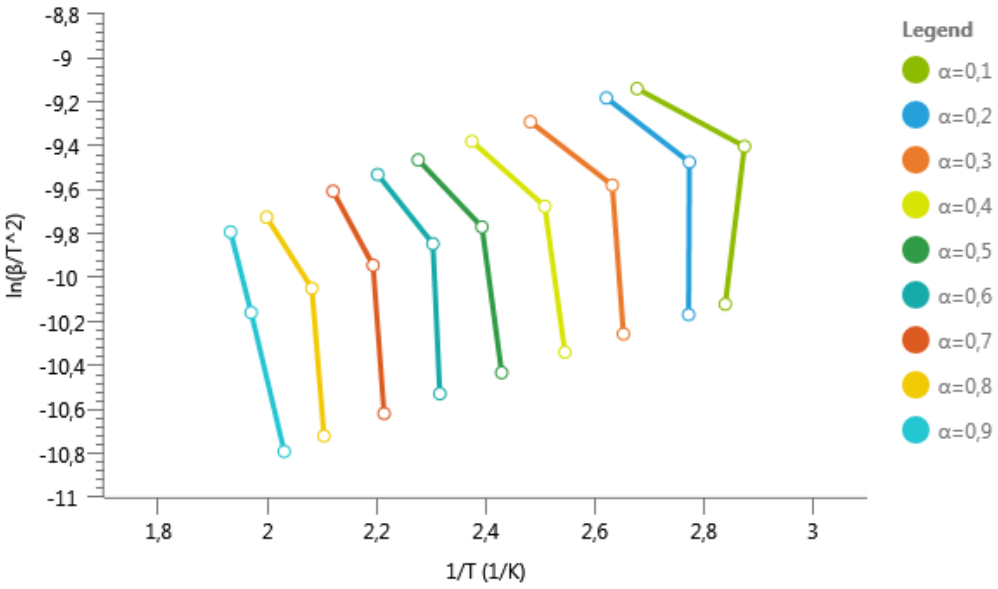

Figure C.II.10 - KAS plot of Crude Oil 2 Saturate for I. Region

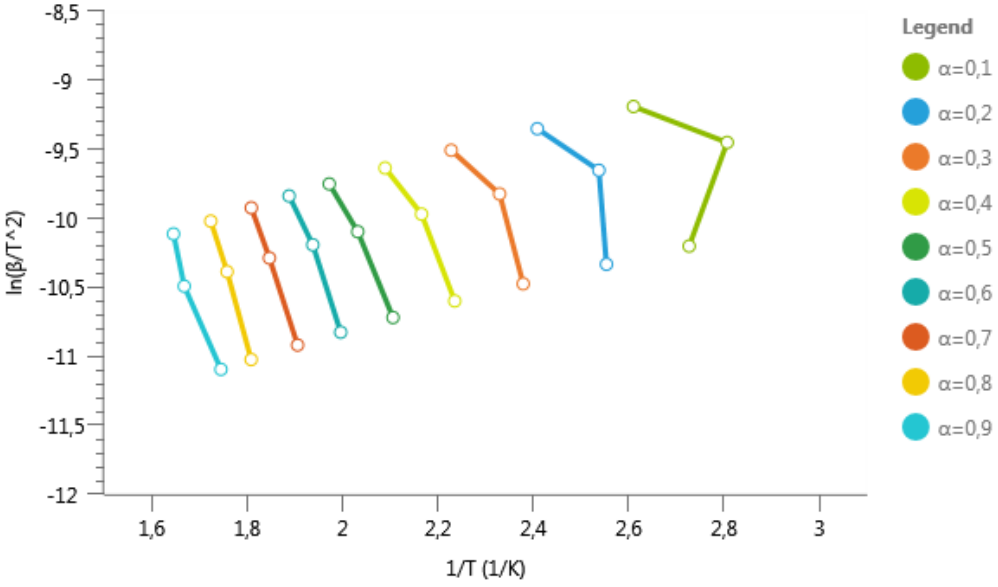

Figure C.II.11 - KAS plot of Crude Oil 2 Aromatic for I. Region

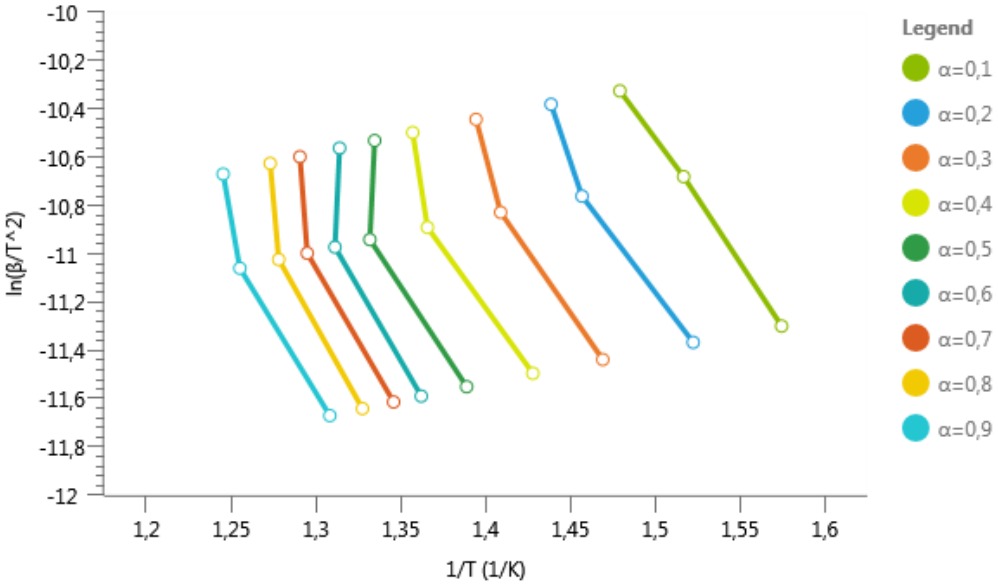

Figure C.II.12 - KAS plot of Crude Oil 2 Aromatic for II. Region

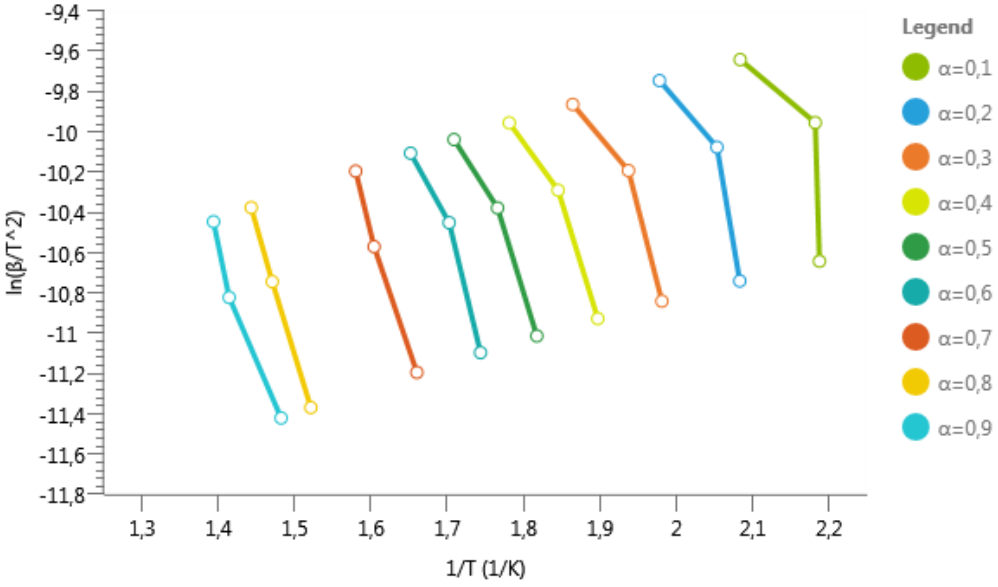

Figure C.II.13 - KAS plot of Crude Oil 2 Resin for I. Region

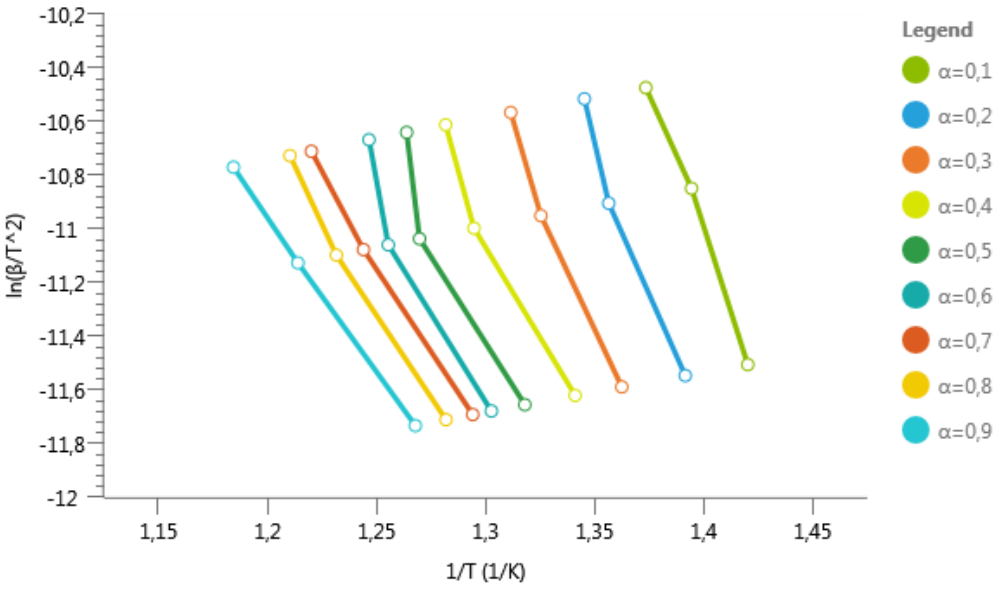

Figure C.II.14 - KAS plot of Crude Oil 2 Resin for II. Region

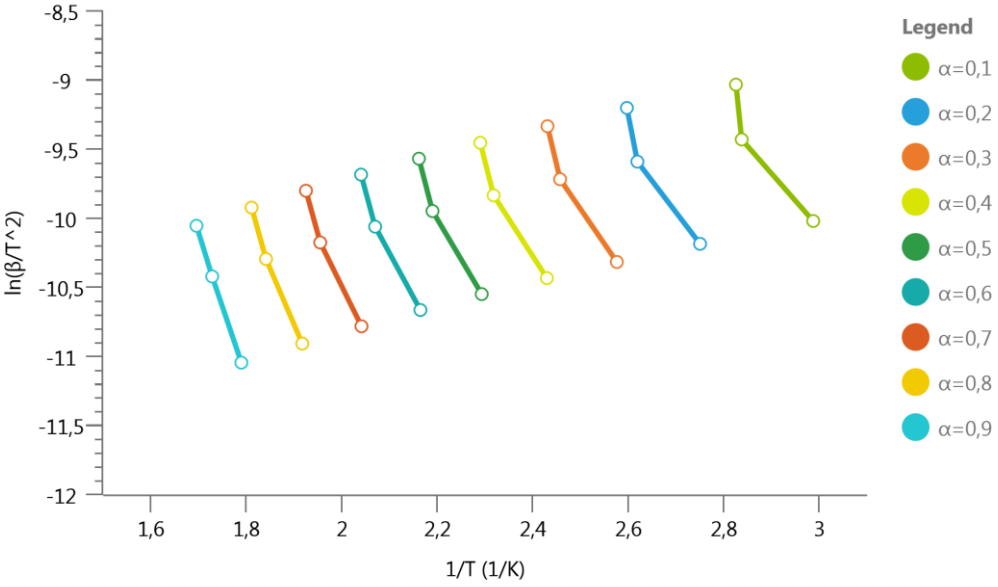

Figure C.II.15 - KAS plot of Crude Oil 3 for I. Region

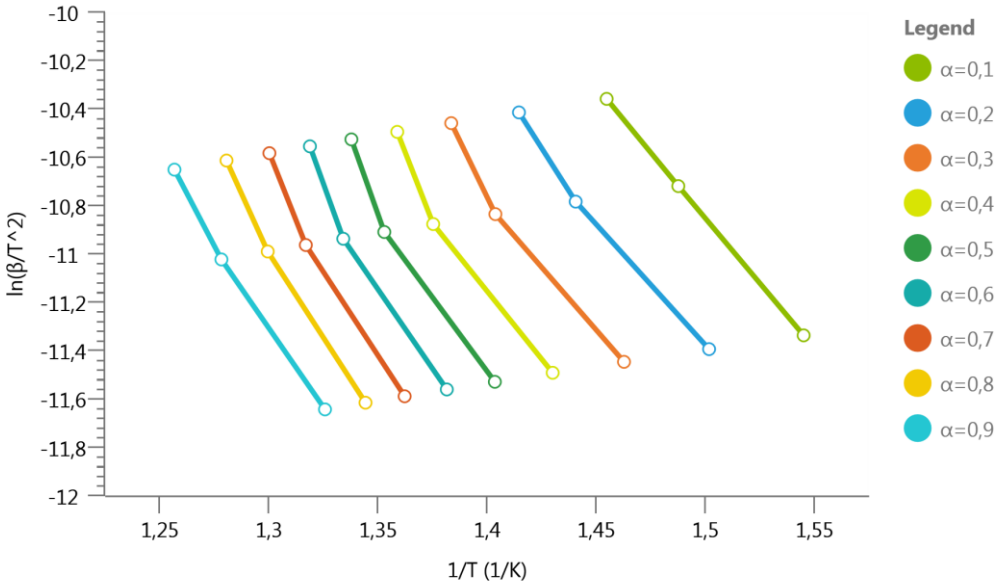

Figure C.II.16 - KAS plot of Crude Oil 3 for II. Region

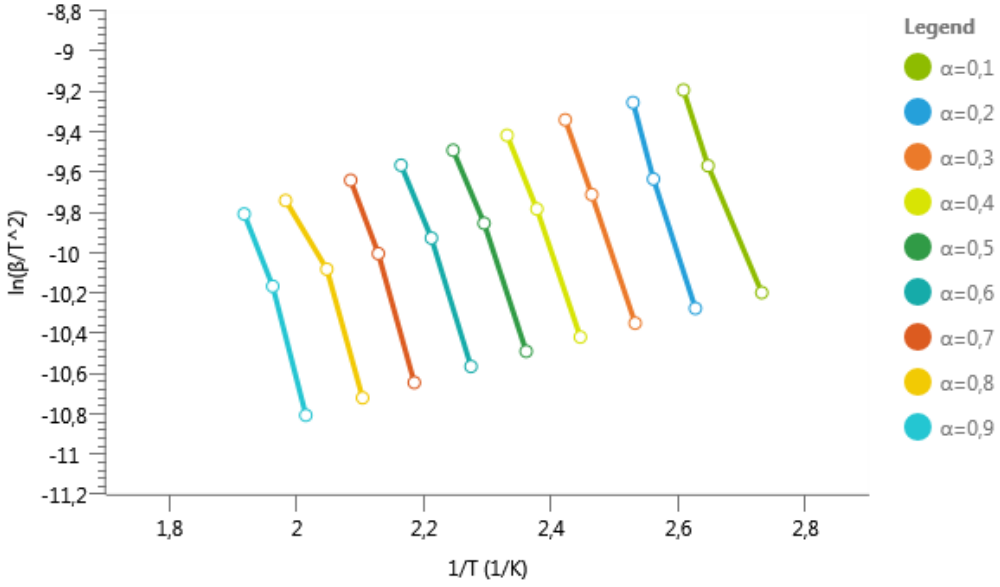

Figure C.II.17 - KAS plot of Crude Oil 3 Saturate for I. Region

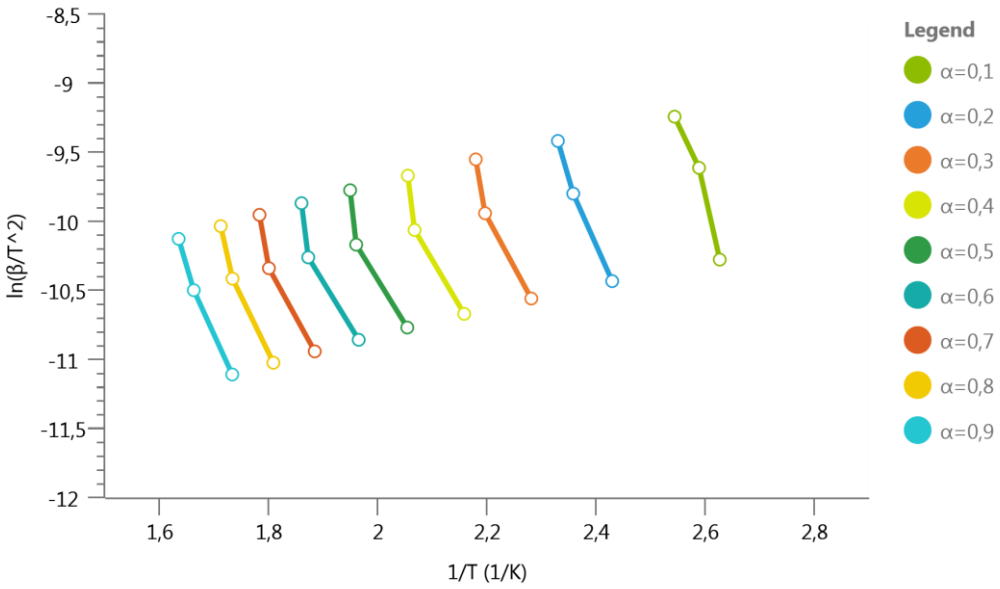

Figure C.II.18 - KAS plot of Crude Oil 3 Aromatic for I. Region

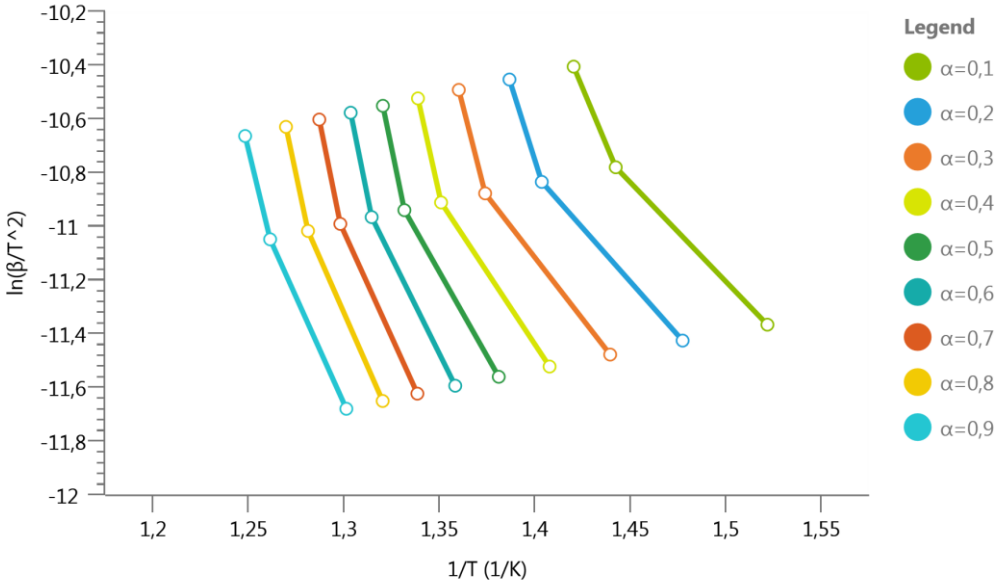

Figure C.II.19 - KAS plot of Crude Oil 3 Aromatic for II. Region

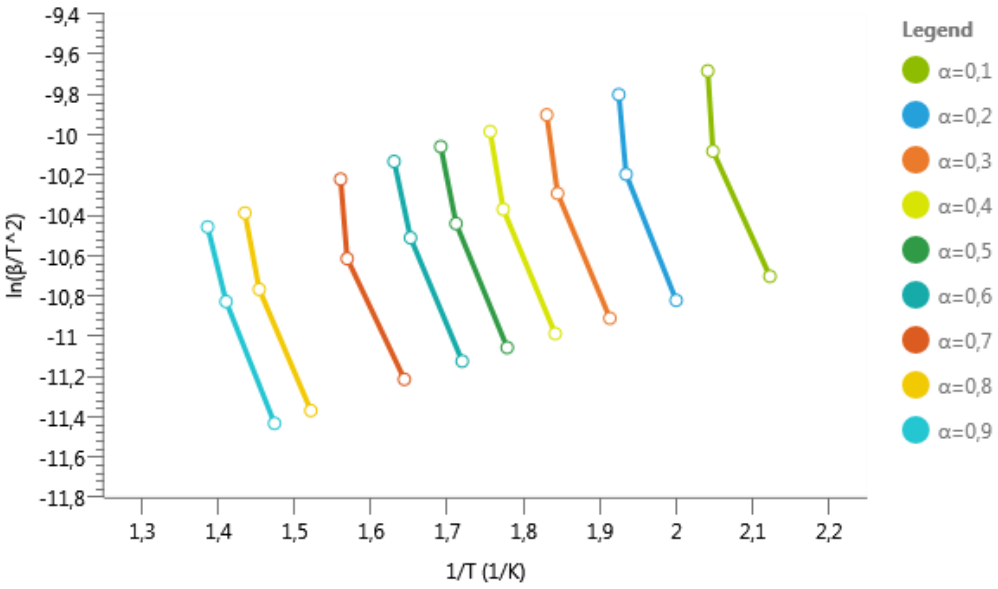

Figure C.II.20 - KAS plot of Crude Oil 3 Resin for I. Region

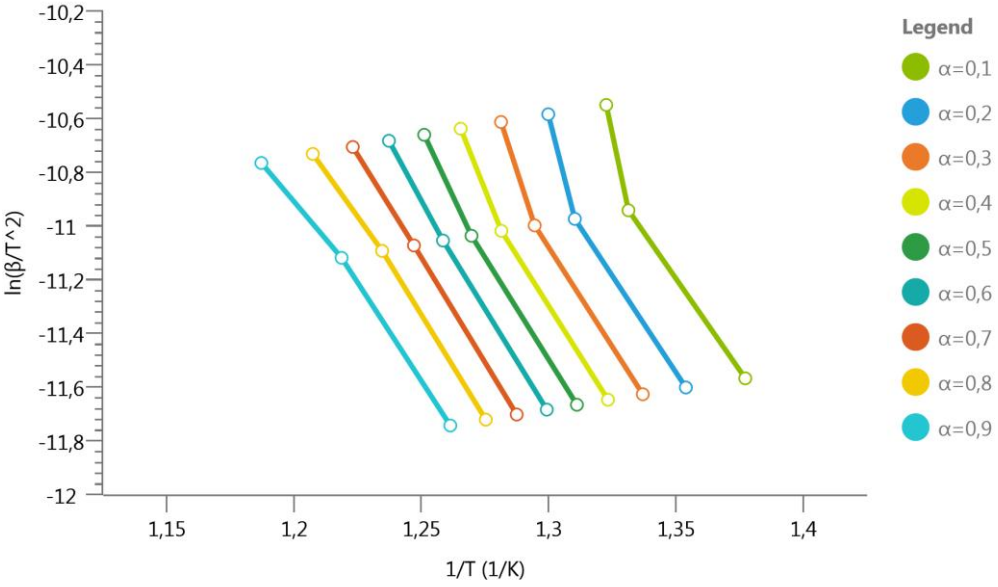

Figure C.II.21 - KAS plot of Crude Oil 3 Resin for II. Region

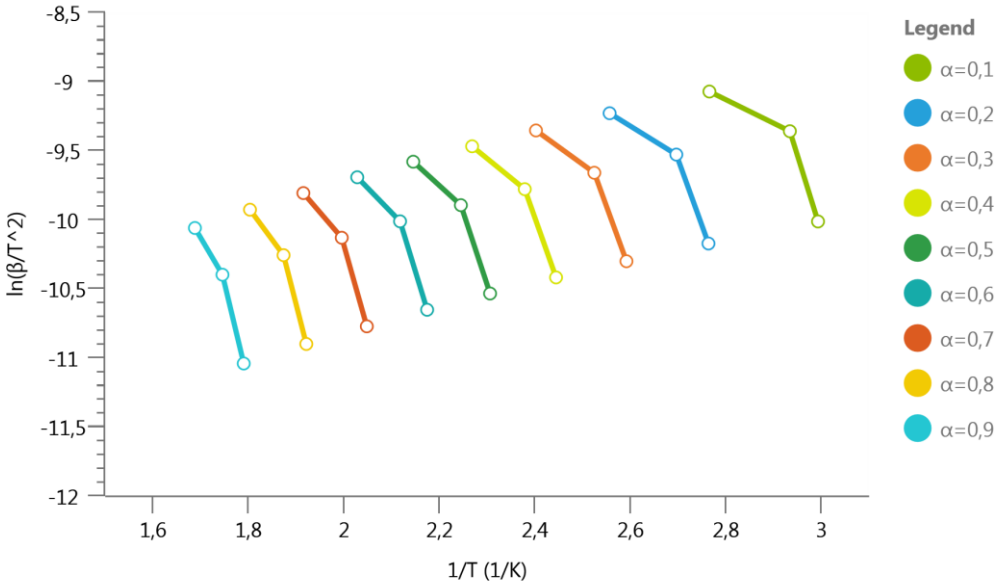

Figure C.II.22 - KAS plot of Crude Oil 4 for I. Region

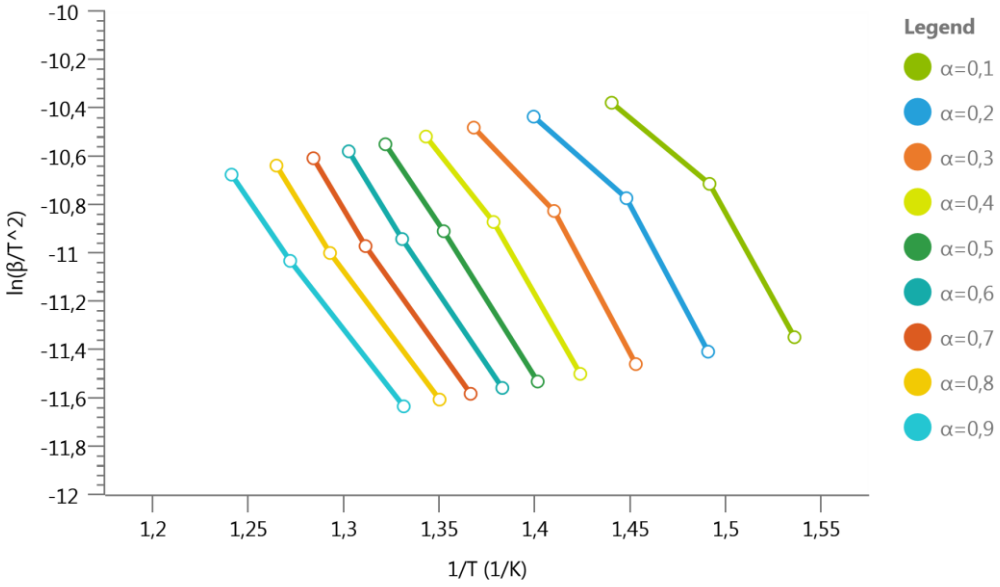

Figure C.II.23 - KAS plot of Crude Oil 4 for II. Region

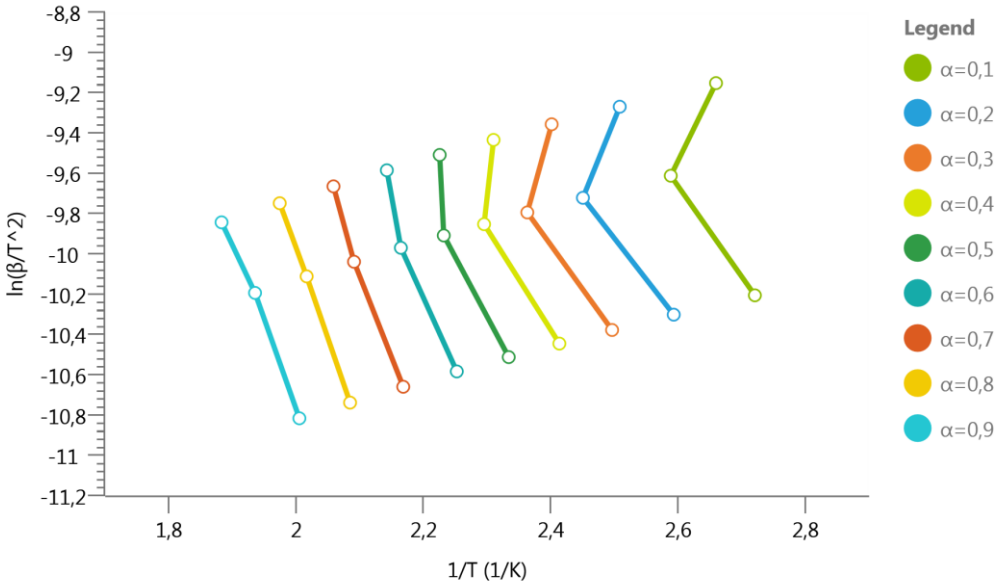

Figure C.II.24 - KAS plot of Crude Oil 4 Saturate for I. Region

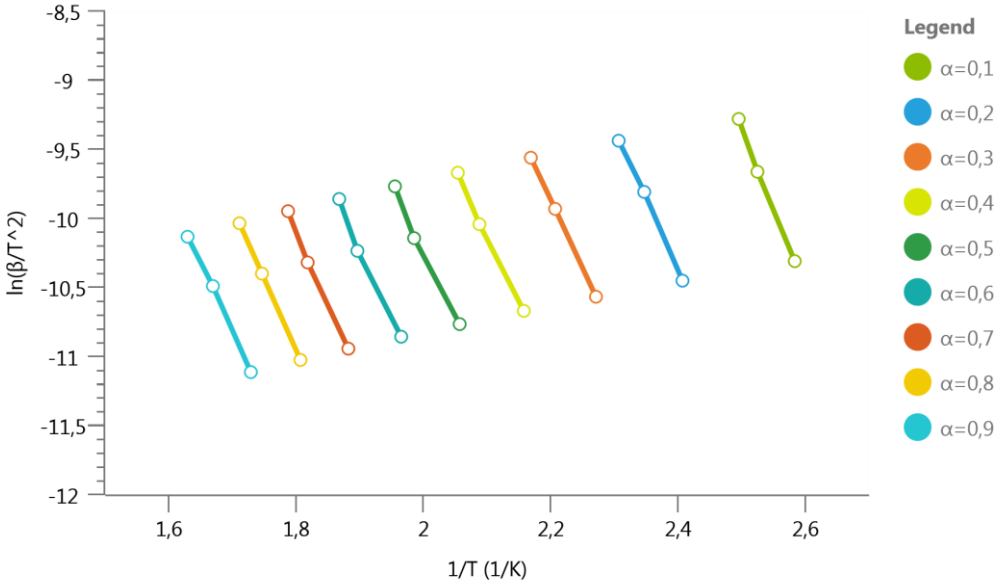

Figure C.II.25 - KAS plot of Crude Oil 4 Aromatic for I. Region

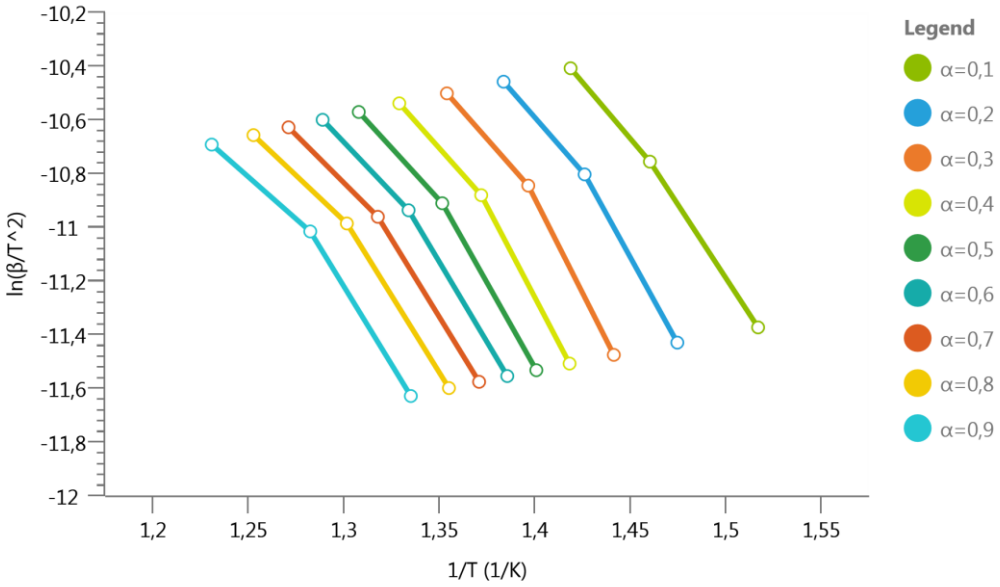

Figure C.II.26 - KAS plot of Crude Oil 4 Aromatic for II. Region

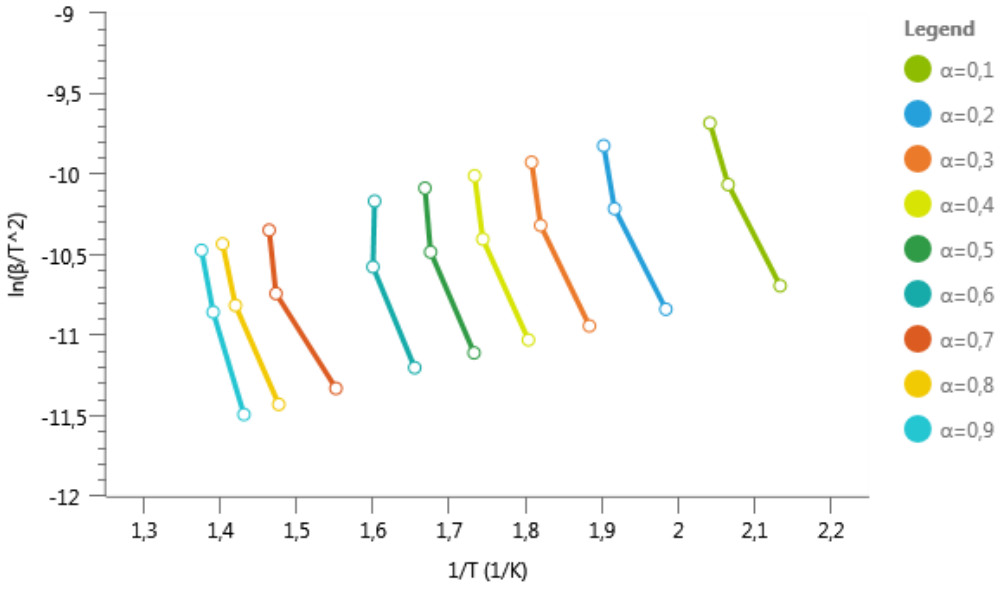

Figure C.II.27 - KAS plot of Crude Oil 4 Resin for I. Region

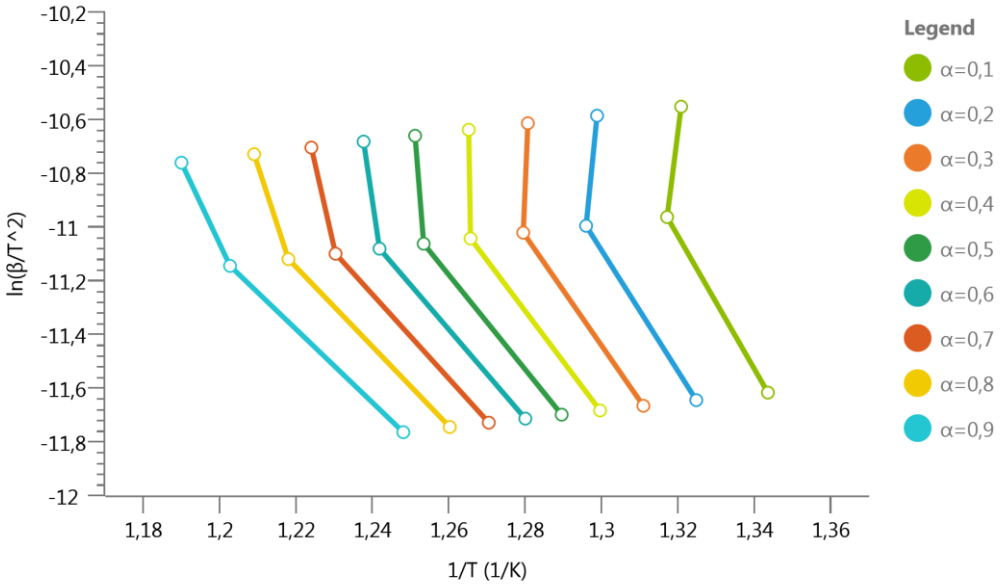

Figure C.II.28 - KAS plot of Crude Oil 4 Resin for II. Region

APPENDIX D

PLOTS OF MODEL FITTING METHODS

D.I. Plots of Arrhenius Methods

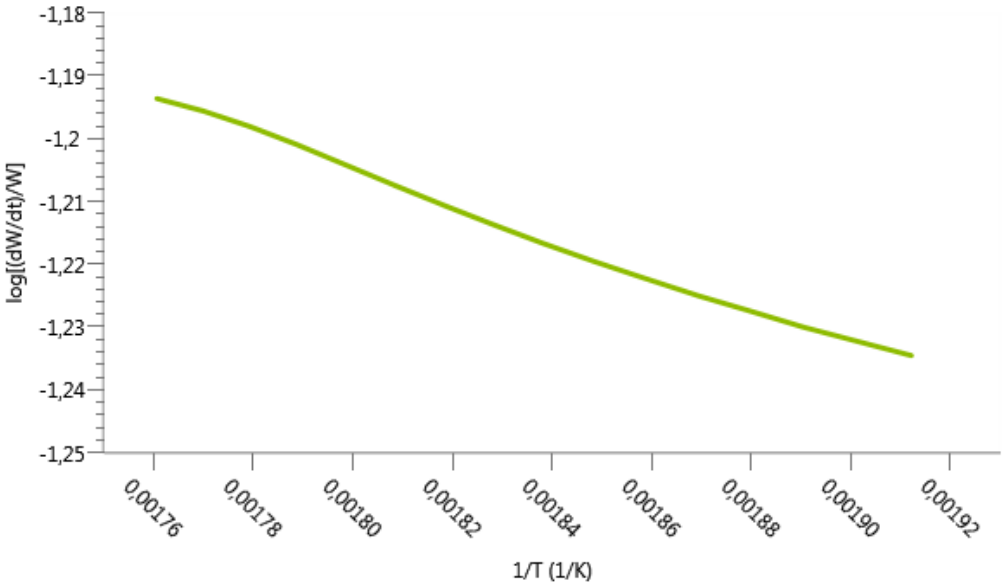

Figure D.I.1 - Arrhenius plot of Crude Oil 1 for I. Region at 10 °C/min

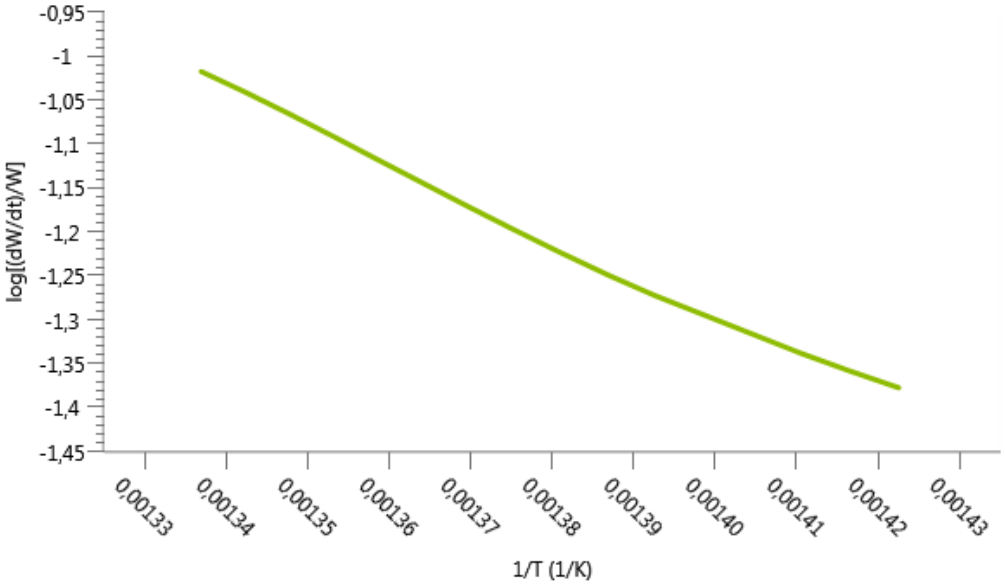

Figure D.I.2 - Arrhenius plot of Crude Oil 1 for II. Region at 10 °C/min

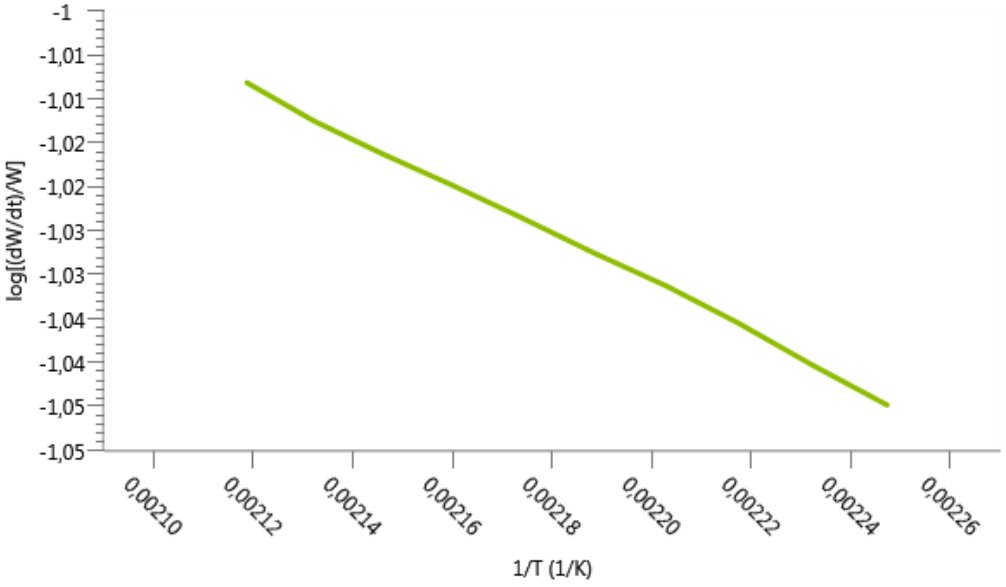

Figure D.I.3 - Arrhenius plot of Crude Oil 1 Saturate for I. Region at 10 °C/min

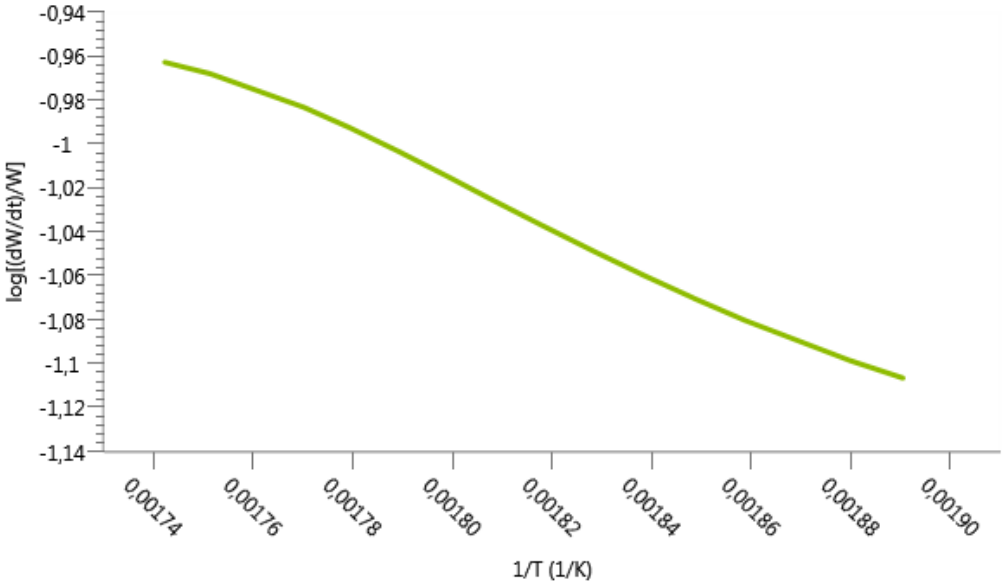

Figure D.I.4 - Arrhenius plot of Crude Oil 1 Aromatic for I. Region at 10 °C/min

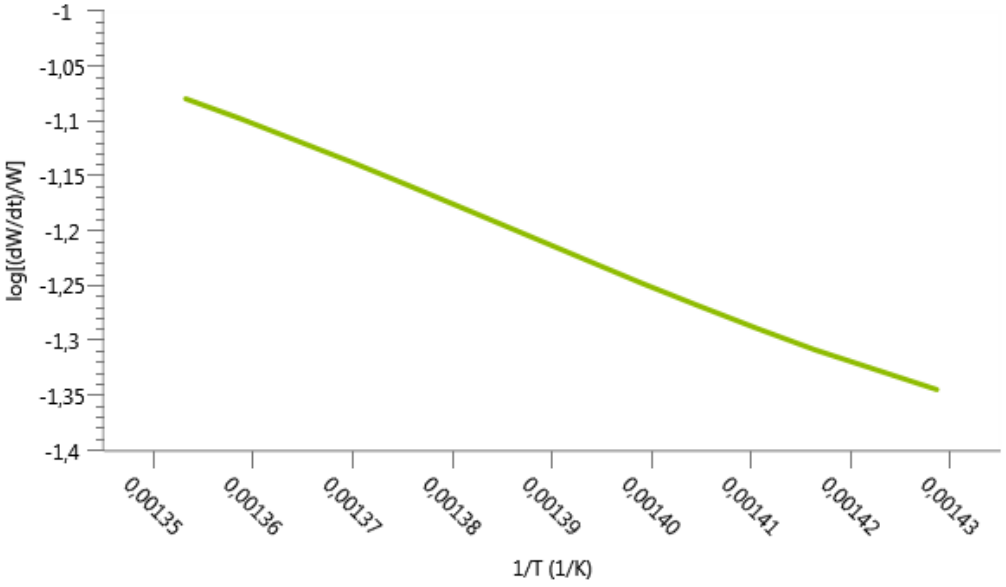

Figure D.I.5 - Arrhenius plot of Crude Oil 1 Aromatic for II. Region at 10 °C/min

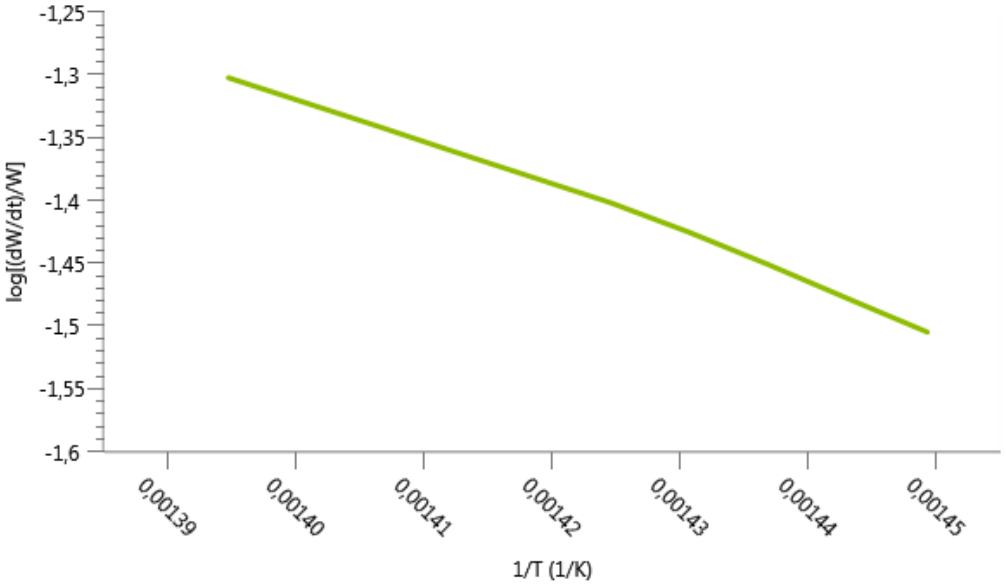

Figure D.I.6 - Arrhenius plot of Crude Oil 1 Resin for I. Region at 10 °C/min

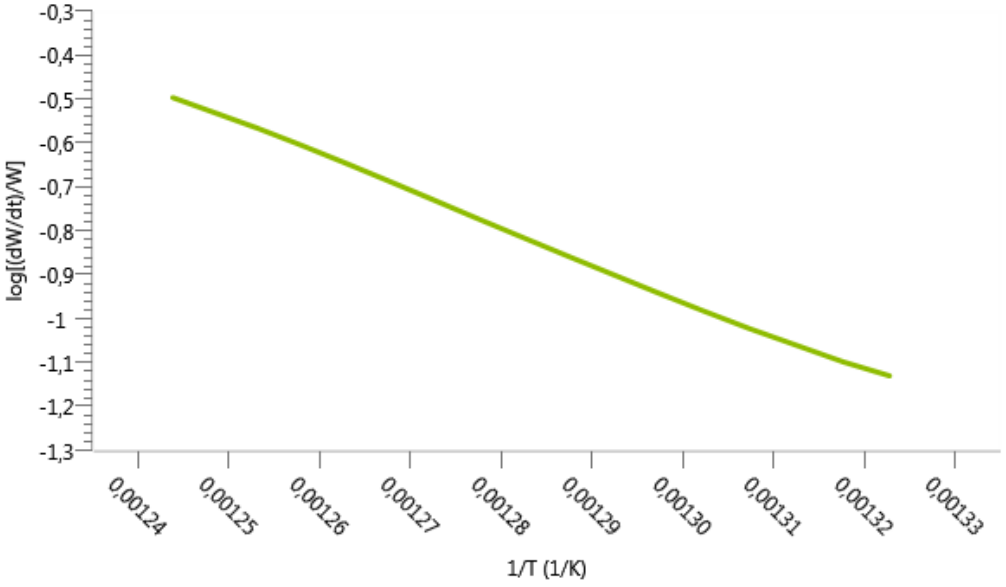

Figure D.I.7 - Arrhenius plot of Crude Oil 1 Resin for II. Region at 10 °C/min

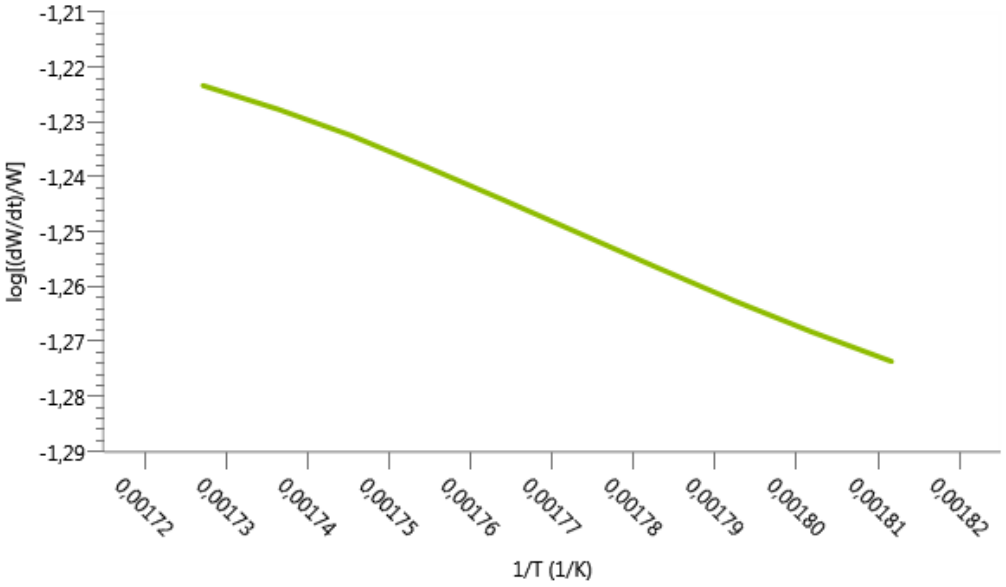

Figure D.I.8 - Arrhenius plot of Crude Oil 2 for I. Region at 10 °C/min

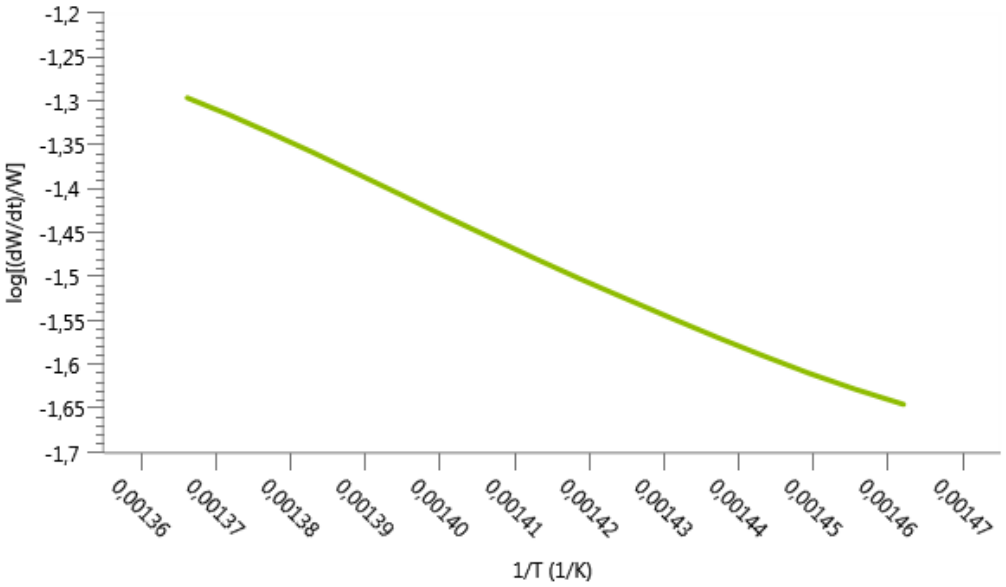

Figure D.I.9 - Arrhenius plot of Crude Oil 2 for II. Region at 10 °C/min

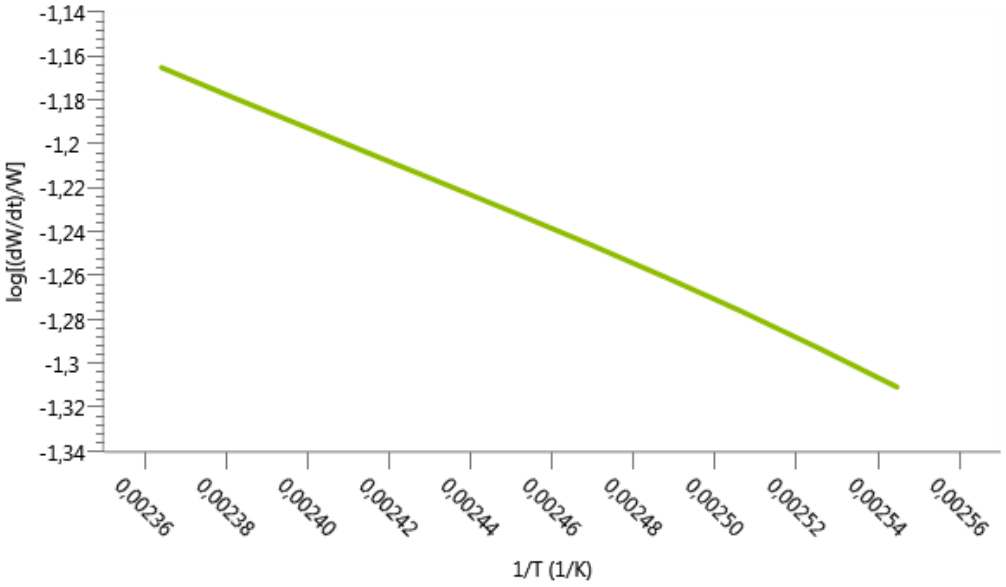

Figure D.I.10 - Arrhenius plot of Crude Oil 2 Saturate for I. Region at 10 °C/min

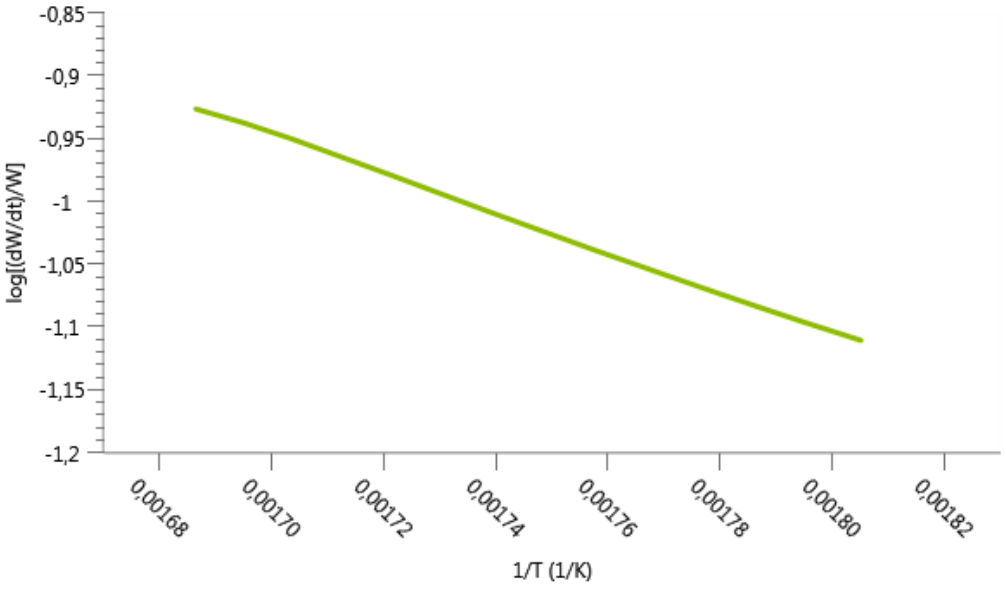

Figure D.I.11 - Arrhenius plot of Crude Oil 2 Aromatic for I. Region at 10 °C/min

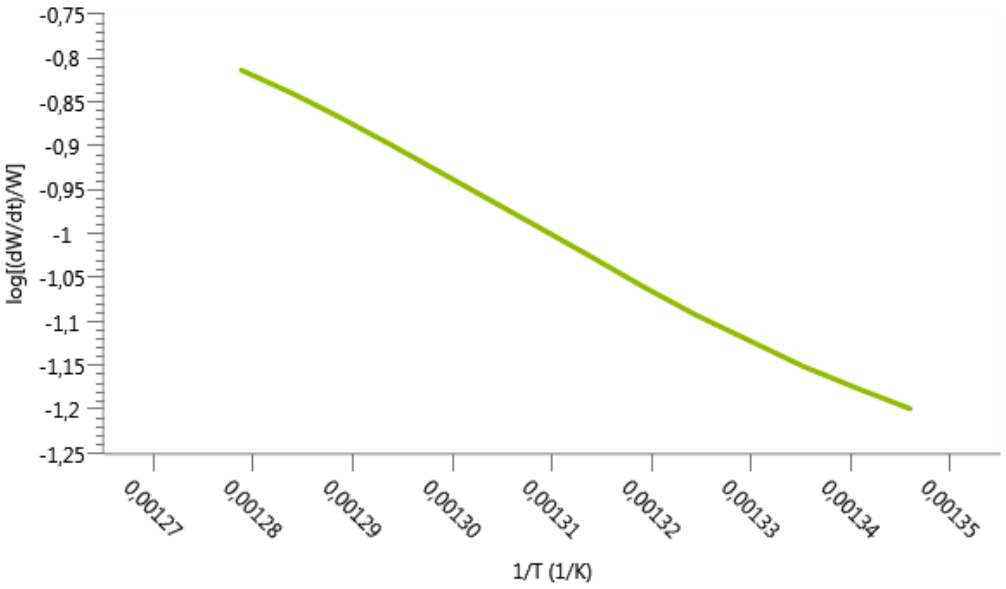

Figure D.I.12 - Arrhenius plot of Crude Oil 2 Aromatic for II. Region at 10 °C/min

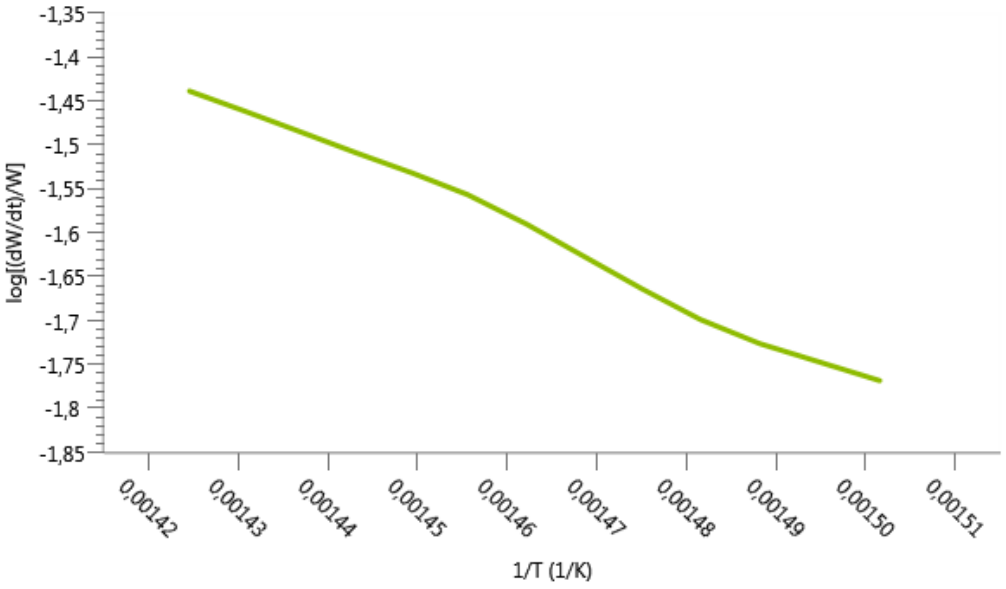

Figure D.I.13 - Arrhenius plot of Crude Oil 2 Resin for I. Region at 10 °C/min

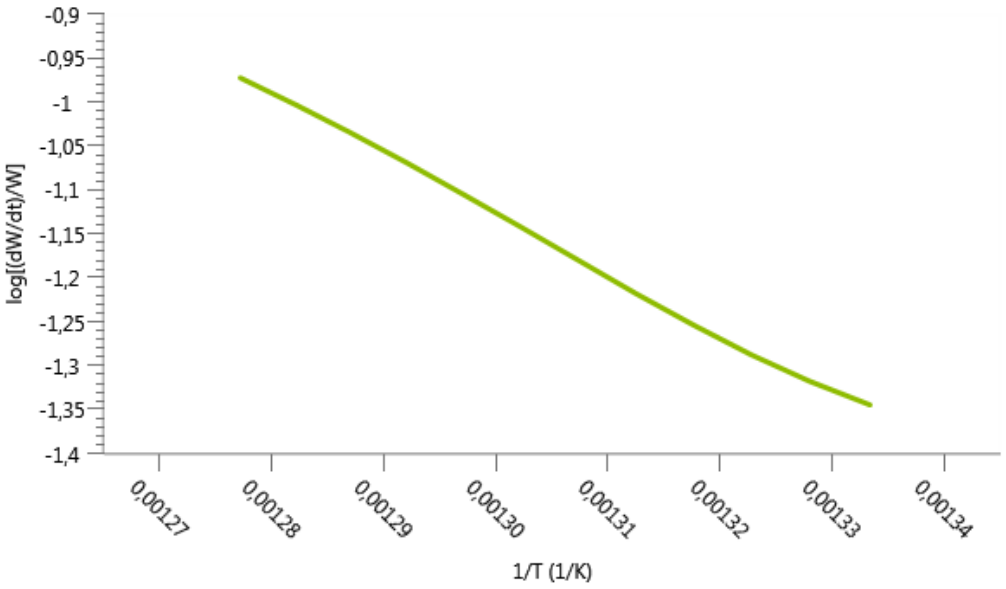

Figure D.I.14 - Arrhenius plot of Crude Oil 2 Resin for II. Region at 10 °C/min

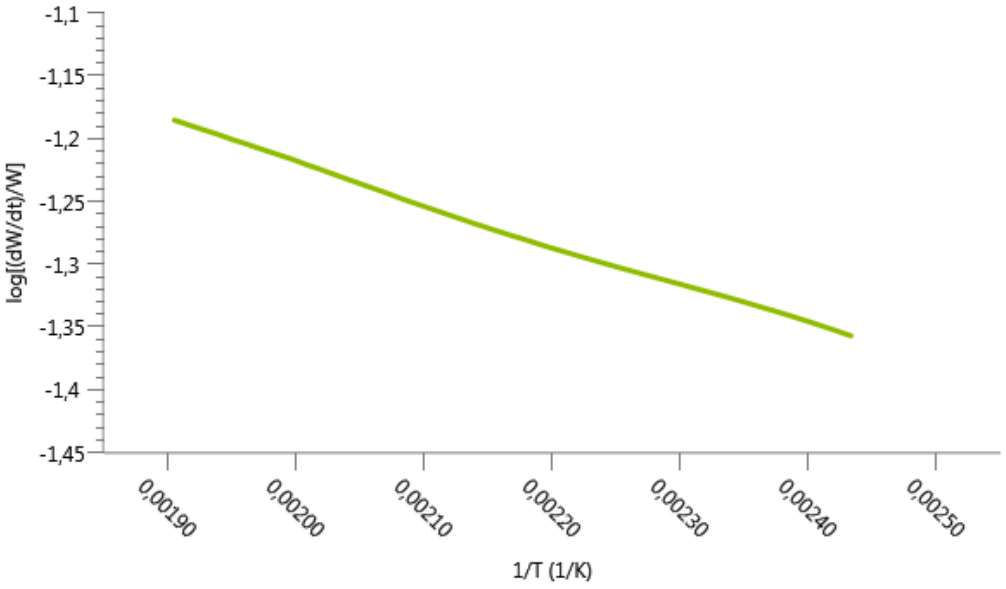

Figure D.I.15 - Arrhenius plot of Crude Oil 3 for I. Region at 10 °C/min

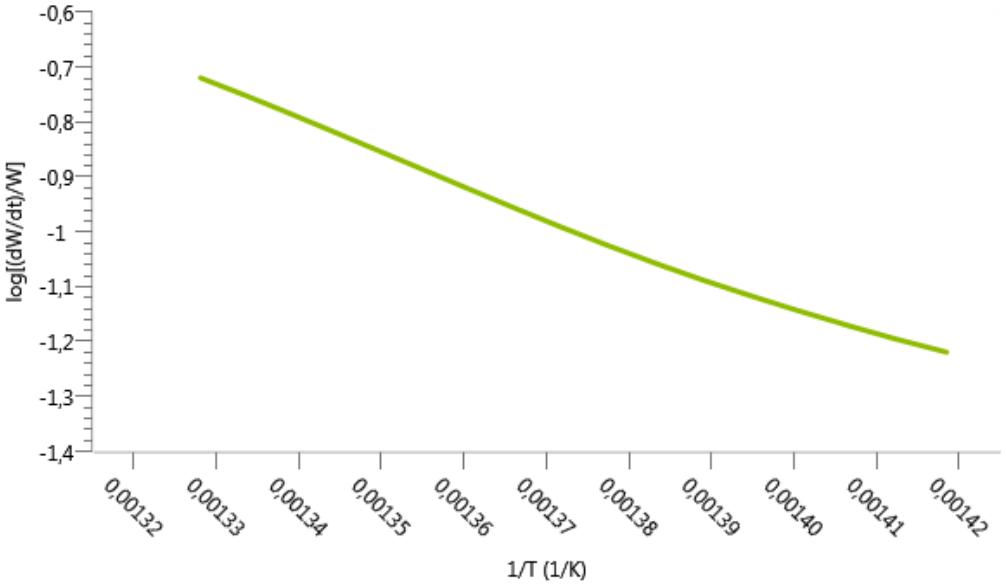

Figure D.I.16 - Arrhenius plot of Crude Oil 3 for II. Region at 10 °C/min

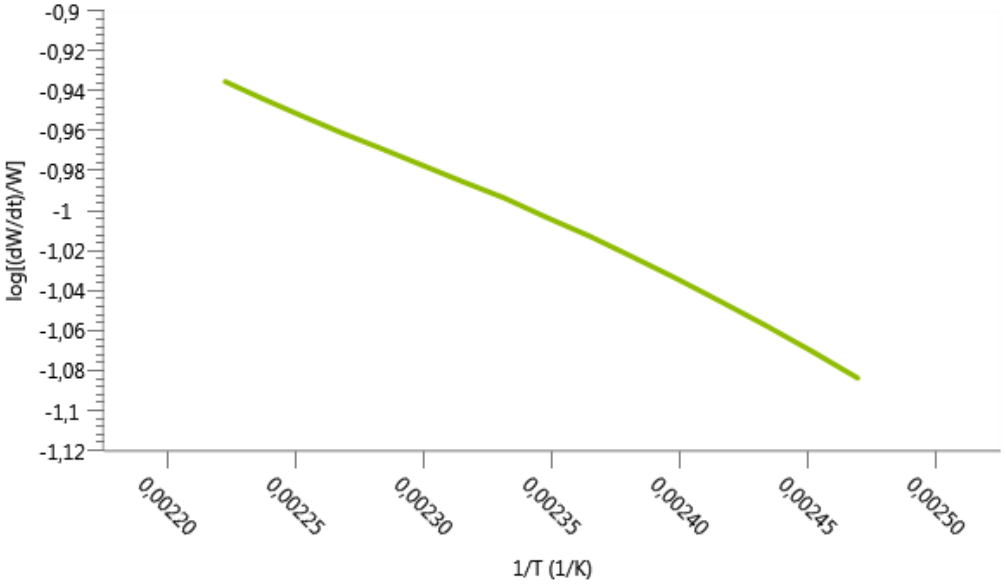

Figure D.I.17 - Arrhenius plot of Crude Oil 3 Saturate for I. Region at 10 °C/min

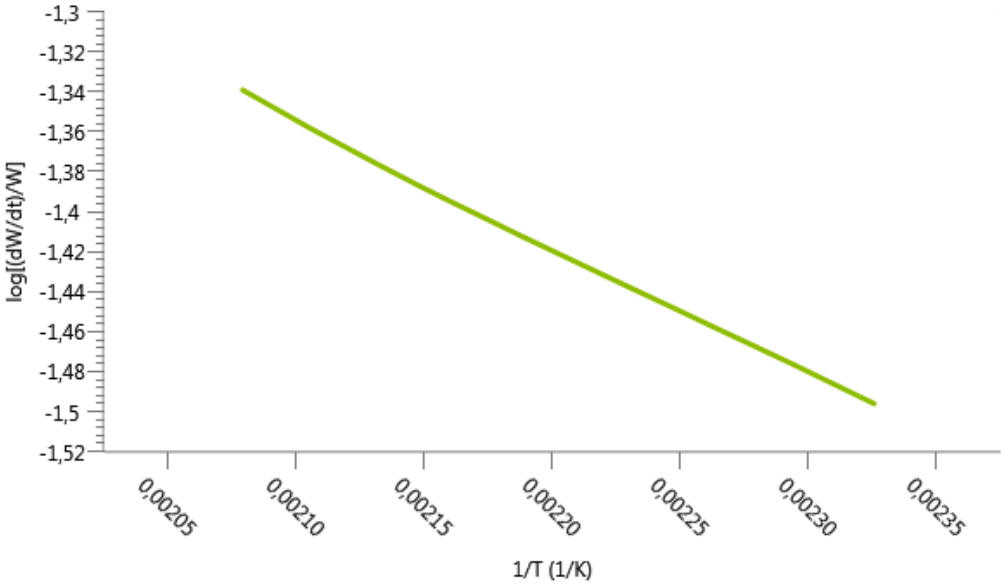

Figure D.I.18 - Arrhenius plot of Crude Oil 3 Aromatic for I. Region at 10 °C/min

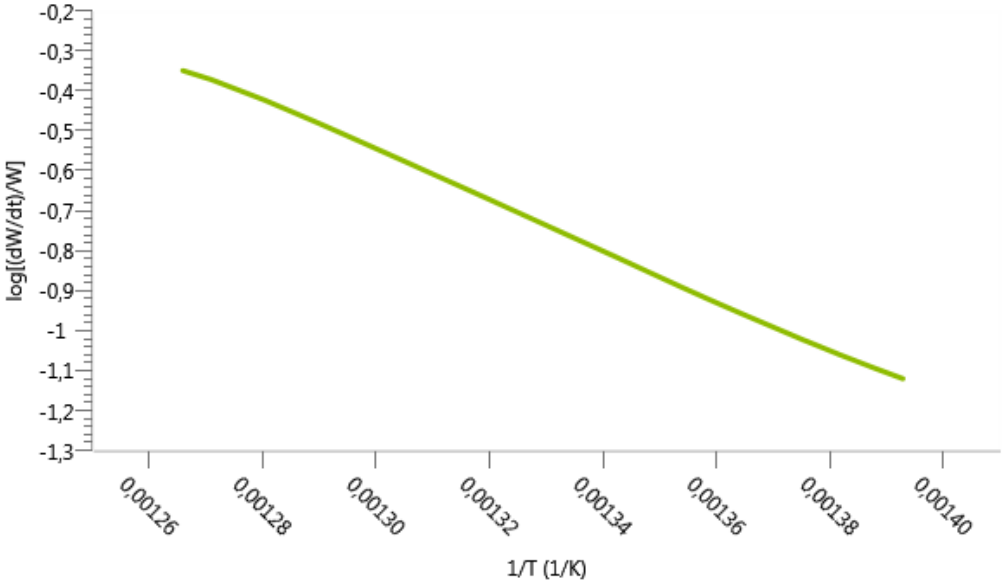

Figure D.I.19 - Arrhenius plot of Crude Oil 3 Aromatic for II. Region at 10 °C/min

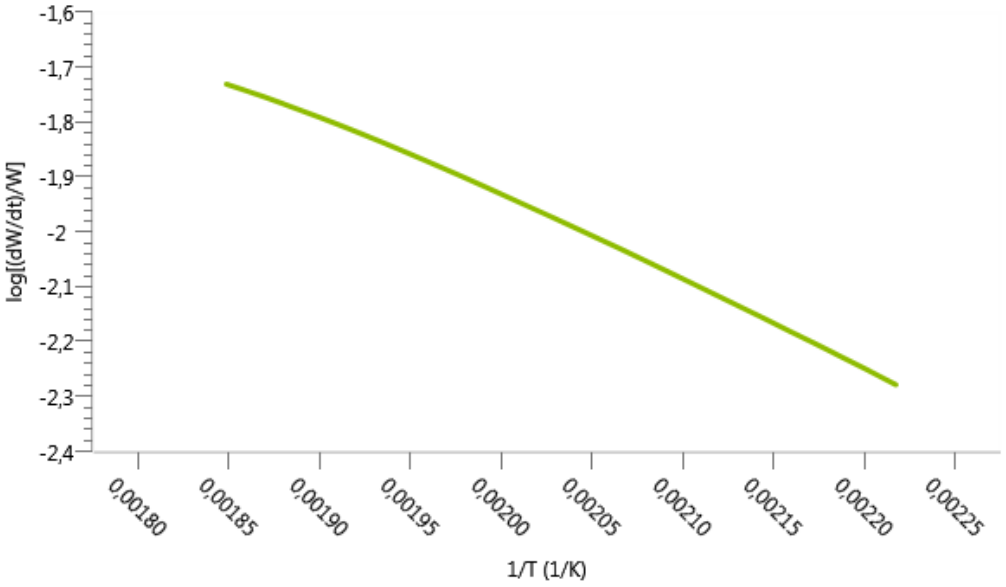

Figure D.I.20 - Arrhenius plot of Crude Oil 3 Resin for I. Region at 10 °C/min

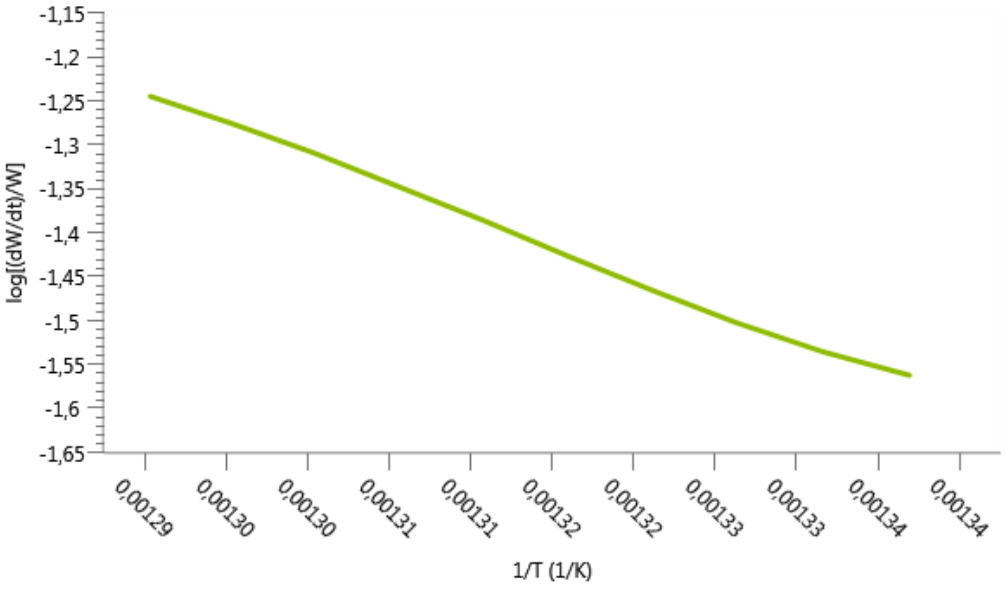

Figure D.I.21 - Arrhenius plot of Crude Oil 3 Resin for II. Region at 10 °C/min

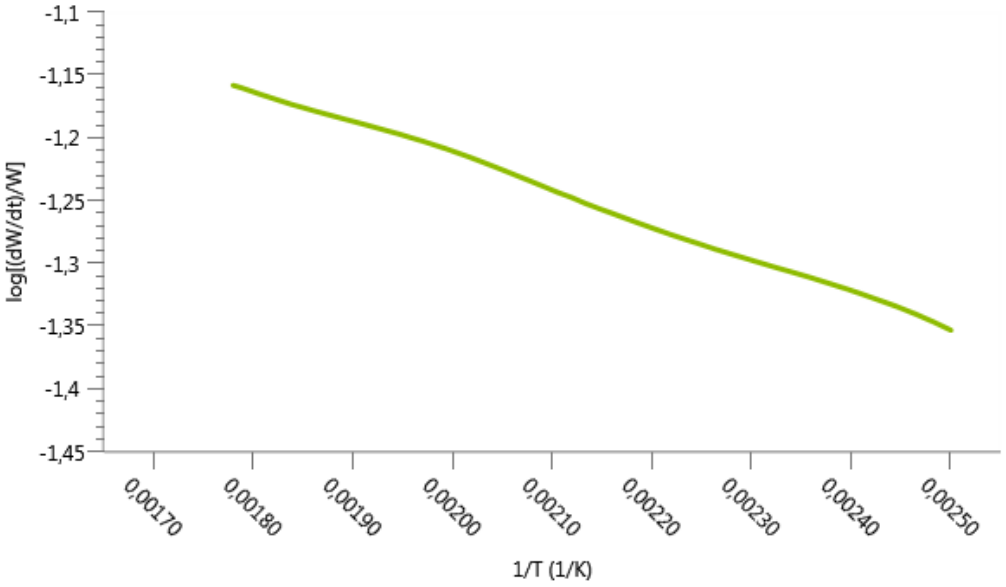

Figure D.I.22 - Arrhenius plot of Crude Oil 4 for I. Region at 10 °C/min

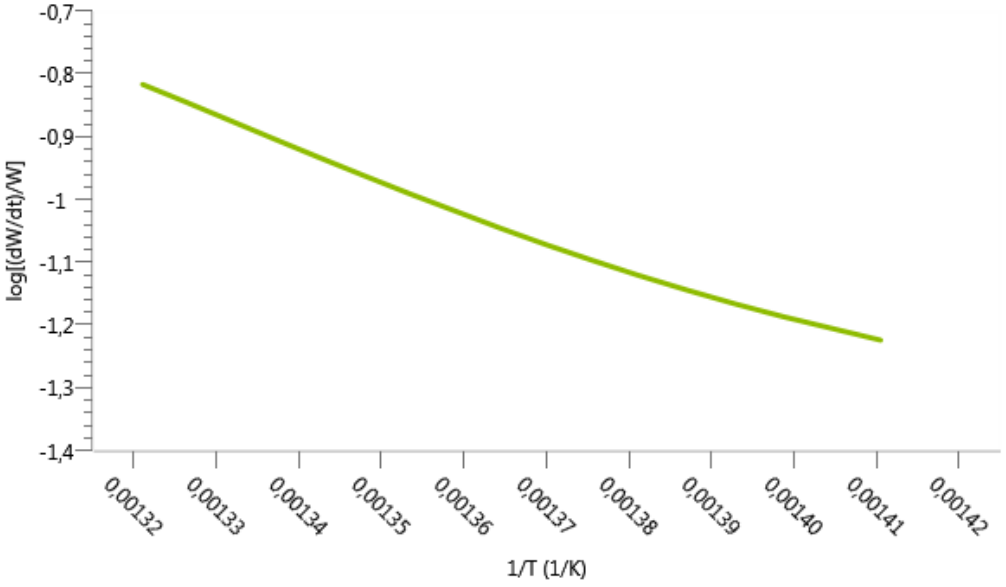

Figure D.I.23 - Arrhenius plot of Crude Oil 4 for II. Region at 10 °C/min

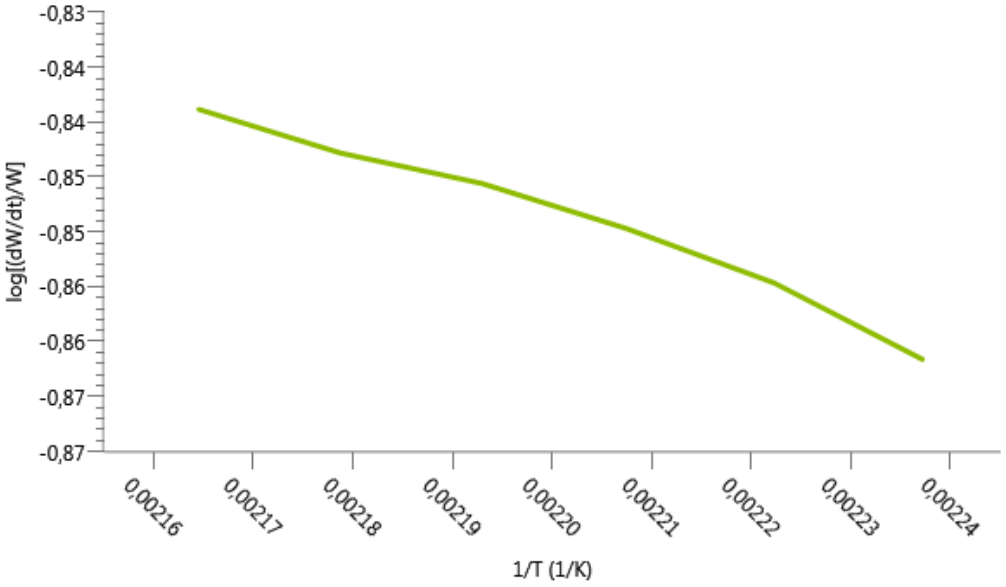

Figure D.I.24 - Arrhenius plot of Crude Oil 4 Saturate for I. Region at 10 °C/min

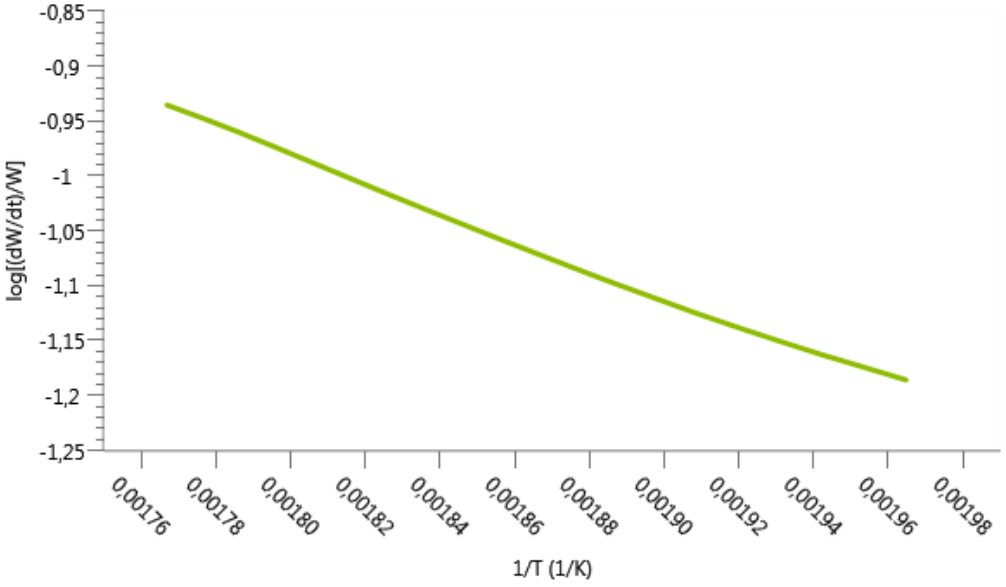

Figure D.I.25 - Arrhenius plot of Crude Oil 4 Aromatic for I. Region at 10 °C/min

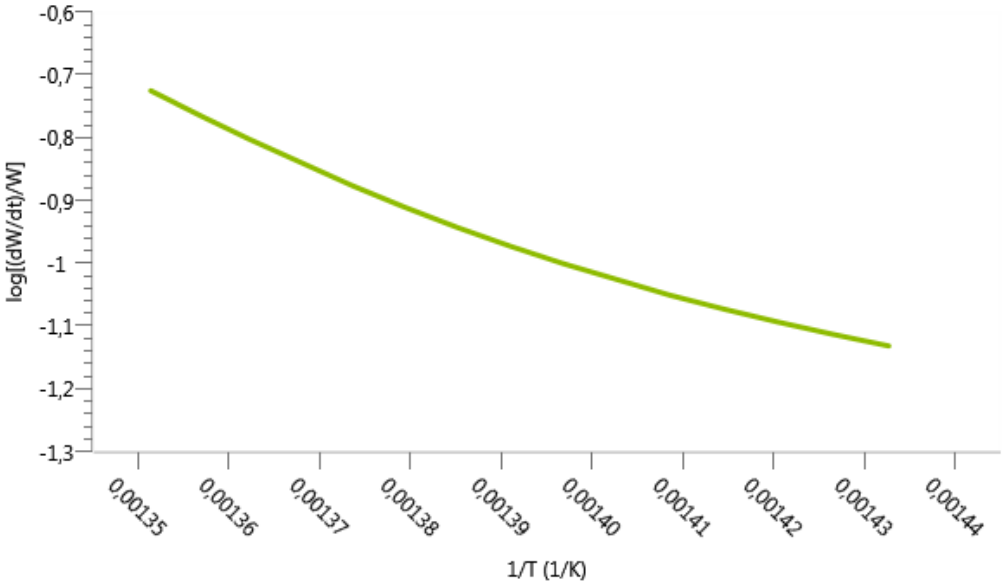

Figure D.I.26 - Arrhenius plot of Crude Oil 4 Aromatic for II. Region at 10 °C/min

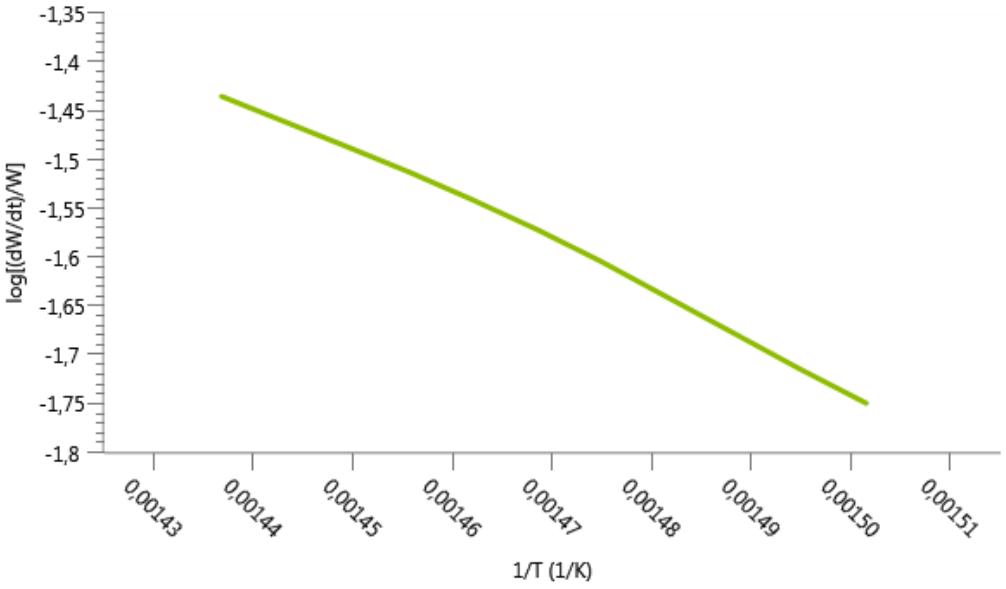

Figure D.I.27 - Arrhenius plot of Crude Oil 4 Resin for I. Region at 10 °C/min

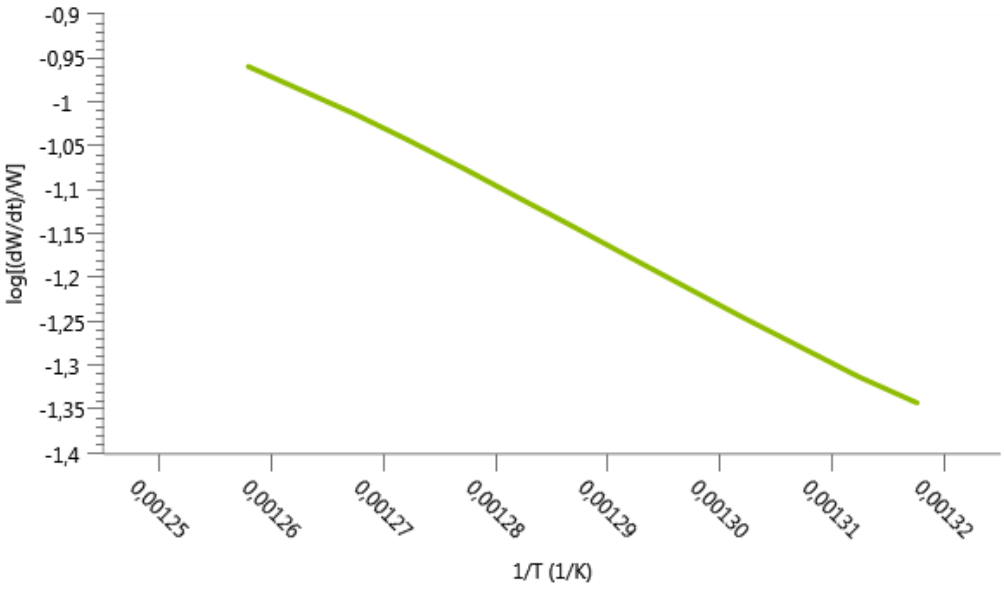

Figure D.I.28 - Arrhenius plot of Crude Oil 4 Resin for II. Region at 10 °C/min

D.II. Plots of Coats and Redfern Method

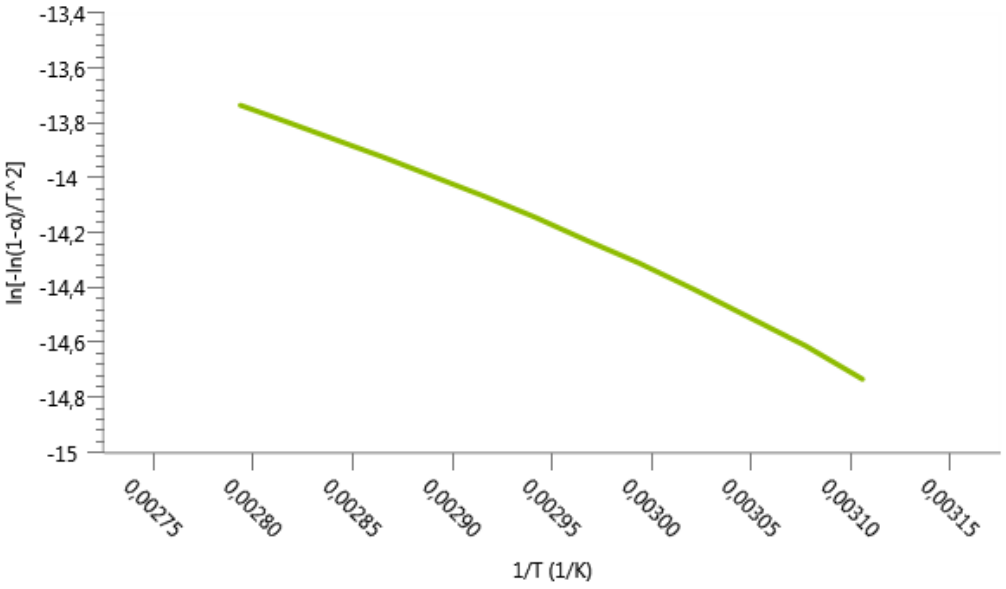

Figure D.II.1 - Coats and Redfern plot of Crude Oil 1 for I. Region at 10 °C/min

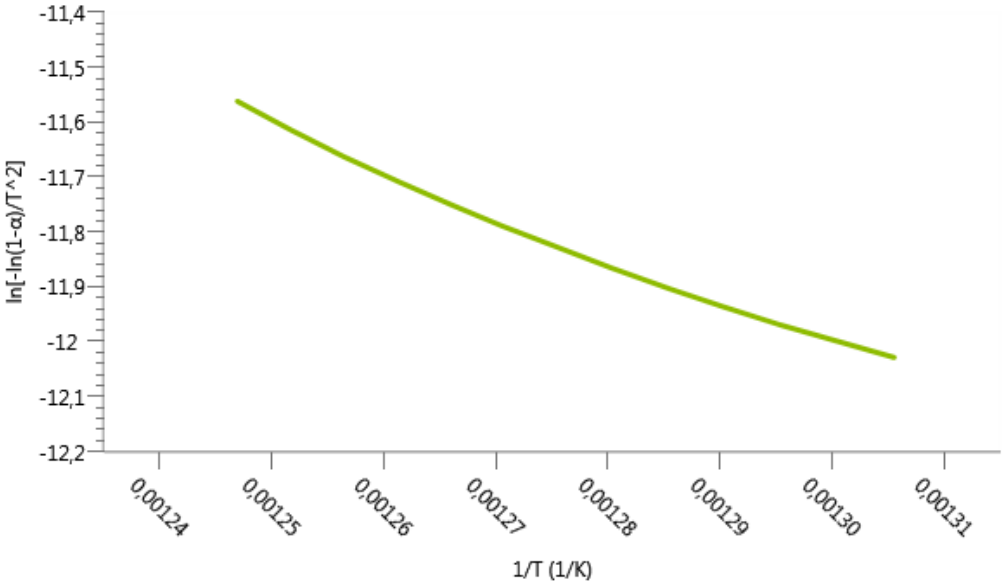

Figure D.II.2 - Coats and Redfern plot of Crude Oil 1 for II. Region at 10 °C/min

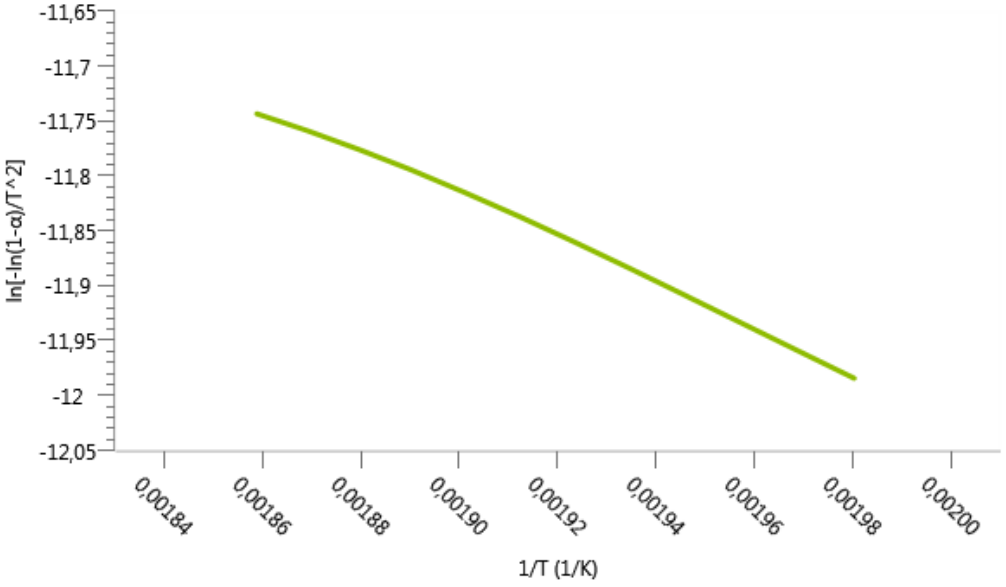

Figure D.II.3 - Coats and Redfern plot of Crude Oil 1 Saturate for I. Region at 10 °C/min

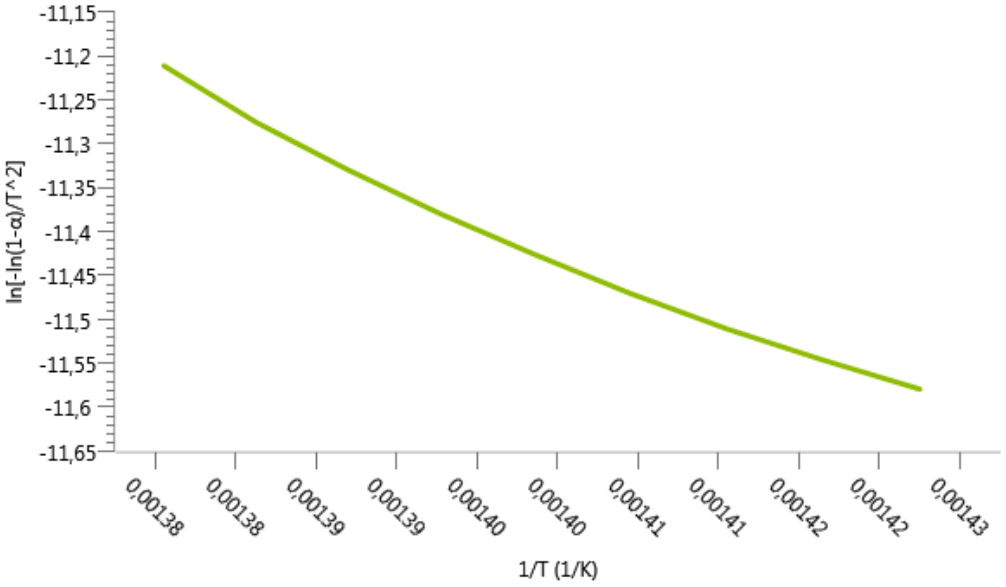

Figure D.II.4 - Coats and Redfern plot of Crude Oil 1 Saturate for II. Region at 10 °C/min

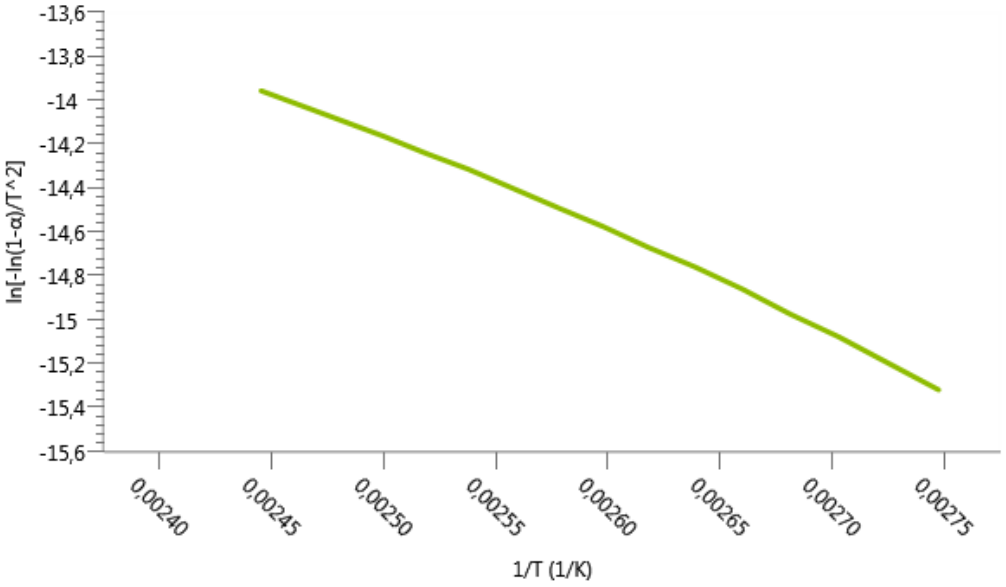

Figure D.II.5 - Coats and Redfern plot of Crude Oil 1 Aromatic for I. Region at 10 °C/min

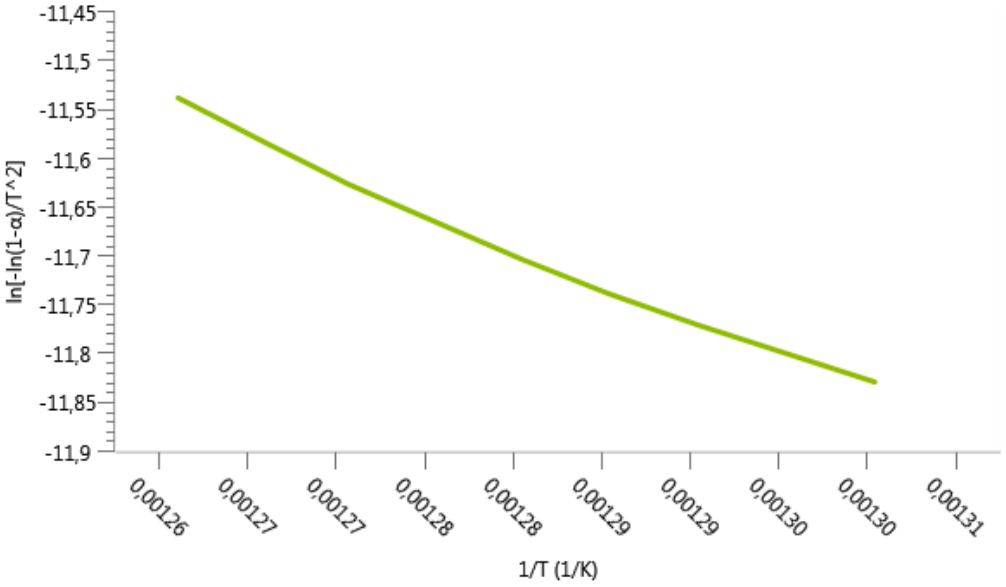

Figure D.II.6 - Coats and Redfern plot of Crude Oil 1 Aromatic for II. Region at 10 °C/min

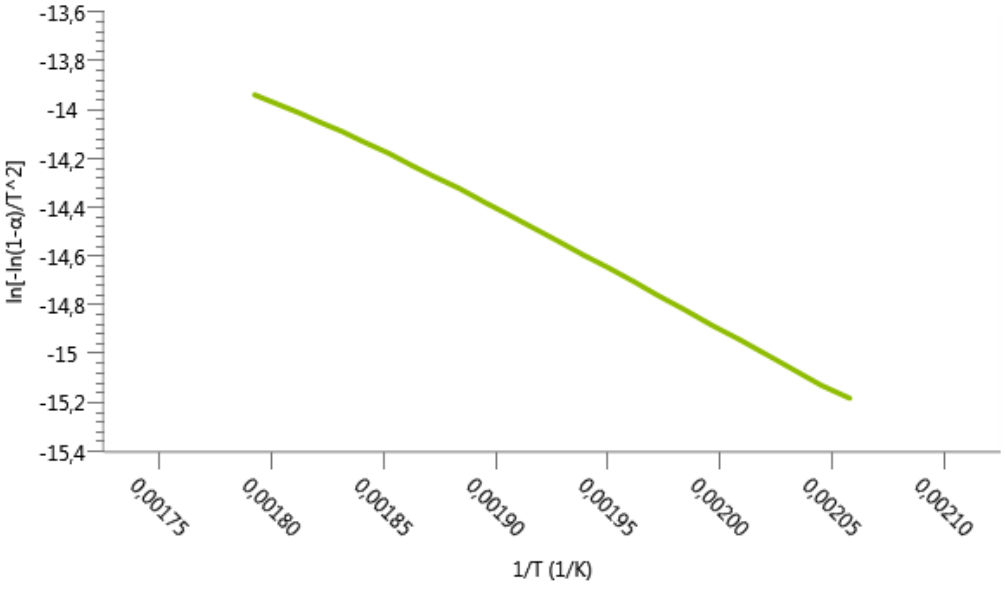

Figure D.II.7 - Coats and Redfern plot of Crude Oil 1 Resin for I. Region at 10 °C/min

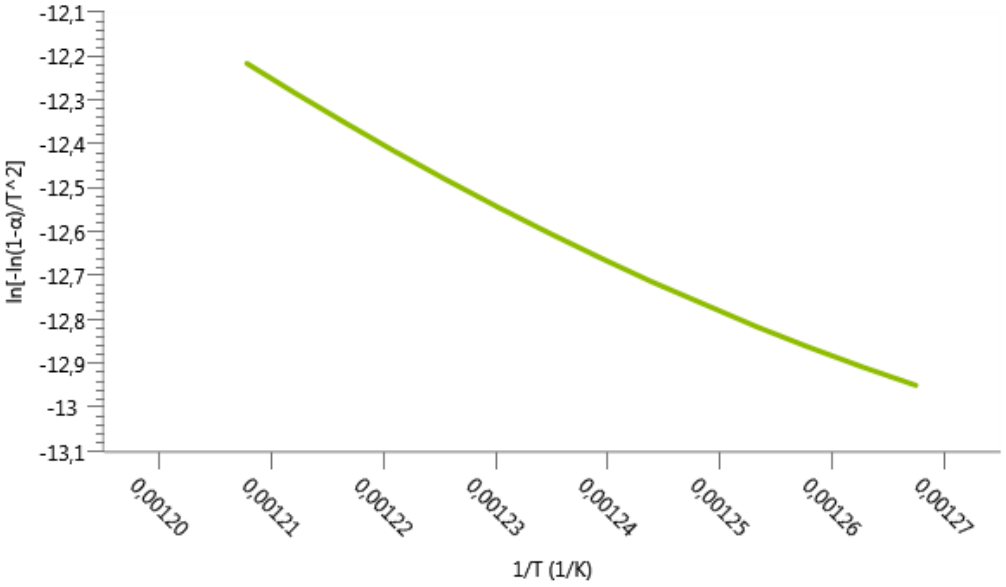

Figure D.II.8 - Coats and Redfern plot of Crude Oil 1 Resin for II. Region at 10 °C/min

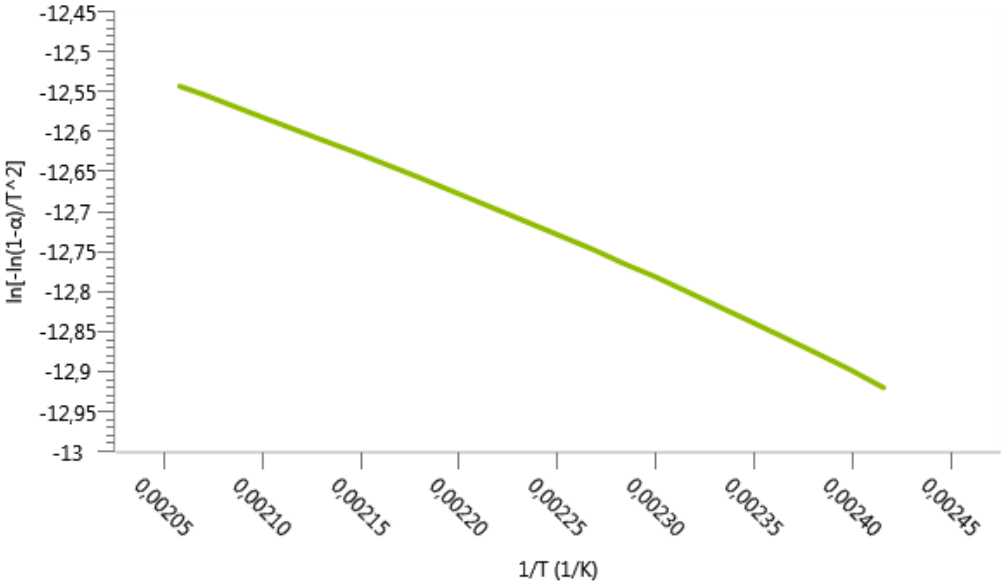

Figure D.II.9 - Coats and Redfern plot of Crude Oil 2 for I. Region at 10 °C/min

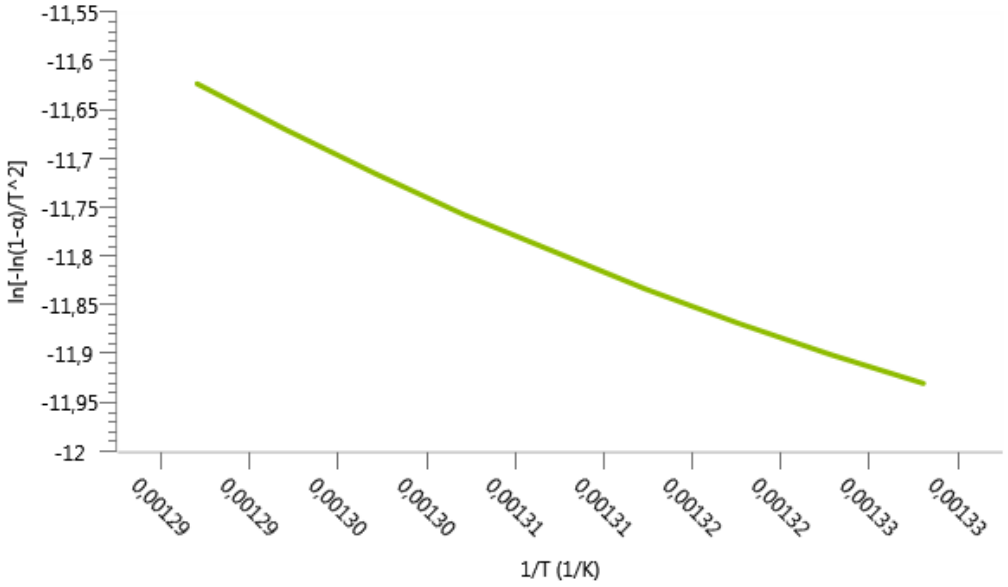

Figure D.II.10 - Coats and Redfern plot of Crude Oil 2 for II. Region at 10 °C/min

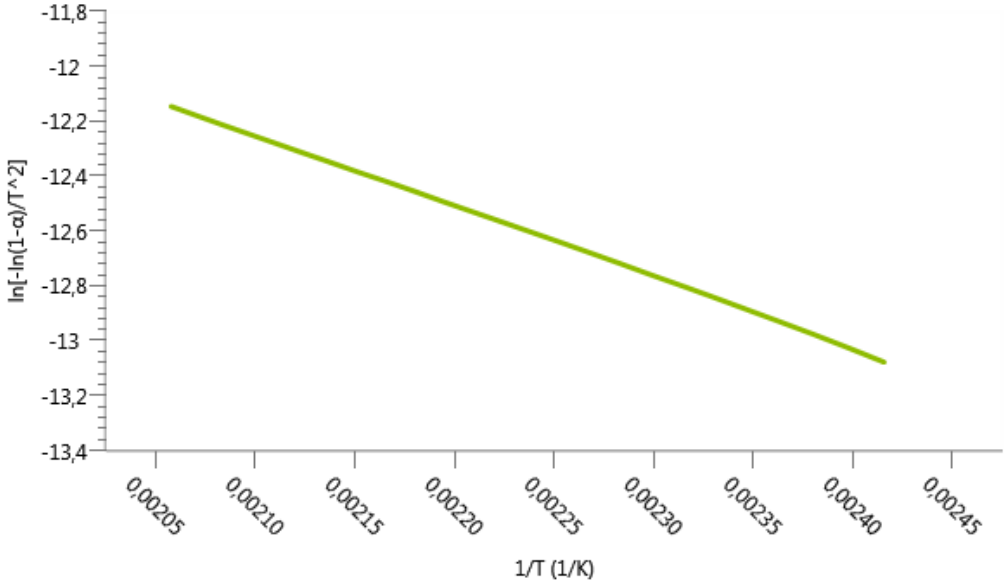

Figure D.II.11 - Coats and Redfern plot of Crude Oil 2 Saturate for I. Region at 10 °C/min

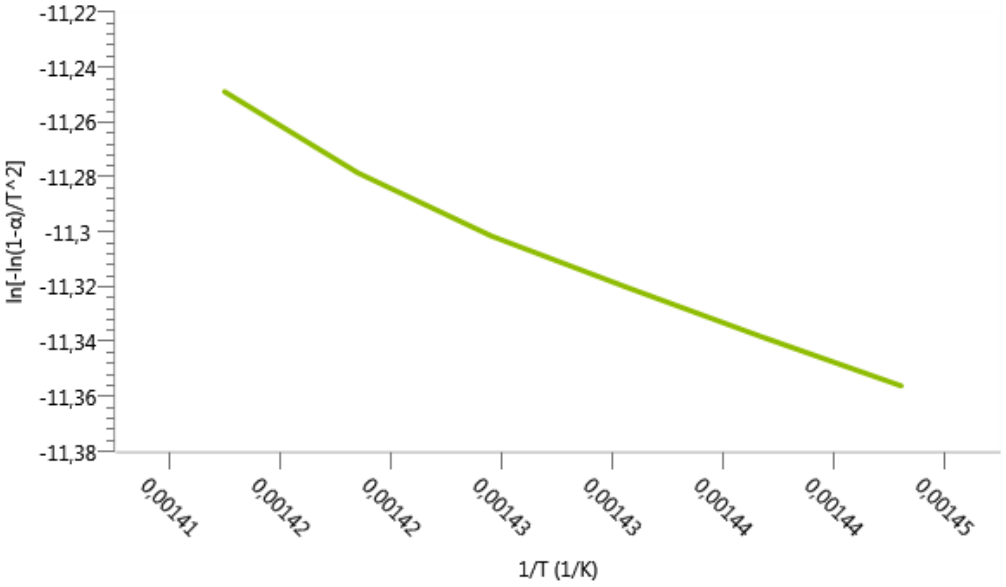

Figure D.II.12 - Coats and Redfern plot of Crude Oil 2 Saturate for II. Region at 10 °C/min

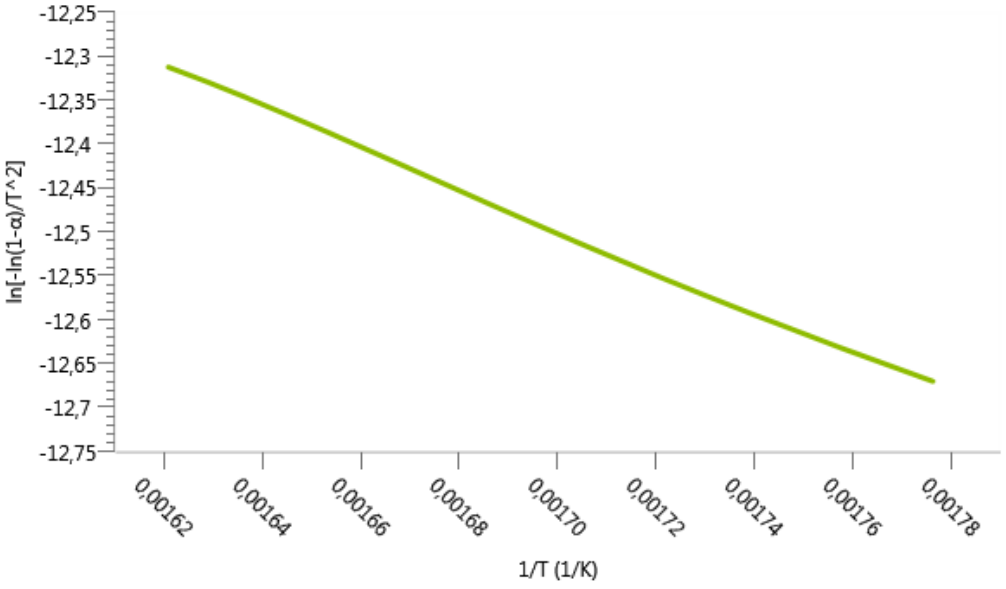

Figure D.II.13 - Coats and Redfern plot of Crude Oil 2 Aromatic for I. Region at 10 °C/min

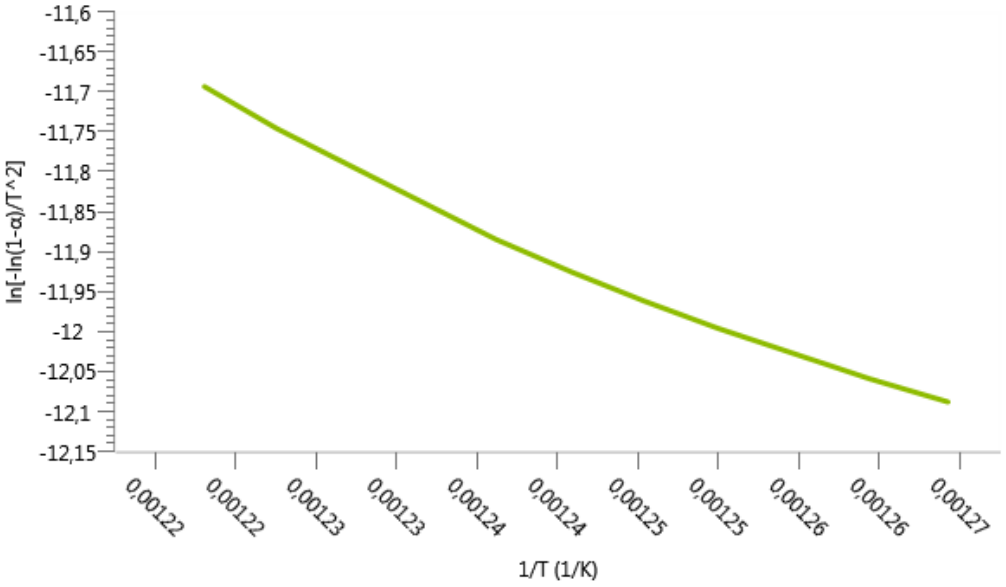

Figure D.II.14 - Coats and Redfern plot of Crude Oil 2 Aromatic for II. Region at 10 °C/min

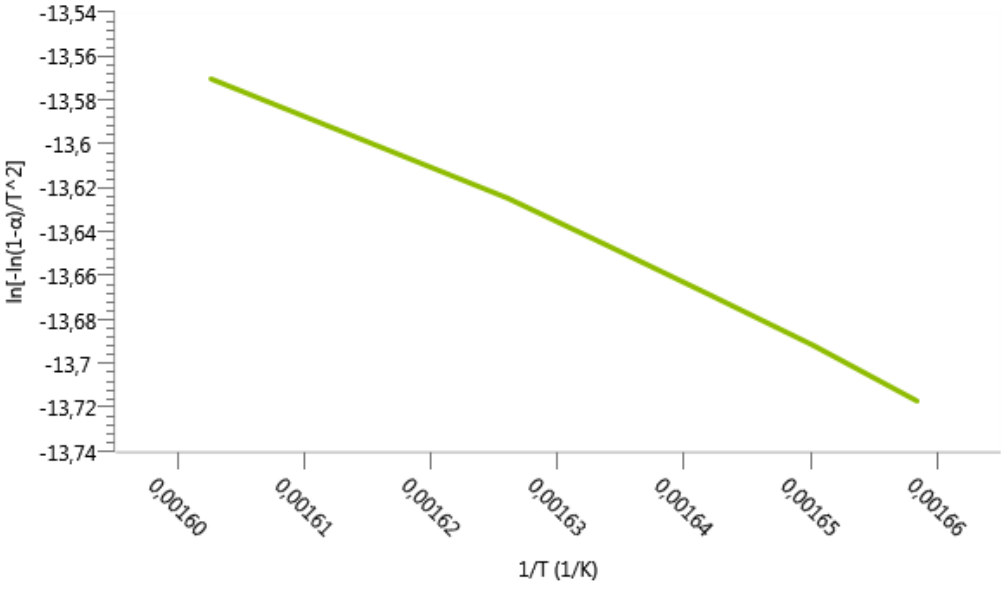

Figure D.II.15 - Coats and Redfern plot of Crude Oil 2 Resin for I. Region at 10 °C/min

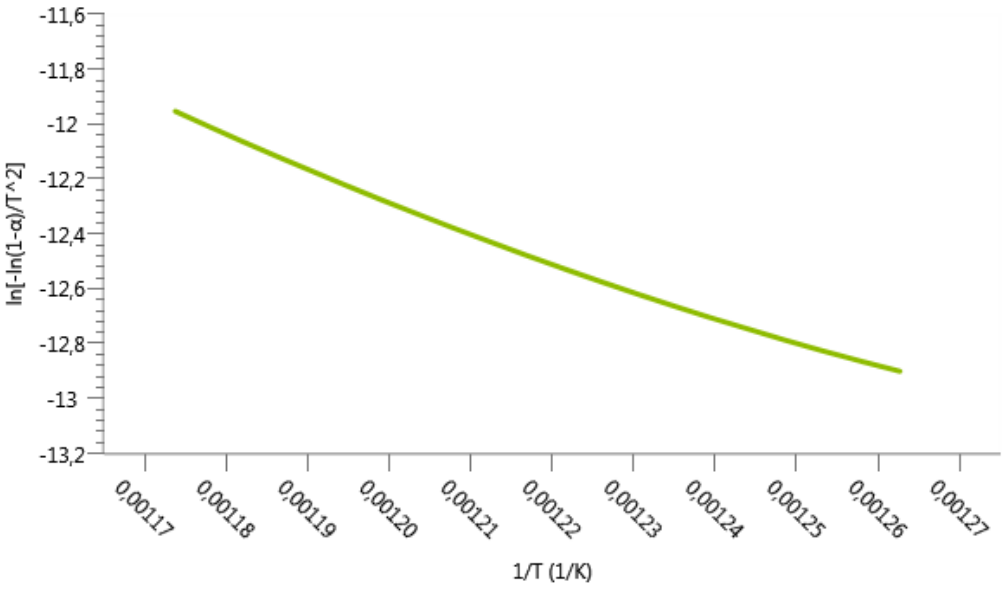

Figure D.II.16 - Coats and Redfern plot of Crude Oil 2 Resin for II. Region at 10 °C/min

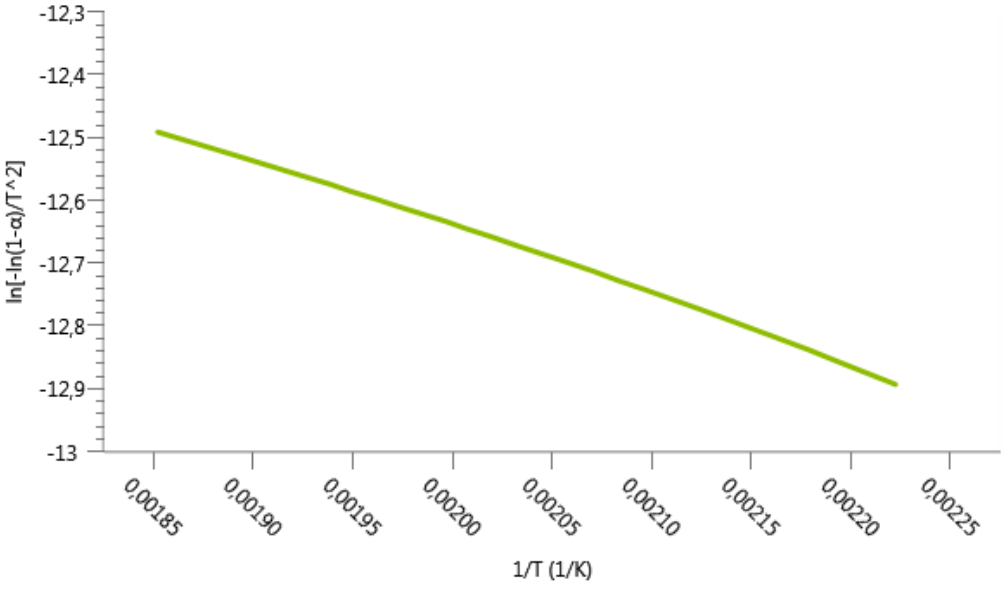

Figure D.II.17 - Coats and Redfern plot of Crude Oil 3 for I. Region at 10 °C/min

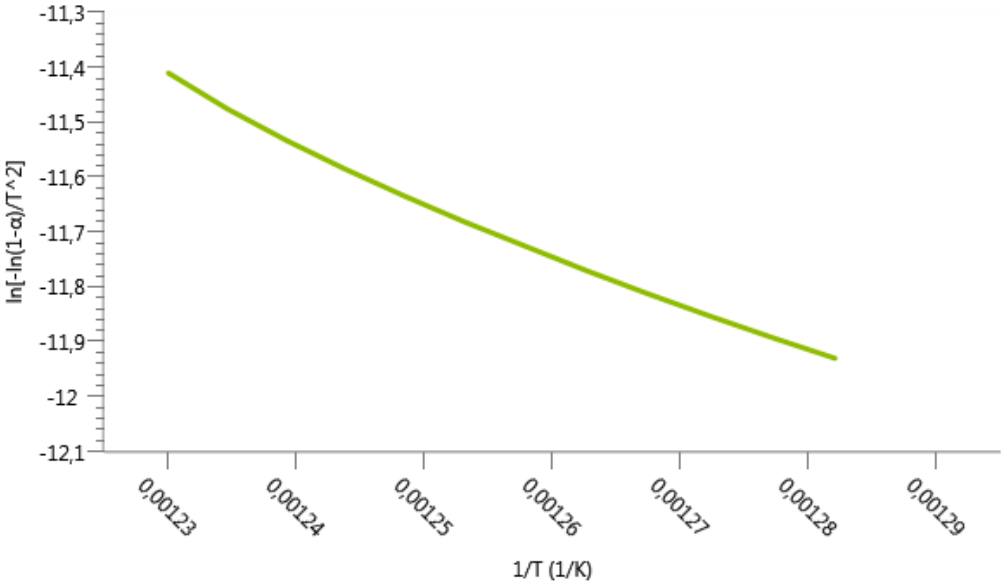

Figure D.II.18 - Coats and Redfern plot of Crude Oil 3 for II. Region at 10 °C/min

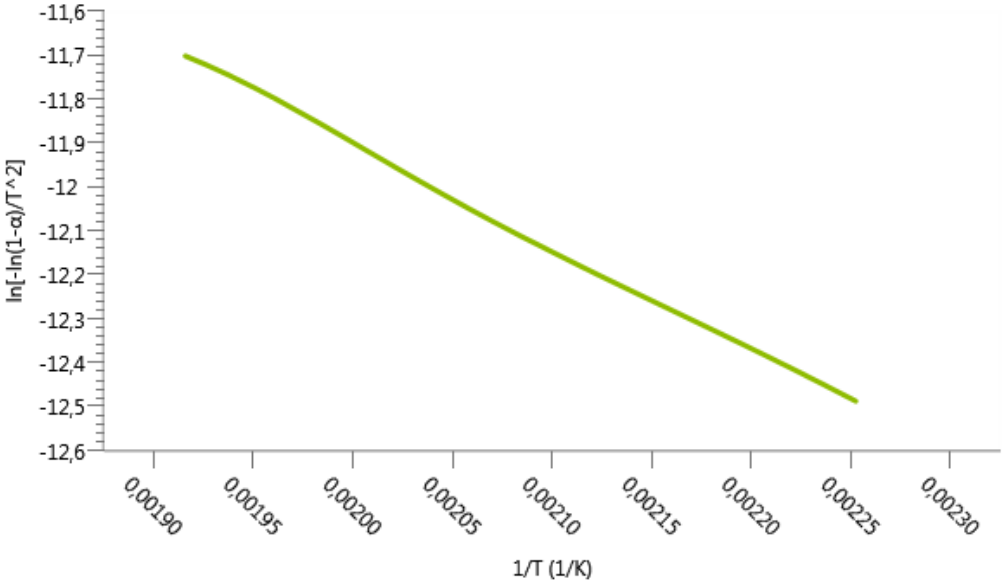

Figure D.II.19 - Coats and Redfern plot of Crude Oil 3 Saturate for I. Region at 10 °C/min

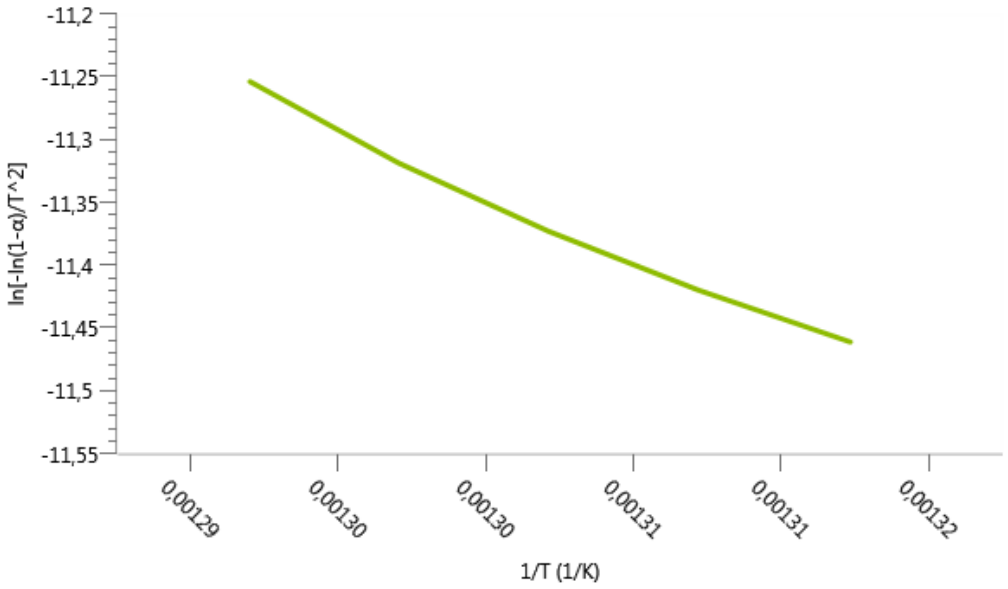

Figure D.II.20 - Coats and Redfern plot of Crude Oil 3 Saturate for II. Region at 10 °C/min

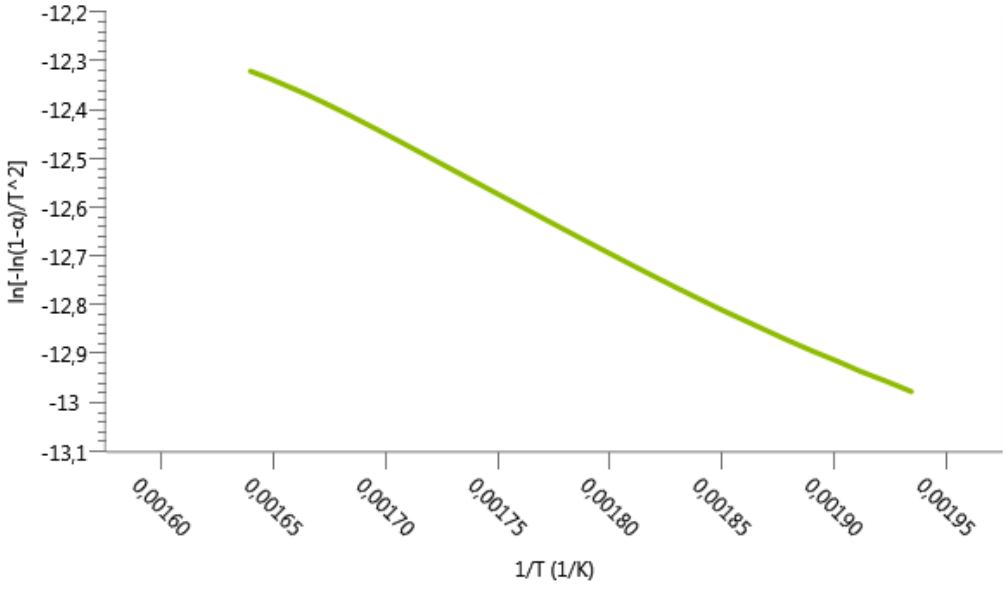

Figure D.II.21 - Coats and Redfern plot of Crude Oil 3 Aromatic for I. Region at 10 °C/min

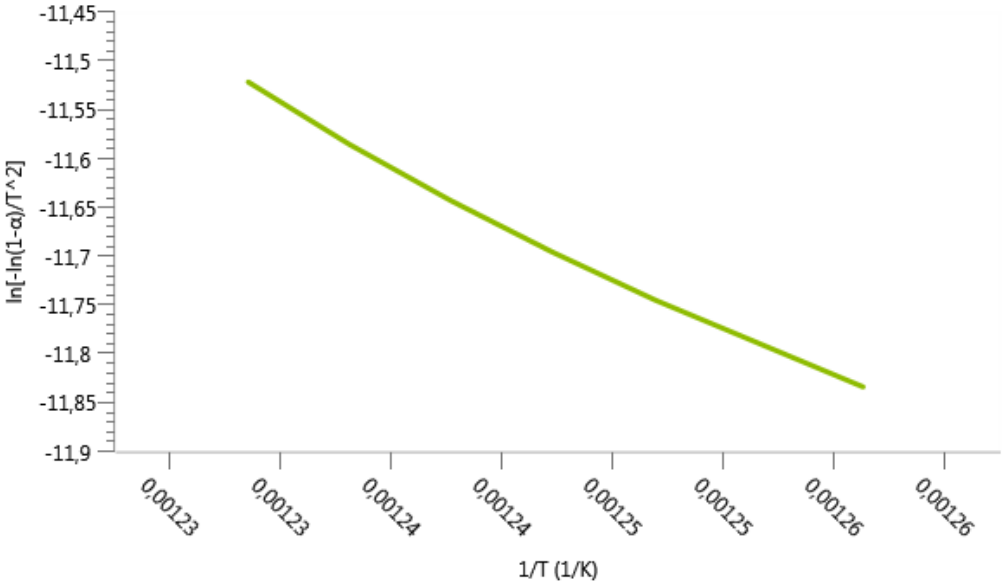

Figure D.II.22 - Coats and Redfern plot of Crude Oil 3 Aromatic for II. Region at 10 °C/min

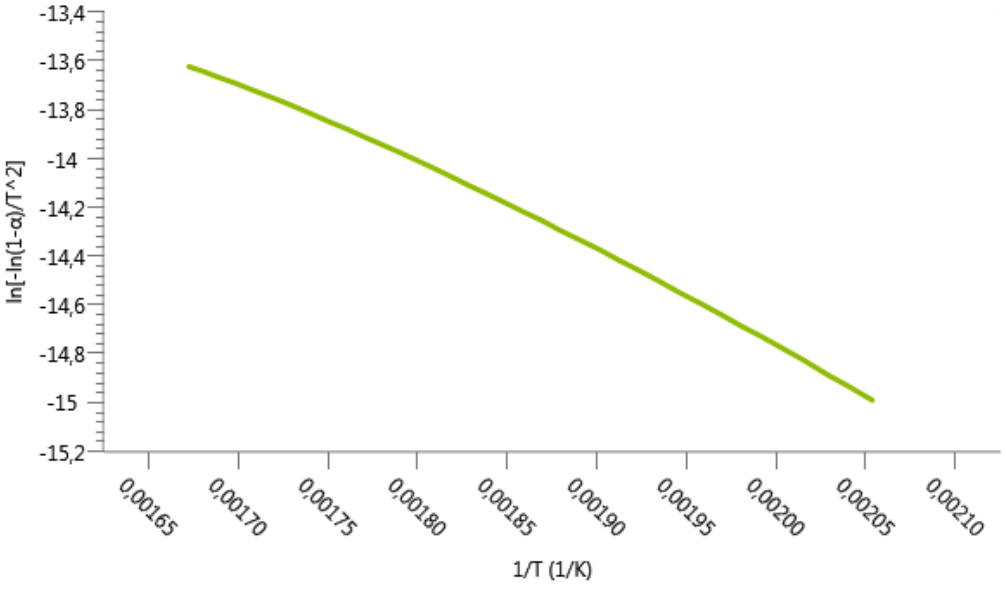

Figure D.II.23 - Coats and Redfern plot of Crude Oil 3 Resin for I. Region at 10 °C/min

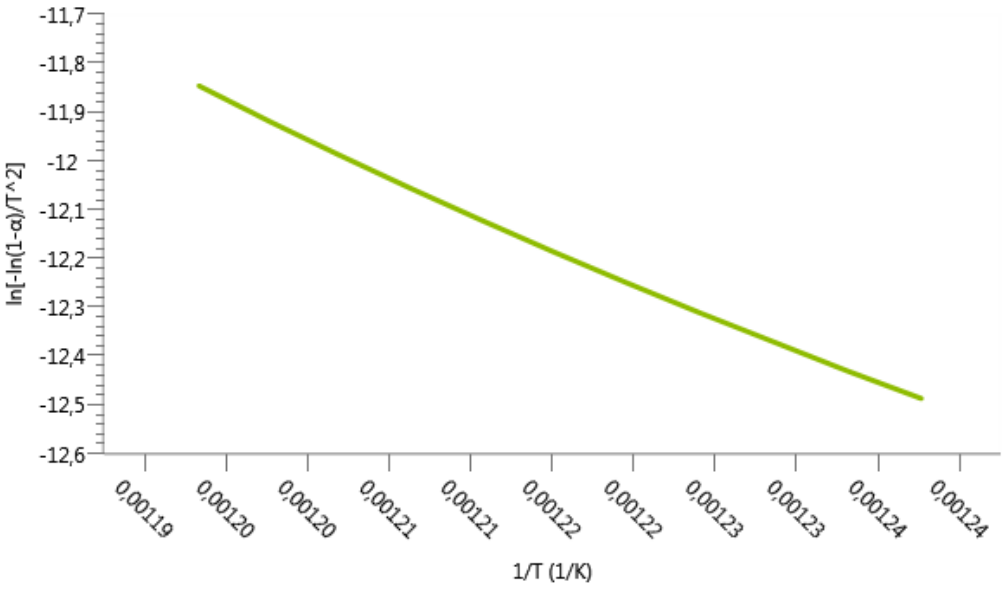

Figure D.II.24 - Coats and Redfern plot of Crude Oil 3 Resin for II. Region at 10 °C/min

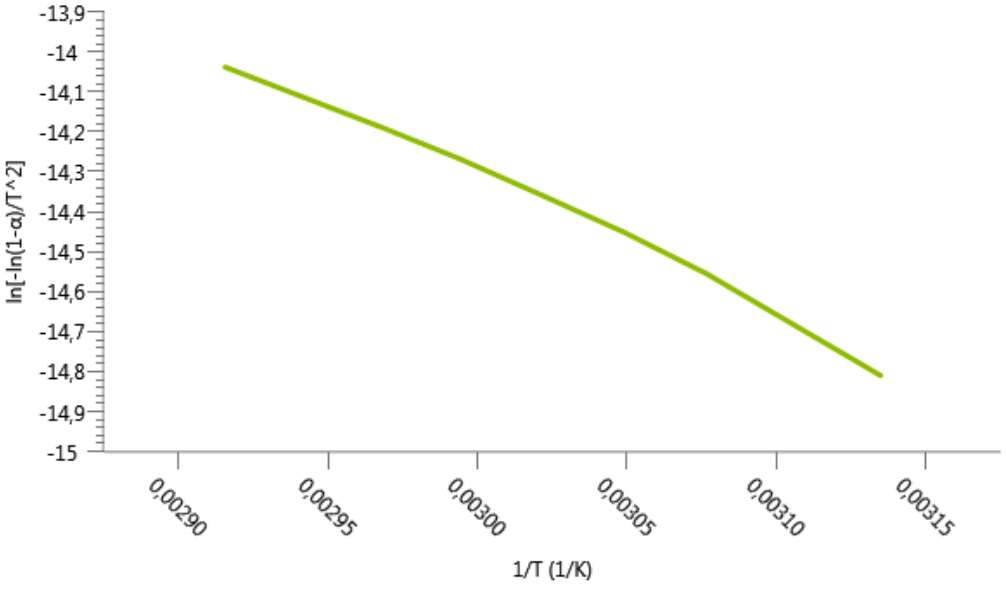

Figure D.II.25 - Coats and Redfern plot of Crude Oil 4 for I. Region at 10 °C/min

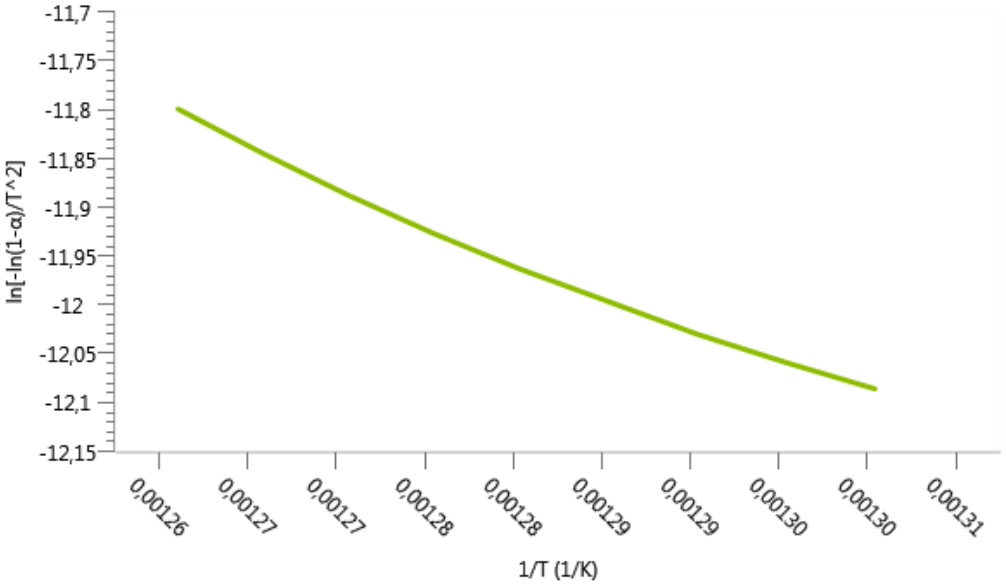

Figure D.II.26 - Coats and Redfern plot of Crude Oil 4 for II. Region at 10 °C/min

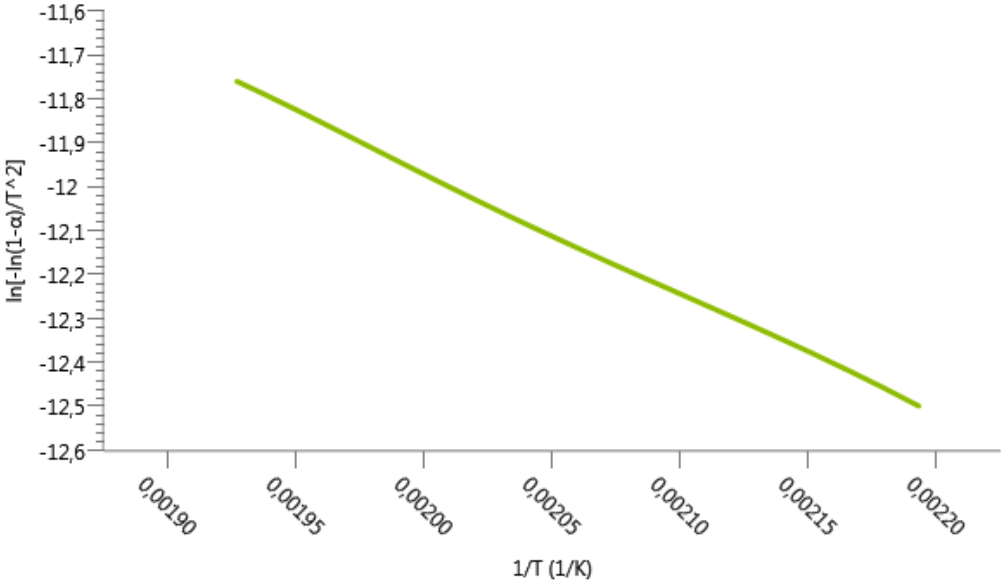

Figure D.II.27 - Coats and Redfern plot of Crude Oil 4 Saturate for I. Region at 10 °C/min

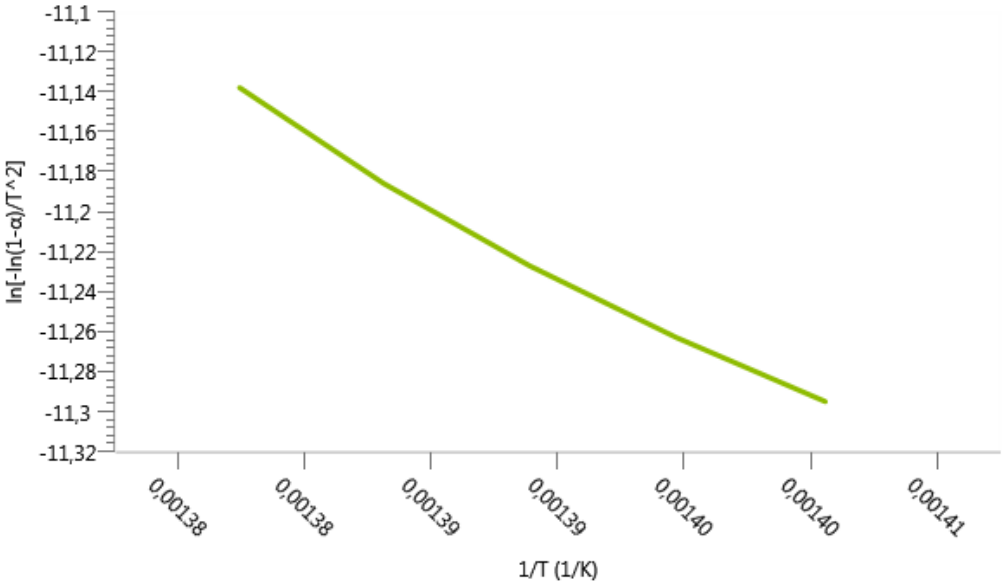

Figure D.II.28 - Coats and Redfern plot of Crude Oil 4 Saturate for II. Region at 10 °C/min

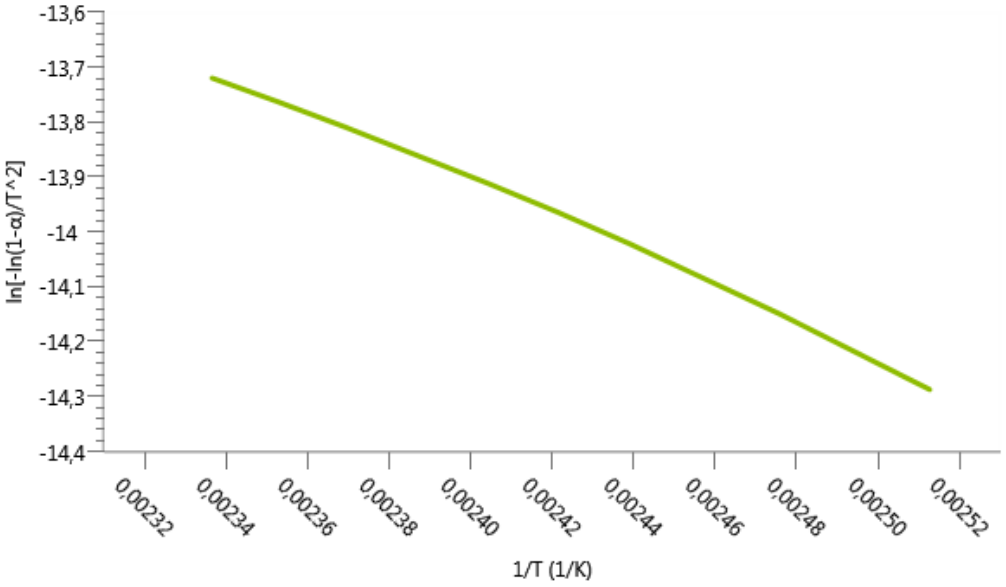

Figure D.II.29 - Coats and Redfern plot of Crude Oil 4 Aromatic for I. Region at 10 °C/min

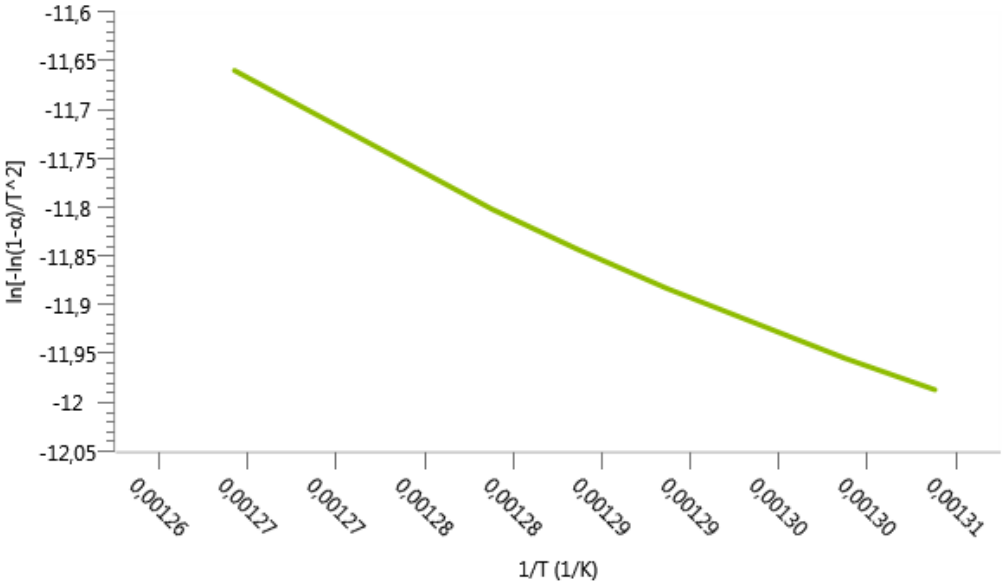

Figure D.II.30 - Coats and Redfern plot of Crude Oil 4 Aromatic for II. Region at 10 °C/min

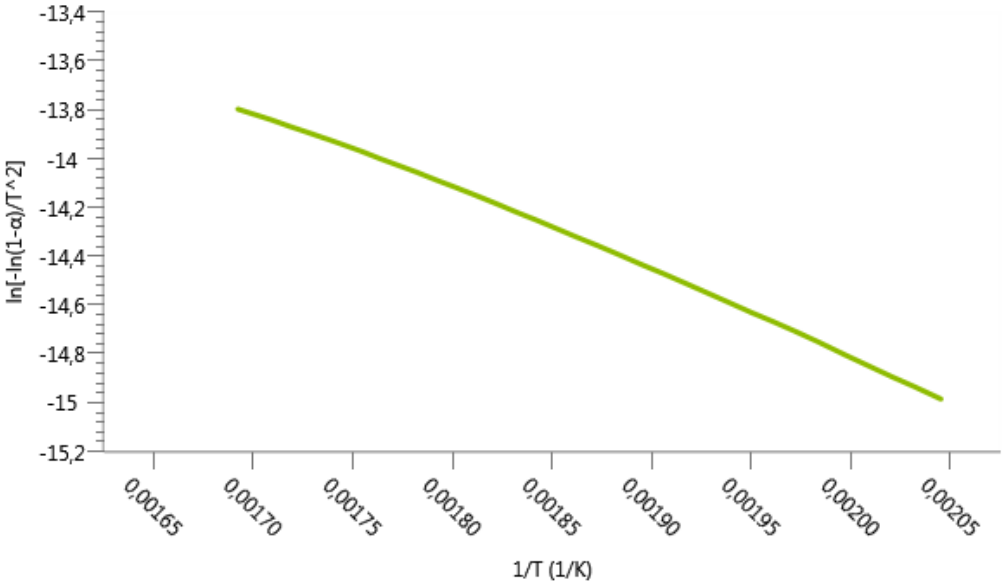

Figure D.II.31 - Coats and Redfern plot of Crude Oil 4 Resin for I. Region at 10 °C/min

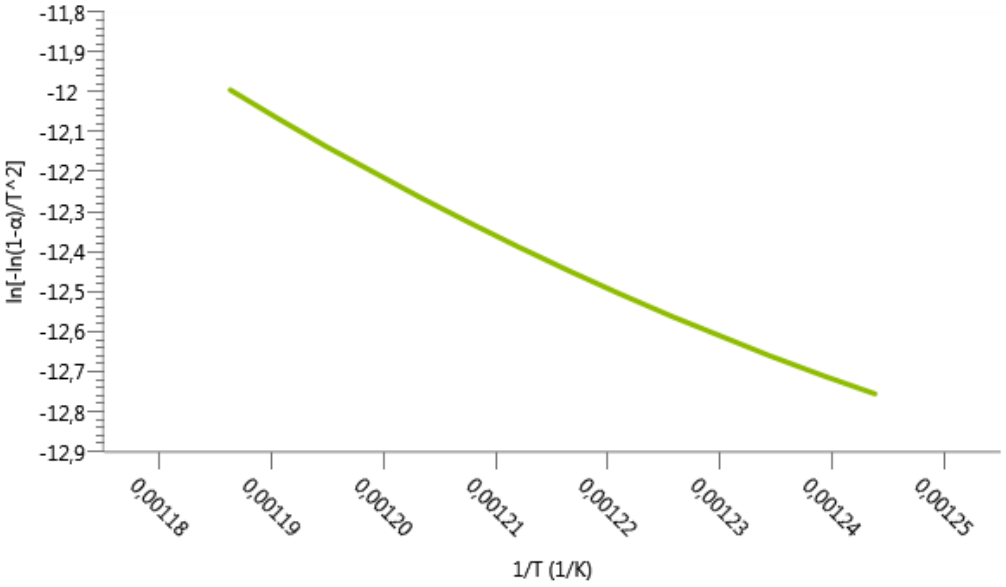

Figure D.II.32 - Coats and Redfern plot of Crude Oil 4 Resin for II. Region at 10 °C/min

APPENDIX E

ASTM E698 METHOD FOR DSC EXPERIMENTS

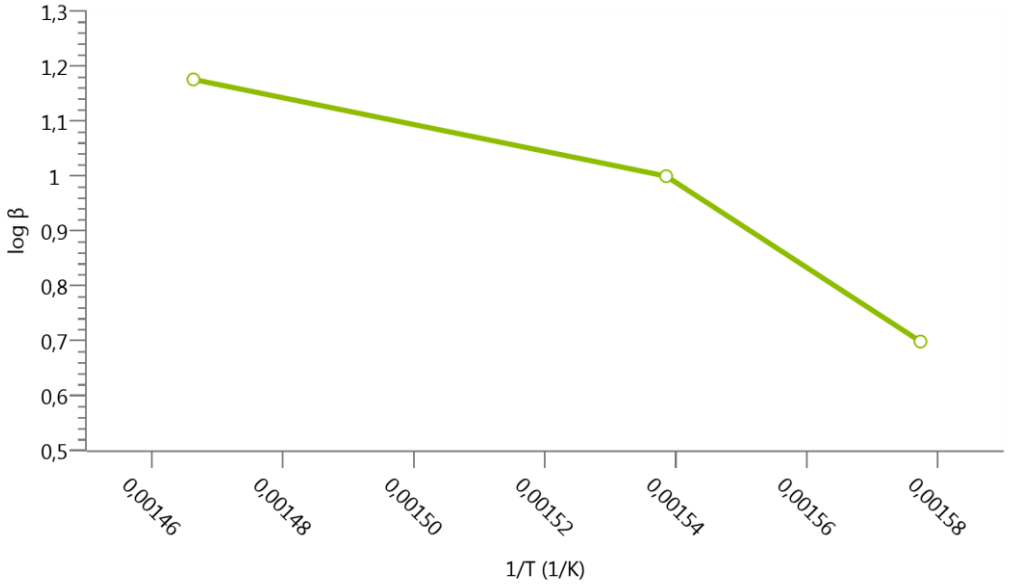

Figure D.II.1 - ASTM E698 Plot of Crude Oil 1

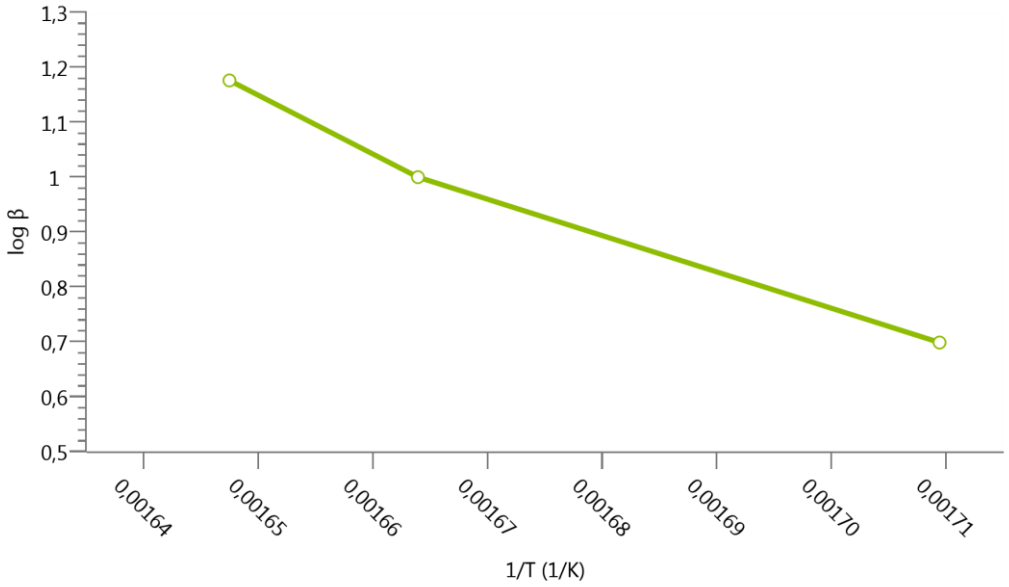

Figure D.II.2 - ASTM E698 Plot of Crude Oil 1 Saturate

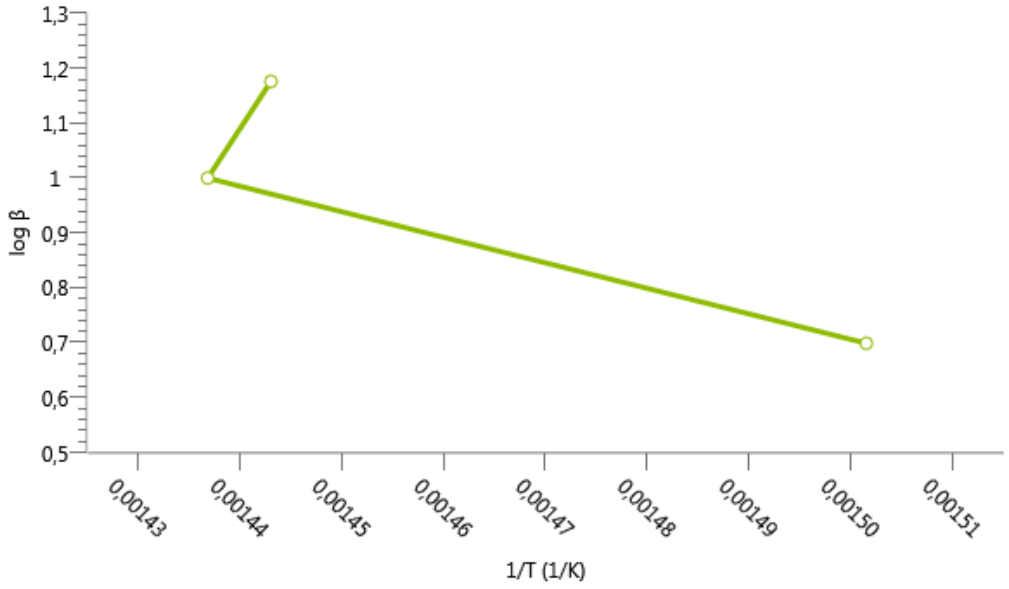

Figure D.II.3 - ASTM E698 Plot of Crude Oil 1 Aromatic

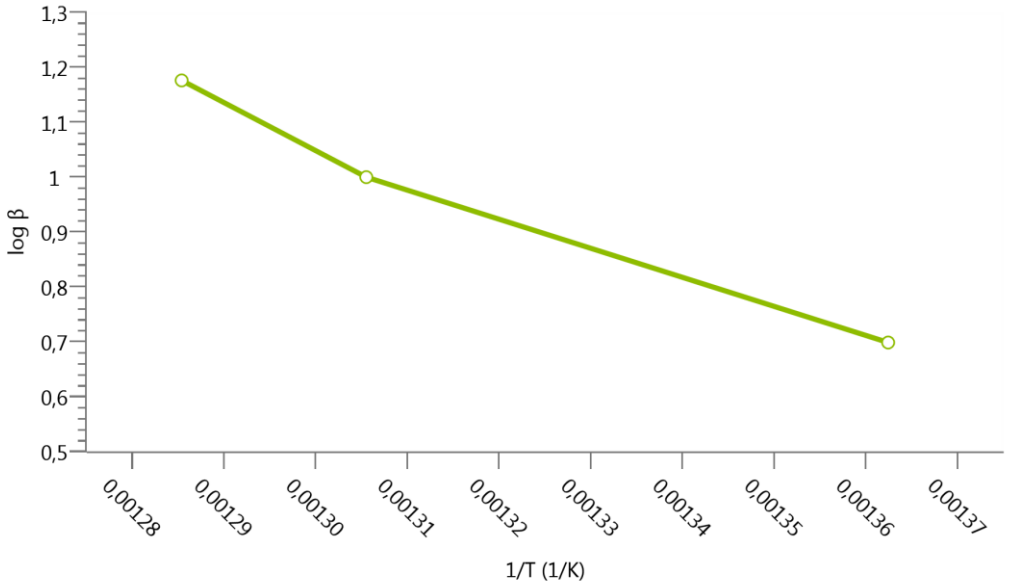

Figure D.II.4 - ASTM E698 Plot of Crude Oil 1 Resin

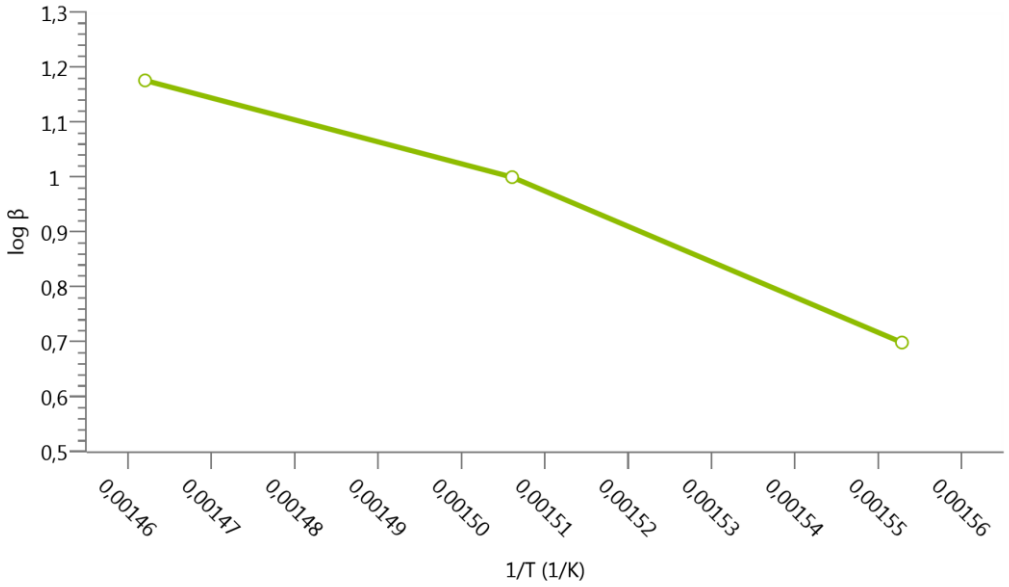

Figure D.II.5 - ASTM E698 Plot of Crude Oil 2

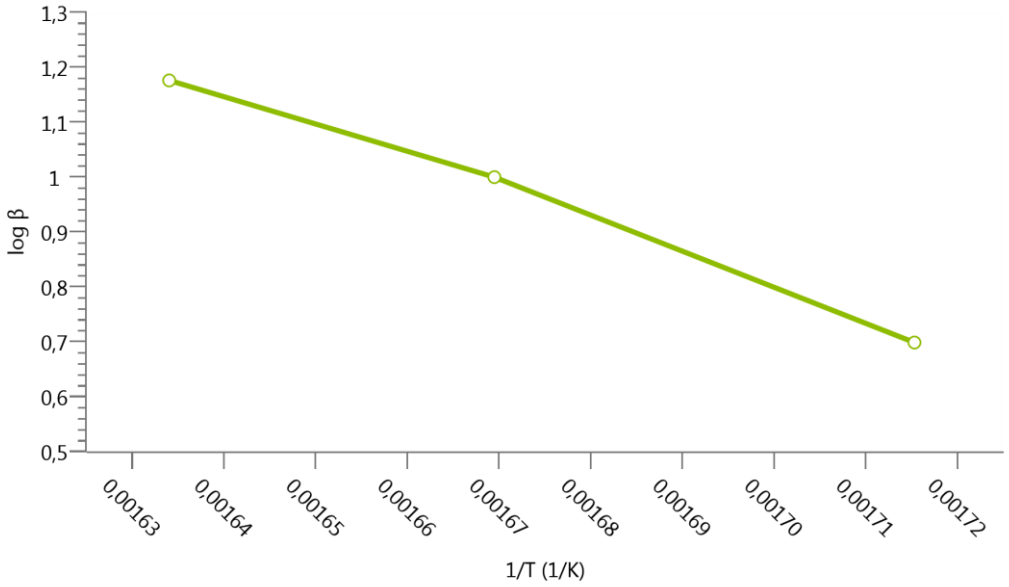

Figure D.II.6 - ASTM E698 Plot of Crude Oil 2 Saturate

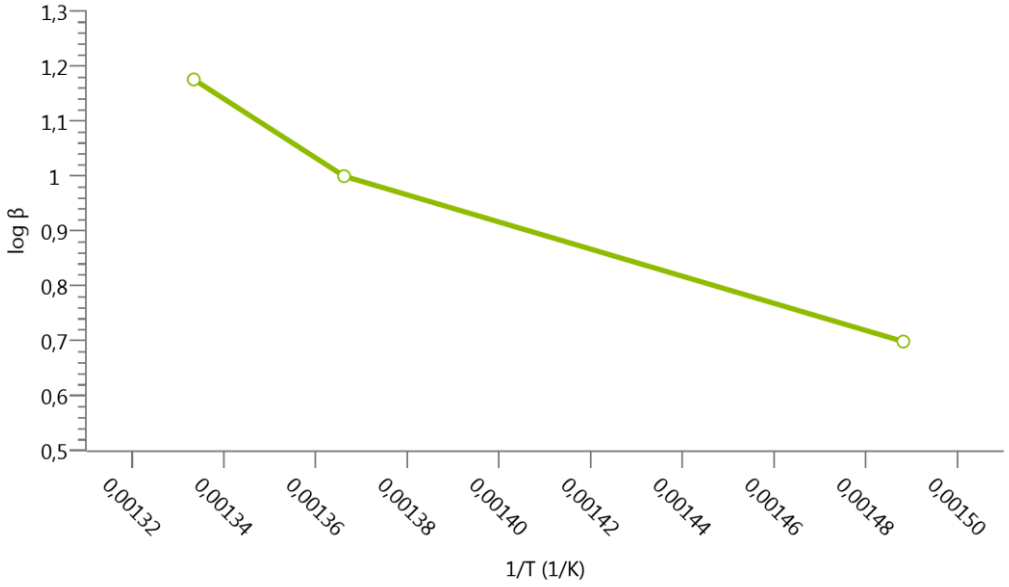

Figure D.II.7 - ASTM E698 Plot of Crude Oil 2 Aromatic

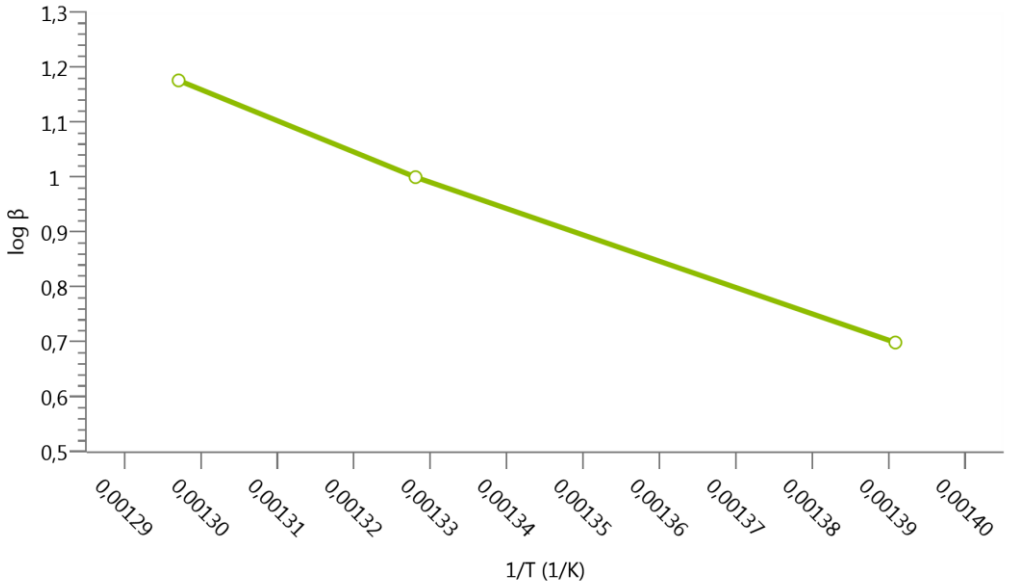

Figure D.II.8 - ASTM E698 Plot of Crude Oil 2 Resin

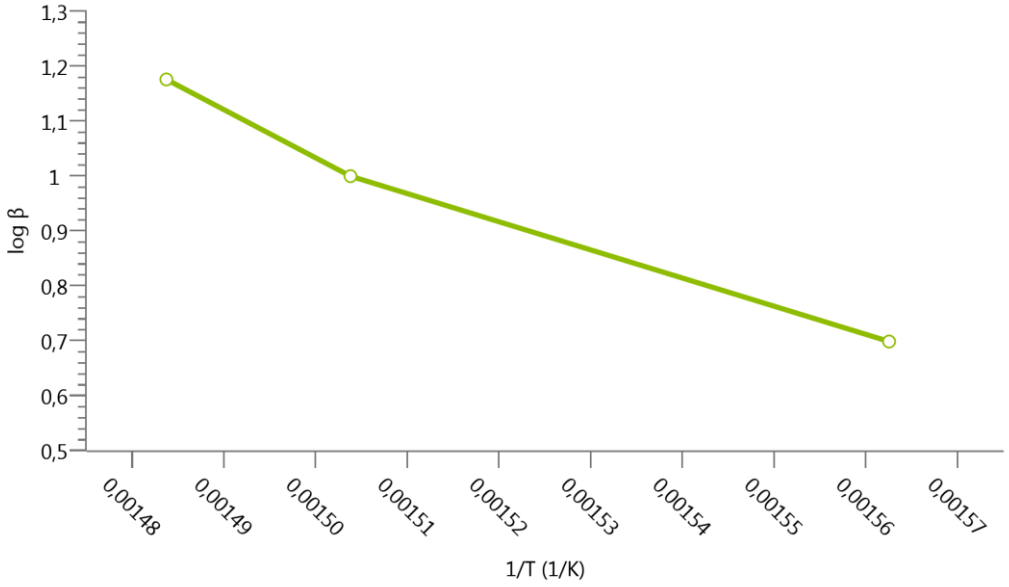

Figure D.II.9 - ASTM E698 Plot of Crude Oil 3

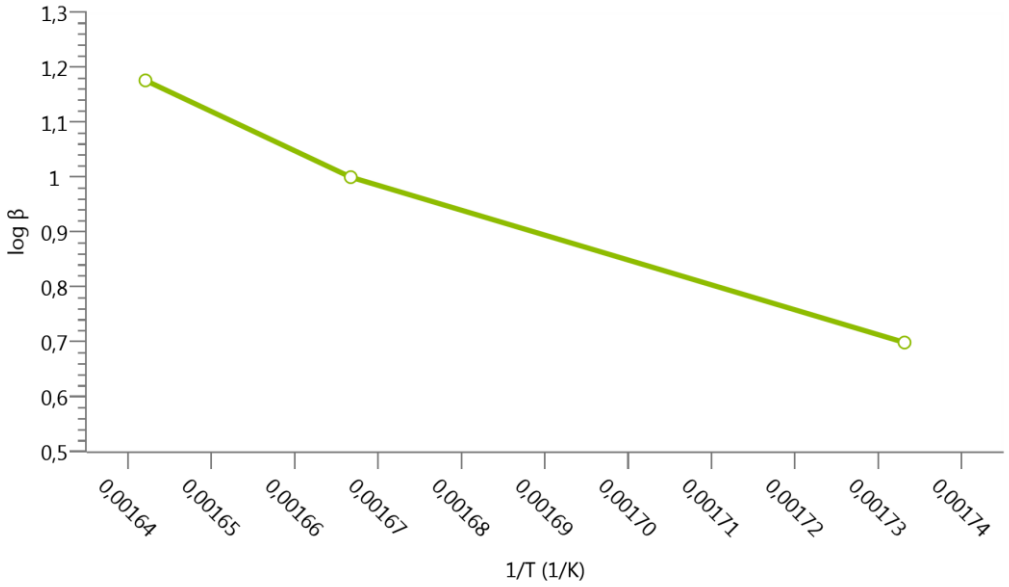

Figure D.II.10 - ASTM E698 Plot of Crude Oil 3 Saturate

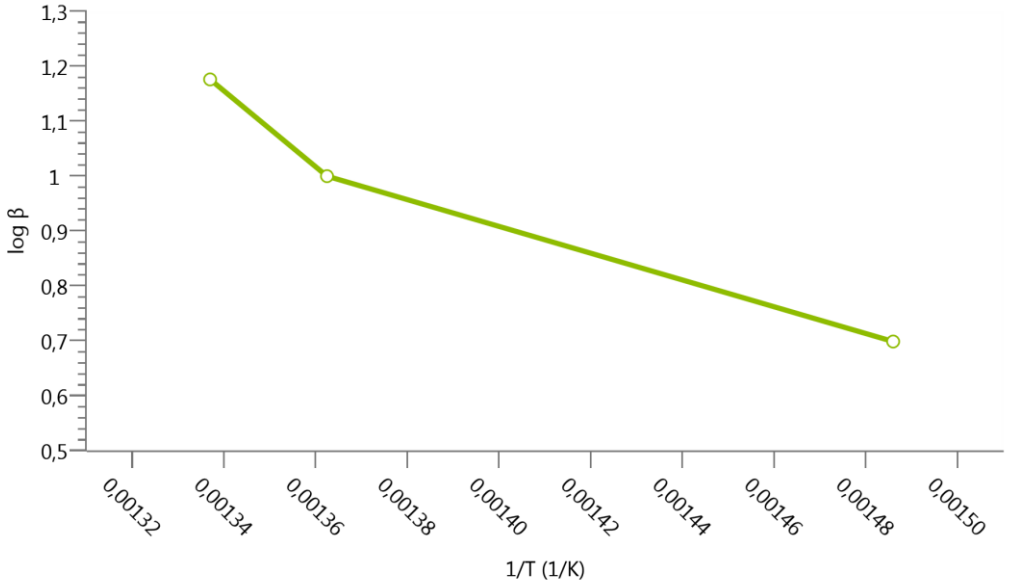

Figure D.II.11 - ASTM E698 Plot of Crude Oil 3 Aromatic

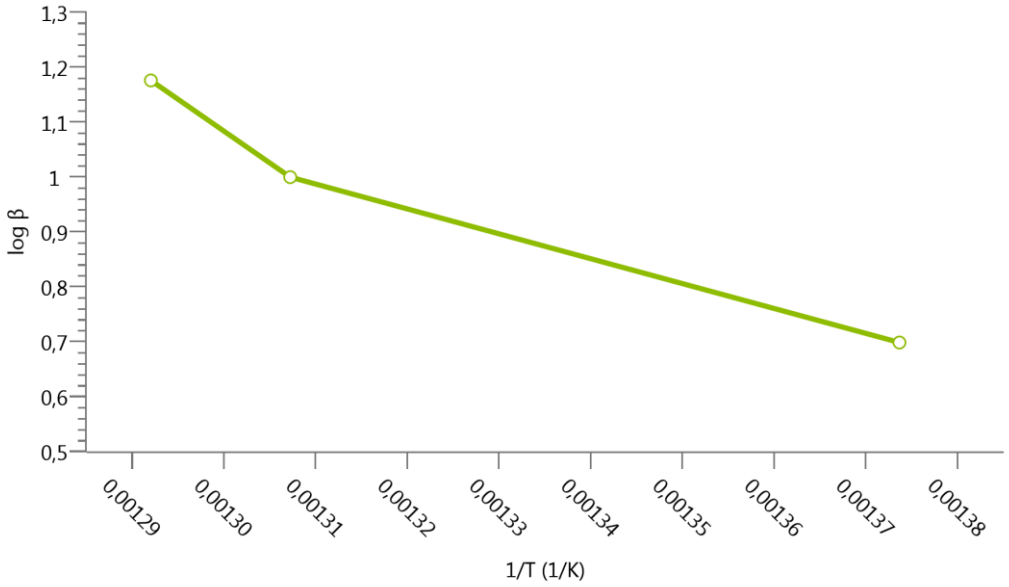

Figure D.II.12 - ASTM E698 Plot of Crude Oil 3 Resin

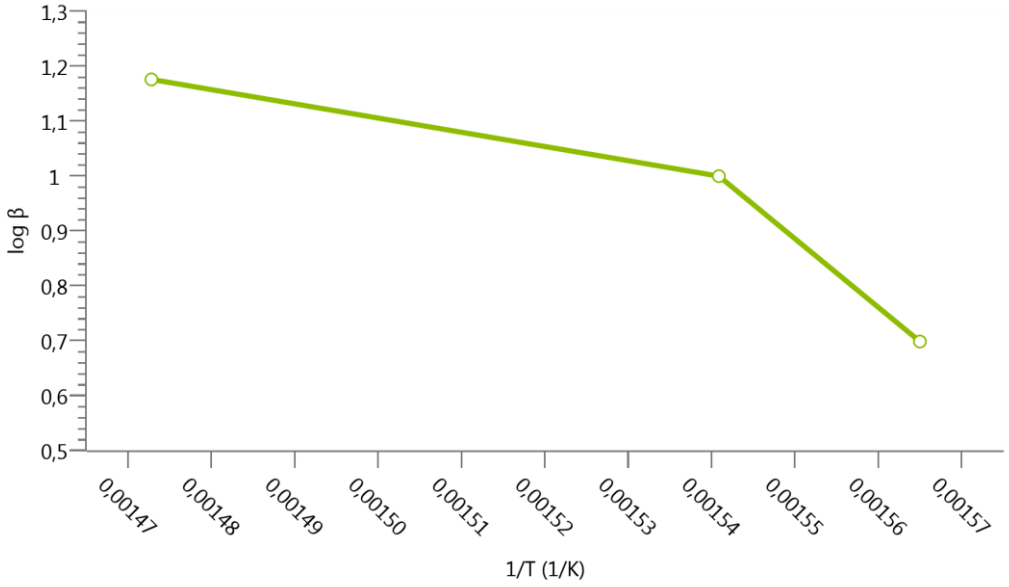

Figure D.II.13 - ASTM E698 Plot of Crude Oil 4

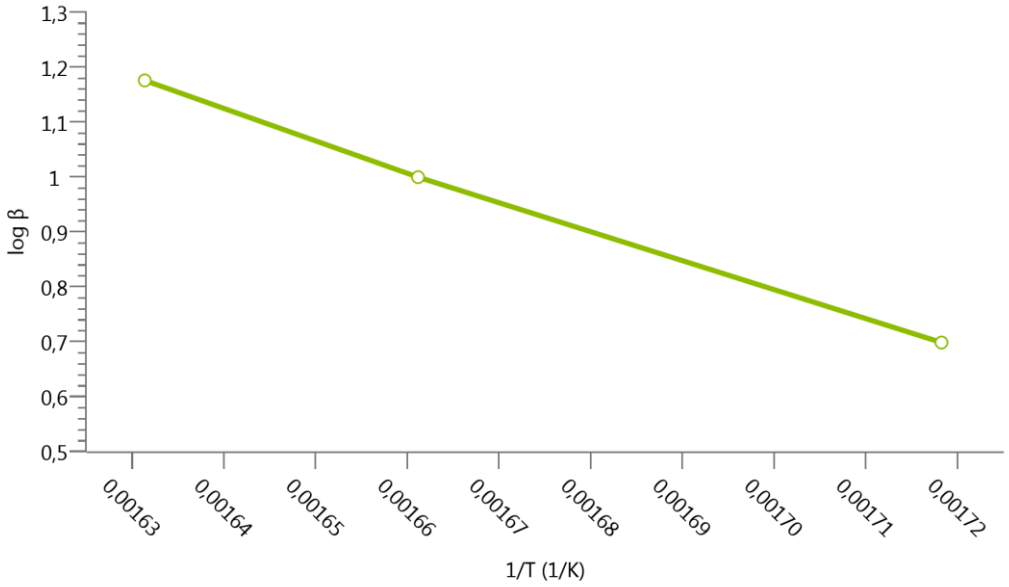

Figure D.II.14 - ASTM E698 Plot of Crude Oil 4 Saturate

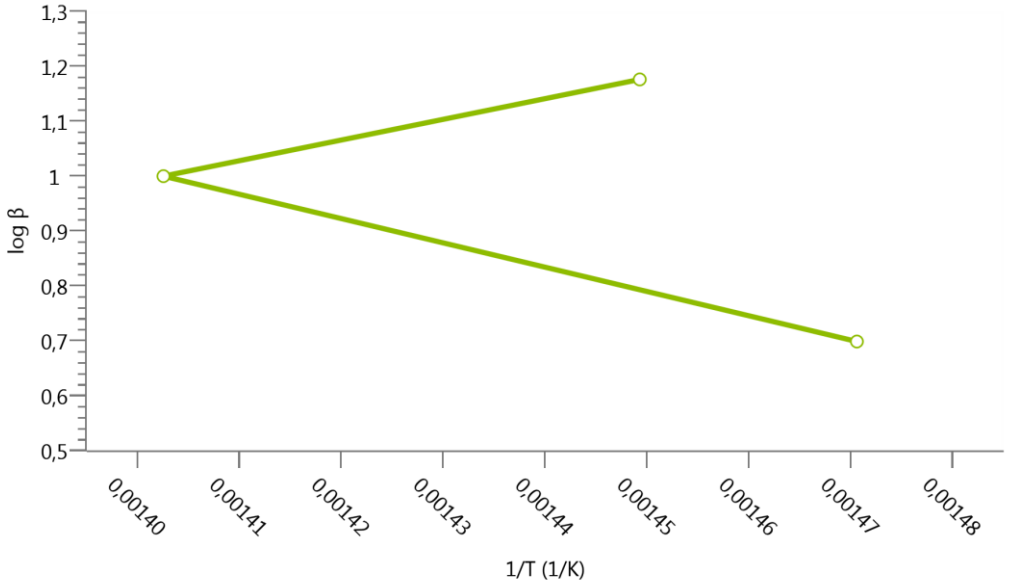

Figure D.II.15 - ASTM E698 Plot of Crude Oil 4 Aromatic

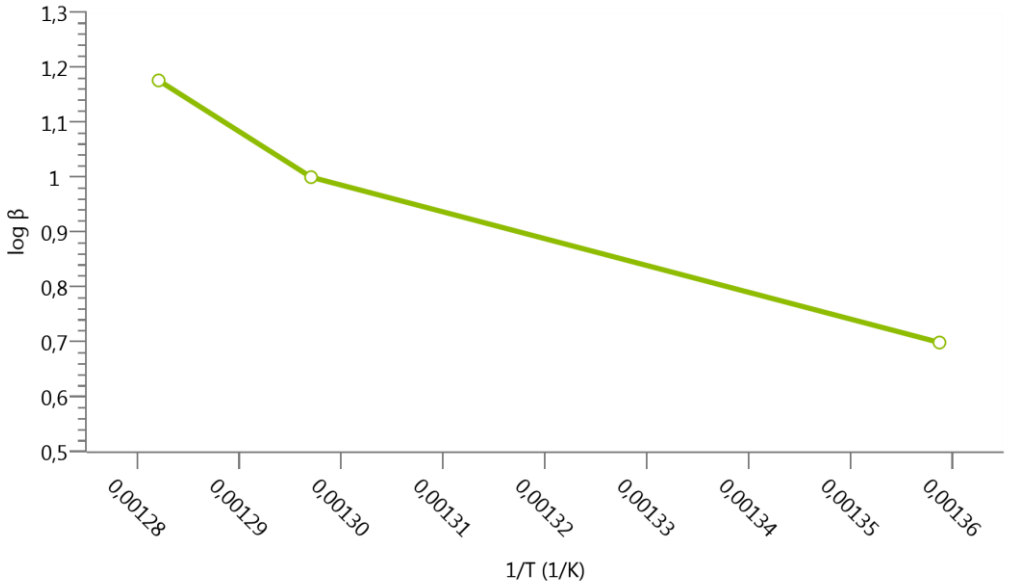

Figure D.II.16 - ASTM E698 Plot of Crude Oil 4 Resin